Insights into late Quaternary vegetation and climate dynamics in Monsoon Asia obtained from numerical pollen-based reconstructions

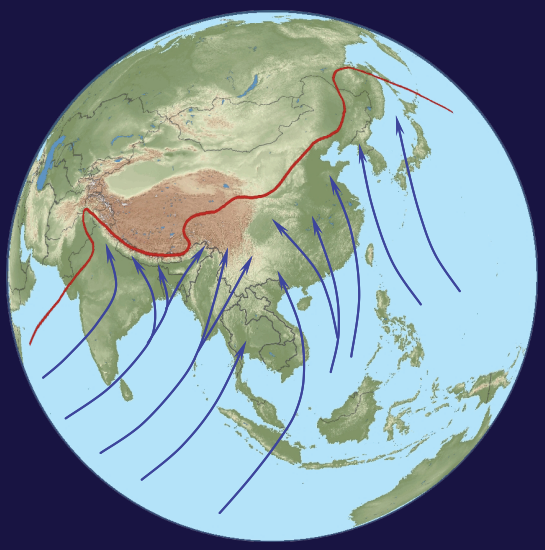

Doctoral thesis

Christian Leipe

Insights into late Quaternary vegetation and climate dynamics in Monsoon Asia obtained from numerical pollen-based reconstructions

Doctoral thesis
submitted in fulfilment of the
requirements for the academic degree
Doctor rerum naturalium (Dr. rer. nat.)

to the Department of Earth Sciences of the
FREIE UNIVERSITÄT BERLIN

by
Dipl.-Geogr.
Christian Leipe

Berlin, May 2014

Front cover figure:

Schematic illustration of the mean main wind directions (arrows) after Kalnay et al. (1996) and the 400 mm precipitation isoline (red line) after New et al. (2002) in Monsoon Asia during summer (June–September).

1st Reviewer: Prof. Dr. Pavel E. Tarasov

2nd Reviewer: Prof. Dr. Frank Riedel

Date of defence: 30 June 2014

Abstract

The Asian monsoon is one of the major components of the world's climate system. The monsoon circulation during the warm half of the year (the Asian summer monsoon) brings significant amounts of precipitation – mainly between May and September – to a vast area of South and East Asia stretching from the western Arabian Sea to the southern Russian Far East. The Asian summer monsoon is generally subdivided into the Indian Summer Monsoon (ISM) and East Asian Summer Monsoon (EASM). Numerous studies have demonstrated that both subsystems have varied significantly over different time scales during the late Quaternary. In order to predict potential future climate dynamics in Monsoon Asia and to provide essential information to build adaptation strategies, it is crucial to understand the spatiotemporal patterns and the magnitude of past variations in the Asian monsoon activity and their relation to other components of the global climate system as well as extraterrestrial forcing factors. Despite considerable progress during the last decades, many issues are still unresolved. To improve existing climate model simulations and to broaden the knowledge about the Asian summer monsoon evolution, additional palaeoclimate proxy studies are required from both subdomains.

This study mainly focuses on the reconstruction of past vegetation and climate dynamics in different regions of Monsoon Asia using numerical approaches (biome reconstruction method and modern analogue technique) based on fossil and modern pollen assemblages. The set of employed fossil pollen records include one from a high-alpine lake (north-western Himalayas, India) located within the ISM domain spanning the last ca. 12 ka and two from peat bogs located within the EASM domain spanning the last ca. 5.5 ka (south-western Hokkaido, Japan) and ca. 44 ka (north-western Sakhalin, Russia). All three climate archives are situated close to the modern summer monsoon limit.

The results suggest that the initial post-glacial ISM strengthening temporally coincides with the termination of the Younger Dryas. The Holocene moisture optimum in the north-western Himalayas prevailed from ca. 11–9.6 cal ka BP. The moisture evolution over the Holocene is marked by a gradual decline, which parallels the southward migration of the mean summer position of the Intertropical Convergence Zone in response to the orbitally induced decrease in summer insolation. The results of the quantitative reconstruction indicate considerable fluctuations in annual precipitation, which was during the wettest interval (early Holocene) ca. 430 mm higher and during the driest interval (late Holocene) ca. 35 mm lower compared to modern conditions (ca. 250 mm). Correlation with other palaeoclimate proxy records suggests that the decrease in precipitation in the regions at the northern limit of the ISM was greater than in the southern parts of the ISM domain.

There is evidence that likely due to Northern Hemisphere ice sheet boundary conditions, the southern ISM domain received more westerly-derived winter precipitation during the early Holocene than during the late Holocene. During the late Holocene, moisture availability is slightly increasing, which is likely a result of strengthened winter westerly disturbances. Holocene centennial-scale intervals of enhanced aridity, which are in concert with North Atlantic cold climate (i.e. Bond) events, probably indicate reduced winter westerly airflow leading to decreased winter precipitation in the north-western Himalayas.

As inferred from the quantitative climate reconstructions, the climate conditions in the northern EASM domain during Marine Isotope Stage 3 were only slightly colder and drier than at present. A significantly strong trend towards climate deterioration is documented during Heinrich event 4. Like in the north-western Himalayas, the onset of Holocene climate amelioration parallels the Younger Dryas termination. While the moisture optimum appears to have occurred in the northern EASM domain during the early Holocene, the thermal optimum was reached during the middle Holocene. Together with the results from Hokkaido, the findings from Sakhalin indicate that the Holocene climate conditions of these islands were considerably influenced by ocean currents.

Palynological and geomorphological analyses suggest that the evolution of the Bronze Age Harappan Civilisation of the greater Indus Valley was linked to short- and long-term climate trends. The gradual decrease in precipitation probably caused crop yields to fall, which promoted the establishment of the mature phase (4.5–3.9 cal ka BP) urban centres to provide an infrastructure for storage, protection, administration, and redistribution of staple crops. Additional pronounced dry spells at ca. 4 and 3.2 cal ka BP in combination with more frequent El Niño–Southern Oscillation-related interannual monsoon fluctuations during the late Holocene probably further hamper sufficient food supply that may have caused the protracted deurbanisation after ca. 4 cal ka BP and eventual demise of the sophisticated Harappan Civilisation between ca. 3.5–3 cal ka BP.

The results of the case studies presented in this thesis yield new insights into late Quaternary Asian monsoon dynamics, possible past climate–human interactions and demonstrate the potential of numerical pollen-based approaches to determine the magnitude of past climate change. They also point out the need for additional palaeoclimate proxy records from different parts of South and East Asia to enhance the understanding of the Asian monsoon system and the underlying driving mechanisms as well as additional modern pollen reference samples to improve numerical pollen-based vegetation and climate reconstructions.

Zusammenfassung

Der asiatische Monsun ist ein Hauptbestandteil des globalen Klimasystems. Während der warmen Jahreshälfte verursacht die Monsunzirkulation (asiatischer Sommermonsun) beträchtliche Niederschläge – hauptsächlich zwischen Mai und September – in einem großen Gebiet Süd- und Ostasiens, welches sich in etwa vom westlichen Arabischen Meer bis zum südlichen Teil des russischen fernen Ostens erstreckt. Der asiatische Sommermonsun ist grundsätzlich unterteilt in den indischen Sommermonsun (ISM) und den ostasiatischen Sommermonsun (EASM). Zahlreiche Studien haben gezeigt, dass beide Subsysteme während des Spätquartärs wesentlichen Änderungen bezüglich ihrer Intensität auf unterschiedlichen Zeitskalen unterworfen waren. Um robuste Vorhersagen über mögliche zukünftige Änderungen im asiatischen Monsunsystem treffen zu können, welche die Grundlagen zur Definition von geeigneten Anpassungsstrategien bilden, ist es unerlässlich die raum-zeitlichen Muster und das Ausmaß vergangener Variabilitäten der Monsunaktivität und deren Beziehung zu anderen Bestandteilen des weltweiten Klimasystems sowie extraterrestrische Einflussfaktoren zu verstehen. Trotz maßgeblicher Fortschritte in den letzten Jahrzehnten sind viele Fragen nach wie vor unbeantwortet. Um die Leistungsfähigkeit bestehender Klimamodelle zu verbessern und das Verständnis der Evolution des asiatischen Sommermonsuns zu erweitern, sind weitere Proxy-basierte Paläoklimastudien in beiden Teilgebieten (ISM und EASM) erforderlich.

Diese Arbeit befasst sich hauptsächlich mit der Rekonstruktion vergangener Vegetations- und Klimaänderungen in verschiedenen Regionen Monsun-Asiens unter Verwendung numerischer Rekonstruktionsmethoden („biome reconstruction method“ und „modern analogue technique“) auf der Grundlage fossiler und rezenter Pollenspektra. Das Set der verwendeten fossilen Pollenprofile beinhaltet ein Profil aus einem hochalpinen See (nordwestlicher Himalaya, Indien) aus dem Einflussbereich des ISM, welches den Zeitraum der letzten ca. 12 ka umfasst und zwei weitere Profile aus Torfmooren aus dem Bereich des EASM, die die letzten ca. 5.5 ka (südwestliches Hokkaido, Japan) bzw. ca. 44 ka (nordwestliches Sachalin, Russland) repräsentieren. Alle drei Klimaarchive befinden sich an der nördlichen Grenze des heutigen Einflussbereichs des asiatischen Summermonsuns und sind deshalb besonders gut geeignet, um Erkenntnisse über vergangene Schwankungen in der Monsunintensität zu erlangen.

Die Ergebnisse der Untersuchungen am Pollenprofil aus dem nordwestlichen Himalaya zeigen, dass der postglaziale Anstieg der ISM-Aktivität zeitlich mit dem Ende der Jüngeren Dryas übereinstimmt. Das holozäne Feuchtigkeitsoptimum datiert zwischen ca. 9.6–11 cal ka BP. Die Entwicklung der holozänen Feuchtigkeits- bzw. Niederschlagsintensität ist gekennzeichnet von einer sukzessiven Abnahme, die mit der südwärts Verlagerung

der durchschnittlichen Sommerposition der innertropischen Konvergenzzone einhergeht. Die Resultate der quantitativen Rekonstruktion ergeben beträchtliche Änderungen in den jährlichen Niederschlägen. Diese waren während der feuchtesten Phase (Frühholozän) um ca. 430 mm höher und während der trockensten Phase (Spätholozän) um ca. 35 mm niedriger als heute (ca. 250 mm). Korrelationen mit anderen Paläoklimarekonstruktionen deuten an, dass die Abnahme der jährlichen Niederschlagsmengen im nördlichen Teil des ISM-Einflussbereichs größer war als im südlichen Teil.

Vergleiche zwischen den hier vorgestellten und anderen Studienergebnissen geben Hinweise darauf, dass im südlichen Bereich des ISM-Gebiets die aus der feuchten ektropischen Westwindströmung resultierenden Niederschlagsmengen während des Frühholozäns höher waren als im Spätholozän. Vermutlich ist dies auf die fortdauernde Vergletscherung in großen Teilen der nördlichen Hemisphäre während des Frühholozäns zurückzuführen, die eine im Vergleich zu heute weiter südlich positionierte Westwindströmung während der kalten und warmen Jahreszeit zur Folge hatte. Der leichte Anstieg der durchschnittlichen Jahresniederschläge im Untersuchungsgebiet des nordwestlichen Himalayas während des Spätholozäns ist wahrscheinlich ein Ergebnis der Intensivierung der ektropischen Westwindströmung. Holozäne Trockenphasen auf einer Zeitskala von Jahrhunderten, die zeitlich synchron mit Klimaschwankungen im nordatlantischen Raum („Bond events“) verlaufen, weisen mutmaßlich auf eine Abschwächung der Westwindströmung hin, welche zu einer Reduktion der Winterniederschläge in den westlichen Randbereichen des ISM geführt hat.

Die Rekonstruktionsergebnisse basierend auf dem fossilen Pollenprofil aus Nordwestsachalin zeigen, dass die Klimabedingungen im nördlichen Teil des EASM-Gebiets während der Sauerstoff-Isotopenstufe 3 nur unwesentlich kälter und trockener waren als heute. Eine Phase bedeutender Klimaverschlechterung mit kalten Wintern und geringen jährlichen Niederschlägen kennzeichnete das Untersuchungsgebiet während des Heinrich-Ereignisses 4. Wie im nordwestlichen Himalaya verlief das Einsetzen der postglazialen Klimaverbesserung parallel zum Übergang Jüngere Dryas/Holozän. Während das warmzeitliche Feuchtigkeitsoptimum in der nördlichen EASM-Zone im Frühholozän belegt ist, ereignete sich das Temperaturoptimum im mittleren Holozän. Die Ergebnisse aus Hokkaido und Sachalin weisen neben der atmosphärischen EASM-Zirkulation als Hauptfaktor für die Steuerung des Klimas dieser Inseln Meeresströmungen als weitere wesentliche Einflussgrößen aus.

Palynologische und geomorphologische Untersuchungen im ISM-Untersuchungsgebiet deuten auf einen Zusammenhang zwischen kurz- und langfristigen Klimaänderungen und der Entwicklung der bronzezeitlichen Harappa-Kultur im nordwestlichen indischen Subkontinent hin. Durch die sukzessive, langfristige Abnahme der jährlichen Niederschlagsmengen kam es wahrscheinlich zu einer landwirtschaftlichen

Ertragsminderung. Letztere führte während der Hauptphase (4.5–3.9 cal ka BP) der Harappa-Kultur zur Gründung urbaner Zentren, die die Infrastruktur für die Lagerung und den Schutz sowie die Verwaltung und Verteilung der Grundnahrungsmittel zur Verfügung stellten. Die in dieser Studie erfassten Trockenphasen um ca. 4 und 3.2 cal ka BP in Verbindung mit häufiger auftretenden El Niño–Southern Oscillation-gesteuerten interannuelle Sommermonsunschwankungen im Spätholozän erschwerten im Folgenden möglicherweise eine ausreichende Versorgung der Bevölkerung mit Nahrungsmitteln und führten somit zu dem nachgewiesenen längerfristigen Verschwinden der urbanen Zentren (ab ca. 4 cal ka BP) und letztendlich zum Niedergang der hochentwickelten Harappa-Kultur (zwischen ca. 3.5 und 3 cal ka BP).

Die Ergebnisse der in dieser Dissertation zusammengefassten Fallstudien liefern neue Erkenntnisse über die spätquartäre Entwicklung des asiatischen Monsuns und möglicher holozäner Mensch–Klima-Wechselbeziehungen im Bereich des nordwestlichen indischen Subkontinents. Ferner veranschaulichen sie das hohe Potenzial numerischer Pollen-basierter Rekonstruktionsmethoden um das Ausmaß vergangener Klimaschwankungen zu erfassen. Die Resultate zeigen zudem die Notwendigkeit weiterer Proxy-basierter Paläoklimastudien aus unterschiedlichen Teilen des ISM- und EASM-Einflussbereichs um ein besseres Verständnis des asiatischen Monsunsystems und seiner zu Grunde liegenden Steuerungsmechanismen zu gewährleisten. Um die Qualität Pollen-basierter numerischer Vegetations- und Klimarekonstruktionen im Untersuchungsgebiet weiter zu steigern, ist eine zusätzliche Erweiterung der bestehenden Referenzdatensätze rezenter Pollenspektra unabdingbar.

Acknowledgements

I am grateful to Frank Riedel and Pavel E. Tarasov, who gave me the opportunity to carry out this interesting research project and to the German Research Foundation (DFG) which financially supported my activities through the grant RI 809/24.

My very special gratitude is extended in particular to my supervisor Pavel E. Tarasov, who has taught me the essentials of scientific work and opened up a new perspective on how to approach all the tricky issues you come across in the scientific realm. I very much appreciate his all-time availability to discuss major and minor difficulties which I run into and to provide valuable feedback and constructive remarks not only in the institute but even from the remotest places via the internet.

I would like to acknowledge the great help and patience of Dieter Demske, who gave valuable advice on sample handling and lab preparation and provided great support in the identification of pollen types from the region of the north-western Himalayas.

I am indebted to Dieter Demske, Sylvia Pinkerneil and Ding Wei for their assistance in sediment core subsampling at the GFZ in Potsdam.

Special thanks go to my officemate Linda Taft for her company and for sharing countless teas and many study-related headaches and to Stefanie Müller for her immense help and encouragement over the last three years. I really enjoyed our inspiring discussions about anything and everything and the hilarious chatter.

Thanks also to all the other "Paläos" of the Freie Universität Berlin especially Steffi Hildebrandt, Wei Ding, Carolina Müller, Wanyi Zhang, Frank Riedel and Annette Kossler for your company, useful ideas, providing literature, and to share heaps of sweets and cakes, not only at the Wednesday afternoon coffee breaks, and to celebrate hilarious barbecue parties on campus together.

Thank you Thomas Schierbaum for accompanying me during sample collection right across the north-western Himalaya and for sharing the breathlessness beyond 5000 m a.s.l. in summer 2011. I owe my thanks to Bernd Wünnemann for the inspiring discussions during the informative excursions around Tso Moriri and for enabling me to see the area through the eyes of an enthusiastic geomorphologist.

Last, but by no means least, I would like to thank the Schuttrutsche-crew for exuberant – not only in terms of music – excursions far from the daily grind, my parents Hartmut and Ursula, for their support and encouragement to follow my interests in research, and my marvellous wife Nao for her unlimited patience, great understanding and overwhelming love.

Table of contents

List of figures

List of tables

List of abbreviations

°C	Degree Celsius
^{14}C	Unstable carbon isotope (half-life: 5730±40 years)
µm	Micrometre
A/C	Ratio of *Artemisia* over Chenopodiaceae
AMS	Accelerator mass spectrometry
AP	Arboreal pollen
a.s.l.	Above sea level
ASM	Asian Summer Monsoon
AVHRR	Advanced Very High Resolution Radiometer
BC	Before Christ
BP	Before present (present = 1950 Anno Domini)
ca.	Circa
cal	Calendar
CLDE	Cold deciduous forest
CLMX	Cold mixed forest
COCO	Cool conifer forest
COMX	Cool mixed forest
DESE	Desert
DO	Dansgaard-Oeschger (events)
EAM	East Asian Monsoon
EASM	East Asian Summer Monsoon
EAWM	East Asian Winter Monsoon
ENSO	El Niño–Southern Oscillation
ESCC	East Sakhalin Cold Current
H	Heinrich (events)
HdV	Hugo-de-Vries Laboratory (University of Amsterdam, The Netherlands)
IPCC	Intergovernmental Panel on Climate Change
ISM	Indian Summer Monsoon
ITCZ	Intertropical Convergence Zone

ka	Kiloyears
km	Kilometre
KWC	Kuroshio Warm Current
LCC	Liman Cold Current
LGM	Last Glacial Maximum
LPZ	Local pollen zone
m	Metre
MAP	Mean annual precipitation
MAT	Modern analogue technique (in Chapters 1, 4 and 5) Mean annual temperature (in Chapter 2)
MIS	Marine Isotope Stage
mm	Millimetre
MTCO	Mean temperature of the coldest month
MTWA	Mean temperature of the warmest month
NAP	Non-arboreal pollen
NH	Northern Hemisphere
NPP	Non-pollen palynomorph
NPPSZ	Non-pollen palynomorph subzone
NPPZ	Non-pollen palynomorph zone
PANN	Mean annual precipitation
PFT	Plant functional type
pH	Potentia hydrogenii
psu	Practical salinity units
PSUM	Mean summer (April–September) precipitation
PsZ	Pollen subzone
PWIN	Mean winter (October–March) precipitation
PZ	Pollen zone
RFE	Russian Far East
SCD	Squared cord distance
SRTM	Shuttle Radar Topography Mission
SST	Sea surface temperature

STEP	Steppe
SWC	Soya Warm Current
TAIG	Taiga
TECO	Temperate conifer forest
TEDE	Temperate deciduous forest
tempLaps	Temperature lapse rate
TMD	Tso Moriri deep water core (composite)
TOC	Total organic carbon
TUND	Tundra
TWC	Tsushima Warm Current
WAMX	Warm mixed forest
YD	Younger Dryas

1. Introduction

1.1 Outline of the thesis

This doctoral thesis constitutes a compilation of four case studies presented in four manuscripts which have been published in or are prepared for submission to international scientific peer-reviewed journals. Each paper represents an individual piece of work, so that in some places (e.g. methods) repetitions are inevitable. An overview of the integrated manuscripts including my own contributions and publication status is given in Chapter 1.2.

Laboratory and analytical work was conducted at the Palaeontology Branch (Institute of Geological Sciences) of the Freie Universität Berlin. The thesis includes case studies (Chapters 2 and 3) which are part of the multidisciplinary Research Unit "Himalaya: Modern and Past Climates" (HIMPAC, http://www.himpac.org/) and were financially supported by the German Research Foundation (DFG) through the grant RI 809/24. This unit was established in 2010 with the aim of elucidating the characteristics of the Indian Summer Monsoon during the late Pleistocene and Holocene. A main component of this research project are studies based on palaeoclimate proxy records—pollen, sediment properties, tree rings, and stable isotopes—from archives located in climatically sensitive regions across the Indian subcontinent (i.e. north-western Himalaya, Meghalaya, Deccan Plateau). The work involved a one-month field campaign through parts of north-western India including the Tso Moriri region (Ladakh).

The thesis is organised into eight chapters:

- **Chapter 1** outlines the general study context including the state of the art of late Quaternary palaeoclimate research in Monsoon Asia and open questions, the study aims and objectives, and the study approach and methods.
- **Chapters 2, 3, 4, and 5** focus on the results of four case studies each presented as self-contained manuscripts.
- **Chapter 6** is concerned with the main conclusions of case studies in **Chapters 2–5** and highlights some directions for future work.
- The bibliography in **Chapter 7** contains all publications cited in this thesis.
- **Chapter 8** gives information on the supplementary material associated with **Chapters 2–4** and how to access the contained data. It also provides a complete list of publications in which I was involved during the time of my doctoral research either as main or co-author. The curriculum vitae is only available in the printed version of this thesis.

1.2 Integrated manuscripts

This manuscript-based doctoral thesis consists of four individual manuscripts, which have been published in or are prepared for submission to international scientific peer-reviewed journals. According to paragraph 7(2) of the doctorate regulations of the Department of Earth Sciences at the Freie Universität Berlin, an overview of these manuscripts including my own contributions regarding the conception, accomplishment of the study and publication is given in Table 1.1.

Manuscript no./chapter	Manuscript (title, author list, own contribution)	Publication status in May 2014
I/2.	A Holocene pollen record from the northwestern Himalayan lake Tso Moriri: Implications for palaeoclimatic and archaeological research *Christian Leipe, Dieter Demske, Pavel E. Tarasov, HIMPAC Project Members* contribution of Christian Leipe — conception: 60%; accomplishment: 70%; publication: 80%	Published in *Quaternary International* 348 (2014) pp. 93–112 doi:10.1016/j.quaint.2013.05.005
II/3.	Potential of pollen and non-pollen palynomorph records from Tso Moriri (Trans-Himalaya, NW India) for reconstructing Holocene limnology and human–environmental interactions *Christian Leipe, Dieter Demske, Pavel E. Tarasov, Bernd Wünnemann, Frank Riedel, HIMPAC Project Members* contribution of Christian Leipe — conception: 70%; accomplishment: 50%; publication: 90%	Published in *Quaternary International* 348 (2014) pp. 113–129 doi:10.1016/j.quaint.2014.02.026
III/4.	Vegetation and climate history of Northern Japan inferred from the 5500-year pollen record from the Oshima Peninsula, SW Hokkaido *Christian Leipe, Norio Kito, Yumi Sakaguchi, Pavel E. Tarasov* contribution of Christian Leipe — conception: 50%; accomplishment: 70%; publication: 60%	Published in *Quaternary International* 290–291 (2013) pp. 151–163 doi:10.1016/j.quaint.2012.07.014
IV/5.	Pollen-inferred late Quaternary vegetation and climate variations from the northern-most part of the East Asian Summer Monsoon domain (Sakhalin, Russian Far East) *Christian Leipe, Yaeko Igarashi, Takeshi Nakagawa, Katsuya Gotanda, Pavel E. Tarasov* contribution of Christian Leipe — conception: 70%; accomplishment: 70%; publication: 90%	Manuscript in review at Quaternary Science Reviews

Table 1.1 Overview of the manuscripts presented in this thesis including my own contribution in percent and the publication status.

1.3 Study background and motivation

The Asian monsoon is the most extensive monsoon system of the world (He et al., 2006) and one of the most important components of the global climate system (Morrill et al., 2006). Like the other major monsoon systems (i.e. the African and American monsoon), the Asian monsoon is generally characterised by a seasonal reversal of atmospheric circulation and associated precipitation. This mechanism is due to the seasonal reversals in temperature and air pressure gradients between the Asian continent and the adjacent oceans, which results in a "wet" and "dry" season in large parts of East and South Asia (Webster et al., 1998; Trenberth et al., 2000). This is expressed in the latitudinal movement of the Intertropical Convergence Zone (ITCZ); a circum-global low pressure belt where the northeast and southeast trade winds converge. In winter, cold air masses (the Siberian High) form over the central Asian continent, while low pressure cells form over the relatively warm surrounding oceans (i.e. Indian Ocean and western Pacific Ocean). This is due to the strong heat capacity of the oceans and the enhanced solar-induced warming of the southern Indian Ocean, which pushes the ITCZ south of the equator. During summer, strong solar-induced heating over the high-elevated Tibetan Plateau forms a massive low pressure cell (Asian continental low), which leads to the enhanced northward migration of the ITCZ. Simultaneously, high atmospheric pressure forms over the relatively cold oceans resulting in a reversed temperature (pressure) gradient (Chang et al., 2006).

In a non-scientific context, the usage of the term "Asian monsoon" is mostly related to the Asian summer monsoon (ASM), which has a far greater meaning for the local societies than the winter monsoon. While winter monsoon circulation leads to cold and dry conditions in continental Asia, the summer monsoon circulation transports large amounts of vapour to the Asian landmass, thus creating warm and wet conditions. The regions which receive significant amounts of atmospheric precipitation associated with the ASM mode make up a vast terrestrial area, which is home to approximately half of the world's population (World Bank, 2014) and characterised by an extremely high population density (CIESIN and CIAT, 2005) (Fig. 1.1) stretching from the western Arabian Sea to the southern Russian Far East (Alpat'ev et al., 1976; Petrov et al., 2000; Wang, 2006; Fig. 1.2). This impressively highlights the direct dependence of the social and economic well-being of the local populations on variations in monsoon intensity (Webster, 2006; Cook et al., 2010).

The ASM is generally divided into the Indian Summer Monsoon (ISM) and the East Asian Summer Monsoon (EASM) (Fig. 1.2), which are independent subsystems with different boundary conditions but at the same time interact with each other (Wang, et al., 2001a, 2003; Ding and Chan, 2005). That both the ISM and the EASM have varied over

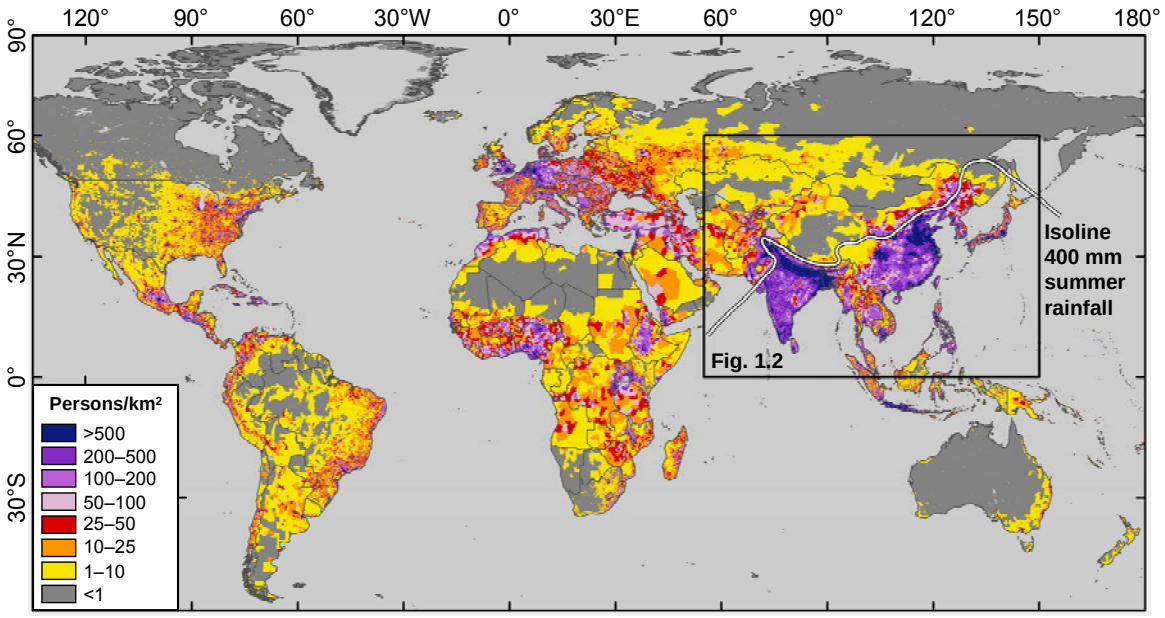

Fig. 1.1 Overview map showing the global population density in 2010 after CIESIN and CIAT (2005), the 400 mm precipitation isoline (white line) in Monsoon Asia during summer (June–September) after New et al. (2002) and the wider study region (black inset).

short- and long-term scales during the late Quaternary is well documented in numerous studies and generally accepted (Clift and Plumb, 2008). In order to predict future dynamics in the ASM and to provide essential information for adaptation strategies and policymakers especially against the background of a global warming scenario (Overpeck and Cole, 2007; Ashfaq et al., 2009), climate model simulations are identified as useful tools (IPCC, 2001, 2007). Although numerous approaches have been proposed (IPCC, 2007, 2013), precise modelling of the Asian monsoon to estimate past fluctuations as well as future trends on multiple time scales (i.e. intraseasonal to orbital time scales) remains a difficult and challenging task (e.g. Webster, 2006; Turner et al., 2011; Sperber et al., 2012; Zhao and Harrison, 2012). This is not least due to the role of the Asian monsoon as a major component of the global climate system with complex spatio-temporal variabilities related to various teleconnections to other climate subsystems e.g. the El Niño/Southern Oscillation (ENSO) (Wallace et al., 1998) and Arctic Oscillation (AO) (Gong et al., 2001) and North Atlantic climate events (Porter and An, 1995). Another important climate feature in the region are the Northern Hemisphere (NH) mid-latitude westerly disturbances, which influence the north-western boundary areas of the Asian monsoon domain (Fig. 1.2) by significant moisture supply during winter (December–March) derived from the Atlantic Ocean, the Mediterranean, Black, and Caspian Sea (Aizen et al., 1996; Gadgil, 2003; Lang and Barros, 2004; Cheng et al., 2012).

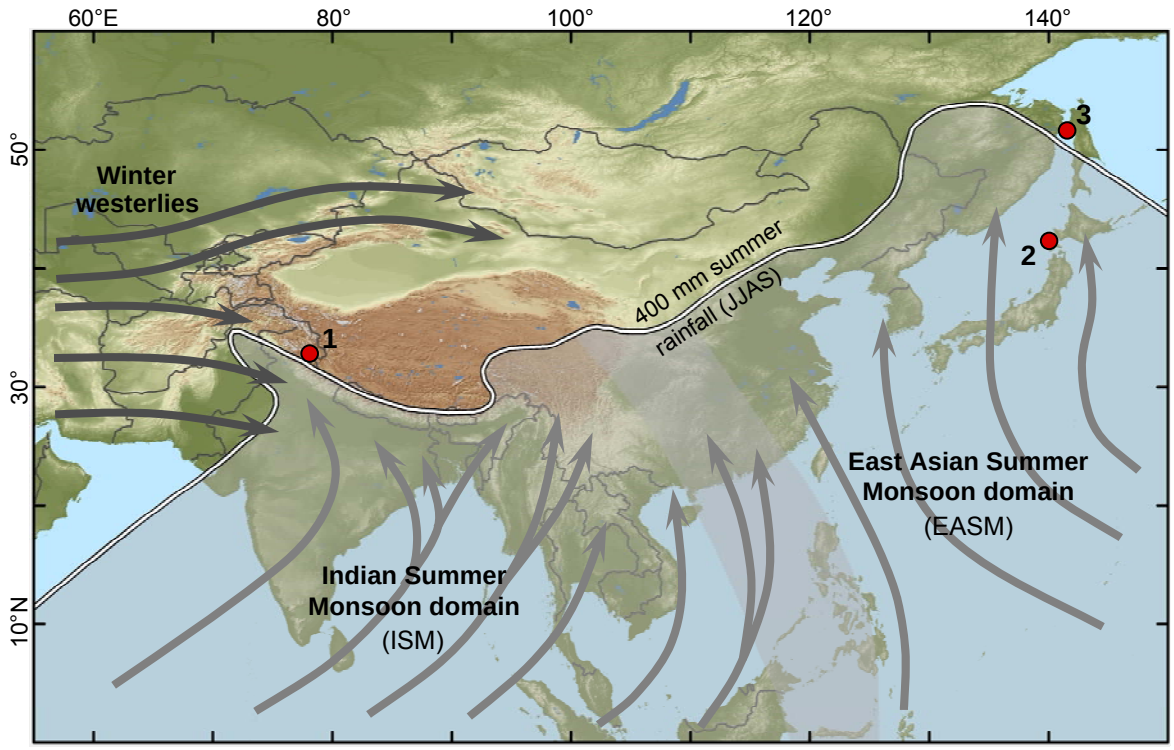

Fig. 1.2 Overview map showing the study area of Monsoon Asia including the schematic domains of the ISM and EASM together with their schematic main wind directions (light grey arrows) during summer (June–September) and the winter (December–February) westerly wind directions (dark grey arrows) after Kalnay et al. (1996). The 400 mm precipitation isoline during summer (June–September) after New et al. (2002) is indicated by a white line. The sites of the employed fossil palynomorph records from Tso Moriri in the NW Himalayas (1), from Yakumo in SW Hokkaido (2) and from Khoe in NW Sakhalin (3) are represented by red dots.

To further improve existing projections of Asian monsoon trends relevant for the livelihood of regional human societies, palaeoclimate reconstructions are essential to uncover monsoon forcing mechanisms and to evaluate climate model outputs (e.g. Otto-Bliesner et al., 2009; Dallmeyer et al., 2010; Braconnot et al., 2012). A large number of palaeoclimate proxy studies have been conducted in both the ISM and EASM realm, and have significantly broadened the knowledge about past dynamics in monsoon activity (see Morrill et al., 2003; Wang et al., 2005a; Herzschuh, 2006; Fleitmann et al., 2007; Wang et al, 2010; Ran and Feng, 2013 and references therein). However, our understanding of the spatiotemporal pattern and the magnitude of past fluctuations in Asian monsoon intensity and its relation with other components of the global climate system as well as extraterrestrial forcing factors remains incomplete (e.g. Clemens and Prell, 2007; Nakagawa et al., 2008; Jin et al., 2014). Moreover, palaeoclimate proxy records not only improve the understanding of the late Quaternary monsoon evolution, but also allow the perception of past human–climate interactions to be broadened. Various studies have suggested a causal relationship between climate deterioration and the demise of early civilisations like the

Akkadian empire of ancient Mesopotamia (Cullen et al., 2000; deMenocal, 2001), Egypt's Old Kingdom (Hassan, 1997; Weiss, 1997), and the Maya in Central America (Haug et al., 2003). Climate change is also hypothesised to have played a key role in the decline of the Harappan Civilisation (e.g. Singh, 1971; Staubwasser et al., 2003; MacDonald, 2011), which at the times of its greatest flourishing (ca. 4.5 and 3.9 cal ka BP) occupied large parts of the greater Indus Valley. However, this interpretation is doubted by different archaeologists (Madella and Fuller, 2006 and references therein), who consider climate change as a negligible factor in the evolution of the Harappans.

The following questions outline some of the main aspects of current research in late Quaternary palaeoclimatology and archaeological research in Monsoon Asia:

- **What is the timing of the Holocene ASM onset?**

  There is disagreement about whether the initial interglacial strengthening of the ASM circulation coincides with the Younger Dryas termination and the Holocene onset around 11.7 cal ka BP (e.g. Overpeck et al., 1996; Dykoski et al., 2005) or occurred no earlier than ca. 10 cal ka BP (e.g. Sirocko et al., 1993; Schulz et al., 1998; Fleitmann et al., 2003).

- **Was the moisture evolution of the ISM and EASM over the Holocene synchronous or asynchronous?**

  While some authors postulate that the developments in the ISM and EASM have been asynchronous (e.g. An et al., 2000; He et al., 2004; Herzschuh, 2006; Maher and Hu, 2006; Wang, et al., 2010) or antiphased (Hong et al., 2005), others have found evidence of their synchronicity (e.g. Zhou et al., 2004; Zhao et al., 2009c; Zhang et al., 2011).

- **What is the phase relationship between the EASM and the East Asian Winter Monsoon (EAWM) on multiple time scales?**

  There is consensus about the anti-phase behaviour of the EASM and the EAWM during the last glacial period. Regarding the Holocene, there is controversy about whether the two components were simply anti-phased (e.g. Yancheva et al., 2007), in phase (e.g. Huang et al., 2011; Steinke et al., 2011) or characterised by a more complex relationship which varied spatially and through time (Wang et al., 2012). At the same time, this demonstrates that the underlying controlling factors of EAWM intensity are not yet identified.

- **What is the interaction between mid-latitude westerly disturbances and the Asian monsoon circulation?**

  There is uncertainty about the interplay between westerly disturbances and the Asian monsoon circulation and their influence in eastern Central Asia and the regions north

of the Tibetan Plateau. While some suggest an anti-phase relationship of westerly disturbances to NH summer insolation, thus ASM intensity, on glacial–interglacial time scales (An et al., 2012), others report strong moisture signals at times of high NH summer insolation in regions of westernmost China (Cheng et al., 2012), which are today clearly dominated by westerlies (Aizen et al., 1996). An inverse behaviour of westerly disturbances and NH summer insolation is also evident during the Holocene interval. Most proxy records indicate dry and moist conditions during the early and late Holocene, respectively (e.g. Chen et al., 2008; Liu et al., 2008; Rudaya et al., 2009). However, inconsistent or contrary findings are documented from other climate archives in the wider region (e.g. Ricketts et al., 2001; Zhao et al., 2009b; Li et al., 2011). Besides external driving forces, internal forcing factors like NH glaciation, snow cover, and ocean circulations may have also affected the spatio-temporal westerly/monsoon influence on seasonal to orbital time scales in these regions, which remain less well understood.

- **How are millennial- to centennial-scale phases of weak ASM linked with cold climate events in the North Atlantic region?**

  Numerous studies have shown that last glacial–Holocene North Atlantic climate events are also imprinted in palaeoclimate records from both the ISM and EASM domains (Bush and Gosling, 2012). There is still debate about the forcing mechanisms (Clement and Peterson, 2008) and why some events are apparently characterised by a particularly high magnitude of change in monsoon activity (Gupta et al., 2003; Wang et al., 2005b). An overview of the suggested mechanisms is outlined by Clement and Peterson (2008) and Marzin et al. (2013). The most likely drivers of abrupt climate oscillations which are discussed include teleconnections to Atlantic meridional overturning variations, which were transmitted by a southward displaced westerly yet causing a weakening of the ITCZ (e.g. Porter and An, 1995; Wang et al., 2005b; Jin et al., 2007; Sun et al., 2012) and direct influence of changes in solar output (Gupta et al., 2005; Wang et al., 2005b).

- **What are the magnitudes of late Quaternary climate fluctuations?**

  Quantitative palaeoclimate reconstructions are of high value in palaeoclimatology and allow direct comparison with (i.e. validation of) climate model outputs (Sawada et al., 2004; Schmidt, 2010). Yet such data for the Asian monsoon realm is still sparse (e.g. Tarasov et al., 2011; Zhao and Harrison, 2012).

- **To what extent was the evolution of the Bronze Age Harappan Civilisation and the Neolithic Yangtze and Central China Cultures influenced by climate change?**

  As (partly) mentioned above, there are still gaps in understanding the role of climate change regarding the demise of the Harappan Civilisation (Madella and Fuller, 2006) and the Yangtze (Yasuda et al., 2004) and Central China (Wu and Liu, 2004) Cultures, which was initiated around 4 cal ka BP.

To solve existing issues in late Quaternary palaeoclimatology addressing the Asian monsoon system including its variations on multiple time scales and underlying driving mechanisms, additional and ideally well-dated continuous high-resolution long-term palaeoclimate proxy records from both subdomains are required (Wang et al., 2005; Ju et al., 2007; Tarasov et al., 2011; Chabangborn et al., 2013; Jin et al., 2014). The basic motivation of this thesis is to make a contribution to a better understanding of the Asian palaeomonsoon dynamics.

1.4 Study aims and objectives

The principle aim of this study is to provide new insights into late Quaternary climate and vegetation variability in different regions within the ASM domain. In particular, it is intended to quantify past climate dynamics by the reconstruction of dominant biomes and various climate and environmental parameters based on fossil and modern pollen assemblages to allow comparison with climate model simulations and to provide awareness of the magnitude of past and possible future climate fluctuations. The reconstruction results are generally discussed in combination with the conventional interpretation of fossil pollen and fern/moss spore assemblages. To make the obtained data easily available to the scientific community, it is provided via open-access databases (Chapter 8.1). The study is based on two fossil pollen records from the EASM and one from the ISM domain, each covering a different time interval. Another concern of this study is to put the fossil pollen records into a robust chronological framework which allows interpretation of vegetation and climate dynamics within a broader spatial context. Besides the reconstruction of the long-term vegetation and climate evolution, focus is also put on detecting short-term (i.e. millennial- to centennial-scale) climate oscillations. The derived reconstructions are correlated with existing regional, extra-regional and global key palaeoclimate records, and records of calculated solar parameters. Against the background of the ongoing debate whether the demise of the Harappan Civilisation was linked to climate change, a further aim is to use the palaeoclimate reconstruction results of the pollen record from the ISM domain to evaluate possible Holocene human–climate interactions. To strengthen the interpretations in view of past climate changes and human development within the northwestern ISM domain and around the study site, the pollen-based reconstruction results are supplemented by the analysis of past palaeolimnologic conditions of the sampled water body on the basis of non-pollen palynomorph (NPP) assemblages.

1.5 Study material and methods

This study combines fossil pollen and NPP records from lacustrine and peat bog sediment profiles from three individual locations situated within the ISM and EASM domain covering different time ranges. Figure 1.2 shows the location of the three study sites and illustrates one basic methodological concept of this study which is to obtain vegetation and climate reconstructions mainly based on fossil pollen records extracted from archives located close to the modern limits of the ASM (i.e. in climatically sensitive regions), thus expected to well reflect past changes in monsoon intensity. More specifically, two fossil pollen records originate from peat bogs at the northern limits of the EASM domain (south-western Hokkaido and northern Sakhalin), whilst one was extracted from a high-altitude lake (Tso Moriri) in the western Trans-Himalaya located close to the northern limit of the ISM, the eastern limits of winter westerly influence (Bookhagen et al., 2010) and northern boundary of the Harappan Civilisation settlement area (Kenoyer, 2010). The contained case studies partly employ palynological records which have been analysed and published within the framework of the HIMPAC project (Chapters 2 and 3) as well as from existing and previously published studies (Chapters 4 and 5). For the quantitative reconstruction of climate parameters, the employed modern pollen reference datasets partly comprise newly analysed samples (Chapter 2), or a combination of new and existing pollen reference samples (Chapters 4 and 5).

Since its establishment in the early 20th century, classic pollen analysis (i.e. the study of past changes of vegetation and climate by means of fossil pollen assemblages) has been extensively applied in late Quaternary palaeoenvironmental studies (Bennett and Willis, 2001). This conventional approach is based on a subjective assessment and interpretation of fossil pollen spectra. The major aim of this study is to decipher past changes in vegetation distribution and climate in the study regions by means of pollen-based objective (semi)quantitative approaches. This mainly includes the modern analogue technique (MAT) and the biomisation method. Since a sufficiently large array of modern pollen assemblages was not at hand for the case study in the ISM domain, a simple transfer function (regression model) was developed to quantify past variations in mean annual precipitation (Chapter 2).

The underlying assumption of the MAT, which is also termed the (best) modern analogue approach, is that pollen assemblages with a similar composition of pollen taxa are produced by compositionally and structurally similar vegetation communities. The principle concept of the method is to compare individual fossil pollen spectra with a comprehensive collection of modern spectra in order to determine whether one or more modern spectrum/spectra numerically "match(es)" the particular fossil spectrum (Jackson and Williams, 2004). Therefore, multivariate distance metrics (e.g. squared cord distance,

Euclidean distance) and empirically determined numerical threshold values are commonly used (Prentice, 1980; Overpeck et al., 1985; Gavin et al., 2003). If a modern spectrum meets the specified statistical criteria, it is considered as a modern analogue of the particular fossil spectrum. The modern environmental conditions (e.g. climate parameters, total tree cover) affiliated with the sites of this modern analogue are then assigned to the fossil spectrum and considered as the reconstructed values of the represented time interval (Guiot, 1990; Jackson and Williams, 2004). To evaluate the robustness of the MAT reconstructions, leave-one-out cross-validation is often applied to the respective compilation of modern reference pollen assemblages (i.e. modern training set) (Birks, 1995, 1998; ter Braak, 1987). Here, each modern spectrum contained in the reference set is compared to the remaining spectra in the set and given the value of the environmental parameter associated with the identified analogues. The performance (i.e. the strength of the relationship between the observed and predicted values) is commonly assessed by different statistical parameters including the coefficient of determination (r^2), root mean square error (RMSE) and root mean square error of prediction (RMSEP).

Another objective pollen-based reconstruction method applied in this study is the semiquantitative biome reconstruction method sometimes referred to as biomisation method. The approach, which was developed and described in detail by Prentice et al. (1996), is based on a fuzzy logic approach and allows the reconstruction of biomes, i.e. major vegetation types, from pollen or plant macrofossil assemblages. The approach basically involves the calculation of numerical "affinity" of the particular assemblage to every biome. This requires for each pollen/macrofossil assemblage (i) the assignment of pollen and/or macrofossil taxa to plant functional types (PFTs), which are plant groups with similar characteristics in stature, leaf form, phenology, and bioclimatic tolerance defined in the global BIOME1 vegetation model (Prentice et al., 1992); (ii) the assignment of PFTs to one or more biome(s) in which they may occur; and (iii) the determination of the affinity scores for each biome by summation of square roots of the abundances of the attributed pollen/microfossil taxa. The biome with the highest affinity score, or the one defined by a smaller number of PFTs (in case several biome scores are equal), is considered as the dominant biome and assigned to the given pollen assemblage. Since the different PFTs and biomes are associated with bioclimatic ranges defined in vegetation models (e.g. the BIOME1 model, Prentice et al., 1992), they allow climatic interpretation of biome reconstruction results which, in turn, may be used for comparison with climate model outputs (Kleinen et al., 2011, 2014).

A schematic overview of the MAT and the biome reconstruction method is given in Figure 1.3. The fundamental advantage of both methods is their objectivity and ability to provide quantitative information on past climate and environmental changes. This is highly beneficial for both the modelling and data community as direct comparison of

model simulations and pollen-based vegetation and climate reconstructions allow validation (Fig. 1.3), thus improvement, of climate models and a better understanding of the role of climate forcings on past environments (Kleinen et al., 2014).

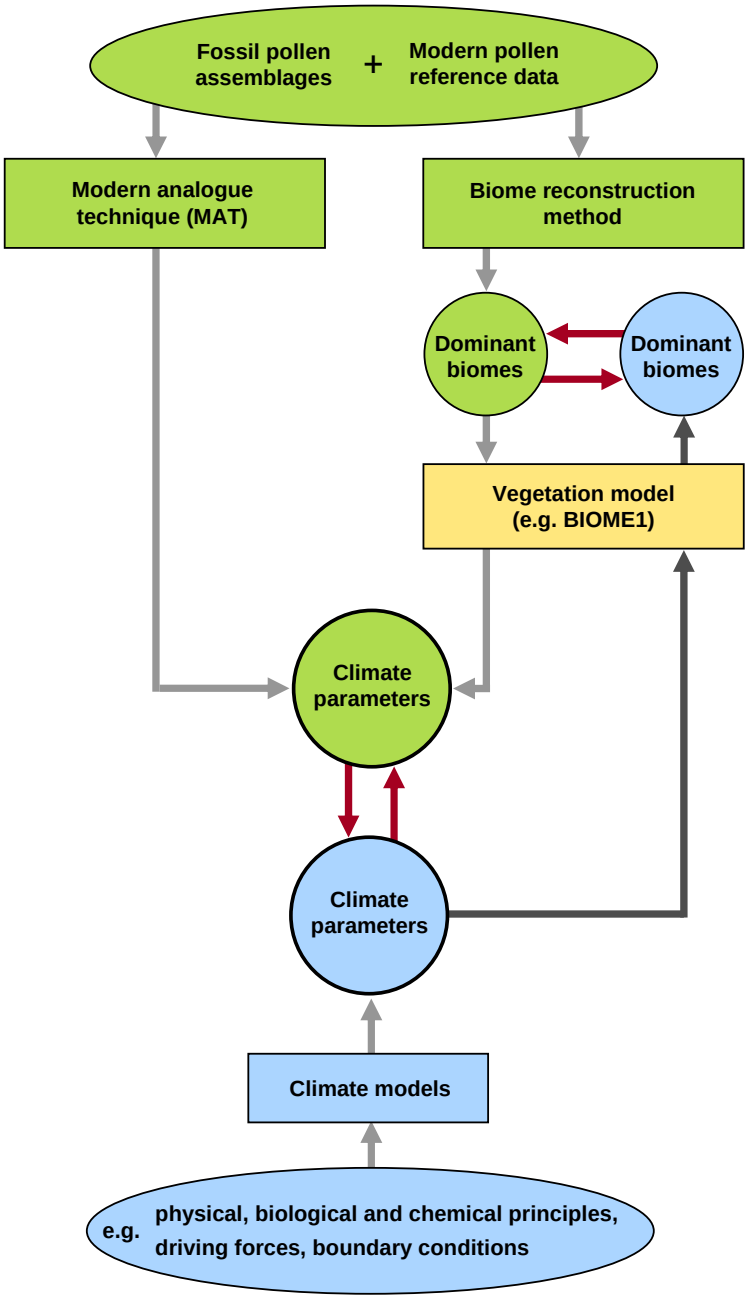

Fig. 1.3 Simple relational schema of pollen-based and model-based approaches to respectively reconstruct and simulate climate parameters.

2. Manuscript I

A Holocene pollen record from the northwestern Himalayan lake Tso Moriri: Implications for palaeoclimatic and archaeological research

Christian Leipe [a], Dieter Demske [a], Pavel E. Tarasov [a],
HIMPAC Project Members [1]

[a] *Institute of Geological Sciences, Palaeontology, Freie Universität Berlin, Malteserstraße 74–100, Building D, 12249 Berlin, Germany*

[1] *http://www.himpac.org/*

Published in *Quaternary International* 348 (2014) pp. 93–112

doi:10.1016/j.quaint.2013.05.005

2.1 Abstract

This paper presents a new fossil pollen record from Tso Moriri (32°54′N, 78°19′E, 4512 m a.s.l.) and seeks to reconstruct changes in mean annual precipitation (MAP) during the last 12,000 years. This high-alpine lake occupies an area of 140 km^2 in a glacial-tectonic valley in the northwestern Himalaya. The region has a cold climate, with a MAP <300 mm, and open vegetation. The hydrology is controlled by the Indian Summer Monsoon (ISM), but winter westerly-associated precipitation also affects the regional water balance. Results indicate that precipitation levels varied significantly during the Holocene. After a rapid increase in MAP, a phase of maximum humidity was reached between ca. 11 and 9.6 cal ka BP, followed by a gradual decline in MAP. This trend parallels the reduction in the Northern Hemisphere summer insolation. Comparison of different palaeoclimate proxy records reveal evidence for a stronger Holocene decrease in precipitation in the northern versus the southern parts of the ISM domain. The long-term trend of ISM weakening is overlaid with several short periods of greater dryness, which are broadly synchronous with the North Atlantic cold spells, suggesting reduced amounts of westerly-associated winter precipitation. Compared to the mid and late Holocene, it appears that westerlies had a greater influence on the western parts of the ISM domain during the early Holocene. During this period, the westerly-associated summer precipitation belt was positioned at Mediterranean latitudes and amplified the ISM-derived precipitation. The Tso Moriri pollen record and moisture reconstructions also suggest that changes in climatic conditions

affected the ancient Harappan Civilisation, which flourished in the greater Indus Valley from approximately 5.2 to 3 cal ka BP. The prolonged Holocene trend towards aridity, punctuated by an interval of increased dryness (between ca. 4.5 and 4.3 cal ka BP), may have pushed the Mature Harappan urban settlements (between ca. 4.5 and 3.9 cal ka BP) to develop more efficient agricultural practices to deal with the increasingly acute water shortages. The amplified aridity associated with North Atlantic cooling between ca. 4 and 3.6 and around 3.2 cal ka BP further hindered local agriculture, possibly causing the deurbanisation that occurred from ca. 3.9 cal ka BP and eventual collapse of the Harappan Civilisation between ca. 3.5 and 3 cal ka BP.

2.2 Introduction

Despite a substantial number of existing marine and terrestrial climate proxy records, especially from the Arabian Sea and the Arabian and Indian Peninsula (e.g. Fleitmann et al., 2007 and references therein), our current knowledge about late Quaternary spatio-temporal variability of the Indian Summer Monsoon (ISM) remains poor. A better understanding of this weather pattern is needed to (i) evaluate relations with climate forcings and other atmospheric circulation features, (ii) build and validate climate models, and (iii) reliably interpret past human climate interactions.

The current underdeveloped state of knowledge regarding the ISM is partly due to a lack of continuous, high-resolution long-term proxy records from the ISM realm (e.g. Fleitmann et al., 2007; Wahl and Morrill, 2010; Ponton et al., 2012). Cook et al. (2010) and Sinha et al. (2011) have also suggested that proxy records from remote areas may not be suitable to explain the evolution of the ISM on the Indian subcontinent, due to its heterogeneous effect reflected at regional scales. It has been accepted that Holocene precipitation changes related to the ISM (Fleitmann et al., 2003) and other tropical atmospheric circulation systems (i.e. the East Asian Summer Monsoon (EASM) (Dykoski et al., 2005; Wang et al., 2005b), African Monsoon (deMenocal et al., 2000; Gasse, 2000), and summer rainfall in northern South America (Haug et al., 2001)) are linked to the migration of the Intertropical Convergence Zone (ITCZ). However, regarding the timing, strength and fluctuations of the late glacial–Holocene hydrological cycle in different parts of the ISM domain, various questions remain unanswered. While the planktonic foraminifera-based $\delta^{18}O$ (Sirocko et al., 1993) and multiproxy (Overpeck et al., 1996) records from the western Arabian Sea show a two-step (ca. 13–12.5 cal ka BP and 11–10 cal ka BP) increase of post-glacial monsoon intensity, Fleitmann et al. (2003, 2007) inferred an onset of enhanced ISM activity from stalagmite $\delta^{18}O$ profiles from Oman no earlier than ca. 10 cal ka BP. A second ongoing discussion focuses on the mode of ISM weakening during the Holocene interval, which has been qualified as occurring abruptly between 5 and 4.5 cal

ka BP and at around 1.3 cal ka BP by Morrill et al. (2003). However, this view has been questioned by Gupta et al. (2003), Wang et al. (2005b) and Fleitmann et al. (2007). They argue that monsoon moisture has declined rather gradually since approximately 8–7 cal ka BP.

The third important puzzle in palaeoclimate research regards the decline of the urban Mature Harappan Civilisation at ca. 4.5–3.9 cal ka BP in the northwestern Indian Peninsula (Fig. 2.1). In particular, we need to clarify whether this decline was brought on by deteriorating climate conditions (see Madella and Fuller, 2006; MacDonald, 2011 for further details). Most palaeoclimate and environmental studies addressing this question are based on proxy records from lacustrine archives. As these are located in the former Harappan Civilisation settlement area (Madella and Fuller, 2006 and references therein), they could have been affected by the human impact on regional environments, as opposed to exclusively recording natural climate change signals. Previous reviews have demonstrated that these records are of limited usefulness, due to their low resolution (e.g. Prasad and Enzel, 2006). Moreover, such studies have yielded contradictory results (e.g. Madella and Fuller, 2006; Wright et al., 2008).

These circumstances highlight the need for supplemental continuous long-term proxy records from terrestrial climate archives capable of providing reliable interpretations and enhancing our understanding of past ISM-related changes on the Indian subcontinent. The high-alpine lakes in the northwestern Himalaya are located in a region that has been little disturbed by human activity and are near the boundary between arid and humid climate conditions (Peel et al., 2007). These lakes have thus been identified as valuable past climate archives able to meet the above stated requirements (Wünnemann et al., 2010). Comprehensive multi-proxy studies have also been conducted in the western end of the adjacent Tibetan Plateau focusing on lake sediment cores from Sumxi Co (Gasse et al., 1991, Fig. 2.1) and Bangong Co (Gasse et al., 1996, Fig. 2.1). A pioneering study on palaeoclimate and vegetation, based on a late glacial–early Holocene pollen profile from the basin of Tso Kar, which is a terminal hyper-saline lake at 4527 m a.s.l. in the Indian northwestern Himalaya, was presented by Bhattacharyya (1989b). More recently, Demske et al. (2009) and Wünnemann et al. (2010) qualitatively reconstructed late glacial and Holocene vegetation and climate changes using palynological, sedimentological, and geomorphological records from the Tso Kar basin. Their results indicate that the region around Tso Kar is even more sensitive to changes in monsoon intensity than the Tibetan lakes located further north that had been investigated earlier (Gasse et al., 1991, 1996). However, the reconstruction results from Tso Kar need to be validated with additional palaeoclimate and environmental proxy data from the region.

This study contributes to the German Research Foundation (DFG) funded multidisciplinary Research Unit “Himalaya: Modern and Past Climates” (HIMPAC). This unit was

established in 2010 with the aim of elucidating the characteristics of the ISM during the late Pleistocene and Holocene (http://www.himpac.org/). A main component of this research project are studies based on palaeoclimate proxy records—pollen, sediment properties, tree rings, and stable isotopes—from archives located in climatically sensitive regions along the Indian subcontinent (i.e. northwestern Himalaya, Meghalaya, Deccan Plateau).

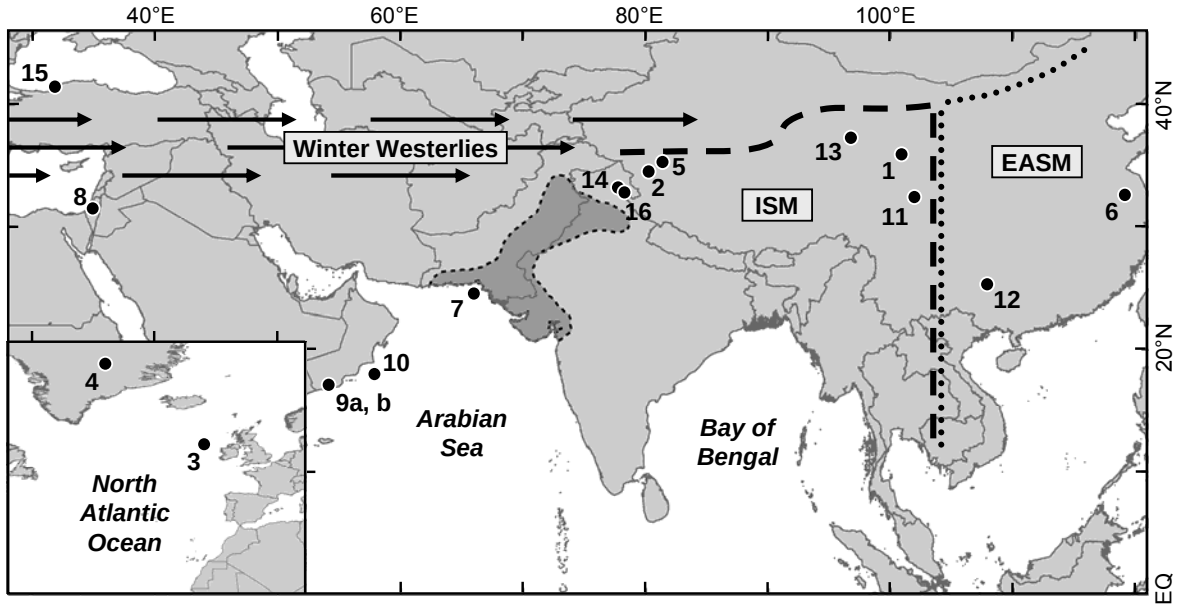

ID	Proxy	Location	Reference
1	$\delta^{18}O$ (lake ostracod valves)	Lake Qinghai (36°45'N, 100°11'E)	Lister et al., 1991
2	Pollen (lake sediment core)	Sumxi Co (34°30'N, 80°23'E)	Van Campo and Gasse, 1993
3	Hematite-stained grains (core VM 29-191) Hematite-stained grains (core MC 52)	North Atlantic (54°16'N, 16°47'W) North Atlantic (55°28'N, 14°43'W)	Bond et al., 1997, 2001 Bond et al., 1997, 2001
4	K^+ ion conc. (ice core)	Greenland (72°35'N, 38°27'W)	Mayewski et al., 1997, 2004
5	$\delta^{18}O$ (ice core)	Guliya ice cap (35°17'N, 81°29'E)	Thompson et al., 1997
6	$\delta^{18}O$ (cave stalagmite PD)	Hulu Cave (32°30'N, 119°10'E)	Wang et al., 2001
7	*G. ruber* $\delta^{18}O$ (63KA/41KL)	Arabian Sea (24°37'N, 65°59'E)	Staubwasser et al., 2002, 2003
8	$\delta^{18}O$ (cave speleothems)	Soreq Cave (31°27'N, 35°02'E)	Bar-Matthews et al., 2003
9a 9b	$\delta^{18}O$ (cave stalagmite Q5) $\delta^{18}O$ (cave stalagmite S4)	Qunf Cave (17°10'N, 54°18'E) Defore Cave (17°07'N, 54°05'E)	Fleitmann et al., 2003 Fleitmann et al., 2007
10	*G. bulloides* conc. (core 723A)	Arabian Sea (18°N, 58°E)	Gupta et al., 2003
11	$N^{13}C$ (plant cellulose)	Hongyuan peat bog (32°46'N, 102°30'E)	Hong et al., 2003
12	$\delta^{18}O$ (cave stalagmite D4)	Dongge Cave (25°17'N, 108°05'E)	Dykoski et al., 2005
13	Pollen (lake sediment core)	Hurleg Lake (37°17'N, 96°54'E)	Zhao et al., 2007
14	Pollen (lake sediment core)	Tso Kar (33°10'N, 78°E)	Demske et al., 2009
15	$\delta^{13}C$ (cave stalagmite So-1)	Sofular Cave (41°25'N, 31°57'E)	Göktürk et al., 2011
16	Pollen (lake sediment core TMD)	Tso Moriri (32°54'N, 78°19'E)	this study

Fig. 2.1 Sketch maps of southern Asia and the North Atlantic region (inset) showing the geographical location of Tso Moriri and other palaeoclimate proxy records (dots) discussed in the text (additional information on the employed proxy, location name, coordinates, and associated references are provided in the table). The main course of the winter westerly storm tracks is shown schematically, along with the spatial extent of the Indian Summer Monsoon (ISM) indicated by a dashed line, the East Asian Summer Monsoon (EASM) indicated by a dotted line, and the Harappan Civilisation settlement area (dark grey area, after Kenoyer, 2010).

Here we present a high-resolution Holocene pollen record from the alpine lake Tso Moriri—the northernmost site along the HIMPAC transect, located near Tso Kar in the northwestern Himalaya (Fig. 2.1). The Tso Kar and Tso Moriri pollen records are compared to verify whether they bear a regional environmental/climatic signal, and are further used to reconstruct regional vegetation and climate changes during the Holocene. These results are then discussed along with other published proxy records from the ISM domain and adjacent regions (Fig. 2.1). This discussion focuses on the context of timing and mechanisms of the reconstructed climatic changes, along with their possible impact on the Indus Valley Neolithic and Bronze Age cultures, primarily the Harappan Civilisation.

2.3 Study site and regional environment

2.3.1 Tso Moriri

Tso Moriri, sometimes referred to as Tso Morari, is a high-alpine lake at 4512 m a.s.l. in the Rupshu area in the south-eastern part of the Ladakh district (32°54'N, 78°19'E, Figs. 2.1 and 2.2A). The lake is in a glacial-tectonic valley bounded by mountain ranges, whose elevation reaches of >6000 m a.s.l., including the Ladakh Range north of the Indus valley and Zanskar Range in the south, in the north-western Himalaya (Negi, 2002; Hedrick et al., 2011). Tso Moriri covers an area of ca. 147 km^2 within a catchment of ca. 2263 km^2. These figures were calculated using ArcGIS v10.0 (ESRI, 2011) and applying a projected coordinate reference system (Beijing 1954/3-degree Gauss–Kruger CM 78E), based on a topographic map (Pointet, 2008, scale 1:150,000), as well as with SRTM v4.1 data (Reuter et al., 2007; Jarvis et al., 2008). The lake is fed by glacier- and snow-melt water, rainwater, and small springs originating within a catchment of about 2250 km^2. The three main perennial rivers flowing into the lake enter in its southern (Phirse Chu), northern (Kyagar Nugma), and western (Korzong Chu) parts (Fig. 2.2B). Since no outlet has been detected (Negi, 2002), Tso Moriri has been classified as a terminal lake. However, a subsurface outflow may exist, as the lake water is only weakly saline, despite the relatively dry climate.

In the global modern (1961–1990) climate dataset (New et al., 2002), the area of Tso Moriri and surrounding mountains is covered by six grid cells (total area 20' × 30') with an average elevation of 5176 m a.s.l. The key bioclimatic variables (*sensu* Prentice et al., 1992) calculated (Guiot and Goeury, 1996) for this immediate pollen source area are as follows. The mean temperature of the coldest month (MTCO) is –15.5 °C, while the mean temperature of the warmest month (MTWA) is 7.7 °C; the annual sum of mean day temperatures over 5 °C (GDD5) is 150. The ratio of actual over potential evapotranspiration (moisture index α) is 0.44. Mean annual precipitation (MAP) amounts to 248 mm,

while the mean annual temperature (MAT) is –4.0 °C. These figures reflect a harsh climate suitable for the alpine cold grass/shrub and tundra vegetation (Prentice et al., 1992).

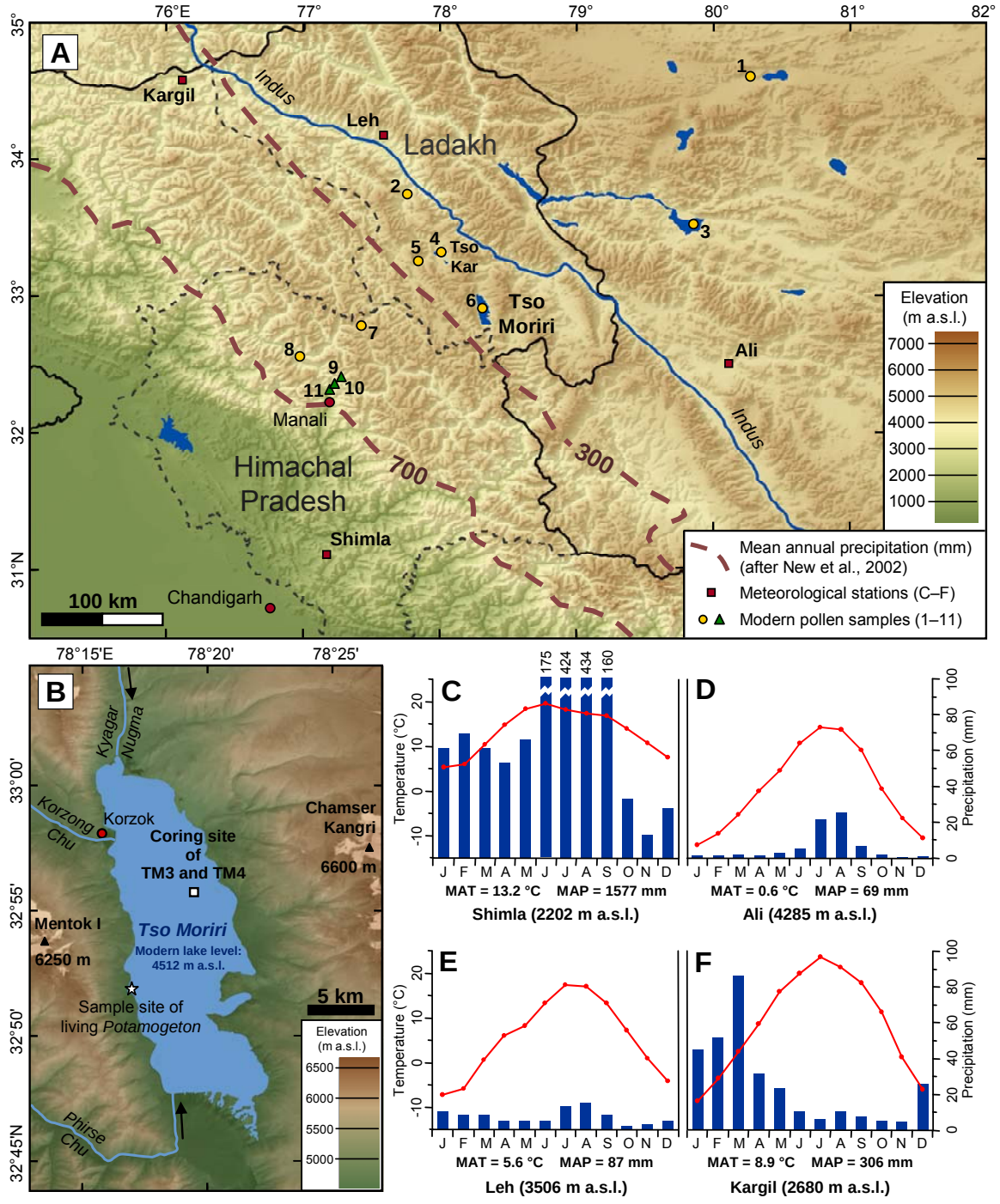

Fig. 2.2 Chart compilation indicating (A) Tso Moriri's location, the spatial distribution of the eleven modern surface pollen spectra from the study region, and positions of the 300 and 700 mm MAP isolines based on the modern climate dataset from New et al. (2002), along with (B) Tso Moriri's local environmental setting, the location site of the TM3 and TM4 cores, and living Potamogeton sample used for ^{14}C reservoir effect evaluation. Graphs C–F show selected climate diagrams of meteorological stations in (C) Shimla (after Müller et al., 1996), (D) Ali (after Chinese Central Meteorological Office, 2010), (E) Leh (after Müller et al., 1996), and (F) Kargil (after Miehe et al., 2001). The graphs also provide information on mean monthly temperature (red curves), mean annual temperature (MAT), mean monthly precipitation (blue bars), and mean annual precipitation (MAP) values.

2.3.2 Regional climate and vegetation

The Ladakh District is in a high altitude mountainous region with a cold, dry climate. Annual temperature variations are very pronounced, with minimum winter temperatures dropping to –20 and even to –40 °C and maximum summer temperatures rising up to 30 °C. The most extreme diurnal oscillations are observed in summer, when maximum daytime temperatures reach ca. 30 °C and drop to subzero during night-time (Bhattacharyya, 1989b; Philip and Mazari, 2000; Philip and Mathew, 2005; Peel et al., 2007; Le Masson and Nair, 2012). Mean temperatures in the area generally follow an altitudinal gradient. Whereas the MAT at Kargil (2680 m a.s.l.) and Leh (3506 m a.s.l.) is 8.9 °C and 5.6 °C, respectively, it only reaches –1.6 °C at 4530 m a.s.l. near Korzok village at Tso Moriri (Müller et al., 1996; Miehe et al., 2001; Reinmüller, 2010). Due to the extreme differences in elevation, the regional distribution of precipitation is strongly controlled by topography and associated rain-shadow effects. However, a general decrease in the MAP values from the south-west to the north-east direction, caused by the ISM attenuation, is well pronounced (Fig. 2.2A).

The regional hydrology is primarily governed by the ISM (Bookhagen and Burbank, 2010 and references therein), which is mainly active from June to September and may contribute up to 76–83% to the MAP sum (i.e. Figs. 2.2C and D). The area around Tso Moriri receives about 70% (ca. 175 mm) of its total annual precipitation from June to September (New et al., 2002).

A further source of precipitation in the region is westerly-associated storm tracks reaching north-western India during winter and spring (Lang and Barros, 2004). Comparison of the climate diagrams of Ali, Leh and Kargil (Figs. 2.2D–F) illustrates that westerly influence considerably decreases in a southeast direction along the high north-western Himalayan mountain ranges. Precipitation falling from October to May can comprise up to 50% of the total annual precipitation at Leh (Fig. 2.2E) in the north-western part of this region, but falls to ca. 30% around Tso Moriri (New et al., 2002). While the total MAP values are relatively small, the impact of westerly-associated precipitation on the water balance and environments of the region should not be underestimated.

The vegetation of Ladakh can mainly be characterised as steppe and desert-steppe (Hartmann, 1997, 1999; Klimeš, 2003). Woody taxa like *Juniperus* spp. and *Betula utilis* are only found in isolated river gorges. Today, *Salix* spp. and *Populus* trees are cultivated along the main river valleys and around human settlements (Fox et al., 1994; Kala and Mathur, 2002). Based on differences in floristic composition, Dvorský et al. (2011) determined eight main vegetation types in eastern Ladakh, including four common and four less common plant communities, in the area between the southern end of Tso Moriri and the north-western end of Pangong Tso (Fig. 2.2A). Among the common vegetation groups, the first is

salt marshes. The second common plant group is semi-deserts and steppes with *Artemisia*, Chenopodiaceae, *Oxytropis*, *Polygonum*, Poaceae, and *Carex* (optimum at 4500–4900 m a.s.l.). The third common plant group consists of alpine grasslands located mostly along streams represented by *Kobresia*, *Potentilla*, *Thalictrum*, and Poaceae (optimum at 4600–4900 m a.s.l.). The last common plant group comprises subnival vegetation with Poaceae, *Potentilla*, *Thylacospermum*, Caryophyllaceae, *Saussurea*, and *Draba* (optimum at 4600–5700 m a.s.l.). Among the four less common vegetation types, the first includes communities with *Halerpestes*, *Potamogeton*, Poaceae, Cyperaceae, and *Ranunculus* around freshwater bodies. A second less common plant group grows around animal resting places and is dominated by Poaceae, Chenopodiaceae, *Artemisia*, *Polygonum*, (optimum at 4600–5000 m a.s.l.). Screes and boulder fields are home to the third less common plant group with Poaceae, *Oxytropis*, *Potentilla*, *Saussurea*, *Thylacospermum caespitosum*, and *Pleurospermum stellatum* (4750–5620 m a.s.l.). Shrublands with Poaceae, *Oxytropis*, *Caragana*, *Ephedra*, *Krascheninnikovia*, *Hippophaë*, and *Myricaria* species (optimum at 4200–5000 m a.s.l.) comprise the final less common plant group and last of the eight main plant communities of the Eastern Ladakh area. The low frequency of shrublands in the area's current vegetation stems from insufficient moisture availability and damage caused by humans and their livestock (Hartmann, 1997, 1999; Murti, 2001; Klimeš, 2003; Dvorský et al., 2011).

Forests are restricted to regions of the Lesser Himalayan Ranges located south to southwest of Tso Moriri, where MAP exceeds 700 mm (Schweinfurth, 1957; New et al., 2002). The shortest linear distance between the forested regions—the Beas River valley and Sutlej River valley—and Tso Moriri is about 120 km. Schweinfurth (1957) and Singh and Singh (1987) have described the five major forest types of this area as follows. The first is low-montane needleleaf forest dominated by *Pinus roxburghii* (ca. 1000–1800 m a.s.l.) with *Olea cuspidata* as the prevailing species in the drier locations. The second is low- to mid-montane hemi-sclerophyllous broadleaf forest of *Quercus* spp. frequently mixed with conifers, such as *P. roxburghii* and *Abies spectabilis*, accompanied by broadleaved evergreen *Rhododendron*, *Lyonia*, and *Ilex*, in areas with MAP of 1000–2500 mm and MAT of 13–16 °C. The third is mid-montane needleleaf evergreen forest largely dominated by *Cedrus deodara* (1700–2500 m a.s.l.), *Abies pindrow* (2500–3000 m a.s.l. or higher), and, more seldom, *Picea smithiana* (2500–2800 m a.s.l.) and *Pinus wallichiana* (2300–3000 m a.s.l.). The fourth is mid-montane deciduous forest mostly located along streams and typically consisting of *Aesculus indica, Acer pictum, Acer caesium, Carpinus viminea, Ulmus wallichiana, Betula alnoides, Pyrus lanata, Morus, Juglans regia, Corylus colurna*, and *Fraxinus micrantha*. And the fifth is high-montane mixed forest (above ca. 3000 m a.s.l.) with *Betula utilis*, *Abies spectabilis*, *Quercus semecarpifolia*, and *Rhododendron*. Drier and

colder areas at 3500–4900 m a.s.l. are marked by steppe-like vegetation with *Caragana*, *Artemisia*, and *Juniperus* growths, including *Juniperus indica* and *Juniperus communis*.

2.4 Material and methods

2.4.1 Drill core recovery and sediment record

In summer 2011, two parallel sediment cores (TM3 and TM4), with a diameter of 90 mm, were recovered at a spot (32°55'46"N, 78°19'24"E) close to the centre of Tso Moriri (Fig. 2.2B). The coring site was selected on the basis of bathymetric information (unpublished data), which uncovered a characteristic glacier influenced U-shaped lake bottom structure. The eastern slope in the northern Tso Moriri basin appears to be less steep than its western slope. The coring site was considered to be less exposed to potential land-slides, slope movement driven by seismic activity, and seasonal fluvial inflows, making it therefore most suitable for coring. Coring was accomplished using a UWITEC piston corer developed by R. Niederreiter at a water depth of 105 m. Correlation of distinct marker layers in the parallel cores TM3 and TM4 made it possible to build up a continuous composite sediment record (briefly referred to as TMD) with a total length of 724 cm. Based on the visual description of the sediment (detailed results of the quantitative sediment analysis will be published in a separate paper), the upper 312 cm part of the TMD composite core discussed in the current study mainly consists of light to dark grey calcareous clay and partly laminated silty clay (Fig. 2.6A). The record does not exhibit any visible disturbances, hiatuses, or turbidite layers, and thus represents continuous sedimentation.

2.4.2 Chronology

Six samples from the analysed part of the TMD core were submitted to the Poznan Radiocarbon Laboratory for AMS age determination. The set consists of five bulk sediment samples and one sample of the macroscopic remains of *Potamogeton* leafs. Dating on the total organic carbon (TOC) of the sample representing the topmost part of the core yielded a ^{14}C age of 3800 ± 35 a BP (Table 3.1). By contrast, a much younger radiocarbon age of 365 ± 30 a BP was determined for the contemporary *Potamogeton* leaf sample collected from Tso Moriri's western littoral region (Fig. 2.2B, Table 2.1). These ages were regarded as representing the constant reservoir effect in the AMS dates obtained on the TOC (i.e. ca. 3800 years) and *Potamogeton* leaf (i.e. ca. 365 years) fossil samples, respectively (see Hou et al., 2012 for discussion). Accordingly, all ^{14}C age determinations (Table 2.1) were first corrected for the reservoir effect and subsequently converted to the calendar ages using the

computer software CalPal-2007 (Weninger and Jöris, 2008; Weninger et al., 2013), along with the online version of the CalPal radiocarbon calibration program (Danzeglocke et al., 2013) based on the CalPal-2007-Hulu calibration curve. The resulting ages, as illustrated in Table 3.1 and in Fig. 2.3, demonstrate some reversals in the middle part of the analysed section (i.e. at 125 and 183.5 cm depth). A similar problem, which raises difficulties for reliable age–depth models, has been recognised in various lakes on the Tibetan Plateau and adjacent regions (Hou et al., 2012 and references therein). This problem may be caused by temporal changes in reservoir age and/or contamination of the bulk samples with reworked organic material.

Due to the observed uncertainties in ^{14}C age determination, we additionally constrained the TMD core chronology by using pollen-based correlation with the radiocarbon-dated Tso Kar record (Demske et al., 2009). The two records are located in very similar climatic environments, i.e. ca. 40 km apart from each other (Fig. 2.2A), and feature highly comparable changes in their pollen assemblages. In the current study, the pollen percentage ratio of *Artemisia* to Chenopodiaceae (A/C) from Tso Kar (Fig. 2.3A) and from the TMD core of Tso Moriri (Fig. 2.3B) is chosen for the pollen-based correlation of the two records. This ratio has been used to reconstruct variations of effective moisture (Demske et al., 2009; Wünnemann et al., 2010) and should represent a regional, rather than local, climatic signal.

Sample ID	ID in Fig. 2.3	Lab. ID	Composite depth (cm, mid point)	Dated material	Radiocarbon date (^{14}C BP)	reservoir effect correction(yr)	Corrected and calibrated age, yr BP (95% conf. interval)
TMD (32°55'46"N, 78°19'24"E)							
TMD 1 (0-1)	a	Poz-48104	0.5	Bulk TOC	3800 ± 35	–3800	Modern
TMD 1 (47.5-47.8)	b	Poz-48105	47.7	Bulk TOC	5050 ± 40	–3800	1200 ± 120
TM 1 (124-126)	c	Poz-45172	125.0	Bulk TOC	9200 ± 50	–3800	6190 ± 160
TMD 3 (30.5)	d	Poz-48133	165.5	*Potamogeton* leaf fragments	4920 ± 35	–365	5200 ± 200
TMD 3 (48-49)	e	Poz-48114	183.5	Bulk TOC	10780 ± 100	–3800	7820 ± 200
TMD 4 (34-34.3)	f	Poz-48134	185.5	Bulk TOC	10080 ± 60	–3800	7190 ± 160
TMD 5 (76-76.3)	g	Poz-48136	276.0	Bulk TOC	14270 ± 80	–3800	12400 ± 360
Nearshore location (32°51'50"N, 78°16'54"E)							
BP10 TM-G-PL-10	–	Poz-48102	–	*Potamogeton* leaf fragments	365 ± 30	–365	Modern

Table 2.1 Radiocarbon dates for samples from the Tso Moriri composite core TMD and one modern sample collected from a nearshore location. All samples were AMS-dated at the Poznan Radiocarbon Laboratory (Poland). Calibrations were performed using CALPAL-2007 (Weninger et al., 2013; Weninger and Jöris, 2008).

The correlation of the Tso Kar and Tso Moriri records is based on the 16 most prominent levels (tie points) identified by visual comparison. The calendar ages assigned to these selected levels in the Tso Kar record were transferred to the corresponding Tso Moriri tie points and utilised for building the TMD chronology outlined in Fig. 2.3C. The age model for the TMD record described here is represented by a second-order polynomial regression. The comparison of the two A/C records shows a reasonably strong correlation ($r^2 = 0.75$). This compatibility (i) suggests that both records archive a regional signal of vegetation/climate change and (ii) enables us to conclude that the upper 312 cm of the analysed TMD core covers the entire Holocene interval between ca. 12 cal ka BP and the present.

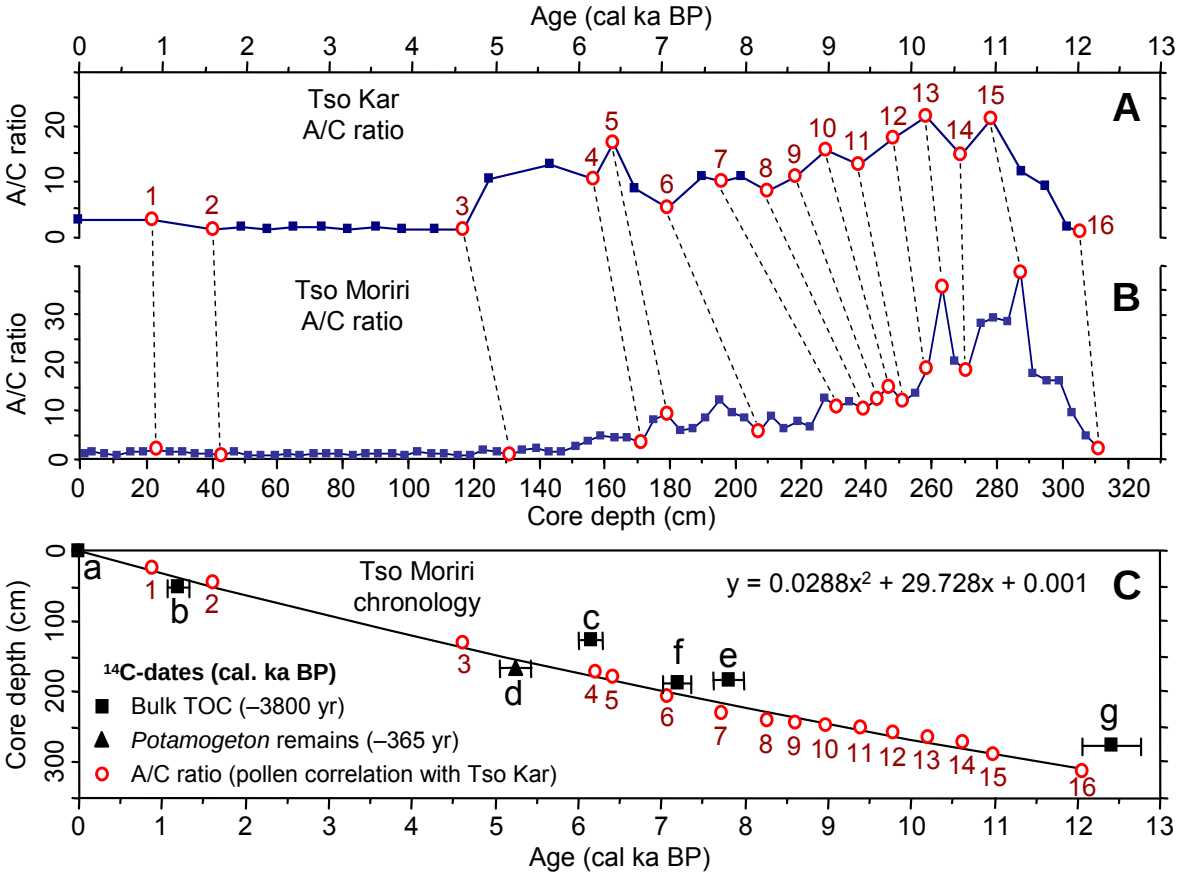

Fig. 2.3 The A/C ratio curves from (A) Tso Kar (TK 106, TK 223, after Demske et al., 2009) and from (B) Tso Moriri (TMD, this study), along with the 16 most prominent levels (open circles), which helped to correlate the two pollen records and construct (C) the age–depth model (black line and equation) for the Tso Moriri composite TMD core. The bottom graph also indicates positions and 95% confidence intervals of the seven calibrated radiocarbon dates (a–g) corrected for the reservoir effect (see Table 3.1 for further details).

2.4.3 Pollen analysis

In this study, we focus on the analysis of terrestrial pollen from the uppermost 312 cm unit of the Tso Moriri composite TMD core, which accumulated during the last ca. 12 cal ka. For palynological analysis, a 2 cm thick sediment layer (volume of 2.3 cm^3) was sampled with a 4 cm step from the TMD core sequence by applying the double-L-channel subsampling method (Nakagawa, 2007). A total of 79 fossil samples were analysed. To allow for a more accurate interpretation of the fossil pollen data, a set of 166 modern surface pollen samples was collected from the wider study region (Fig. 2.2A) in 2009–2012. In the current study, we first analysed seven representative samples from this reference dataset, which are distributed along a transect crossing the north-western Himalaya.

Palynomorphs were extracted from each fossil and modern sample in the pollen laboratory of the Freie Universität Berlin (FU Berlin) following standard procedures, including HF treatment and acetolysis (Fægri and Iversen, 1989). To calculate the total terrestrial pollen concentration, each sample was spiked with one tablet of modern *Lycopodium* spores prior to chemical treatment (Stockmarr, 1971). In each sample, a minimum number of 400 pollen and spores were counted with the aid of compound light microscopy at magnifications of ×400 and ×600. We used several palynomorphological keys (Punt and Malotaux, 1984; Gupta and Sharma, 1986; Moore et al., 1991; Wang and Feng, 1994; Wang et al., 1997; Beug, 2004; Fujiki et al., 2005) to determine the pollen and spores of ferns and fern allies. Arboreal pollen types belonging to the Rosaceae family, including the *Sorbus*, *Cotoneaster*, *Prunus*, *Rosa*, and *Spiraea* types, were summarised as Rosaceae (arboreal).

For all surface and fossil pollen spectra, the relative abundance of each taxon was calculated based on the sum of all terrestrial pollen excluding indeterminable pollen grains. For spores, percentages were calculated using the total terrestrial pollen sum, plus the sum of spores. Based on these percentage values, total sums of arboreal pollen (AP) and non-arboreal pollen (NAP) taxa were calculated for each sample. The Tilia/TiliaGraph/TGView software set (Grimm, 1993, 2004) was employed to statistically calculate the pollen percentages and construct pollen assemblage diagrams (Figs. 2.4 and 2.6).

Local pollen zones (LPZ) were derived from visual examination supported by stratigraphically constrained cluster analysis using CONISS (Grimm, 1987) integrated in the Tilia package.

2.4.4 Biome reconstruction

To objectively evaluate changes in the major regional natural vegetation types, which are primarily driven by regional climate changes (Prentice et al., 1992), we employed the

biome reconstruction method first presented in Prentice et al. (1996). This quantitative approach makes it possible to reconstruct major vegetation types (i.e. biomes) on a regional to global scale using pollen data. It was successfully tested in various regions of Eurasia, including areas influenced by the EASM and the ISM in China (e.g. Yu et al., 1998; Herzschuh et al., 2004) and Japan (e.g. Takahara et al., 2000; Gotanda et al., 2002; Leipe et al., 2013). However, we are not aware of publications applying the biome reconstruction method to fossil pollen data from the Indian Peninsula.

Following a standard methodology (see Prentice et al., 1996 for details), all terrestrial pollen taxa identified in the analysed samples were assigned to one or several regional biomes following knowledge of the modern geographical plant distribution and bioclimatic tolerance. The resulting biome-taxa matrix shows the taxa which may occur in each biome (Table 3.2). The biome with the highest affinity score, or the one defined by a smaller number of PFTs (in case several biome scores are equal), is considered as the dominant biome and assigned to the given pollen spectrum. To provide a basis for the regional biome-taxa matrix (Table 3.2), as applied to the TMD pollen record, we adopted previously published biome-taxa matrixes representing characteristic vegetation types of the Inner Asia region (Tarasov et al., 1998; Yu et al., 1998; Herzschuh et al., 2004). Biome score calculations were made using PPPBase software (Guiot and Goeury, 1996).

2.4.5 Moisture availability reconstruction

The ratio of arboreal to non-arboreal pollen percentage (AP/NAP) is frequently applied to discuss changes in forest distribution and regional moisture availability (Favre et al., 2008 and references therein). However, in the steppe, desert, and tundra regions with harsh climate and relatively low pollen productivity (i.e. decreased pollen concentration), this ratio appears to be an inappropriate measure for moisture availability (Tarasov et al., 1998), even though it is useful tool for evaluating the contribution of far-distant transported tree pollen to the local pollen assemblages (Birks, 1973; Van Campo and Gasse, 1993; Herzschuh et al., 2004). Pollen studies done on the north-western Himalaya (Bhattacharyya, 1989a; Demske et al., 2009) and north-western Tibet (Cour et al., 1999) show that variations in the long-distant transported AP percentages, together with pollen concentration data, can be used to evaluate pollen productivity of the local plants and ISM intensity and westerly disturbances during the Holocene period.

Demske et al. (2009) demonstrated the usefulness of the pollen percentage ratio of *Artemisia* to Chenopodiaceae (A/C) for reconstructing qualitative centennial to millennial changes in the moisture availability in the Tso Kar area during the late glacial and Holocene. As suggested by El-Moslimany (1990), the approach assumes that *Artemisia*, as

Biome name/ Abbreviation	Pollen taxa assigned
Tundra/TUND	*Aconogonon*, *Alnus fruticosa* type, *Betula* undiff., Cyperaceae, *Knorringia* type, Poaceae undiff., *Polygonum*, *Primula* type, *Salix*, *Saxifraga cernua* type, *Saxifraga granulata/hirculus* type, *Scrophularia* type
Steppe/STEP	*Aconogonon*, *Allium* type, *Anthemis* type, *Artemisia*, *Aster/Gnaphalium* type, Asteraceae subfam. Cichorioideae undiff., Brassicaceae, *Caltha/Isopyrum* type, *Cannabis* type, Caryophyllaceae undiff., Chenopodiaceae/*Amaranthus*, *Galium* type, *Geum/Potentilla* type, *Hippophaë*, *Knorringia* type, *Mentha/Elsholtzia* type, *Papaver* type, Poaceae undiff., *Polygonum*, *Potentilla/Chamaerhodos* type, *Ranunculus* type, *Rosa* type, Rosaceae undiff., *Scrophularia* type, *Sedum* type, *Spergularia* type, *Spiraea* type, *Thalictrum*, *Veronica* type
Cold deciduous forest/CLDE	*Alnus* undiff., *Betula* undiff., *Betula* utilis type, *Juniperus* type, *Pinus* Diploxylon type, *Pinus* Haploxylon type, *Pinus sylvestris* type, *Pinus* undiff., *Primula* type, *Salix*
Taiga/TAIG	*Abies*, *Alnus* undiff., *Betula* undiff., *Betula utilis* type, *Juniperus* type, *Picea*, *Pinus* Diploxylon type, *Pinus* Haploxylon type, *Pinus sylvestris* type, *Pinus* undiff., *Primula* type, Rosaceae undiff., *Salix*, *Sorbus/Cotoneaster* type
Cold mixed forest/CLMX	*Alnus* undiff., *Betula* undiff., *Betula utilis* type, *Cedrus*, *Corylus*, *Juniperus* type, *Pinus* Diploxylon type, *Pinus sylvestris* type, *Pinus* undiff., *Primula* type, Rosaceae undiff., *Salix*, *Sorbus/Cotoneaster* type
Cool conifer forest/COCO	*Abies*, *Alnus* undiff., *Betula* undiff., *Betula utilis* type, *Carpinus* undiff., *Carpinus viminea* type, *Corylus*, *Juniperus* type, *Picea*, *Pinus* Diploxylon type, *Pinus* Haploxylon type, *Pinus sylvestris* type, *Pinus* undiff., *Primula* type, Rosaceae undiff., *Salix*, *Sorbus*/*Cotoneaster* type
Cool mixed forest/COMX	*Abies*, *Alnus* undiff., *Betula* undiff., *Betula utilis* type, *Carpinus* undiff., *Carpinus viminea* type, *Corylus*, *Juniperus* type, *Picea*, *Pinus* Diploxylon type, *Pinus* Haploxylon type, *Pinus sylvestris* type, *Pinus* undiff., *Primula* type, *Quercus* undiff., Rosaceae undiff., *Salix*, *Sorbus*/*Cotoneaster* type
Temperate deciduous forest/TEDE	*Alnus* undiff., *Betula* undiff., *Betula utilis* type, *Carpinus* undiff., *Carpinus viminea* type, *Cedrus*, *Corylus*, *Juglans*, *Juniperus* type, *Morus*, *Pinus* Diploxylon type, *Pinus sylvestris* type, *Pinus* undiff., *Primula* type, *Quercus* undiff., Rosaceae undiff., *Salix*, *Sorbus*/*Cotoneaster* type
Warm mixed forest/WAMX	*Alnus* undiff., *Betula* undiff., *Betula utilis* type, *Carpinus* undiff., *Carpinus viminea* type, *Corylus*, *Juglans*, *Juniperus* type, *Morus*, *Pinus* Diploxylon type, *Pinus sylvestris* type, *Pinus* undiff., *Primula* type, *Quercus* undiff., Rosaceae undiff., *Salix*, *Sorbus*/*Cotoneaster* type
Desert/DESE	*Aconogonon*, Chenopodiaceae/*Amaranthus*, *Ephedra distachya* type, *Ephedra fragilis* type, *Knorringia* type, *Myricaria* type, *Polygonum*

Table 2.2 Biome-taxa matrix based on previous publications (Tarasov et al., 1998; Yu et al., 1998; Herzschuh et al., 2004) and used in the calculation of biome affinity scores. The matrix includes all taxa presented in the 79 fossil pollen spectra from the analysed TMD core from Tso Moriri which exceed the universal threshold of 0.5% as suggested by Prentice et al. (1996). The affinity score for each potential biome is calculated by summation of the square roots of all attributed pollen taxa percentages. The biome with the highest affinity score or the one defined by a smaller number of PFTs (when scores of several biomes are equal) is treated as the dominant biome.

characteristic of steppe environments, requires higher effective moisture compared to Chenopodiaceae, which is typically found in desert environments. Thus higher *Artemisia* percentages in the pollen spectra (and higher A/C values) in arid and semi-arid environ-

ments are linked to increased moisture availability. Numerous studies have shown that in the arid regions of Inner Asia, the A/C ratio is a reliable qualitative to semi-quantitative measure for inferring soil/atmospheric moisture availability and distinguishing between steppe and desert vegetation communities (e.g. El-Moslimany, 1990; Van Campo et al., 1996; Cour et al., 1999; Demske and Mischke, 2003; Zhao and Herzschuh, 2009).

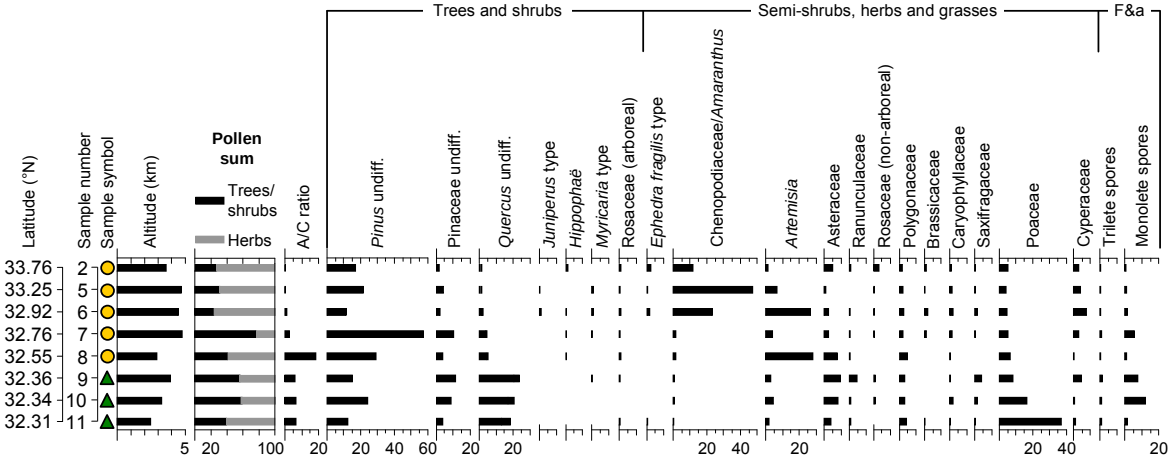

Fig. 2.4 Simplified percentage pollen diagram showing eight modern surface pollen spectra (analysed in this study) arranged by latitude and providing altitudinal information and sample numbers and symbols used in Figs. 2.2A and 2.5. The pollen percentages of each taxon are calculated using the total sum of all arboreal and non-arboreal pollen taxa. Fern and fern allies' (F & a) spore percentages were calculated using the total sum of all terrestrial pollen taxa and spores.

The above research has demonstrated the positive correlation between the A/C ratio and measured humidity or precipitation records. Zhao et al. (2008) presented a near-annual resolution pollen record from a lake in the north-eastern Qaidam Basin and compared the A/C ratio over a 50 year interval to the relative humidity record from a nearby meteorological station. They reported that the A/C ratio is very sensitive to changes in effective moisture and corresponds well to the instrumental data. Two other studies based on modern pollen and climate data from the Tibetan Plateau (Herzschuh, 2007) and Alashan Plateau/Qilian Mountains region (Herzschuh et al., 2004) revealed a relatively weak correlation between the A/C and the instrumentally measured MAP values ($r^2 = 0.25$ and $r^2 = 0.39$, respectively). However, these studies also showed that the A/C ratio can serve as a good qualitative indicator of the past vegetation and moisture conditions. More recently, Zhao et al. (2012) demonstrated that in the arid and semi-arid environments of China, the correlation between A/C and MAP values may be enhanced by applying non-linear regression models. But they also denoted considerable disturbances, which are mainly due to a strong human impact, in their study areas affecting the A/C ratio.

In the current study, we tested the A/C ratio approach using available modern surface pollen data. In the set of eleven samples, seven represent moss polsters and surface sediment samples analysed in this study (Fig. 2.4), while the other four represent lake

sediment core top samples. The lake sentiment core top samples include the TMD pollen record (this study), TK 223 pollen record from Tso Kar (Demske et al., 2009), and pollen profiles from Sumxi Co (Van Campo and Gasse, 1993) and Bangong Co (Van Campo et al., 1996). The two latter A/C ratio values were digitised from figures provided in Van Campo and Gasse (1993) and Van Campo et al. (1996). Details on all eleven modern surface samples are included in the supplementary material associated with this article. The samples are roughly distributed along a northeast–southwest transect (Fig. 2.2A), following the ISM-derived precipitation gradient across the north-western Himalaya and parts of the western Tibetan Plateau (see Figs. 2.2A and C–F). The samples come from sites characterised by a low degree of human disturbance, so the A/C values likely reflect the natural composition of vegetation controlled by the regional climate. Modern MAP was derived from a gridded (10' × 10') global dataset of surface climate averaged over a thirty-year (1961–1990) interval (New et al., 2002). For each surface sample (and associated A/C ratio), we adopted the estimated MAP value of the corresponding grid cell. The relation between the modern A/C and MAP values shown in Fig. 2.5 is well described by the exponential regression function explaining ca. 71% of the variation. The samples 9–11 from forest-dominated sites reveal lower A/C ratios compared to the sample originating from the wettest steppe site (8 in Fig. 2.5). Previous studies (e.g. El-Moslimany, 1990; Zhao and Herzschuh, 2009; Zhao et al., 2012) have also highlighted that A/C ratios from relatively moist environments, like forests and meadows, show lower values compared to steppes. Because the TMD and Tso Kar pollen records indicate a predominance of the treeless vegetation around the study lakes during the Holocene interval, the data from the forest site samples was not considered in the transfer function (Fig. 2.5) applied to the fossil A/C pollen ratio from Tso Moriri (Fig. 2.3B). The transfer function applied in the current paper is an attempt to quantify past changes in the study region's MAP using pollen data. Completing the pollen analysis of the remaining surface samples collected in the region will allow for further statistical tests of the A/C approach, as well as the application of other reconstruction methods (i.e. modern analogue technique), which requires a more representative and spatially extended reference pollen dataset.

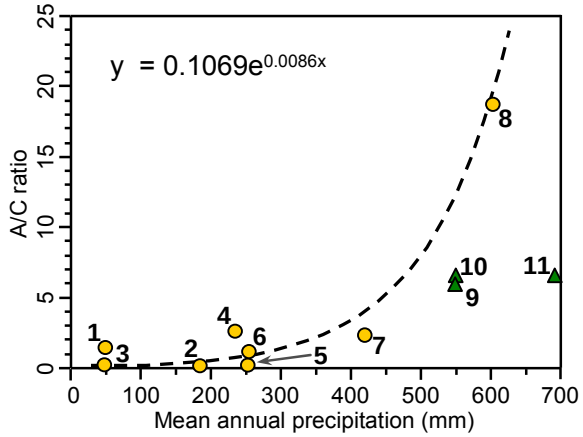

Fig. 2.5 Relationship between the A/C ratio and mean annual precipitation derived from the dataset from New et al. (2002) for eleven modern pollen spectra (see Fig. 2.2A for spatial distribution) from the study region. Samples 9–11 (triangles) from forested locations demonstrating substantially lower A/C ratios were not considered in the regression model (dashed line and equation).

2.5 Results and interpretation

2.5.1 Fossil pollen record and biome reconstruction

We identified 141 terrestrial pollen taxa and differentiated two morphological groups of spores in the analysed fossil spectra from the TMD core. The majority of the taxa are generally represented by only small frequencies. The assemblage diagram shows relative percentage values for selected major pollen types and monolete and trilete spores (Fig. 2.6B). The major pollen types were arranged into two groups: (i) trees and shrubs (i.e. AP) and (ii) semi-shrubs (i.e. *Ephedra* and Chenopodiaceae), herbs and grasses (i.e. NAP). A complete dataset is provided in the supplementary material published online. Figure 2.6 also provides records of pollen concentration (Fig. 2.6C), AP/NAP (Fig. 2.6D) and A/C (Fig. 2.6E) ratios, and the dominant biome scores (Fig. 2.6F), which are used in the qualitative interpretation of the pollen record. The pollen record is subdivided into five main local pollen zones (LPZ TMD-1 to TMD-5) by means of visual inspection and statistical cluster analysis (Fig. 2.6G). The LPZ TMD-1 indicates the top of the core, thus allowing a consequent numbering through the not yet analysed glacial part of the TMD pollen record.

All analysed spectra are clearly dominated by NAP, namely *Artemisia*, Chenopodiaceae, Cyperaceae, and Poaceae, which are the most characteristic elements of the alpine environments. While frequencies of *Artemisia*, Chenopodiaceae, and Cyperaceae show considerable changes, Poaceae frequencies remain more or less constant. The amounts of AP throughout the record are relatively stable and do not exceed ca. 20%. The AP sum is mainly comprised of wind transported pollen of *Pinus*. Pollen percentages of other trees and shrubs appear in small quantities. The most prominent changes in the fossil pollen spectra and the results of biome reconstruction and their interpretation are presented in the following paragraphs organised by LPZs.

LPZ TMD-5 (312–285 cm; ca. 12–10.8 cal ka BP) exhibits a rapid increase in *Artemisia* pollen abundances (from ca. 40 to 64%) accompanied by a decrease in Chenopodiaceae (from ca. 18 to 1%). Percentages of Cyperaceae pollen remain stable (between ca. 10 and 13%) before they start to increase, albeit in a somewhat delayed manner, from the rise in *Artemisia*, at about 11 cal ka BP, towards the top of the zone. Desert-associated *Ephedra fragilis*-type features declining abundance from ca. 4 to 2%, suggesting a decreasing aridity trend during this time. Decreases in *Pinus* and Pinaceae pollen percentages, together with a simultaneous rapid increase in total pollen concentrations from ca. 6500 to ca. 10,000 grains/cm^3, likely indicate increase in pollen productivity and/or local vegetation cover density. This interpretation is further supported by a major increase in A/C values, from ca. 2 at the bottom to 39 at the top of this zone. The increase in A/C values is

strongest in the entire record and indicates a trend towards the spread of *Artemisia*-dominated communities and substantially wetter regional climate. The low AP/NAP values, together with the lowest pollen concentrations revealed at the bottom of LPZ TMD-5, likely reflect a very limited presence of trees in the whole region by the end of the Younger Dryas stadial. At the beginning of the Holocene, interglacial climate amelioration significantly improved growth conditions of the herbaceous plant communities around Tso Moriri, as reflected by the changes in the pollen assemblages and in the pollen concentration values. The biome reconstruction demonstrates that steppe is a dominant vegetation type, and scores for desert decrease in favour of tundra, thus suggesting a transition from relatively dry to substantially wetter environments.

LPZ TMD-4 (285–193 cm; ca. 10.8–6.8 cal ka BP) is characterised by the lowest Chenopodiaceae (ca. 1–3%) percentages in the whole pollen record. *Artemisia* abundance decreases from ca. 40% at the bottom of the pollen zone to ca. 30% near its top. The increase in *Thalictrum*, Polygonaceae, and Caryophylaceae percentages is accompanied by decreasing percentages of Cyperaceae. The growing frequencies of *Betula*, *Hippophaë*, *Salix*, *Myricaria*, and arboreal Rosaceae pollen reflect the establishment of stream-side associated shrubby/woody vegetation communities. The gradual increase in *Pinus* percentages is paralleled by the slight decline in the pollen concentrations, which explains growing contribution of wind-transported AP taxa to the local pollen assemblages. The highest pollen concentrations are recorded in the lower part of TMD-4 (up to 14,000 grains/cm^3), suggesting favourable growing conditions around Tso Moriri during the early Holocene. This conclusion is supported by the highest A/C ratios, which are registered between ca. 11 and 9.5 cal ka BP. Afterwards A/C values show a moderate decrease towards the top of this zone. The biome scores for tundra continue to increase and reach almost the same level as steppe at ca. 9.6 cal ka BP, marking the maximum extension of meadow communities in the Tso Moriri region. The numerical score of desert remains lowest in the whole record, suggesting that the Tso Moriri region experienced the wettest Holocene climate during this time interval. The reduced pollen contribution of local plants towards the middle Holocene may explain the moderate decrease in pollen concentrations, accompanied by the relative increase in wind transported arboreal pollen, as indicated by the increase in AP/NAP values from 0.12 to about 0.3.

LPZ TMD-3 (193–133 cm; ca. 6.8–4.5 cal ka BP) reveals a continuous increase in Chenopodiaceae, accompanied by decreasing percentages of *Artemisia* and Cyperaceae. Though percentages of wind transported *Pinus* remain stable, percentages of riparian woody taxa, including *Betula*, *Hippophaë*, *Salix*, and *Myricaria*, as well as arboreal Rosaceae, decline. At the same time, *Ephedra* percentages show a moderate increase, from 0.4 to ca. 4%, while the overall pollen concentration becomes lower compared to LPZ TMD-4. A remarkable feature in the TMD-3 pollen spectra is the highest taxa diversity—or highest

average of the number of identified pollen taxa in all samples—of the entire record. This might indicate a transitional phase in the regional vegetation development. Despite a short phase of climate amelioration, suggested by an increase in A/C ratios at around 6.2 cal ka BP, the changes in the pollen spectra, along with reduced local pollen production, indicate a further reduction of moisture availability in the study region. This is in line with increasing scores of desert and decreasing scores of tundra revealed in the biome reconstruction.

LPZ TMD-2 (133–37 cm; ca. 4.5–1.1 cal ka BP) is generally characterised by considerably high percentages of Chenopodiaceae (27–42%). Cyperaceae continues to slowly decrease during this interval. The average abundance of E. fragilis remains comparatively high (>2%). On the other hand, regional shrubby taxa (i.e. Juniperus type, Hippophaë, Salix, Myricaria) reveal decreasing percentages and are frequently absent in the pollen spectra. The more frequent presence of Cannabis type pollen grains is registered from ca. 3.5 cal ka BP, while Urtica also appears more frequently in the pollen spectra after ca. 1.7 cal ka BP. These taxa may indicate human presence (e.g. Demske et al., 2009), though both may naturally grow in the study region. Pollen spectra composition, lowest pollen concentrations, very low A/C values, ranging between 0.7 and 1.7, and the highest desert biome scores together suggest that this period constituted the driest time interval of the entire record. In particular, short-term intervals of increased aridity are indicated by several distinct peaks in Chenopodiaceae percentages, accompanied by relatively low contribution of Artemisia, at about 4.4, 3.2, 2.7, and 1.3 cal ka BP.

LPZ TMD-1 (37–0 cm; ca. 1.1–0 cal ka BP) is characterised by the almost complete disappearance of Hippophaë, Salix, and Myricaria. In the lower half of the pollen zone, Chenopodiaceae is moderately decreasing, while Artemisia slightly increases in abundance, reflecting a short climate amelioration interval between ca. 1.1 and 0.5 cal ka BP. The A/C ratios show a peak value of 1.9 at around 0.7 cal ka BP, a decline to 0.9 at ca. 0.3 cal ka BP, and subsequent moderate increase towards the core top. Similarly, biome scores for desert generally decrease from the base of the pollen zone to ca. 0.5 cal ka BP, but subsequently increase again afterwards.

The results of the pollen analysis and pollen-based biome reconstruction applied to the TMD record suggest that alpine steppe (cool grass/shrub biome sensu Prentice et al., 1992) was a dominant vegetation type in the Tso Moriri region through the entire Holocene, though the scores of alpine tundra and desert remained relatively high, confirming local presence of both vegetation types. These results are in line with Hartmann (1997, 1999) and Klimeš (2003), who defined the modern vegetation in the study area as desert-steppe. The pollen-based biome reconstruction approach does not allow for the reconstruction of intermediate vegetation types, i.e. desert-steppe, tundra-steppe, and the

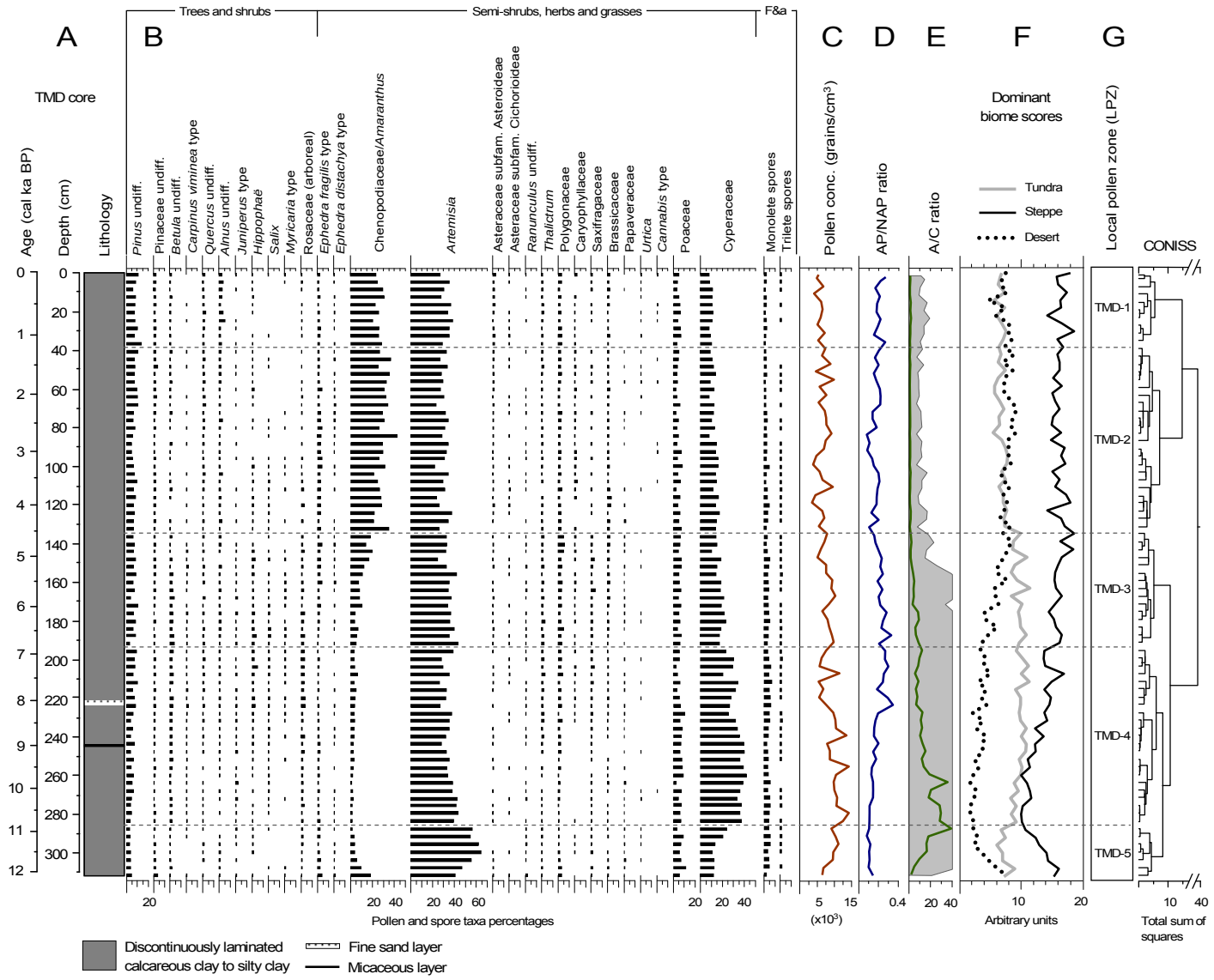

Fig. 2.6 Overview chart illustrating (A) the simplified lithology of the analysed Holocene part of the TMD record from Tso Moriri plotted along the depth and age scale; (B) the simplified assemblage diagram of terrestrial pollen taxa and spores of ferns and fern allies (F & a) from 79 fossil pollen spectra; (C) the pollen concentrations as an indicator of the local pollen production; (D) the AP/NAP ratio used to interpret the contribution of the far-distant pollen transport; (E) the A/C ratio as an index of moisture availability (shaded area shows 10-times exaggeration); (F) the dominant biome scores used for the qualitative evaluation of vegetation and climate changes in the study area and indicating contribution of desert, tundra, and steppe communities to the alpine vegetation around Tso Moriri; and (G) the local pollen zones (LPZ).

like (Prentice et al., 1996).Nevertheless, the analysis of the broader spectrum of biome scores (i.e. Fig. 2.6F)—not just those of the dominant biome—helps to partly overcome this methodological constraint.

2.5.2 Quantitative climate reconstruction

The positive results of the test with the modern surface pollen and climate data from the study region encouraged us to apply the obtained transfer function (Fig. 2.5) to the fossil A/C record from the TMD core (Fig. 2.7A) for reconstructing regional changes in MAP since ca. 12 cal ka BP.

The reconstruction results are shown in Fig. 2.7B. For the topmost sample, the reconstructed MAP of 276 mm strongly reflects the modern value of ca. 250 mm (New et al., 2002). During the covered time interval, the reconstructed MAP in the Tso Moriri region ranged from 215 mm at 2.1 cal ka BP to 685 mm at 10.9 cal ka BP. This suggests that the 700 mm isoline of MAP (Fig. 2.2A), which limits modern forest distribution in the northwestern Himalaya (Schweinfurth, 1957), was situated much closer to the study site between ca. 11 and 9.6 cal ka BP than it is today. Though pollen data indicate the higher occurrence of trees in the study area during the first half of the Holocene (Fig. 2.6D), the AP percentages are not high enough to assume that the altitudinal forest belt expanded to the Tso Moriri area. However, the results do not contradict each other, as the upper forest limit there is primarily controlled by the low summer temperatures and low GDD5 values (Prentice et al., 1992), rather than being exclusively determined by MAP, as indicated by the modern climate data (New et al., 2002).

In line with the pollen record and the biome reconstruction results (Fig. 2.6), the increase in precipitation promoted the local spread of arboreal vegetation at lower altitudes, but mainly favoured the spread of alpine steppe (i.e. cool grass/shrub biome) and meadow (i.e. tundra biome) communities in the Tso Moriri region between ca. 11 and 9.6 cal ka BP. Since that time, the reconstructed MAP decreased gradually until about 5.4 cal ka BP. It then declined more rapidly until ca. 4.4 cal ka BP. Subsequently, a dry period, with reconstructed MAP values generally below 300 mm, persisted until ca. 1.3 cal ka BP, followed by a slight increase (≥ 300 mm) during the last millennium (ca. 1–0.4 cal ka BP). After that, MAP depleted towards the present. This millennial-scale general trend was complicated by shorter-term century-scale oscillations, including phases of pronounced aridity at ca. 4.4, 3.2, 2.7, 2.1, and 1.3 cal ka BP with precipitation of around 220 mm/a.

2.6 Discussion

The Holocene pollen record from Tso Moriri allows for the qualitative and quantitative reconstruction of millennial- to centennial-scale changes in vegetation and climate around this high-alpine lake. The good match between the A/C records from Tso Moriri and Tso Kar (situated ca. 40 km to the north-west) show that the reconstructed environmental changes mirror a regional climatic signal, mainly the ISM Holocene activity. In the following discussion, the results from Tso Moriri are reviewed, along with other published proxy records from the ISM domain and adjacent regions (Fig. 2.1). This review has the following four focal points. The first is the timing and magnitude of the ISM strengthening in the early Holocene. The second is the attenuation of the ISM during the Holocene. The third is the occurrence of century-scale oscillations in the Tso Moriri record of precipitation and their possible background mechanisms. And the fourth is the reconstructed climatic changes and their possible impact on the Indus Valley Neolithic and Bronze Age cultures, primarily on the Harappan Civilisation.

2.6.1 The early Holocene strengthening of the ISM: A spatio-temporal comparison

Both qualitative and quantitative interpretation of the Tso Moriri pollen record (Figs. 2.6 and 2.7B) suggests a rapid increase in moisture availability and MAP, from very low values by the end of the Younger Dryas ca. 12 cal ka BP to a maximum value ca. 10.9 cal ka BP. The interval between ca. 11 and 9.6 cal ka BP can be regarded as the wettest interval of the entire Holocene, as reflected by the highest A/C ratio (Fig. 2.7A) and reconstructed MAP values (Fig. 2.7B), accompanied by the highest pollen concentrations (Fig. 2.6C) and minimum scores of desert biome (Fig. 2.6F). Similar trends could be observed in the pollen record from Tso Kar (Demske et al., 2009). The first peak of humidity around 11 cal ka BP corresponds to the summer insolation maximum at 30°N (Laskar et al., 2004, Fig. 2.7C). Previous palaeoclimatic studies from north-western India and adjacent regions (e.g. Gasse et al., 1991; Van Campo and Gasse, 1993; Gasse et al., 1996; Demske et al., 2009; Wünnemann et al., 2010) argue that the ISM has been the major source of moisture during the Holocene interval in these areas and past variations in precipitation are mainly controlled by the monsoon strength. Up to now, the Arabian Sea region has served as a key focus area of studies aimed at reconstructing the late Quaternary ISM history. However, the published climate proxy records from this region are temporally inconsistent regarding the onset of the ISM. Evidence for an early maximum, from ca. 11.4 cal ka BP onwards, is only reported from an investigation done on three individual marine pollen and foraminifera records from the western Arabian Sea (Overpeck et al., 1996). By contrast, two studies on marine sediment cores, including a foraminifera $\delta^{18}O$ profile from the

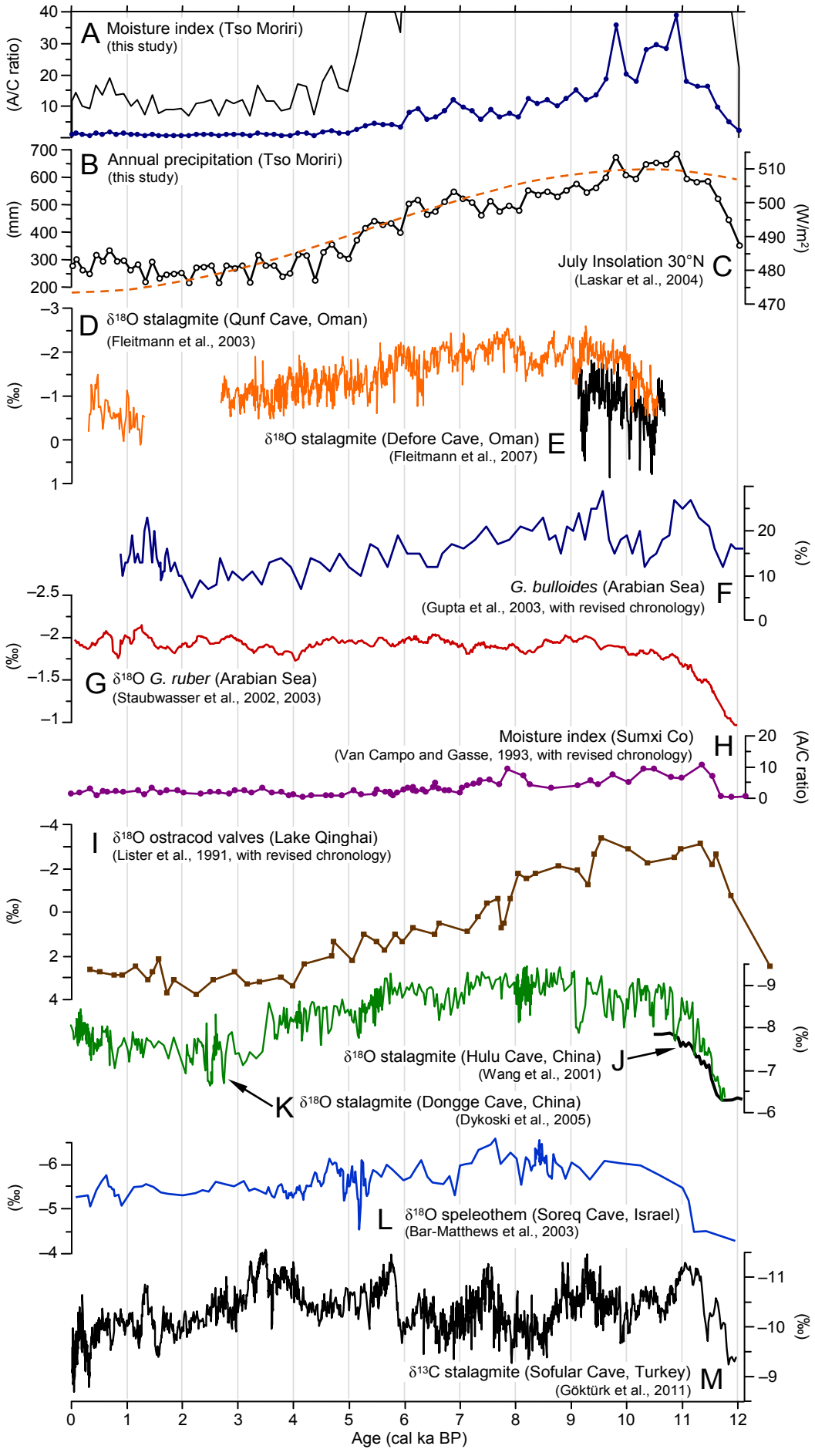
A Moisture index (Tso Moriri)
(this study)
(A/C ratio)
B Annual precipitation (Tso Moriri)
(this study)
(mm)
July Insolation 30°N C
(Laskar et al., 2004)
(W/m²)
D δ18O stalagmite (Qunf Cave, Oman)
(Fleitmann et al., 2003)
(‰)
δ18O stalagmite (Defore Cave, Oman) E
(Fleitmann et al., 2007)
G. bulloides (Arabian Sea) F
(Gupta et al., 2003, with revised chronology)
(%)
G δ18O G. ruber (Arabian Sea)
(Staubwasser et al., 2002, 2003)
Moisture index (Sumxi Co) H
(Van Campo and Gasse, 1993, with revised chronology)
(A/C ratio)
I δ18O ostracod valves (Lake Qinghai)
(Lister et al., 1991, with revised chronology)
δ18O stalagmite (Hulu Cave, China) J
(Wang et al., 2001)
K δ18O stalagmite (Dongge Cave, China)
(Dykoski et al., 2005)
L δ18O speleothem (Soreq Cave, Israel)
(Bar-Matthews et al., 2003)
δ13C stalagmite (Sofular Cave, Turkey) M
(Göktürk et al., 2011)
Age (cal ka BP)

Fig. 2.7 Summary chart used to discuss the Holocene onset and evolution of the ISM showing (A) the A/C record (thin line shows 10-times exaggeration) and (B) the mean annual precipitation (MAP) reconstruction from Tso Moriri (this study) compared with (C) the mean July insolation at 30°N (after Laskar et al., 2004) and other palaeoclimate proxy records referred to in the Discussion chapter (see Fig. 2.1 for geographical locations), including the stalagmite $\delta^{18}O$ records from (D) Qunf Cave (Q5) and (E) Defore Cave (S4) in Oman indicating ISM precipitation intensity (after Fleitmann et al., 2003, 2007); (F) the Globigerina bulloides record from Hole 723A in the western Arabian Sea indicating ISM upwelling intensity assigned to the revised chronology (see Chapter 2.6.1 and Supplementary data for further details) (after Gupta et al., 2003); (G) the 63KA/41KL Globigerinoides ruber $\delta^{18}O$ record (210-year average) from the northern Arabian Sea implying Indus River discharge (after Staubwasser et al., 2002, 2003); (H) the A/C record from Sumxi Co assigned to the revised chronology (see Chapter 2.6.1 and Supplementary data for further details) based on calendar ages BP (after Van Campo and Gasse, 1993; Van Campo et al., 1996); (I) the ostracod valves $\delta^{18}O$ record from Lake Qinghai on the northern Tibetan Plateau in China assigned to the revised chronology (see Chapter 2.6.1 and Supplementary data for further details) (after Lister et al., 1991); (J) the PD stalagmite $\delta^{18}O$ record from Hulu Cave (after Wang et al., 2001b) and (K) the D4 stalagmite $\delta^{18}O$ record from Dongge Cave (after Dykoski et al., 2005), reflecting summer monsoon intensity in China; (L) the speleothem $\delta^{18}O$ record from Soreq Cave in Israel representing annual precipitation (after Bar-Matthews et al., 2003); and (M) the So-1 stalagmite $\delta^{18}O$ record from Sofular Cave in Turkey controlled by temperature and precipitation variations (after Göktürk et al., 2011).

western Arabian Sea (Sirocko et al., 1993) and an upwelling record based on total organic carbon concentration from the north-eastern Arabian Sea (Schulz et al., 1998), suggest a peak of the ISM strength occurring no earlier than ca. 10 cal ka BP. Similarly, Fleitmann et al. (2003), based on the analysis of the Q5 stalagmite $\delta^{18}O$ profile (Fig. 2.7D) from Qunf Cave in Oman (Fig. 2.1), concluded that the maximum level of precipitation was reached at about 10 cal ka BP, or approximately 1000 years later than the Tso Moriri date.

The Q5 record does not have the potential to show an earlier initial Holocene ISM strengthening, as it only covers the past 10.6 cal ka interval. The S4 stalagmite $\delta^{18}O$ record (Fig. 2.7E) from nearby Defore Cave (Fleitmann et al., 2007, Fig. 2.1), which starts ca. 140 years earlier than Q5, indicates a phase of higher ISM-driven precipitation prior to the minimum observed ca. 10.5 cal ka BP. Moreover, it has to be noted that the trough in the $\delta^{18}O$ cave record prior to 10 cal ka BP (Fig. 2.7E) corresponds to a simultaneous decrease in the A/C values from Tso Kar and Tso Moriri. This drop in monsoon activity may be associated with a climate anomaly recorded in the glacial GISP2 ion records at ca. 10.3 cal ka BP (Mayewski et al., 1997, 2004), which Weninger et al. (2009) evaluated as one of the most intense cooling events during the last 50 ka. A similar strong attenuation of the ISM is also evident in a coastal upwelling record based on *Globigerina bulloides* concentrations (Gupta et al., 2003, Fig. 2.1). Initial results based on the chronology developed by Gupta et al. (2003) suggest peak ISM intensity at ca. 10 cal ka BP, which correlates with the timing of the monsoon onset proposed by Fleitmann et al. (2007). To allow comparison with Tso Moriri and the other records discussed here, we adjusted the given chronology, which was initially based on the MARINE98 calibration dataset (Stuiver and Reimer, 1993), by

converting the ^{14}C ages using the online version of the CalPal radiocarbon calibration program (Danzeglocke et al., 2013). To our satisfaction, the resulting curve (Fig. 2.7F, see supplementary material for further details) not only points to a significantly earlier ISM maximum (ca. 11 cal ka BP) than was reported in the original publication, but also shows a substantial depression in *G. bulloides* concentrations at around 10.3 cal ka BP. This finding coincides with the $\delta^{18}O$ peaks in the Q5 and S4 stalagmites from Oman (Fleitmann et al., 2007, Figs. 2.7D and E) and corroborates the low MAP values seen in the Tso Moriri reconstruction (Fig. 2.7B).

Another proxy reflecting the ISM activity is the *Globigerinoides ruber* $\delta^{18}O$ record from the northern Arabian Sea (Staubwasser et al., 2002, 2003, Figs. 2.1 and 7G). The changes in oxygen isotope composition were interpreted as an indicator for the discharge of the Indus River, whose watershed largely covers the region of northern Pakistan and north-western India. According to Staubwasser et al. (2002), the major strengthening of the ISM occurred between ca. 12 and 11 cal ka BP and the maximum Indus water discharge (i.e. lowest $\delta^{18}O$ value) was reached at ca. 9.4 cal ka BP. This dovetails closely with the results from north-western India.

Our synthesis also reveals similar trends in the monsoon-related moisture availability in other palaeoclimate records northeast of the Tso Moriri/Tso Kar region, for example, in the A/C ratio curves from Sumxi Co (Van Campo and Gasse, 1993; Van Campo et al., 1996) and Bangong Co (Van Campo et al., 1996). Both records are located in the south-western Tibetan Plateau (Fig. 2.1); however, their published chronologies were established based on uncalibrated ^{14}C dates. For consistency, we digitised the A/C ratio record from Sumxi Co (Van Campo et al., 1996) and then replaced the assigned radiocarbon ages with calendar ages obtained using the CalPal-2007-Hulu calibration curve (Fig. 2.7H, see supplementary material for further details). The variations in the A/C values from Sumxi Co are in strong temporal agreement with the A/C record from nearby Bangong Co (Van Campo et al., 1996). Consequently, both records indicate a rapid moisture increase from ca. 11.6 cal ka BP, quickly reaching maximum Holocene level within the next hundred of years (Fig. 2.7H). But the absolute values of A/C at Sumxi Co and Bangong Co are lower than these in the Tso Moriri record, which is in line with the generally drier climate of south-western Tibet.

A similar climatic change pattern has been reported from Qaidam Basin in the north-eastern Tibetan Plateau (Zhao et al., 2007), where a wet climate phase occurred ca. 11.9–9.5 cal ka BP inferred from a Hurleg Lake pollen record (Fig. 2.1). Lister et al. (1991) presented a study on changes in ostracod oxygen isotopes from Lake Qinghai (Fig. 2.1), which are related to the precipitation–evaporation budget controlling the lake levels and thus may be interpreted as a proxy for humidity. For consistency, we digitised the ostracod $\delta^{18}O$ values from this early publication and calibrated the associated radiocarbon ages using

CalPal online (Danzeglocke et al., 2013). The resulting curve (Fig. 2.7I) reveals a phase of minimum $\delta^{18}O$ values (i.e. increased humidity) starting at ca. 11.6 cal ka BP and persisting until ca. 9.4 cal ka BP (see supplementary material for further details).

Though, the northern part of the Qinghai-Tibetan plateau may also receive precipitation from other sources, including the EASM and the Atlantic westerlies, there is a striking similarity with the ISM domain. While the ISM and EASM are often regarded as two different subsystems of the Asian summer monsoon, both directly respond to the strength of the developed low-pressure cell over the Asian continent (Wang et al., 2005a) linked to the insolation anomaly and position of the ITCZ during the Northern Hemisphere (NH) summer. If we assume that this constitutes a common driving force of the Asian summer monsoon, then the post-glacial strengthening of the ISM and EASM should be fairly synchronous. This general assumption is supported by the comparison of the early Holocene part of the PD $\delta^{18}O$ stalagmite record (Wang et al., 2001b, Fig. 2.7J) from Hulu Cave (Fig. 2.1), interpreted as a proxy for EASM intensity, with the D4 $\delta^{18}O$ stalagmite record (Dykoski et al., 2005, Fig. 2.7K) from Dongge Cave (Fig. 2.1), which was mainly influenced by ISM-related precipitation. Both signatures show a steep increase in monsoon intensity between ca. 11.7 and 11 cal ka BP.

In sum, the majority of the discussed proxy records from the ISM domain suggest an abrupt intensification of the summer monsoon had already occurred at the end of the Younger Dryas and the early Holocene phase of the most active monsoon starting at ca. 11 cal ka BP. This finding, in turn, strongly dovetails with the reconstruction results from both Tso Moriri and China. One of the reasons for the disagreement in the ISM evolution reported in some records from the western Arabian Sea may be chronological uncertainties related to ocean upwelling and surface convection caused by south-westerly and north-easterly winds, respectively. As both upwelling and convection vary in time, reservoir ages have been fluctuating in the past, which hampers the development of robust age-depth models (Staubwasser et al., 2002). Another explanation for the "later onset of the ISM" suggested in some publications may be the insufficient length of these records, which are missing the late glacial/early Holocene interval, as demonstrated in Fig. 2.7D. The differences seen in the records from the southern and northern part of the ISM domain may also reflect some differences in the regional atmospheric circulation during the early Holocene. For example, westerly disturbances may have possibly governed the precipitation in the northern parts of the ISM area during the early Holocene. Today, the westerly system carries vapour from the Atlantic Ocean, Eastern Mediterranean region and the Caspian Sea as far as north-western India (Aizen et al., 1996) and controls the hydrology of the Karakorum and parts of the north-western Himalaya during the winter and spring (Figs. 2.2C, E and F). Stable isotope records from the Eastern Mediterranean region reveal a quick and relatively early increase in precipitation ca. 11 cal ka BP in the speleothem $\delta^{18}O$

record from Israel (Bar-Matthews et al., 2003, Figs. 2.1 and 2.7L) and ca. 11.2 cal ka BP in north-western Turkey (Göktürk et al., 2011, Figs. 2.1 and 2.7M). These records are comparable with the early Holocene humidity peak recorded at Tso Moriri. As suggested for the Eastern Mediterranean (Rohling, 1994; Rossignol-Strick, 1999), this early Holocene precipitation maximum may be interpreted as the effect of both winter and summer rainfall. In this case, the presence of the early Holocene ice sheet in Scandinavia meant that the summer westerly precipitation belt did not migrate as far northwards as today (Litt et al., 2009). This feature of the early Holocene atmospheric circulation may have led to enhanced moisture transmission to the Eastern Mediterranean and further eastwards, thus contributing to the rapid increase in precipitation suggested by the north-western Himalaya proxy records. To further evaluate the timing of the initial onset and maximum activity of the ISM, we need additional well-dated palaeoclimate proxy records from the southern ISM region, which could not been influenced by low-latitude westerly disturbances.

2.6.2 The long-term evolution of the ISM during the middle and late Holocene

To date, no general agreement exists about how the ISM has developed since the hydrological optimum conditions during the early Holocene. Morrill et al. (2003) did the first published statistical analysis of palaeoclimate records and argued for significant weakening of the summer monsoon between ca. 5 and 4.5 cal ka BP. However, their study covered the entire Asian monsoon domain. More recently, Wang et al. (2010) postulated that the Holocene evolution of the ISM and EASM has been asynchronous, arguing that the ISM has weakened since the early Holocene maximum, while the EASM reached its maximum ca. 7 cal ka BP. This conclusion, however, requires further empirical verification and is not easily traceable in the most representative records from both regions (Fig. 2.7).

The MAP reconstruction (Fig. 2.7B) derived from the TMD record shows an overall gradual decrease in available moisture, which closely parallels the reduction in NH summer insolation (Fig. 2.7C). This continuous decrease in monsoon strength accords with the majority of available terrestrial proxy records (Wang et al., 2010 and references therein), as well as the ISM domain's marine component (e.g. Overpeck et al., 1996; Gupta et al., 2003; Ivanochko et al., 2005; Fleitmann et al., 2007; Ponton et al., 2012). The consensus is that this continuous attenuation of the ISM (e.g. Fleitmann et al., 2007), also seen in other parts of the tropical belt (e.g. Haug et al., 2001), follows the southward migration of the mean position of the ITCZ, which occurred in response to the reduction in NH summer insolation. Nevertheless, the data syntheses from the EASM (An et al., 2000; He et al., 2004) and the ISM (Fleitmann et al., 2007) regions also indicates that spatial heterogeneity in the Holocene moisture climate evolution can not be completely excluded. Comparing Fig. 2.7B

and Fig. 2.7D, suggests two precipitation trends. First, in response to the southward shift of the mean ITCZ position during summer, precipitation in areas closer to the equator experienced a less pronounced decrease during the middle Holocene. Second, precipitation has been decreasing more steadily in the northern parts of the ISM domain since the early Holocene towards minimum values ca. 3–2 cal ka BP.

2.6.3 Centennial-scale climate oscillations

In addition to the overall trend towards drier conditions in the study region during the Holocene, there is evidence for climatic oscillations of much shorter duration in the MAP record from Tso Moriri, as well as in the other proxy records (Fig. 2.8).

The A/C record (Fig. 2.8A) and MAP reconstruction results (Fig. 2.8B) from Tso Moriri reveal several phases of reduced precipitation (grey bars, Fig. 2.8). Similar abrupt variations in the ISM strength, which correspond to climate events in the North Atlantic (Bond et al., 1997, 2001), were first found in the Holocene $N^{13}C$ time series based on plant remains from the Hongyuan peat bog on the eastern Tibetan Plateau (Hong et al., 2003, Fig. 2.1). Later, Wang et al. (2005b), who interpreted the summer monsoon intensity record from Dongge Cave, also noted that the gradual trend in the monsoon development is punctuated by eight centennial-scale weak monsoon events, centred at ca. 8.3, 7.2, 6.3, 5.5, 4.4, 2.7, 1.6, and 0.5 cal ka BP, and further linked them to solar changes and North Atlantic climate. A comparison of the Tso Moriri Holocene climate record with millennial-scale cold/dry cycles recognised in the North Atlantic region (Bond et al., 1997, 2001, numbered 0–8, Fig. 2.8C) and Greenland ice cores (Mayewski et al., 1997, 2004, Fig. 2.8D) shows a remarkable synchrony. That synchrony suggests a link with the North Atlantic century-scale climate oscillations.

On the other hand, monsoon proxy records from the region of the western Arabian Sea do not imply dry climate fluctuations, which are clearly coeval with the cold events documented in the North Atlantic during the mid to late Holocene (e.g. Fleitmann et al., 2003, 2007, Fig. 2.8F; Gupta et al., 2003, Fig. 2.8E). However, in the Q5 record from Oman, Fleitmann et al. (2007) identified pulses of reduced $\delta^{18}O$ values during the early Holocene (Fig. 2.8F), which are also found in the stalagmite record from Dongge Cave (Dykoski et al., 2005, Fig. 2.8G) from the northeastern ISM domain. These pulses are synchronous with the 9.2 and 8.2 events (i.e. Bond cycles 6 and 5, respectively). Moreover, the period of decreasing $\delta^{18}O$ values between ca. 10.6 and 10 cal ka BP in the Q5 and S4 record (Fig. 2.8F), which is interpreted as the Holocene onset of the ISM by Fleitmann et al. (2007), may reflect the end of a pronounced phase of dry climate synchronous with the Bond cycle 7 (Bond et al., 2001, Fig. 2.8C) and 10.2 event described from Greenland ice core data (Mayewski et al., 1997, 2004, Fig. 2.8D; Weninger et al., 2009). This interval of climate

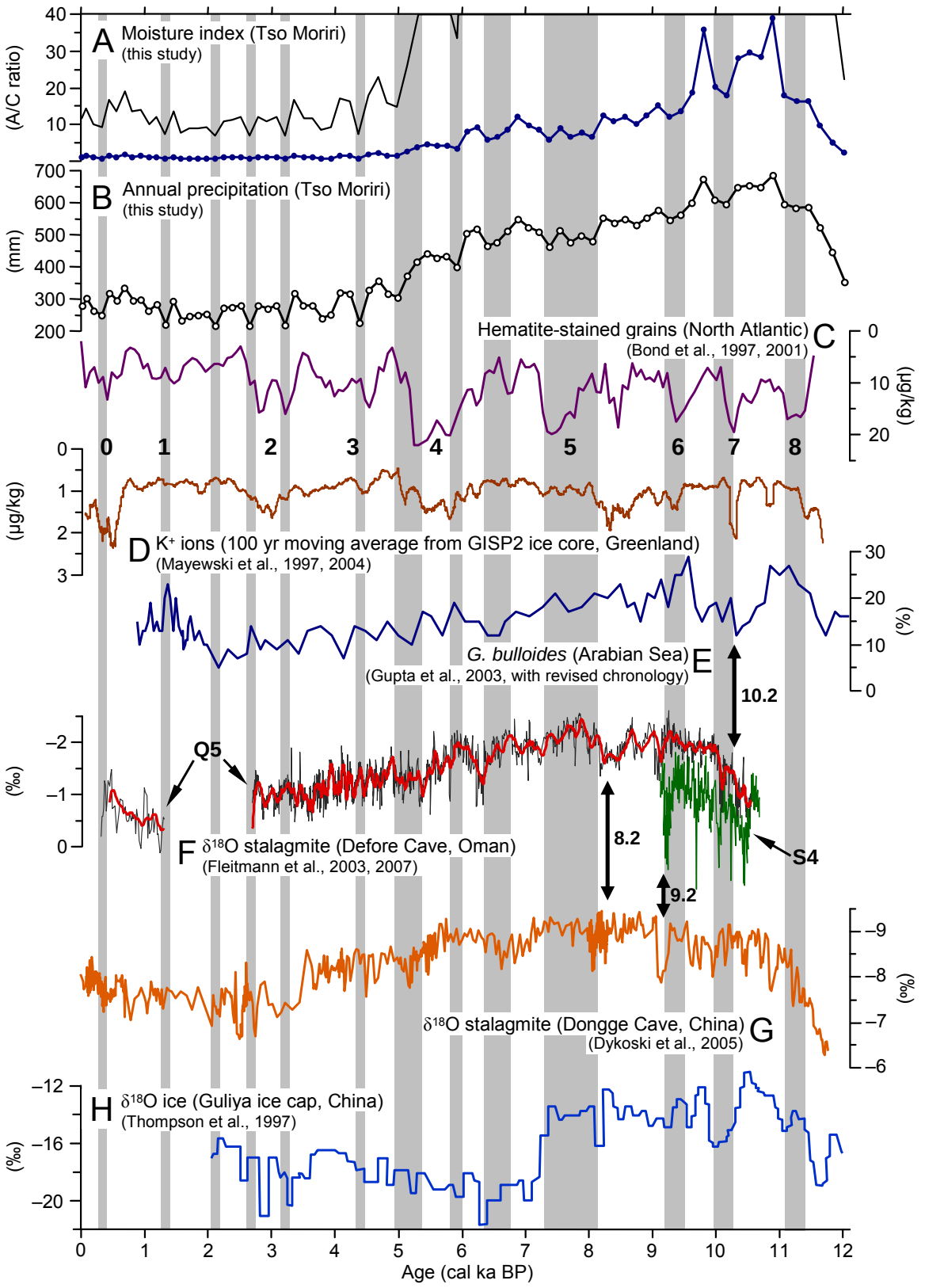

Fig. 2.8 Summary chart used to discuss the centennial-scale dry oscillations in (A) the A/C record (thin line shows 10-times exaggeration); (B) the Tso Moriri MAP reconstruction; (C) the hematite-stained grains record as a drift ice indicator from North Atlantic deep-sea sediment cores with numbered Bond events (after Bond et al., 1997, 2001); (D) the concentrations of K^+ ions in the GISP2 Greenland ice core as a signature of polar circulation-linked atmospheric dust flux (after Mayewski et al., 1997, 2004); (E) the Globigerina bulloides record from Hole 723A in the western Arabian Sea showing ISM upwelling intensity assigned to the revised chronology (see Chapter 2.6.1

and Supplementary data for further details) (after Gupta et al., 2003); (F) the stalagmite $\delta^{18}O$ records from Qunf Cave (Q5), including the ten-point running average (thick line) and Defore Cave (S4) in Oman, indicating ISM precipitation intensity (after Fleitmann et al., 2003, 2007); (G) the stalagmite $\delta^{18}O$ record from Dongge Cave in southern China showing variations mainly in the ISM (after Dykoski et al., 2005); and (H) the $\delta^{18}O$ record from the Guliya ice core from the western Kunlun Shan showing temperature changes (after Thompson et al., 1997). Vertical grey bands indicate dry spells in the Tso Moriri moisture and MAP reconstructions.

deterioration is also indicated by a large-amplitude shift in the foraminifera upwelling record, combined with the revised chronology from the Oman margin (Gupta et al., 2003, Fig. 2.8E), reduced moisture/precipitation availability values in the Tso Moriri reconstructions (Fig. 2.8A and B), and the expansion of the Guliya ice cap in north-western Tibet (Thompson et al., 1997, Fig. 2.8H).

If our interpretations are correct, then it appears that North Atlantic influence is more pronounced in the records from the southern part of the ISM domain during the early Holocene, but does not play a significant role during the middle and late Holocene. This may be explained by the higher summer and winter westerly-derived rainfall during the early Holocene, which likely had a greater impact on the regional hydrology. By contrast, the North Atlantic cooling events significantly affected the hydrology in the north, including the Tso Moriri area following the Holocene onset. This is probably due to the significant contribution of westerly-driven precipitation to the overall water budget throughout the Holocene interval.

2.6.4 Possible impact of climate variations on early human civilisations

Like the Akkadian Empire and Ancient Egypt, the Harappan Civilisation was one of the world's first great urban societies (see MacDonald, 2011 and Giosan et al., 2012 for summary and references). At times of maximum flourishing, marked by the highest degrees of urbanisation, between ca. 4.5 and 3.9 cal ka BP, defined as the Mature Harappan phase (Figs. 2.9A and B), the civilisation occupied large parts of the alluvial lowlands of the greater Indus Valley and adjacent regions in present-day Pakistan and north-western India (dark grey area in Fig. 2.1). The subsequent phase, known as the Late Harappan stage (3.9–3 cal ka BP), is marked by a cultural demise related to prolonged deurbanisation. This deurbanisation was accompanied by a more dispersed settlement structure, migration, and shifts in agriculture, all of which eventually resulted in the vanishing of prominent artefacts and the Harappan script in the archaeological records after 3 cal ka BP (Possehl, 2002; MacDonald, 2011). As is the case for the collapse of several other early civilisations (e.g. deMenocal, 2001; Weiss and Bradley, 2001; Yasuda et al., 2004a), several authors regard climate deterioration as being mainly responsible for the demise of the Mature Harappan

cities, though this climatic hypothesis is not indisputably accepted by all scientists (Madella and Fuller, 2006 and references therein).

Like the region's earliest sedentary communities first discovered at the Mehrgarh site (Baluchistan, Pakistan) and dated to ca. 9 cal ka BP, the diet of the Early (5.2–4.5 cal ka BP) and Mature Harappans was mainly based on winter crops, like wheat and barley (Weber, 2003; Fuller, 2006). MacDonald (2011) pointed out that good harvests of such crops not only depended on westerly-controlled winter precipitation, but needed sufficient ISM rainfall as well. The latter was essential to provide enough soil moisture for the germination of grains after sowing during September or October. We assume that, like today, the climate in the former settlement area of the Harappan Civilisation (Fig. 2.1) has been influenced by both westerly-controlled and ISM precipitation throughout the Holocene. Consequently, the wider plains of the Indus and its tributaries in the north-western Indian subcontinent appear to have been a highly suitable environment for the rise of the sophisticated urban culture of the Mature Harappan Civilisation. Most astonishing is that this cultural development was accompanied by the following three climate features. The first was a general trend towards increasingly arid climate (Figs. 2.9C and E) caused by the identified ISM weakening (e.g. Overpeck et al., 1996; Gupta et al., 2003; Fleitmann et al., 2007) linked to a decrease in NH summer isolation (e.g. Fleitmann et al., 2007; Marzin and Braconnot, 2009). The second were several centennial-scale dry events (Figs. 2.9C and D) superimposed on this long-term climate trend (Figs. 2.9C and E). And the third was increasing interannual variability in monsoon precipitation caused by El Niño events, which started occurring during the mid Holocene (Moy et al., 2002; Gagan et al., 2004).

A period of intensified aridity, due to severe cold spells in the North Atlantic (Bond cycle 3 in Fig. 2.9F) and referred to as the 4.2 event, has been associated with the demise of the Akkadian empire (Cullen et al., 2000; deMenocal, 2001) and Egypt's Old Kingdom (Hassan, 1997; Weiss, 1997). Although called the 4.2 event, this cold climate oscillation extended over several centuries, i.e. from ca. 4.2 until 3.8 cal ka BP (Redman et al., 2007). However, the cooling possibly started as early as ca. 4.5–4.4 cal ka BP, which may be traced in a rather short-term peak in hematite-stained grains (Bond et al., 2001, Fig. 2.9F) and Greenland ice core ion concentration (Mayewski et al, 1997, 2004, Fig. 2.9G). An abrupt shift towards aridity in the Tso Moriri MAP record is dated to ca. 4.4 cal ka BP, and a second distinctly dry oscillation took place around 4 cal ka BP (Fig. 2.9C). Taking into account minor chronological uncertainties, the recognised trends in the MAP reconstructions and during the Bond cycle 3 represented in the ice-rafted debris record from the North Atlantic (Fig. 2.9F) are well synchronised. Equivalent tendencies are documented in the oxygen isotope record from the continental margin off Pakistan interpreted as a proxy for Indus River discharge (Staubwasser et al., 2002, 2003). The record does not indicate a general trend of discharge decrease during the middle and late Holocene, but shows

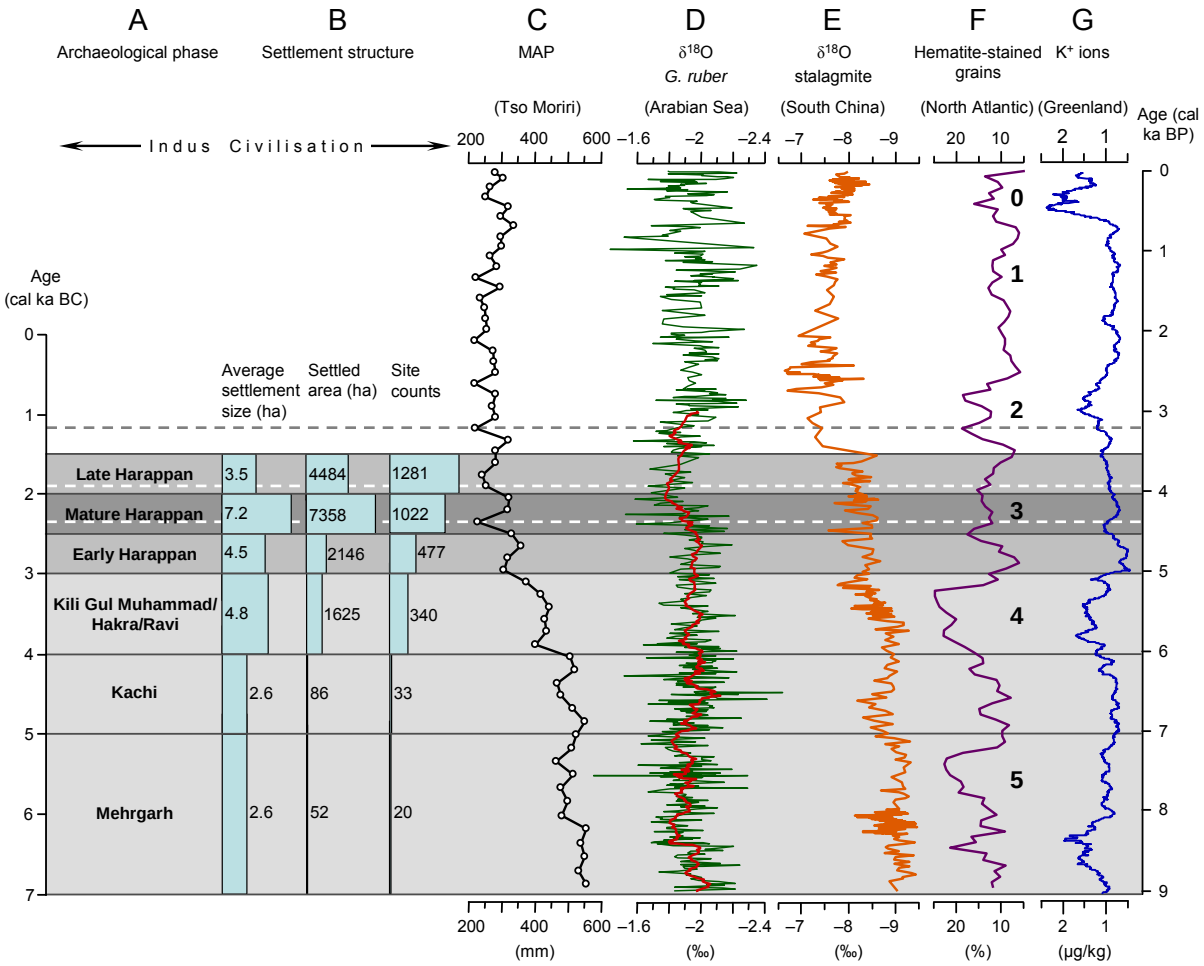

Fig. 2.9 Overview of (A) the chronology of the approximate archaeological periods in the greater Indus Valley (after Madella and Fuller, 2006) and (B) associated information on settlement structure (after Madella and Fuller, 2006) compared to palaeoclimate proxy records (see Fig. 2.1 for geographical location) including (C) the reconstruction results for MAP derived from the TMD record from Tso Moriri; (D) the 63KA/41KL Globigerinoides ruber $\delta^{18}O$ record from the northern Arabian Sea, implying Indus River discharge, with thick line showing the 10-point running average (after Staubwasser et al., 2002, 2003); (E) the stalagmite $\delta^{18}O$ record from Dongge Cave in southern China showing variations mainly in the ISM (after Dykoski et al., 2005); (F) the hematite-stained grains record as a drift ice index from North Atlantic deep-sea sediment cores with numbered Bond events (after Bond et al., 1997, 2001); and (G) the concentrations of K^+ ions in the GISP2 Greenland ice core as indicators of polar circulation-linked atmospheric dust flux (after Mayewski et al., 1997, 2004). Dashed lines indicate pronounced dry events mentioned in the Discussion.

small-scale oscillations from a relatively stable $\delta^{18}O$ level (Fig. 2.9D). It might be possible that changes in $\delta^{18}O$ are no more visible after the discharge exceeds a certain threshold or that only very significant variations in the water discharge can be recognised. Such large-scale fluctuations, with maximum $\delta^{18}O$ values (i.e. a minimum in the Indus River discharge), are visible during the middle Holocene, between approximately 4.5 and 4.3 cal ka BP, with a more prolonged phase of heavier $\delta^{18}O$ beginning at ca. 4 cal ka BP (Fig. 2.9D). The correlation of these records suggests that the north-western Indian subcontinent was already exposed to short-term dry events during the early Mature Harappan phase,

characterised by the most intensive urbanisation (Figs. 2.9A and B). Madella and Fuller (2006) propose that such changing (and unstable) climate conditions might have promoted the diversification of agriculture, which then contributed to the appearance of the Mature Harappan urbanism. Likewise, the emergence of urbanism in southern Mesopotamia after ca. 6 cal ka BP is thought to be the result of adaptation to severe drought and unpredictable periodic flooding (Adams, 1981; Nissen, 1988).

Alternatively, Giosan et al. (2012) attest a long-term trend of increasing aridification in the Harappan Civilization domain during the middle Holocene based on an investigation of the fluvial landscape morphology of the western Indo-Gangetic Plain. The latter study suggests that after ca. 5 cal ka BP diminished river discharge and decreased flood intensity might have improved habitation environments of this initially unstable fluvial landscape, facilitated agricultural and stimulated urban development during the Mature Harappan Civilisation (Giosan et al., 2012). The relationship between the inferred middle Holocene decrease in regional fluvial discharge and the ISM weakening derived from the Himalayan pollen record (Fig. 2.9C) is obvious, though understanding the links between climate change and societal developments require further considerations.

Under conditions of continuous drying, which possibly culminated at ca. 4 cal ka BP (Figs. 2.9C and D), there is evidence of deurbanisation starting in the period between 4.2 and 4 cal ka BP (Madella and Fuller, 2006). The Tso Moriri MAP reconstruction (Fig. 2.9C), together with the Indus discharge record (Fig. 2.9D), strongly suggests that a period of enhanced aridity, which probably persisted until ca. 3.8–3.6 cal ka BP and is associated with the Bond cycle 3, caused the adverse changes in sociocultural adaptation (Possehl, 1997; Fuller and Madella, 2001). These climate changes coincide with the termination of the Mature Harappan phase. As MacDonald (2011) concludes, more frequently appearing interannual monsoon fluctuations, caused by a higher density of El Niño events after ca. 4 cal ka BP (Moy et al., 2002; Abram et al., 2007), further complicated sustaining agricultural subsistence. The subsequent agrarian, social, and economic transformations include: (i) agricultural diversification (i.e. double-cropping) marked by the additional cultivation of summer crops, such as millet, (ii) population dispersion, reflected in the abandonment of cities and an increase in the number of smaller, separated rural settlements (Fig. 2.9B), and (iii) reduction in long-distance trade and production of luxury items (Possehl, 1997; Fuller and Madella, 2001). The most significant causal relationship between Late Harappan communities and climate deterioration is probably the migration to moister regions in the east, northeast (i.e. the Ganges plains and the Himalayan foothills) and south (Gujarat Province), which left many western areas abandoned (Gaur and Vora, 1999; Fuller and Madella, 2006). From ca. 3 cal ka BP, traces of the Harappan Civilisation start to disappear from archaeological records, pointing to the end of the Harappan Civilisation as a complex sociocultural system (Possehl, 2002). Despite continued habitation in the Harappan

settlement area (Fig. 2.1) at much lower density, Possehl (2002) states that the people were no longer organised by class and occupation and partly gave up their identity by adopting new customs and beliefs. As is the case for the decline of the urban period, we see strong evidence that this downfall was climate-induced. Around 3.2 cal ka BP, the region is characterised by distinctly low levels of MAP (Fig. 2.9C) and Indus River discharge (Fig. 2.9D). These increasingly severe environmental conditions were likely due to a further weakening in ISM circulation (Figs. 2.9C and E), which was reinforced by a decrease in the westerly-transported winter precipitation during the phase of North Atlantic cooling identified as Bond cycle 2 (Fig. 2.9F).

Up to now, it has been acknowledged that the Harappan Civilisation's rise, decline, and disappearance were accompanied by a gradual trend towards a more arid climate (Madella and Fuller, 2006; MacDonald, 2011; Giosan et al., 2012). On the basis of the foregoing discussion, we conclude that the continuous reduction of ISM precipitation and more frequent ENSO-related interannual Asian monsoon fluctuations may be considered as the fundamental driving force for climate deterioration recognised in much of South Asia. This deterioration was further amplified by North Atlantic cold events, especially in large parts of the north-western Indian subcontinent, including the former Harappan settlement area. This is mainly due to the region's location at the interface of two major atmospheric circulation systems, where, in addition to the ISM, annual precipitation is significantly influenced by westerly disturbances immediately linked to North Atlantic climate. Consequently, we hypothesise that it was the interplay of both long- and short-term trends of climate change which triggered the Harappan Civilisation's rise, development and flourishing, and then decline and eventual disappearance.

2.7 Conclusions

In this study, we analysed the Holocene part of the 7.24 m long deep-water core from Tso Moriri for terrestrial pollen. The strong fit between the pollen record from Tso Moriri, and pollen record from Tso Kar, situated ca. 40 km north of Tso Moriri, suggests that they reflect regional changes in vegetation and climate. Based on the published pollen studies from the broader region, we used the A/C ratio as an indicator for moisture availability. Furthermore, using a limited set of modern surface pollen spectra and modern climate data assigned to the pollen sampling sites, we found a significant statistical correlation between the A/C ratio and MAP. Thus, we applied the obtained transfer function to the Tso Moriri fossil pollen record to quantify past changes in MAP.

Both qualitative and quantitative interpretations of the Tso Moriri pollen record imply that moisture availability had already increased rapidly at the end of the Younger Dryas, with hydrological optimum conditions in the study region occurring between ca. 11

and 9.6 cal ka BP. The subsequent climate is characterised by a gradual decline in humidity, which is only interrupted by a centennial-scale reversal trend between ca. 1 and 0.4 cal ka BP, which is also observed in the EASM domain. The Holocene development of regional moisture availability parallels the evolution of the NH mean summer insolation. This suggests that the regional hydrology is primarily governed by ISM strength, which is coupled to the mean summer ITCZ position as a response to the precessional isolation cycle controlled warming over Asia.

The persistent decline of MAP in the Tso Moriri record is superimposed by several prominent centennial-scale intervals of enhanced aridification, which are closely synchronised to North Atlantic cold climate events. It appears that the latter reduced the winter westerly air flow, which decreased regional winter precipitation, thereby amplifying the underlying steady weakening of the ISM.

The comparison of the Tso Moriri record with the published moisture reconstructions suggest that the decrease in precipitation in the regions at the northern limit of the ISM (i.e. the north-western Himalaya) was greater than in the southern parts (i.e. the western Arabian Sea region) of the ISM domain. In the latter region, we also see evidence for stronger dependence on North Atlantic climate conditions throughout the early Holocene, which is probably linked to the westerlies' maximum intensity during this time period.

The reconstructed moisture evolution supports previous hypotheses that the emergence and decline of the urban Harappan Civilisation coincided with periods of severe drought. The overall gradual decrease in MAP may have caused crop yields to fall. That, in turn, promoted the establishment of urban centres to facilitate the storage, protection, administration, and redistribution of staple crops. Moreover, there is evidence for pronounced dry spells at ca. 4 and 3.2 cal ka BP, which possibly further hindered food ensuring sufficiency and may have caused the protracted deurbanisation after ca. 4 cal ka BP and eventual demise of the Harappan Civilisation between ca. 3.5 and 3 cal ka BP in the greater Indus Valley.

2.8 Acknowledgements

The present study is a contribution to the current project 'Himalaya: Modern and Past Climates (HIMPAC)' funded by the German Research Foundation (DFG Research Unit 1380) and to the ongoing research initiative "Bridging Eurasia". The work of C. Leipe and D. Demske is funded via the DFG grant RI 809/24. P. Tarasov acknowledges the DFG Heisenberg Program (TA 540/5). We would like to express our thanks to B. Wünnemann (Freie Universität Berlin, Germany; Nanjing University, China) and T. Schierbaum for great help during the field work, W. Ding (Freie Universität Berlin, Germany) and S.

Pinkerneil (GFZ, Potsdam, Germany) for their committed assistance in core subsampling as well as F. Riedel, S. Müller, S. Hildebrandt and L. Taft (all Freie Universität Berlin, Germany) for valuable discussions and providing literature. We are grateful to two anonymous reviewers for their constructive comments and to Daniel Garst for his useful suggestions and linguistic improvements.

2.9 Supplementary data

Supplementary material associated with this article is provided in the online version of this published article at doi:10.1016/j.quaint.2013.05.005 and in the Open Access information system PANGAEA at doi:10.1594/PANGAEA.808958.

3. Manuscript II

Potential of pollen and non-pollen palynomorph records from Tso Moriri (Trans-Himalaya, NW India) for reconstructing Holocene limnology and human–environmental interactions

Christian Leipe [a,*], Dieter Demske [a], Pavel E. Tarasov [a], Bernd Wünnemann [b,c], Frank Riedel [a], HIMPAC Project Members [1]

[a] *Institute of Geological Sciences, Palaeontology, Freie Universität Berlin, Malteserstrasse 74–100, Building D, 12249 Berlin, Germany*

[b] *Institute of Geographical Sciences, Freie Universität Berlin, Malteserstrasse 74–100, Building H, 12249 Berlin, Germany*

[c] *School of Geographic and Oceanographic Sciences, Nanjing University, Nanjing, China*

[1] http://www.himpac.org

Published in *Quaternary International* 348 (2014) pp. 113–129

doi:10.1016/j.quaint.2014.02.026

3.1 Abstract

The high-altitude lake Tso Moriri (32°55'46"N, 78°19'24"E; 4522 m a.s.l.) is situated at the margin of the Indian Summer Monsoon and westerly influences in the Trans-Himalayan region of Ladakh. Human settlements are rare and domestic and wild animals are concentrated in the alpine meadows. A set of modern surface samples and fossil pollen from a deep-water core was evaluated with focus on indicator types revealing human impact, grazing activities and lake system development during the last ca. 12 cal ka BP. The non-pollen palynomorph (NPP) record, comprising remains of limnic algae and invertebrates as well as fungal spores and charred plant tissue fragments, were examined in order to attest palaeolimnic phases and human impact, respectively. Changes in the early and middle Holocene limnic environment are mainly influenced by regional climatic conditions and glacier-fed meltwater flow in the catchment area. The NPP record indicates low lake productivity with high influx of freshwater between ca. 11.5 and 4.5 cal ka BP which is in agreement with the regional monsoon dynamics and published climate reconstructions. Geomorphologic observations suggest that during this period of enhanced precipitation the lake had a regular outflow and contributed large amounts of water to the

Sutlej River, the lower reaches of which were integral part of the Indus Civilisation area. The inferred minimum freshwater input and maximum lake productivity between ca. 4.5–1.8 cal ka BP coincides with the reconstruction of greatest aridity and glaciation in the Korzong Valley, resulting in significantly reduced or even ceased outflow. We suggest that lowered lake levels and river discharge at a larger regional scale may have caused irrigation problems and harvest losses in the Indus Valley and lowlands occupied by sedentary agricultural communities. This scenario, in turn, supports the hypothesis that Mature Harappan urbanism (ca. 4.5–3.9 cal ka BP) emerged in order to facilitate storage, protection, administration, and redistribution of crop yields, and secondly, the eventual decline of the Harappan Culture (ca. 3.5–3 cal ka BP) was promoted by prolonged aridity. There is no clear evidence for human impact around Tso Moriri prior to ca. 3.7 cal ka BP, with a more distinct record since ca. 2.7 cal ka BP. This suggests that the sedimentary record from Tso Moriri primarily archives the regional climate history.

3.2 Introduction

At present, the climate conditions in the western Trans-Himalaya are mainly influenced by the Indian Summer Monsoon (ISM) and westerly disturbances (Wünnemann et al., 2010). Previous studies from this region (Bhattacharyya, 1989b; Wünnemann et al., 2008, 2010; Demske et al., 2009; Leipe et al., 2014) and the adjacent westernmost Qinghai–Tibet Plateau (e.g. Gasse et al., 1991, 1996) indicate significant variations in palaeoenvironmental conditions throughout the late-glacial and Holocene in this arid high-alpine part of Asia. In contrast to the palaeoenvironmental archives, the human prehistory of this region remains poorly studied. It is unclear when the first human activities occurred in the Indian part of the Trans-Himalaya (Dollfus, 2012). Only limited archaeological evidence is reported from this region (e.g. Ganjoo and Ota, 2012). Tripathi et al. (1988) discovered stone artefacts from several sites in the Indus Valley 60–150 km downstream of Leh, which according to sediment stratigraphy are regarded as Lower and Middle Palaeolithic. Early to late Holocene (Neolithic–Iron Age) human presence, at least temporary, in Ladakh is described from a set of sites in the Indus Valley ~100 km upstream of Leh, which are radiocarbon-dated to 7.7–2.7 cal ka BP (Sharma et al., 1989; Ota, 1993; S.B. Ota, personal communication 2013). It is believed that nomadic pastoralists, who originated from ancient tribes on the Qinghai–Tibet Plateau, were among the earliest permanent inhabitants (Dollfus, 2012). Today, their descendants in Ladakh, called Changpas, mainly subsist through pastoralism.

Similarly, the prehistory of the Qinghai–Tibet Plateau is poorly understood (Miehe et al., 2009a; Brantingham et al., 2010; Aldenderfer, 2011 and references therein). Archaeological finds from the plateau suggest that hunter-gatherer populations were at

least seasonally present at ca. 11–8 cal ka BP (Brantingham et al., 2007, 2010) in areas ≥4000 m a.s.l. Year-round habitation of nomadic pastoralists based on domesticated yaks (*Bos grunniens*) is claimed to have occurred not before ca. 4 cal ka BP (Flad et al., 2007; Rhode et al., 2007). By contrast, other archaeological studies suggest that the occupation started already at ca. 10 cal ka BP (Aldenderfer, 2003). A yet earlier colonisation is hypothesised by several genetic investigations, which date the onset of permanent human occurrence to ca. 21 cal ka BP (Zhao et al., 2009a) or even to ca. 30 cal ka BP (e.g. Moore et al., 2000; Beall, 2001).

Since the establishment of modern palynology, the analysis of fossil palynomorphs has been demonstrated a useful tool for identifying the presence and dynamics of human activities (e.g. Firbas, 1937; Iversen, 1949; Behre, 1981, 1988; Dimbleby, 1985; Gaillard et al., 1992, 1994; van Geel, 2001), applied to various environmental settings (e.g. Birks et al., 1988 and references therein; Rösch, 1992; Yasuda et al., 2000; van Geel et al., 2003). In the high altitudinal regions of Asia, such works have been conducted in the Nepal Himalaya (Miehe et al. 2002, 2009b; Schlütz and Zech, 2004) and the Pakistani Hindu Kush (Miehe et al., 2009b), suggesting that human impact caused deforestation. Considering the eastern part of the Qinghai–Tibet Plateau, several studies (e.g. Thelaus, 1992; Frenzel, 1994, Miehe et al. 2006; Kaiser et al., 2008; Schlütz and Lehmkuhl, 2009) aimed at identifying the onset of regional nomadic pastoralism, which was dated to ca. 8.8 cal ka BP (Miehe et al., 2009a). However, the interpretations of the above mentioned studies are still under debate (e.g. Ren, 2007; Herzschuh et al., 2009, 2010), and contradict other studies which assume a climate-induced Holocene vegetation change on the Qinghai–Tibet Plateau (e.g. Herzschuh et al., 2006).

The application of non-pollen palynomorphs (NPPs) in palaeolimnological research is a comparatively young discipline (van Geel, 1978, 1986, 2001). Many of the described microscopic botanical and zoological remains are yet unknown and their ecology is scantily understood. However, today the value of NPPs in palaeoecology is generally recognised (Aichner et al., 2012; Hooghiemstra, 2012) and numerous studies have used them for the reconstruction of late Quaternary limnological changes (e.g. van Geel et al., 1989; Rull et al., 2008; Kramer et al., 2010). In a recent multi-proxy study, Wünnemann et al. (2010) applied fossil NPP assemblages from Tso Kar in Ladakh to infer late-glacial–Holocene climate and limnological changes.

The present study contributes to the multidisciplinary Research Unit "Himalaya: Modern and Past Climates" (HIMPAC) which involves the analysis of palaeoclimate proxy records from archives located in climatically sensitive regions distributed over the Indian subcontinent (http://www.himpac.org). Besides elucidating late-glacial–Holocene variations in the ISM and its global teleconnections, these proxy records are aimed at enhancing our understanding of past human-environment interactions.

Here, we present a Holocene record of fossil pollen and NPPs based on a composite sediment core from Tso Moriri, a high-alpine lake located in the Indian Trans-Himalaya. Based on the terrestrial pollen record from the same sediment profile, Leipe et al. (2014) reconstructed regional Holocene vegetation and climate changes and correlated them with other palaeoclimate records. The results suggest that the terrestrial vegetation in the Tso Moriri region was relatively undisturbed by human activities. With the current study, we expand our analysis about deciphering human impact in the region and for tracing palaeolimnological variation in the lake by using different types of palynomorphs including arboreal and non-arboreal pollen, spores of ferns, fern allies and fungi, remains of algae, zoobenthos and zooplankton, and plant tissue fragments. Further, the palaeolimnological reconstructions are used to evaluate how climate and environmental conditions could have influenced cultural changes in the ancient Harappan Civilisation which prospered in the greater Indus Valley between ca. 5.2 and 3 cal ka BP. The fossil pollen and NPP records are complemented by a new set of regional modern palynological surface samples and recent observations of geomorphological features within the lake basin. The discussion of the presented results considers previously published regional palaeoenvironmental studies including the glaciation history in the Korzong Valley.

3.3 Study site and modern environment

3.3.1 Characteristics of lake and catchment area

The high-alpine lake Tso Moriri is situated in the Trans-Himalayan region of north-western India in the Rupshu area, south-eastern Ladakh district (Figs. 3.1A and B). This part of Ladakh southeast of Leh (Fig. 3.1B) is characterised by high average altitudes ranging from around 3000 m a.s.l. in the Indus Valley to above 6500 m a.s.l. at the highest peaks (Reuter et al., 2007; Jarvis et al., 2008). Tso Moriri spans a surface area of ~147 km^2 (Leipe et al., 2014) at an elevation of 4522 m a.s.l. according to Shuttle Radar Topography Mission (SRTM) v4.1 data (Reuter et al., 2007; Jarvis et al., 2008). It has been considered a closed-basin lake (Hutchinson, 1937; Lesher, 2011). Gujja et al. (2003) and Panigrahy et al. (2012) noted a former outlet in the south, but they did not describe related hydromorphological features nor did they indicate during which period the outlet was active. Thickness of the lacustrine basin sediments has not been explored, but from the chronology of a 724 cm sediment core it can be inferred that the lake has existed at least since the Last Glacial Maximum (Leipe et al., 2014).

The maximum depth of Tso Moriri is not known, but exceeds 105 m (Mishra et al., 2013). Secchi disc transparency of 9 m (Hutchinson, 1937) defines the lake as ultra-oligotrophic. From the electric conductivity data published in Singh et al. (2008), a salinity

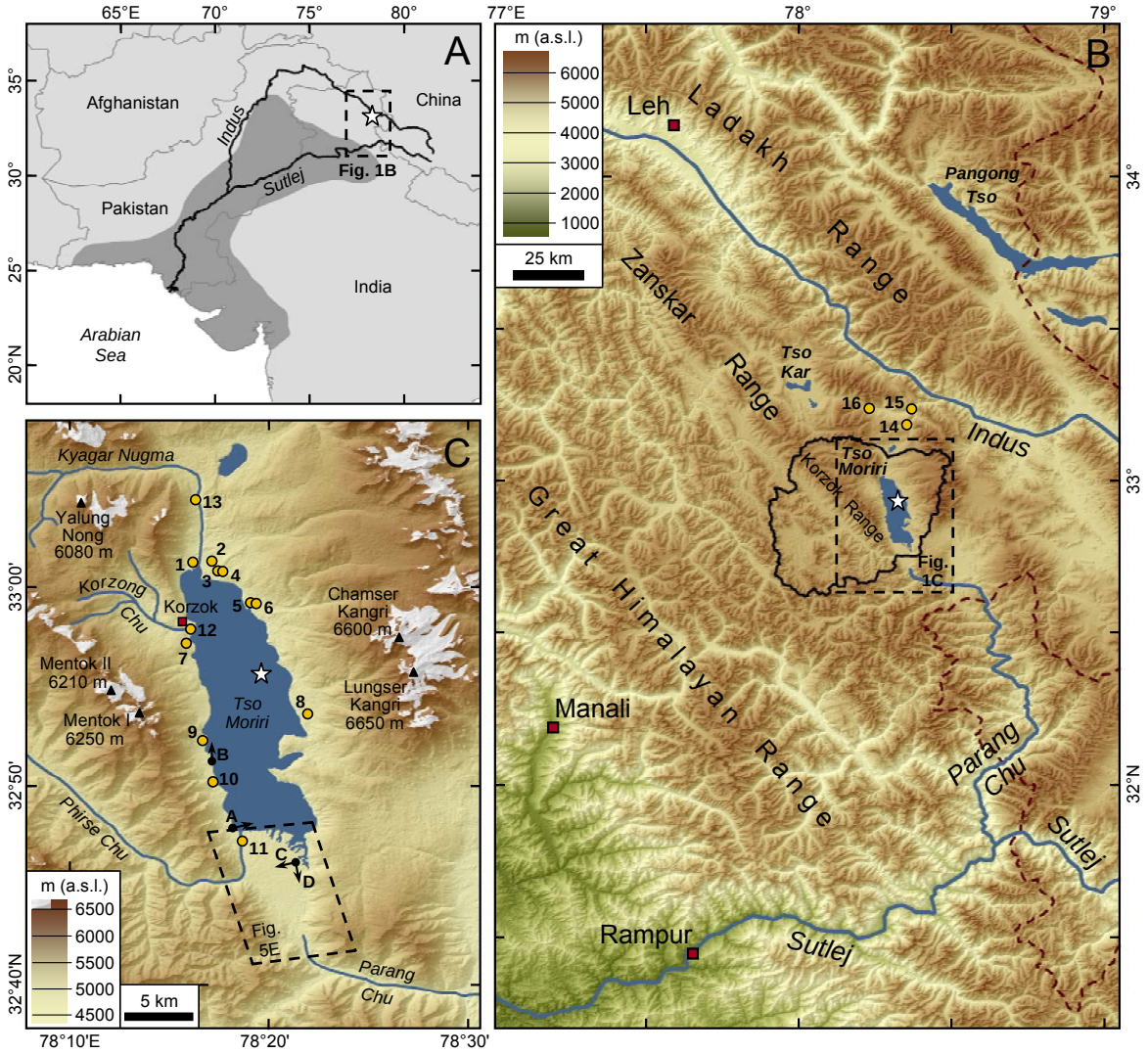

Fig. 3.1 Chart compilation including (A) the geographical distribution of the Mature Harappan Culture (dark grey area, after Kenoyer, 2010) and the location of the study region (inset) in north-western India; (B) topographic map of the study region showing the Tso Moriri watershed (black contour line, after Leipe et al., 2014), rivers discussed in the text and site of the local environment of Tso Moriri (inset) presented in chart (C). Spatial distribution of modern surface pollen spectra is indicated by circles. The TMD coring site is shown by a star. Arrows A–D show position of photographer in Figs. 3.5A–D. Inset in (C) marks the spatial extent of the non-orthorectified CORONA image in Fig. 3.5E. Topography is based on ASTER GDEM V2 data (NASA Land Processes Distributed Active Archive Center, 2011); distribution of snow and ice fields (September 2006) in chart (C) is derived from Landsat 7 ETM+ imagery (NASA Landsat Program, 2009).

of 2–3 psu can be calculated, which is low for an endorheic lake. The pH is ~9 (Hutchinson, 1937; Singh et al., 2008). The vertical distribution of temperature and of oxygen saturation in late August (Hutchinson, 1937) indicates stratification at ~25 m water depth. Water temperature near the surface was 12 °C and 4.8 °C in 50 m water depth (Hutchinson, 1937). The mixing type is unclear but it is possibly monomictic-meromictic. However, during years with a short ice cover period, the lake water may overturn twice (in spring and autumn) and mix completely. The ice cover period is from January/February to April/May, with a range of 75–140 days during 2001–2010 (Lesher, 2011). Despite the oxygen

saturation, which is sufficient in all studied water depths to sustain macro-invertebrates (data in Hutchinson, 1937), we assume a low biodiversity in Tso Moriri. The only group of macro-invertebrates occurring in larger numbers is amphipods, which points to a low macro-invertebrate biodiversity compared to other previously studied high altitude lakes in Ladakh and across the Qinghai–Tibet Plateau (personal observations, F. Riedel, 2008, 2009, 2012, 2013). Concerning phytoplankton, Hutchinson (1937) listed *Oocystis* (Chlorophyceae) and *Cyclotella* (Bacillariophyceae). Zooplankton such as rotifers, cladocerans and copepods were not listed for the lake proper but from the estuary of the northern inflow (see Hutchinson, 1937). Chironomids are mentioned to occur in Tso Moriri (Ramachandra et al., 2011).

The precipitation pattern in the western Himalayas is characterised by pronounced seasonal and spatial variations (Bookhagen and Burbank, 2010). A mean annual precipitation of 248 mm (including rain- and snowfall) can be inferred from the global surface climate dataset (10′ × 10′ resolution) from New et al. (2002), which is averaged over a thirty-year (1961–1990) interval based on meteorological station data. According to the latter dataset, the area around Tso Moriri receives ~70% of its total annual precipitation during June to September (Leipe et al., 2014). Tropical Rainfall Monitoring Mission (TRMM) 2B31 data (Kummerow, et al., 1998) averaged over 10 years (1998–2007) show that the main amount of rainfall (excluding snow precipitation) in the lake area falls during summer (May–October) (Bookhagen and Burbank, 2010). Based on their estimates, Bookhagen and Burbank (2010) suggest that summer rainfall (mainly ISM-derived) decreases rapidly west of 77°E (~120 km west of Tso Moriri), which approximately equals the western boundary of the Sutlej river catchment, where the annual rainfall sum becomes dominated by westerly-derived rainfall. TRMM 2B31 data mainly represent rainfall, thus excluding most snow precipitation (B. Bookhagen personal communication 2013). In contrast to the long-term climate dataset from New et al. (2002), Wulf et al. (2010) calculated average monthly precipitation based on data measured over a ten-year interval (1998–2007) at 16 meteorological stations in the semi-arid to arid Himalayan orogenic interior (70–160 km south–southwest of Tso Moriri) and found that precipitation (including rain- and snowfall) during the cold season (November–April) exceeds that in the warm season (May–October).

The catchment area of Tso Moriri is 2263 km^2 (Leipe et al., 2014). The larger part of it is in the Zanskar Range, particularly in the sub-system Korzok Range (Fig. 3.1B). The maximum elevation of this part of the catchment is the peak of Mentok I at ~6250 m a.s.l. (Fig. 3.1C). Small glaciers exist at Yalung Nong, whose meltwater feeds the perennial Kyagar Nugmar (enters the lake from the north) and at Mentok II within the drainage area of the perennial Korzong Chu which enters the lake near Korzok village in the northwest (Fig. 3.1C). The largest of the three perennial rivers, the southern inflow Phirse Chu, runs

along the south-western and southern flanks of Korzok Range before the main water flow is directed NNW towards the lake. The Phirse Chu alluvium delimits the lake basin in the south. In the eastern part of the catchment area, two larger snow- and ice fields cover the neighbouring peaks of Chamser Kangri (6600 m a.s.l.) and Lungser Kangri (6650 m a.s.l.) (Fig. 3.1C). In September 2013, two small rivers from this sub-catchment were still active while most other river beds entering the lake were already dry. Several large alluvial fans indicate that water flow was much stronger in the past. Based on Landsat image analysis, Lesher (2011) calculated lake area changes from 1972 to 2009 and concluded significant inter-annual lake level fluctuations. Because the nine images analysed were partly from different seasons, Lesher's data, however, may equally describe intra-annual lake level fluctuations.

3.3.2 Natural flora and fauna

Modern vegetation in the Tso Moriri region is represented by desert-steppe and alpine/high alpine steppe communities, which are characteristic for the Trans-Himalayan landscape. In addition to general studies on the vegetation in the north-western Trans-Himalaya (e.g. Polunin and Stainton, 1984) detailed phytosociological records are available for Ladakh (Hartmann, 1983, 1987, 1990, 1995, 1997, 1999; Klimeš, 2003; Klimeš and Dickoré, 2005) including the Rupshu area (Dvorský et al., 2011). Summaries of the main plant community characteristics are outlined in Demske et al. (2009) and Leipe et al. (2014). In this study, we exclusively focus on vegetation types which are related to human activities in the Tso Moriri region.

The alpine environment of Ladakh is a habitat for numerous species of ungulates, rodents, lagomorphs and birds, which affect the regional vegetation by grazing or may influence the nutrient cycle of Tso Moriri and other lakes, respectively. Further details on mammals and birds in the region of Tso Moriri are outlined in Pfister (2004) and Chandan et al. (2008).

3.3.3 Human activities

For the local nomadic pastoralists (Changpas), the Trans-Himalayan region of north-western India represents an important highland grazing system for their livestock (Goldstein und Beall, 1990; Gautam et al., 2007). Today, the tent-dwelling Changpas mainly subsist on different livestock including yak, sheep, goat, donkey and horse (Namgail et al., 2012 and personal observations). These livestock types, which are well adapted to the harsh environmental conditions, strongly depend on the available grazing ground. With almost ten times the population (~200,000) of their wild counterparts,

today's domestic ungulates of Ladakh severely impact the natural vegetation by grazing and trampling (Gautam et al., 2007; Namgail et al., 2009, 2012). Open and closed alpine meadows, which are usually dominated by Cyperaceae (mostly Kobresia) species, are a widespread vegetation type in the Tso Moriri region including the upper Korzong Valley of the Korzong Chu river (Hartmann, 1999). These alpine meadow communities are influenced by grazing and pastoralism (Miehe et al., 2008) constituting important resources for domestic livestock but also wild herbivores (Hartmann, 1997, 1999; Gautam et al., 2007). The principal woody taxa found in the study area are shrubs of Caragana, Astragalus, Ephedra, Krascheninnikovia, Hippophaë and Myricaria, which are intensively harvested as fuel by the local people (Rawat and Adhikari, 2005; Srivastava, 2010; Dvorský et al., 2011; Khuroo et al., 2011). Animal resting places, which are in use throughout the grazing season in summer, represent further plant communities related to human impact, characterised by Knorringia, Aconogonon, Physochlaina, Lindelofia, Microula and several grass taxa including Elymus (Dvorský et al., 2011).

Historically, farming only played a minor role in the area of Ladakh mainly due to the severe environmental conditions along with a short growing season (Namgail et al., 2007). The main crops cultivated in Ladakh are cereals including barley (Hordeum), wheat (Triticum), buckwheat (Fagopyrum) and millet (Panicum) (Bhattacharyya, 1991; Hartmann, 1999). Despite the more recent introduction of improved crop varieties by the regional authorities, agricultural patches cover less than 1% of the Tso Moriri region today (Chandan et al., 2008). Permanent settlements are commonly found in the lower reaches of valleys running towards the major rivers crossing the region. Most other settlements on higher altitudes are seasonal camp sites. One of the few permanent settlements in Rupshu is the village of Korzok on the north-western shore of Tso Moriri (Fig. 3.1C) with its ca. 400 year-old Buddhist temple (gompa) and one of the highest cultivated areas world-wide (Gujja et al., 2003; Gautam et al., 2007).

3.4 Study material and methods

3.4.1 Sampling and chronology

The composite Tso Moriri deep-water core (TMD) was recovered from the north-western part of the lake (32°55'46"N, 78°19'24"E; Fig. 3.1C) at a water depth of 105 m. It provides a continuous sedimentary sequence based on two parallel cores (TM3 and TM4). Further details about core extraction and a rough overview about the lithology are presented in Leipe et al. (2014). The part of the TMD core analysed in this paper has a length of 312 cm. The age–depth model for this section relies on eight AMS ^{14}C dates and has been additionally constrained using pollen-based correlation with the record from Tso

Kar (Demske et al., 2009) situated ~40 km northwest of Tso Moriri (for details see Leipe et al., 2014). For a more precise interpretation of the fossil palynological data from the Tso Moriri TMD core, we collected a total of 166 modern surface pollen samples from the wider study region during several field campaigns between 2007 and 2012. In this study, we selected 16 representative samples from this reference dataset, which are distributed around Tso Moriri and in valleys ~25 km north of the lake (Figs. 3.1B and C). The surface samples were taken from the uppermost layer (~1.5–3 cm) of the top soil following the sampling technique described in Adam and Mehringer (1975).

3.4.2 Hydromorphological analysis

The analysis of hydromorphological features of the Tso Moriri basin is mainly based on personal observations of F. Riedel during a field campaign in September 2013, which are documented by photography, and/or on reported observations from local people and a Manali-based mountaineer, who has tracked the lake area many times during the last two decades. In addition, we utilised non-orthorectified CORONA imagery (entity ID: DS1107-1104DA026) provided by the United States Geological Survey EROS Center (1995) to illustrate the hydromorphological situation of the alluvial fan at the southern end of Tso Moriri.

3.4.3 Palynological analysis

The current research focuses on the analysis of pollen and non-pollen palynomorphs (NPPs) from the Holocene part of the composite TMD core and a set of 16 surface samples from the study area. For the analysis of fossil palynomorphs, volumetric subsamples of 2.31 cm^3, each representing a 2 cm thick sediment layer, were continuously picked from the TMD core sequence by applying the double-L-channel subsampling method (Nakagawa, 2007). Due to lack of sediment material, the uppermost two samples from the core top comprise 2.0 cm^3. To allow pollen and NPP taxa identification, every second sample was submitted to standard laboratory processing including treatment with hydrochloric acid, 50% hydrofluoric acid and ultrasonic fine-sieving on 7 µm meshes (Fægri and Iversen, 1989). The initial treatment with hydrochloric acid allowed estimation of the carbonate content in the sediments. Accumulation rate (influx) can significantly improve the interpretation as it also considers the sedimentation rate. In order to calculate absolute concentrations and influx of palynomorphs, one *Lycopodium* marker spore tablet was added to each fossil sample (Stockmarr, 1971; Maher, 1981). The marker spore frequencies together with estimated ages for the analysed TMD core samples then allowed for the calculation of influx values expressed as number of palynomorphs deposited per square

centimetre per year (n/cm^2/y). Results of the pollen and NPP analysis of the surface samples are presented in percentages. The relative abundance of each terrestrial pollen taxon was calculated based on the sum of all terrestrial pollen taxa excluding indeterminable pollen grains. For aquatic pollen, spores, algae and other NPPs percentages were calculated using the total terrestrial pollen sum, plus the respective subsum.

Altogether, 79 fossil samples were analysed for pollen and NPP assemblages, except for charred and uncharred grass epidermis fragments, which were only counted in every second sample (n = 40). Arboreal and non-arboreal pollen from terrestrial plants were identified to reach a minimum basic sum of 400 grains (for details, see Leipe et al., 2014 and supplementary material published in PANGAEA at doi:10.1594/PANGAEA.808952). Microscopic slides were counted across evenly spaced lines using a light-transmitting microscope (Axiophot, Carl Zeiss) at magnifications of 400× and, in combination with Nomarski Differential Interference Contrast (NDIC), at 600×. The preservation of palynomorphs was mostly good to very good. The determination of pollen types mostly followed Punt et al. (1976–2009), Moore et al. (1991), Gupta and Sharma (1986) and Beug (2004). Identification of NPPs was based on a variety of publications referring to fern plant spores (Sorsa, 1964), algal remains (Jankovská and Komárek, 2000), charred and non-charred grass epidermis fragments (Ralska-Jasiewiczowa and van Geel, 1992) and other palynomorphs (van Geel 1978, 1986, 1989, 2001, 2003; Pals et al., 1980). The complete pollen and NPP datasets of the Holocene TMD section are published as supplementary data in the PANGAEA Open Access information system at doi:10.1594/PANGAEA.808958 and at doi:10.1594/PANGAEA.829753.

The distinguished Poaceae pollen types comprise undifferentiated small grains (Poaceae undiff.) and larger grains of the wild grass type and cereal type. Cereal type pollen were identified on the basis of the grain size (>37 µm) and characteristics of the anulus (Beug, 2004). For the surface samples we used a lower grain size limit of 40 µm, in order to enhance the confidence of correct identification. The wild grass type pollen have a grain size >37/40 µm but do not meet the criteria for the cereal type anulus characteristics.

The identification of fungal spores was limited to endomycorrhizal *Glomus* chlamydospores and ascospores of coprophilous taxa given in van Geel et al. (2003) indicated as HdV (Hugo-de-Vries Laboratory, University of Amsterdam, The Netherlands) type, which include *Sporormiella* (HdV-113), *Sordaria* (HdV-55A) and *Gelasinospora* (HdV-1) (van Geel, 1978). Coenobia of *Pediastrum*, which could only partly be determined (see supplementary data for further details), mainly include *P. orientale* and *P. boryanum* (including var. *longicorne*), but also a substantial fraction of crumpled undifferentiated remains. Therefore, only the summary curve is presented in this paper.

Pollen and NPP taxa identified in the surface samples are presented in one diagram (Fig. 3.2), whereas fossil palynomorphs related to the terrestrial (Fig. 3.3) and limnic

environment (Fig. 3.4) are shown separately in order to facilitate presentation and discussion of the results. For the purpose of the current study, selected pollen taxa (Fig. 3.2 and 3.3) are grouped in several categories potentially relevant in terms of past human activities at regional to local scale. Pollen types of woody taxa are grouped according to their upper altitudinal distribution limits (Fig. 3.3), including a *Betula* zone (including *B. utilis*; <3200 m a.s.l.), a *Juniperus* zone (*Juniperus* type, *Rosa* type, *Spiraea* type, *Myricaria* type, *Tamarix* type, *Lycium* type, *Capparis* type, *Viburnum*; <3500 m a.s.l.), a *Sorbus* zone (*Sorbus/Cotoneaster* type, *Hippophaë*, *Salix*, *Anemone/Clematis* type, *Berberis*, *Rhododendron*, *Thymelaea* type; <4000 m a.s.l.) and a *Lonicera* zone (*Lonicera*, Ericaceae undiff. including *Cassiope*, *Ribes*; ca. >4000 m a.s.l.) (Klimeš and Dickoré, 2005; Khuroo et al., 2011). *Astragalus/Oxytropis* type (partly including *Caragana* pollen), *Caragana* type and *Ephedra* are shown separately for discussing potential alpine wood resources (Srivastava, 2010). The NPP diagram (Fig. 3.4) contains grouped aquatic life forms, fungal and moss spores and unidentified NPPs.

3.5 Results

3.5.1 Hydromorphological analysis

Information on seasonal lake level fluctuation was obtained from local people (September 2013) and inferred from shore zone observations and analyses. During the last decades the lake level varied within a range of 1–3 m, with a high stand in June/July when melt water inflow and rainfall peak. In late summer and autumn, evaporation dominates over precipitation, and a low lake level is reached in December before the lake freezes. Geomorphic features on the south-western shore can be related to such short-term lake level fluctuations. The high level is featured by a pronounced gravel beach delimiting a lower lying stretch of hummocked earth with minor shore-line features intercalated (Fig. 3.5A). The hummocked earth is free of marmot and pika burrows, which can regularly be found in areas which are not periodically flooded. This interpretation was confirmed by Mehar Chand (Mountaineering Institute Manali) who passed this area repeatedly in July.
Long-term lake level fluctuation could not be examined in detail and the study was confined to geomorphic features above modern lake level. There is no evidence of palaeo-shoreline features higher than 6–7 m above the September 2013 lake level. Palaeo-estuary deposits near the western shore (Fig. 3.5B) exhibit the interaction of shallow riverine inflow and lake water at this level. Palaeo-beaches and erosional features at 6–7 m above the September lake level can be traced along the slopes and the mountain range, which is delimiting the wetland south of the lake. This wetland has formed along the edge of the northern and north-western part of the large alluvial fan bounding the lake basin to the

south. The alluvial fan is very gently down-sloping from the valley of Phirse Chu (Fig. 3.5C). Its central sector forms the watershed. About 2 km northeast of the distal central alluvium, the continuation of the erosional line, which is 6–7 m above the lake surface, levels at ~2 m above the front of the fan. Across the watershed, a shallow channel (Fig. 3.5D) indicates former surface outflow to the south into the Parang Chu Valley. Analysis of a CORONA image (Fig. 3.5E) shows that the ground along the lower lying front of the alluvial fan is water saturated. The orientation of channels in the southern part of the alluvium indicates that subsurface flow is feeding Parang Chu (Fig. 3.1C), which is a tributary of the Sutlej River (Fig. 3.1B). Mehar Chand (personal communication) who has trekked across this area many times over the last two decades, reported in September 2013 that during seasonal Tso Moriri high stands lake water flowed into Parang Chu.

3.5.2 Palynological analysis of modern surface samples

An overview of the palynomorph assemblages of the 16 selected modern surface samples from the wider Tso Moriri area is given in a percentage diagram (Fig. 3.2). The samples are arranged according to the collecting locations (Figs. 3.1B and C) into six groups including a northern area (20–25 km north of Tso Moriri), the Korzok area, and areas northwest, southwest, northeast and east of Tso Moriri. The cultivation of cereals (mostly *Hordeum*) is reflected in the pollen spectra from the village of Korzok and its vicinity (samples no. 1, 7 and 12). Especially, sample number twelve, from the area known to be currently used for crop cultivation (personal observations), shows a high frequency of the cereal pollen type. This coincides with similarly high pollen abundance of the wild grass type, which shows a wider spatial coverage. The presence of *Cannabis* type pollen (sample no. 10, 11 and 14) does not show a spatial distribution related to human settlements. Pollen of *Aconogonon* and *Physochlaina* type are more frequently found in samples from locations in the northern part of the study area (samples no. 13, 15 and 16), where nomadic camp sites were present in summer 2011 (personal observations). *Aconogonon* is also recorded in the pollen assemblages (no. 4–6 and 8) from the eastern and north-eastern shore area of Tso Moriri. The abundances of these pollen types coincide with presence of *Knorringia*, *Thalictrum* and Gentianaceae type pollen. Several samples (1–6, 11 and 13–15) from sites, which are temporarily moist or submerged, expose a significant percentage of algae.

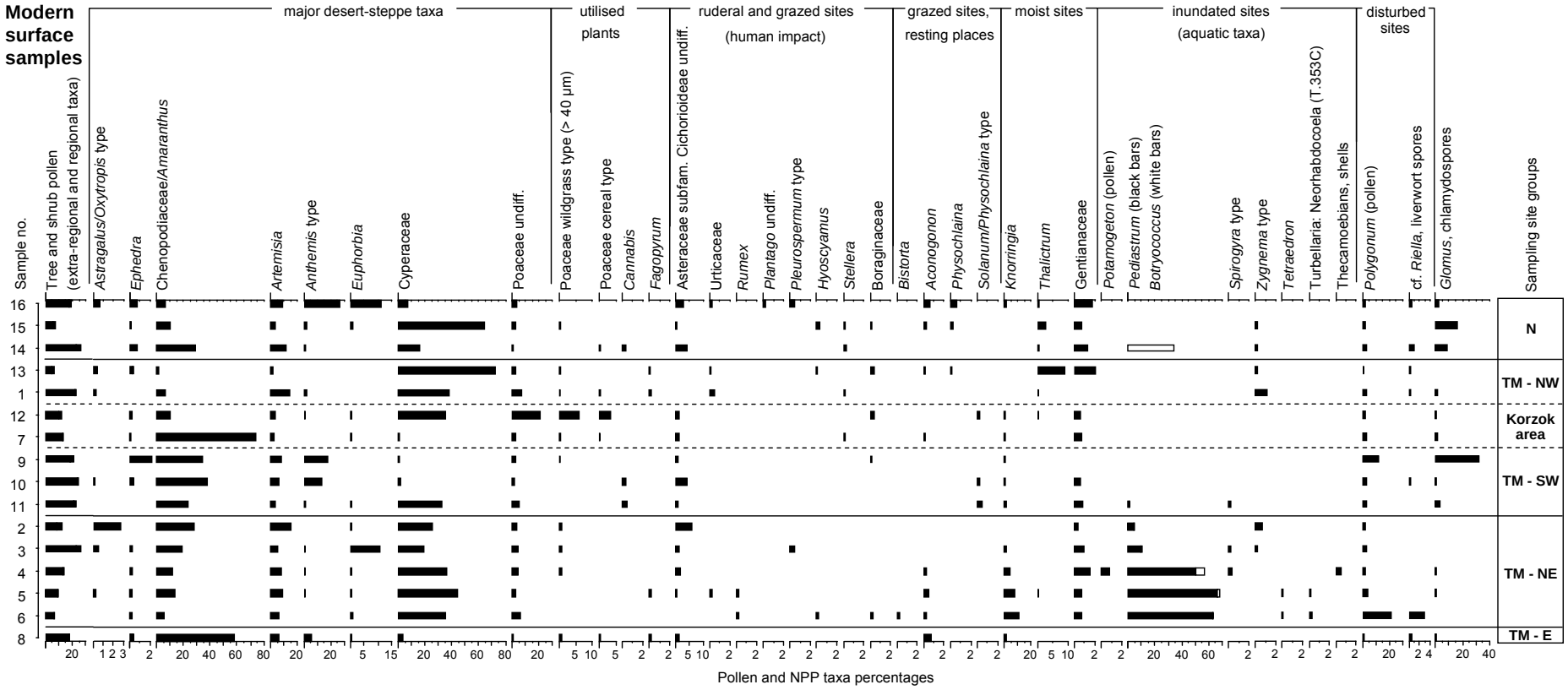

Fig. 3.2 Diagram illustrating the percentage abundances of selected identified palynomorphs for the analysed set of 16 modern surface samples from the Tso Moriri (TM) area (see Fig. 4.1B and C for geographical distribution). Samples are grouped according to the collecting locations including a northern area (ca. 20–25 km north of Tso Moriri), the Korzok area, and areas northwest, southwest, northeast and east of Tso Moriri. Percentages are calculated based on the sum of all terrestrial pollen plus subsums of aquatics pollen, spores, algae and other non-pollen palynomorphs (NPPs). Taxa are grouped in the context of wood resources, human impact and grazing as well as in relation to moist, inundated or disturbed sites.

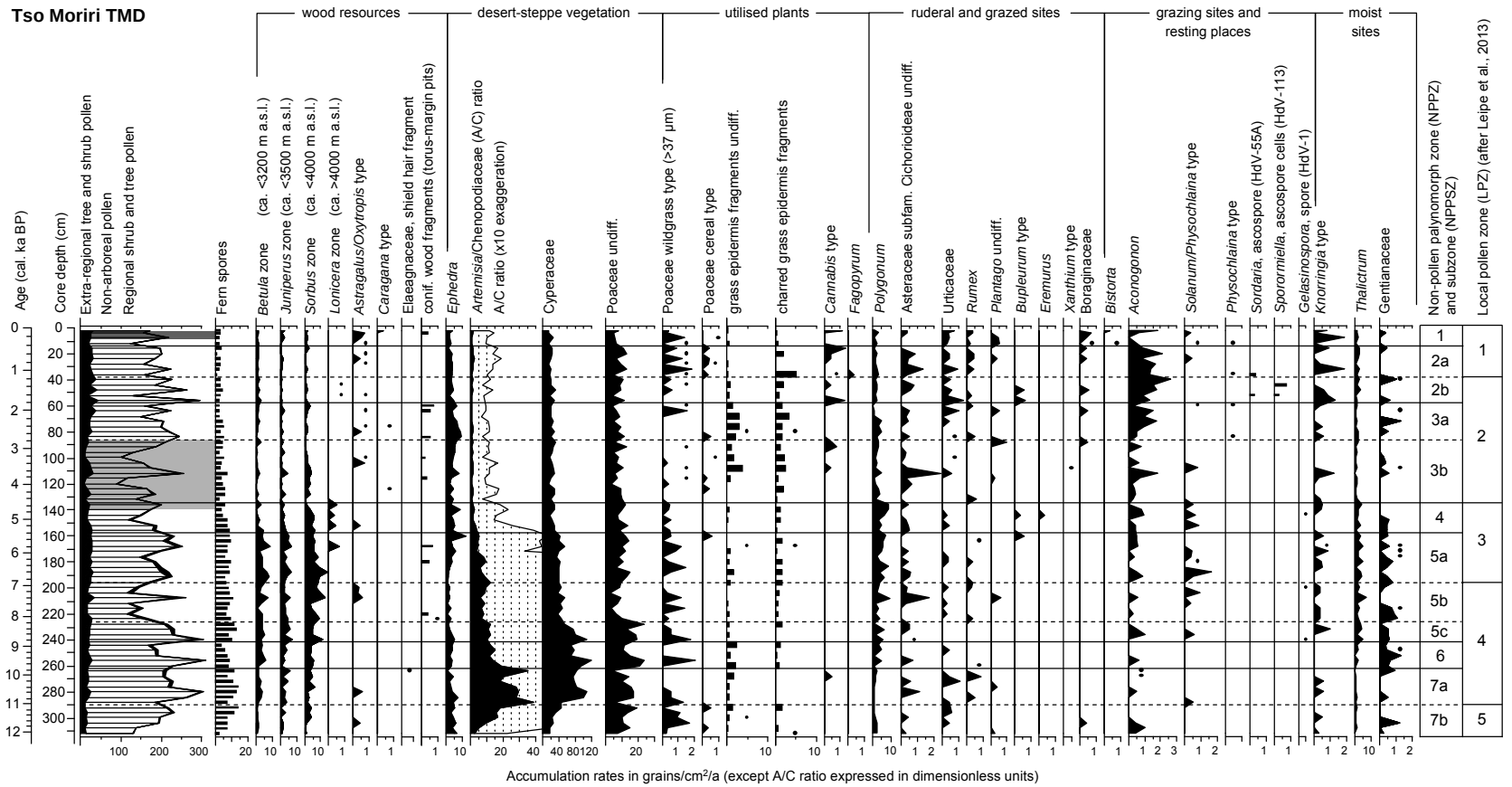

Fig. 3.3.Diagram showing assemblages of selected terrestrial pollen types (after Leipe et al., 2014) and non-pollen palynomorph taxa (this study) based on 79 fossil palynomorph spectra from the Tso Moriri TMD core thematically grouped into potential wood resources, human impact and grazing intensity. Pollen data are shown as silhouette curves, non-pollen palynomorph taxa as histogram bars. Dots indicate additional observations beyond the regular count. Pollen types of woody taxa are grouped into zones according to their altitudinal distribution limits, including a Betula zone (including B. utilis), a Juniperus zone (Juniperus type, Rosa type, Spiraea type, Myricaria type, Tamarix type, Lycium type, Capparis type, Viburnum), a Sorbus zone (Sorbus/Cotoneaster type, Hippophaë, Salix, Anemone/Clematis type, Berberis, Rhododendron, Thymelaea type) and a Lonicera zone (Lonicera, Ericaceae undiff. including Cassiope, Ribes). Both, local pollen zones (LPZs, solid lines) adopted from Leipe et al. (2014) and non-pollen palynomorph zones (NPPZs, solid lines) and subzones (NPPSZs, dotted lines) visually defined in this study are given for better orientation. Intervals of glacial advance in the Korzong and Puga Valley (Hedrick et al., 2011) discussed in the text are indicated by a light and dark grey bar, respectively.

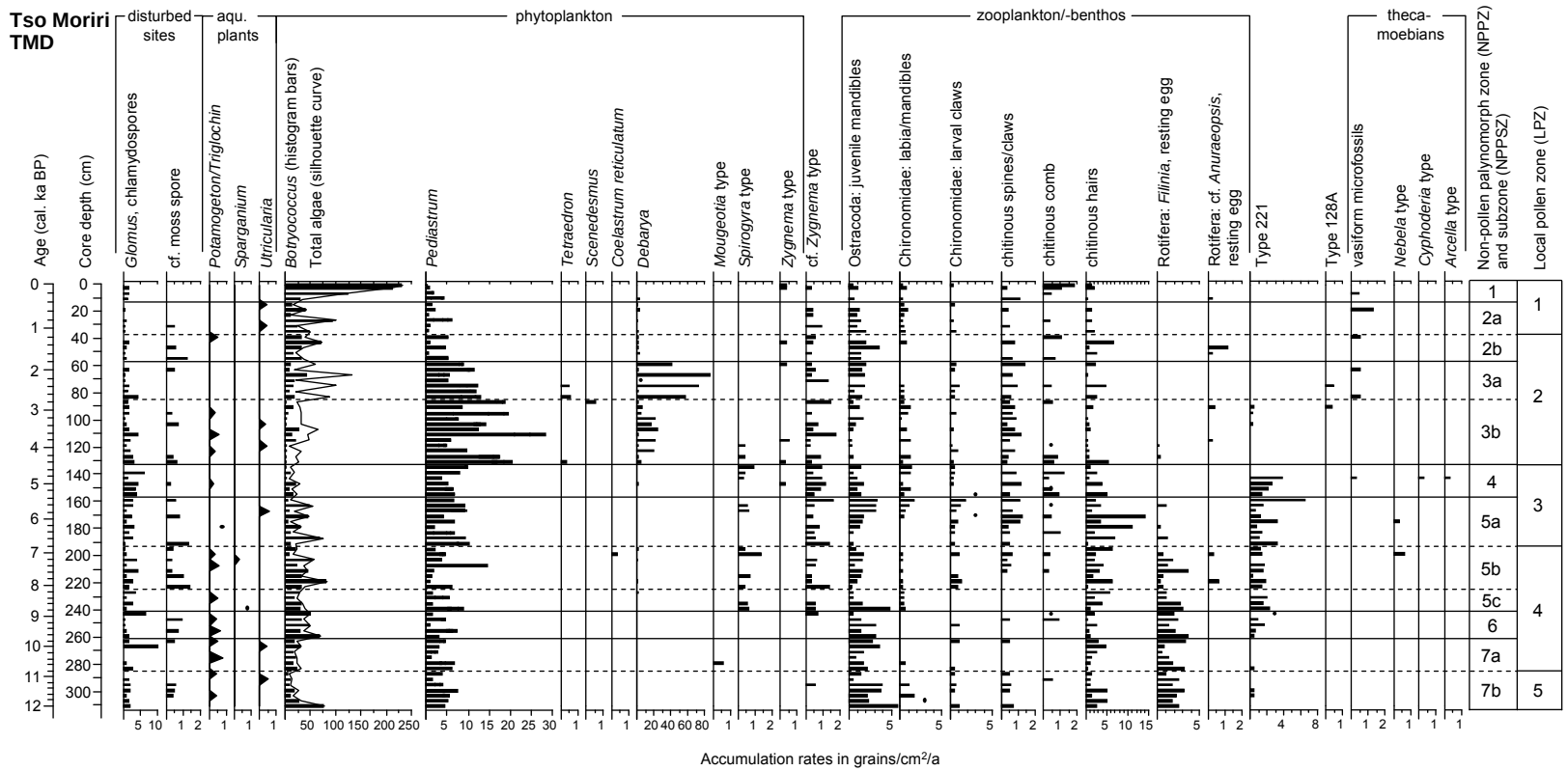

Fig. 3.4 Diagram showing assemblages of selected non-pollen palynomorph taxa (this study) and terrestrial pollen types (after Leipe et al., 2014) based on 79 fossil palynomorph spectra from the Tso Moriri TMD core used to reconstruct variations in palaeolimnological conditions. Pollen data are shown as silhouette curves, non-pollen palynomorph taxa as histogram bars. Dots indicate additional observations beyond the regular count. The *Pediastrum* curve includes influx values of *Pediastrum orientale*, *P. boryanum* and *P.* undiff. Both, local pollen zones (LPZs, solid lines) adopted from Leipe et al. (2014) and non-pollen palynomorph zones (NPPZs, solid lines) and subzones (NPPSZs, dotted lines) visually defined in this study are given for better orientation.

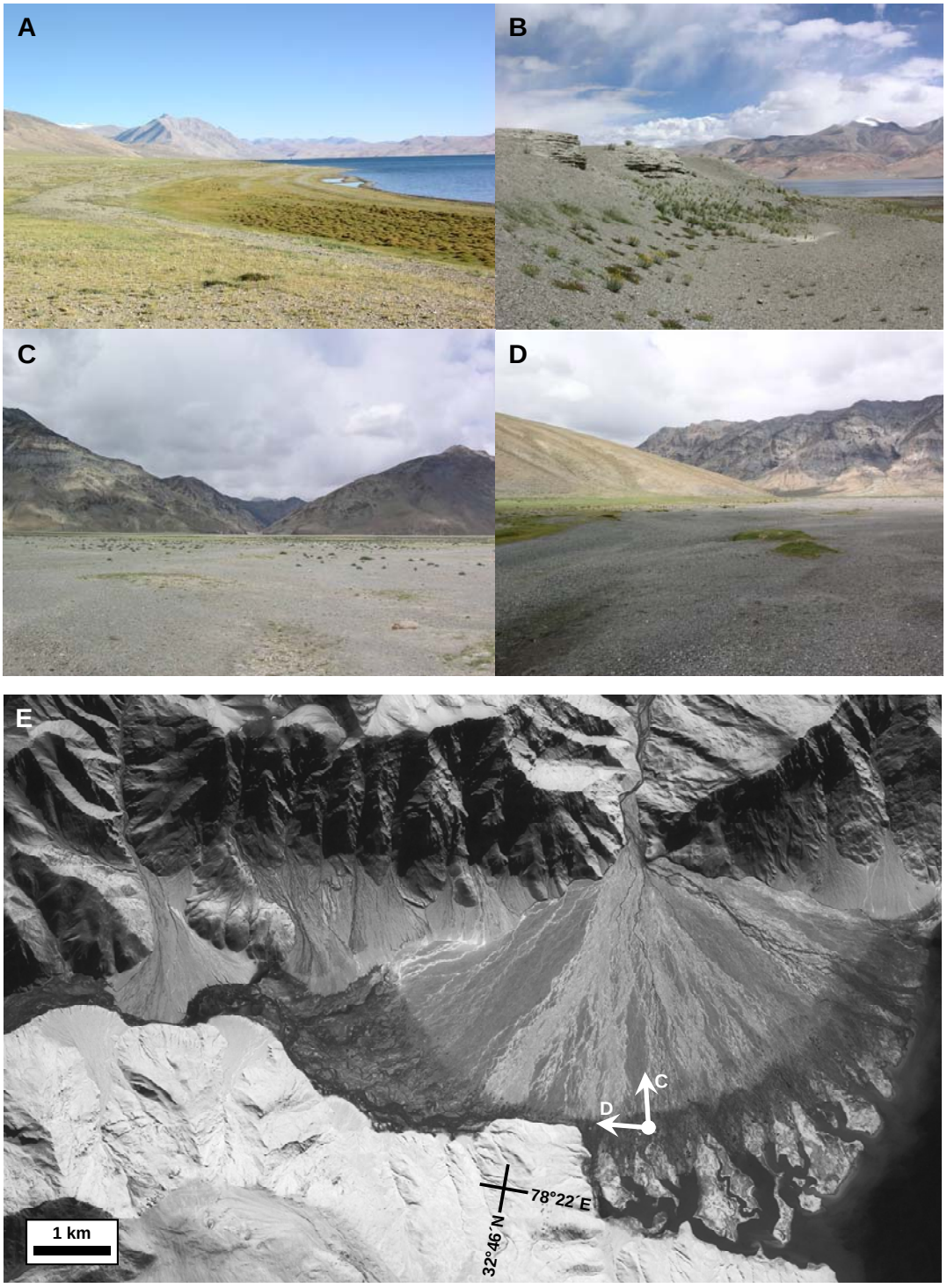

Fig. 3.5 A: Inter- and intra-annually active beach zone of Tso Moriri, characterised by earth hummocks and absence of mammal burrows; B: The top of fluvio-lacustrine, palaeo-estuarine sediments is located 6–7 m above early September lake level indicating the maximum palaeo-highstand of Tso Moriri; C: The alluvial fan of the river Phirse Chu is very gently sloping; D: Geomorphic evidence for a former outflow of Tso Moriri along the lowest part of the Phirse Chu alluvial fan. E: Clip of a non-orthorectified CORONA image (entity ID: DS1107-1104DA026; United States Geological Survey EROS Center, 1995) taken on 30th July 1969 showing the alluvial fan of Phirse Chu which delimits Tso Moriri to the south. Photos were taken in 2013 on September 4 (B), September 5 (C and D) and September 6 (A); positions of photographer and directions of view (A–D) are indicated in E and Fig. 3.1C.

3.5.3 Palynological analysis of the TMD sediment core

The record of terrestrial pollen from the TMD core covers the last ca. 12 cal ka BP as outlined in Leipe et al. (2014). In this section, we present the assemblages of (a) terrestrial pollen, coprophilous fungi and grass remains, which are potentially relevant in terms of past human activities (Fig. 3.3), along with (b) aquatic pollen, spores of mosses and fungi, remains of algae, Ostracoda, Chironomidae, Rotifera and other aquatic and terrestrial organisms (Fig. 3.4), which are used for the reconstruction of limnological conditions. A total of 141 terrestrial pollen types (Leipe et al., 2014) and 78 types of NPPs (see Supplementary material for further details) were identified. Local pollen zones (LPZs) in Fig. 3.3 were adopted from Leipe et al. (2014). Palynostratigraphic intervals of NPP assemblages (NPP zones and subzones) in Fig. 3.4 were visually delineated. Both zonations are shown in each diagram.

The influx of extra-regional arboreal pollen shows only minor variations along the entire record with slightly higher values in the upper part (ca. 2.7–0 cal ka BP). More pronounced changes are recognised for the accumulation of the (mostly regional) herbaceous taxa, which varies between ca. 80 and 270 grains/cm^2/y, showing several clear minima. The abundances of spores show a long-term decrease, with high values until ca. 5 cal ka BP corresponding to the maxima in pollen of regional alpine woody taxa (including taxa of the *Juniperus* zone and *Sorbus* zone). The sequence of NPP zones (NPPZs) and subzones (NPPSZs) follows prominent changes in fossil NPP assemblages, which are compared to the record of selected pollen types within corresponding sections of the local pollen zones (Figs. 3.3 and 3.4).

NPPSZ 7b (312–285 cm; ca. 12–10.8 cal ka BP) is characterised by decreasing abundances of *Botryococcus*, *Pediastrum* and ostracod remains. *Filinia* resting eggs remain at a constant proportion. Pollen numbers of the woody taxa *Juniperus* and *Sorbus* are slightly rising. Pollen grains of ruderal plants are mostly absent. Poaceae wild grass type pollen is relatively abundant. Pollen assigned to the cereal type occurs in this zone.

In NPPSZ 7a (285–261 cm; ca. 10.8–9.7 cal ka BP) influx of *Botryococcus* and *Pediastrum* is relatively low. *Glomus* chlamydospore abundances show high variations but are mostly comparatively low. Ostracoda values increase in this zone. In the lower part of LPZ 4 pollen abundance of Poaceae wild grass type is very low. Pollen of taxa assigned to regional wood resources (i.e. *Betula*, *Juniperus* and *Sorbus* zones) show a slight increase.

NPPZ 6 (261–241 cm; ca. 9.7–8.8 cal ka BP) is marked by increased influx values of *Botryococcus* and the appearance of the undetermined Type 221 and cf. *Zygnema*. *Filina* is detected in high abundances while ostracod remains diminish. The upper part of LPZ 4 shows a slight increase in *Thalictrum* abundance. In this zone, Gentianaceae shows the

highest influx values along the record. Pollen abundances of regional woody taxa (*Juniperus* zone and *Sorbus* zone) remain unchanged.

In NPPSZ 5c (241–225 cm; ca. 8.8–8.1 cal ka BP) *Spirogyra* type first appears. Ostracod remains and *Filinia* resting eggs decrease. In this part of LPZ 4 the accumulation rates of *Juniperus* and *Sorbus* zones continue to slightly rise while pollen of *Ephedra* shows decrease in abundance.

NPPSZ 5b (225–193 cm; ca. 8.1–6.8 cal ka BP) exhibits distinctly lowered pollen accumulation rates (increased sediment accumulation rates) which coincide with very low abundances of *Pediastrum*, reduced frequencies of *Filinia* and presence of cf. *Anuraeopsis* resting eggs (Rotifera). While abundances of ostracod remains are comparatively low, numbers of zooplanktonic and other zoobenthic microfossils rise. The influx of the *Sorbus* zone continues to increase in the uppermost part of LPZ 4. *Ephedra* abundance reaches the lowest level of the record. In this zone, pollen of *Solanum*/*Physochlaina* type starts to appear more regularly than in the lower part of the record.

In NPPSZ 5a (193–157 cm; ca. 6.8–5.4 cal ka BP) *Botryococcus* slightly diminishes and *Pediastrum* shows an increase. *Filinia* resting eggs decline in abundance and appear only sporadically. By contrast, ostracods, chironomids and other chitinous remains appear more abundantly in the spectra. In this part of LPZ 3 regional shrub and tree pollen influxes are highest of the entire record; *Thalictrum* and Gentianaceae are continuously very abundant and *Ephedra* abundances start to increase.

NPPZ 4 (157–133 cm; ca. 5.4–4.5 cal ka BP) is characterised by the increase in *Pediastrum* remains, lack of *Filinia* and the decline and disappearance of organisms represented by Type 221, as well as by decreased abundances of ostracod and chironomid remains. Within the upper part of LPZ 3 frequencies of *Polygonum* pollen reach maximum levels.

The most distinctive feature of NPPSZ 3b (133–85 cm; ca. 4.5–2.7 cal ka BP) is the strong increase of *Pediastrum* and the minimum influx of *Botryococcus*. In addition, *Debarya* appears in considerable frequencies while *Spirogyra* vanishes. *Glomus* chlamydospores start to appear in smaller numbers. In most samples, Type 221 is absent. In this section, corresponding to the lower part of LPZ 2, regional arboreal taxa are represented by significantly lowered abundances. However, pollen grains of *Astragalus/Oxytropis* type and *Ephedra* are noted more regularly.

NPPSZ 3a (85–57 cm; ca. 2.7–1.8 cal ka BP) is delineated by highest frequencies of *Debarya*, presence of *Tetraedron* and relatively high influx rates of ostracod remains. While *Pediastrum* remains abundant, *Botryococcus* is slightly increasing. In the corresponding part of LPZ 2, *Aconogonon* shows high influx for the first time. Highest influx rates for *Ephedra* are encountered.

In NPPSZ 2b (57–37 cm; ca. 1.8–1.1 cal ka BP) *Botryococcus* and *Pediastrum* show opposite trends towards higher and lower abundances, respectively. *Debarya* influx

dropped sharply and is considerably lower compared to NPPZ 3a. Spores of coprophilous fungi are first time recorded in this zone. This is related to increasing frequencies of *Aconogonon* pollen in the upper part of LPZ 2.

In NPPSZ 2a (37–13 cm; ca. 1.1–0.4 cal ka BP), compared to the preceding zone, *Botryococcus*, *Pediastrum* and *Debarya* abundances remain unchanged. Both Poaceae wild grass and cereal type pollen influx are relatively high and regular. In this part of LPZ 1 pollen of *Cannabis* type and *Fagopyrum* are present in the record. *Aconogonon* accumulation rate diminishes, but remains on comparatively high levels.

NPPZ 1 (13–0 cm; ca. 0.4–0 ka BP) is characterised by strongly rising frequencies of *Botryococcus* and further decreasing of *Pediastrum*. Poaceae wild grass and cereal type pollen are also present in this part of LPZ 1. *Aconogonon* influx varies strongly with comparatively low influx values.

3.6 Interpretation and discussion

3.6.1 Hydromorphological analysis

There is no indication that the level of Tso Moriri has ever been higher than 6–7 m above modern lake level. This is due to the low, broad and gently sloping alluvial fan of Phirse Chu delimiting the lake to the south. The surface outflow has probably been activated at levels 4–5 m above modern lake level. Adding another 2 m of water to the lake level, the outlet would become significantly wider preventing the lake level from further increase. The outlet was thus able to constrain the lake level even during periods of particular high inflow. Considering the hydromorphology of the alluvial fan, it is not likely that in present times Tso Moriri has a surface outflow every late spring–early summer but possibly during years with exceptionally high amounts of melt water and atmospheric precipitation. The outflow observed by mountaineering people is related to Parang Chu, which emerges from Phirse Chu water penetrating through the alluvial sediment but also receives subsurface water originating from Tso Moriri by flowing through the distal alluvial fan into Parang Chu. This small scale regular seasonal outflow in combination with a larger scale periodical surface outflow probably explains why Tso Moriri is only slightly saline. On the other hand, it also explains why Tso Moriri is not a freshwater lake. That Tso Moriri is not a freshwater lake is probably also related to former low lake levels preventing any outflow. During such periods of low lake levels, salinity would increase significantly. An indication for repeated former low stands in combination with increased salinity might be the presumed low modern macro-invertebrate diversity likely reflecting an ecologically unstable system (Filippov and Riedel, 2009) characterised by environmental changes to which gastropods such as *Radix* and *Gyraulus*, which are widely distributed across the

Tibet Plateau (von Oheimb et al., 2011, 2013), cannot adapt (ecological traits of Tibetan Plateau *Radix* summarised in Taft et al., 2012). Potential colonisation of Tso Moriri by such molluscs characteristic of oligohaline environments has probably been difficult or only short-term.

3.6.2 Holocene environmental and limnological evolution of the Tso Moriri basin

Pollen-inferred vegetation changes (Bhattacharya, 1989; Demske et al., 2009) and precipitation reconstructions (Leipe et al., 2014) indicate an early Holocene climatic amelioration likely due to the warming and strengthening of the ISM in the high mountain region of Rupshu in the NW Himalayas. The following moist interval, which continues until the middle to late Holocene transition (ca. 11.5–4.5 cal ka BP), is characterised by an expansion of relatively moist desert steppe communities, grassland and meadows in the study region (Leipe et al., 2014). After ca. 4.5 cal ka BP, moisture availability in the Tso Moriri region became considerably lower. This is designated by high abundances of Chenopodiaceae and reduced values of Poaceae and *Artemisia* pollen (Leipe et al., 2014). This climate change towards aridity is well documented by the TMD *Artemisia*/Chenopodiaceae (A/C) ratio (ranging between 0.68 and 1.9; Fig. 3.3), commonly used as a moisture index in arid environments (e.g. El-Moslimany, 1990), and annual precipitation reconstruction (Leipe et al., 2014).

During the early to middle Holocene interval (ca. 12–4.5 cal ka BP; NPPZ 7–4), relatively low influx values of algae remains of *Botryococcus* and *Pediastrum* are recorded. The low abundances of these taxa can tentatively be associated with nutrient poor freshwater lakes (Jankovská and Komárek, 1995, 2000; Kuhry, 1997). This interpretation would also explain the pronounced minima in the *Botryococcus* curve (Fig. 3.4) during the phase of reconstructed maximum humidity (up to ca. 600–680 mm mean annual precipitation) between ca. 11–9.6 cal ka BP (upper NPPSZ 7b–7a) (Leipe et al., 2014). These findings corroborate the inferred interval of enhanced precipitation (ca. 11.5–4.5 cal ka BP; upper NPPSZ 7b–NPPZ 4), which presumably led to open lake (exorheic) conditions and a reduced residence time induced by a rising lake level and the consequent surface outflow via the detected channel on the alluvial fan at the southern end of Tso Moriri (Figs. 3.5D and E). In contrast to low algal abundance, remains of zooplanktonic and zoobenthic taxa, especially of ostracods (juvenile mandibles) and *Filinia* (Rotifera) are recorded in high frequency. During the interval ca. 12–4.5 cal ka BP, ostracod remains show highest abundances including some minor trends. The latter may point to changes in lake level and/or salinity. However, since taxa differentiation was not conducted, the ostracod mandible assemblages cannot be further interpreted. The growth of *Filinia* (ca. 12–6.8 cal ka BP; NPPSZ 7b–5b) might be promoted by a somewhat higher water

temperature and shorter ice cover period (Gauthier et al., 2010) in response to enhanced early Holocene summer insolation (Berger and Loutre, 1991). Earlier studies have shown that Rotifera sensitively react to temperature changes (Andrew and Fitzsimons, 1992) and that some *Filinia* species are associated with warmer water bodies (Basińska et al., 2010). Chironomidae are widely used in lacustrine palaeoenvironmental studies for reconstructing e.g. water temperature, salinity and lake productivity (Walker, 2001 and references therein). A limnological interpretation of the chironomid assemblages in the TMD samples was not conducted, since a more detailed identification of their remains to genus or species level is not feasible.

The appearance of the *Spirogyra* type (Zygnemataceae) at ca. 8.8–6.6 cal ka BP (NPPSZ 5c–upper NPPSZ 5b), after the interval of maximum humidity, might be related to water conditions of lowered pH values and likely augments the evidence for enhanced freshwater influx to the lake. Many of the Zygnemataceae are reported to be acidophilic and abundant in acidic habitats (Zippi et al., 1991 and references therein). Low-pH conditions are typical for high-altitude cold-water bodies with a low photosynthetic activity and low concentration of other green algae (Kramer et al., 2010). Interestingly, the attendance of the yet unidentified Type 221 (e.g. van Geel et al. 1989, van Geel, 2001) is more or less isochronous with that of *Spirogyra*. As the origin of this microfossil remains unknown, its record does not allow a reliable limnological interpretation, but clearly delimits a middle Holocene palaeolimnic interval comprising NPPZs 3–5 (Fig. 3.4).

The NPPZ 4 (ca. 5.4–4.5 cal ka BP) is marked by a climatic transition towards significantly more arid conditions (Leipe et al., 2014). This is accompanied by the decrease in *Botryococcus*, a slight increase in *Pediastrum* and the abrupt decline of NPP Type 221, which likely point to changing limnological conditions driven by aridification. The aridification trend, which is characterised by reduced precipitation and/or reduced meltwater flow, is supported by increased abundances of *Glomus* chlamydospores, which are associated with roots of various terrestrial plants (van Geel, 2001). The increase in *Glomus* probably indicates intensified soil erosion by wind during this interval due to a more reduced vegetation cover than during the previous moister interval (ca. 11.5–5.4 cal ka BP; Leipe et al., 2014) where *Glomus* influx was generally lower. Correspondingly, Kramer et al. (2010), who studied an NPP record from a lake on the south-eastern Qinghai–Tibet Plateau, argue that enhanced *Glomus* influx is related to sparse vegetation cover due to increased aridity.

The following interval ca. 4.5–1.8 cal ka BP (NPPZ 3) is characterised by substantial changes in the phytoplankton composition. We assume that the maximum abundance of *Pediastrum* along with the presence of different genera of green algae (*Tetraedron*, *Scenedesmus* and *Debarya*) indicate reduced inflow of freshwater combined with enrichment of nutrients from nearby terrestrial surfaces. Fossil *Debarya* zygospores, which

show highest influx values during NPPSZ 3a (ca. 2.7–1.8 cal ka BP), have been recorded in palaeoenvironmental settings of shallow sandy pools (van Geel et al., 1989), and are observed in both fossil sediments and surface samples of high-mountain zones in the Colombian and Venezuelan Andes (van Geel and van der Hammen 1978; Montoya et al., 2010; Kołaczek et al., 2012).

Although observed ca. 1 ka earlier (ca. 5.5 cal ka BP), a comparable onset of decreasing *Botryococcus* influx is found in the NPP record from the neighbouring (~40 km northwest of Tso Moriri) lake Tso Kar (Wünnemann et al., 2010), indicating a tendency towards lowering of the lake level caused by a relatively dry climate. In the Tso Kar record, this decline in lake level was accompanied by highest water salinity values reconstructed after ca. 4.2 cal ka BP (Wünnemann et al., 2010). Increased salinity caused by reduced freshwater influx was probably also a feature of Tso Moriri during the interval of highest aridity (ca. 4.5–1.8 cal ka BP; NPPZ 3). This would well agree with our hypothesis that the modern lake's low salinity and low biodiversity are due to prolonged endorheic conditions in the past.

Interestingly, there is evidence for glacial advance in the Korzong (Chu) Valley (Fig. 3.1C) which was dated to ca. 4.7–2.7 ka BP (Fig. 3.3) based on ^{10}Be dating of moraine boulders, with an average exposure age of 3.6 ±1.1 ka BP (Hedrick et al., 2011). This is overlapping with the age of glaciation in the Puga Valley ~25 km north of Tso Moriri, which is documented between ca. 7.6–2.1 ka BP, with an average age of 4.2 ±2.2 ka BP (Hedrick et al., 2011). Given these average ages, which correspond well to NPPSZ 3b (ca. 4.5–2.7 cal ka BP), the glacial phase might corroborate the inferred low level of freshwater input when assuming enhanced glacial accumulation of winter precipitation in the Tso Moriri catchment. Evidence for climatic deterioration in the TMD pollen record is given by peak abundance of Cichorioideae pollen (Fig. 3.3), likely related to a spread of pioneer vegetation on bare ground, and two minima in pollen accumulation rates during NPPSZ 3b.

However, the ^{10}Be ages from the Korzong Valley need to be considered with caution. The distinct boulder moraine ~3 km northwest of Lake Tso Moriri, that blocked the narrow Korzong Valley there, was not described and dated by Hedrick et al. (2011). Due to the shape and unweathered surfaces of the moraine's granite boulders, it may represent a glacier advance during the late-glacial period. This moraine is located between the stratigraphically corresponding moraine complex KM-1 further upstream that was dated between ca. 12.5–135 ka (mean age ca. 80 ka; Hedrick et al., 2011) and the oldest moraine boulders (KM-0) with a mean age of ca. 310.5 ±4.1 ka situated further downstream, thus younger than the two latter moraine fields. The reason for this may be that the identified moraine represents a younger advance which overrun the moraine complex KM-1 or that the KM-1 average age given by Hedrick et al. (2011) is too old. This demonstrates the need

for further glaciological studies to establish a more reliable glacial chronology for the Korzong Valley.

Starting at ca. 4.5 ka BP towards the TMD core top, *Glomus* continuously shows lowered accumulation rates. We hypothesise that this is caused by a reduced vegetation cover in combination with decreased atmospheric precipitation (i.e. surface runoff) which led to reduced transportation of erosional matter (organics, humic acids) into the lake. After a phase (ca. 5.4–4.5 cal ka BP; NPPZ 4) of most intensive outwash of *Glomus* chlamydospores remaining in the soil from formerly more dense vegetation cover between ca. 11.5–5.4 cal ka BP, their amount is continuously reduced after ca. 4.5 cal ka BP.

During the interval at ca. 1.8–0.4 cal ka BP (NPPZ 2) the phytoplankton record is very similar to that of the interval ca. 11.5–5.4 cal ka BP, thus likely indicates a shift towards enhanced freshwater influx. This interpretation is consistent with the reconstructed regional increase in precipitation (Leipe et al., 2014).

For the youngest phase representing the last ca. 300 years of the lake history, after foundation of the Korzok gompa ca. 400 years ago, the abrupt increase in *Botryococcus* algae accompanied by a pronounced decrease in *Pediastrum* likely indicate a rapid change in limnic conditions including an increase of lake productivity. Similar interpretations are published by Lami et al. (2010), who related the autochthonous algal growth during the last century in a series of lakes on the Qinghai–Tibet Plateau to the distinct increase in primary production. The rise in *Botryococcus* abundances cannot be explained by changes in precipitation (i.e. freshwater influx) given the results of the precipitation reconstructions, which suggest slightly drier conditions compared to the previous interval (ca. 1.8–0.4 cal ka BP). It also might be considered that the extremely high abundance of *Botryococcus* in the uppermost (core top) sample is connected to the contemporary trans-regional climate warming (e.g. Ren et al., 2004; Gou et al., 2007; Holmes et al., 2009) leading to increased evaporation and salinity and/or the strongly increased livestock populations as seen during the past decades (Namgail et al., 2007; Cui and Graf, 2009).

3.6.3 Potential human impact in the Tso Moriri region during the Holocene

During the early and middle Holocene (prior to ca. 4.5 cal ka BP), the TMD pollen and NPP records do not provide clear evidence for human activities around the study site, thus strengthening our original interpretation that the Tso Moriri pollen record primarily indicates regional vegetation and climate history. Though, the documented increase in regional shrubby taxa pollen in LPZ 4 and 3 (ca. 5.4–2.7 cal ka BP; Fig. 3.3) suggests an increased availability of fuel wood, it remains unclear whether these wood resources were utilised by humans in the region. Similarly, the increased pollen influx of moisture indicators like *Thalictrum* and Gentianaceae points to more developed grassland and

meadows offering improved grazing conditions for nomadic livestock. However, there is no further support for pastoralism recognised at this time. The stable but relatively low influx rates of charred grass epidermis fragments until ca. 4.5 cal ka BP coincide with maximum abundance of regional woody taxa and indicator taxa of moist sites. We assume that during this climatically favourable interval (ca. 11.5–4.5 cal ka BP) of enhanced ISM activity the charred grass epidermis fragments may indicate a more frequent occurrence of fires (e.g. Bos et al., 2005) in the forested lower ranges of the Himalayas probably caused by lightening related to stronger than present monsoonal convection.

The study region experienced climate aridity with notably lower moisture availability between ca. 4.5 and 2.7 cal ka BP (NPPSZ 3b) (Leipe et al., 2014). Several changes in the TMD record presented here, such as the increase in grass epidermis fragments, including charred particles, paralleled by low Poaceae pollen influx, more frequently recorded cereal type pollen and the occurrence of *Cannabis* type pollen may be tentatively interpreted as indicators for permanent human presence in the Tso Moriri region. A good potential indicator for human activities related to use of fire is the increased record of charred grass epidermis fragments after ca. 3.7 cal ka BP. In contrast, maximum frequencies of charred plant tissue remains in the NPP record from Tso Kar occur even earlier (ca. 6.9–5.3 cal ka BP) (Wünnemann et al., 2010). *Cannabis* type starts to appear more frequently after ca. 3.5 cal ka BP and especially after ca. 1.8 cal ka BP. Until ca. 2.7 ka BP pollen of herbaceous plants typical for grazing sites (Dvorský et al., 2011), as well as ruderal plant pollen, show no change (Fig. 3.3). The pronounced reduction of wood resources (e.g. *Betula*, *Juniperus*, *Sorbus* and *Hippophaë*), which require moister habitats (Fig. 3.3), likely reflects the decline in precipitation and not the increased firewood consumption. In accordance, pollen frequencies of *Ephedra*, a typical dry-tolerant shrubby taxon, which may be also used as firewood, show an increase.

Archaeological evidence of human presence prior to ca. 3.7/2.7 cal ka BP in the wider Tso Moriri region is documented by fire place remains from the upper Indus Valley ~60 km north of Tso Moriri dated to ca. 7.7–2.7 cal ka BP (Sharma et al., 1989; Ota, 1993). However, these oldest human traces rather indicate temporal than permanent presence of agro-pastoralists in the study region thus show that the Indus Valley likely served as a connecting route between the Indian subcontinent and Central and East Asia already since ancient times. It may be further hypothesised that the human remains from the Indus Valley are related to trading activities of sedentary communities reported from the greater Indus plains. Here, the earliest evidence of sedentary lifestyle was found at Mehrgarh (Pakistani Baluchistan) and appeared as early as ca. 9 cal ka BP (Possehl, 2004).

From ca. 2.7 cal ka BP until present (NPPSZ 3a–NPPZ 1), the terrestrial pollen record from Tso Moriri suggests the persistence of arid climate with a weak reversal towards slightly moister conditions between ca. 1.1–0.5 cal ka BP (Leipe et al., 2014), with glacial

advance after ca. 1.0 cal ka BP (Fig. 3.3) as documented for the Puga Valley (Hedrick et al., 2011). This interval exhibits most evidence for human activities affecting the regional landscape. Pollen of herbaceous taxa indicating grazing sites (Dvorský et al., 2011), in particular *Aconogonon*, as well as some ruderal taxa like Urticaceae, show highest or generally increased accumulation rates. Likewise, the presence of coprophilous fungi arguing for an enhanced number of animals in the lake catchment area (van Geel et al., 1983, 2003; van Geel, 2001) may be explained by presence of herdsmen and their livestock. Enhanced disturbance of the natural vegetation, which would be expected under enhanced grazing pressure, is supported by the generally augmented influx of ruderal plant pollen. On the contrary, there is no significant change in Cyperaceae influx after ca. 5.4 cal ka BP (NPPSZ 5a), which may point to a spread of *Kobresia* mats. Regarding large parts of the Qinghai–Tibet Plateau, the latter were hypothesised to be the result of grazing pressure by nomadic livestock (Miehe et al., 2008).

Pollen of the Poaceae wild grass type starts to appear more frequently in the pollen assemblages after ca. 1.8 cal ka BP (NPPSZ 2b–NPPZ 1). As suggested by the results of the modern surface sample analysis regional wild grass type pollen may partly represent taxa of cultivated crops (Fig. 3.2), but primarily includes large pollen types, e.g. of *Elymus* (Beug, 2004), which after Dvorský et al. (2011) is characteristic for moist sites and animal resting places. On the other hand, the increased presence of wild grass type pollen may demonstrate the expansion of grassland. Previous studies have shown that intensified grazing activities in an alpine meadow ecosystem on the northern Qinghai–Tibet Plateau can enhance the productivity of grass vegetation (Klein et al., 2007). Consequently, the above interpretations would suggest that the rise in wild grass type pollen indicates an onset or increase of either pastoral or farming or both activities around Tso Moriri.

Poaceae pollen grains assigned to the cereal type appear more frequently after ca. 1.1 cal ka BP (NPPSZ 2a–NPPZ 1) (Fig. 3.3), but this pollen morphological type may also include wild grass taxa to some extent (Beug, 2004). Clear distinction is further hampered by the possibility that the pollen grains of the local cereals are particularly smaller in size due to the harsh growing conditions in the study area. Therefore, the interpretation of cereal type pollen should be evaluated critically. While in Europe numerous detailed palynological investigations (e.g. Andersen, 1979; Moore et al., 1991; Beug, 2004; Tweddle et al., 2005) allow for a more reliable differentiation between cereal and wild grass types in fossil pollen assemblages, such a distinction is postulated to be much more difficult in other regions, including the Middle East or South and East Asia (e.g. Behre, 2007 and references therein). Although *Fagopyrum* is a cultivated crop in Ladakh today (Bhattacharyya, 1991; Hartmann, 1999), the record of its pollen at around 1.1 cal ka BP (lower NPPSZ 2a) cannot be interpreted beyond doubt as an indicator for human presence. This is due to the distribution of wild *Fagopyrum* species (i.e. *F. cymosum* and *F. tataricum*) in the

north-western Himalayas (Kumaun, Garhwal and Kashmir region) (Ohnishi, 1998), which cannot be differentiated from cultivated species by microscopic analysis of their pollen.

Despite the reconstructed minor trend towards climate amelioration (Leipe et al., 2014), the pollen sums of regional shrubby taxa (including e.g. *Juniperus*, *Sorbus*, *Lonicera* and *Ephedra*) potentially used as firewood show lowest values during this phase, suggesting enhanced human impact on vegetation. Other plants commonly used as firewood in the study region are *Astragalus* (*Astragalus*/*Oxytropis* pollen type) and the insect-pollinated shrub *Caragana* (Srivastava, 2010), with the latter being generally underrepresented in pollen records (Beug and Miehe, 1999). In contrast to the generally lower influx of the previously mentioned shrubs, both taxa are more frequently found in the uppermost part (NPPZ 1) of the TMD core. An alternative or additional explanation for the minor presence of regional shrubs may be the enhanced grazing activities of nomadic livestock, indicated by high influx of wild grass and *Aconogonon* pollen, which prevented the growth of these taxa (Vera, 2000; Klein et al., 2007).

An interesting feature at ca. 0.4 cal ka BP (lower NPPZ 1) are the distinctly lowered frequencies of *Aconogonon* and *Cannabis* type pollen and charred grass remains, which likely indicate reduced human impact around this time. This may provide evidence for a short period of reduced agro-pastoral activities due to unfavourable climate conditions, which coincide with glacial advance in the region as documented by boulders in the Puga Valley dated to ca. 1.2–0.2 cal ka BP (Hedrick et al., 2011).

3.6.4 Possible influence of climate dynamics on the Harappan Civilisation

There is still debate on whether there was an interaction between climate dynamics and the evolution of the Harappan Civilisation, which flourished ca. 5.2–3 cal ka BP and occupied a large part of the greater Indus plains (Fig. 3.1A) during its greatest expansion (Madella and Fuller, 2006; MacDonald, 2011). The palaeolimnological record from Tso Moriri provides arguments for a possible relationship between climate deterioration and documented cultural changes in the Harappan Civilisation. In combination with the TMD terrestrial pollen record (Leipe et al., 2014), the NPP record supports the onset of a phase of enhanced aridity by significantly increased *Pediastrum* influx together with the occurrence of different genera of green algae, which indicate reduced inflow of freshwater combined with enrichment of nutrients between ca. 4.5–1.8 cal ka BP (NPPZ 3). The evidence of arid conditions corroborates the hypothesis that deteriorated climate conditions may have promoted the diversification of agriculture and the emergence of urbanism during the Mature (ca. 4.5–3.9 cal ka BP) Harappan phase (see Leipe et al., 2014 for further discussion). Moreover, we propose that the fossil algae record also implies a prolonged residence time of water in the Tso Moriri basin resulting in a minimised or ceased outflow

at its southern end (Fig. 3.1C and 3.5E). If these interpretations are correct, they not only illustrate that during the time interval in focus the Harappans were facing reduced precipitation. They also suggest diminished discharge of the Indus and its tributaries (e.g. Sutlej and Beas), with large parts of their catchments situated in the north-western Himalayas and the Qinghai–Tibet Plateau, which was mainly due to reduced monsoon precipitation (Leipe et al., 2014). According to Giosan et al. (2012), the late Holocene drying of the Ghaggar-Hakra drainage system located between today's Indus and Ganges watersheds augments the hypothesis that aridification was mainly driven by declining ISM precipitation that could affect the Harappan Civilisation. On the basis of fluvial landform analyses on the Indo-Gangetic plains, the authors argue that the Ghaggar-Hakra was a monsoon-controlled perennial river system without access to a glacier-fed river when numerous settlements flourished along its channels during the urban Harappan phase (ca. 4.5–3.9 cal ka BP). Later, through the Late Harappan phase (ca. 3.9–3 cal ka BP) when the number of Harappan sites along the middle Ghaggar-Hakra course decreased (Possehl, 2002), the channels of the fluvial system dried (Giosan et al., 2012).

3.7 Conclusions

The record of non-terrestrial pollen and non-pollen palynomorphs from the high-alpine lake Tso Moriri in north-western India exhibits prominent changes in its ecosystem during the Holocene interval. In combination with the geomorphologic analysis of the lake basin, these variations yield insight into Tso Moriri's palaeolimnology and hydromorphology and underpin the proposed regional palaeoclimate evolution through the last ca. 12 ka outlined in Leipe et al. (2014). The NPP record indicates conditions of low lake productivity with high influx of freshwater between ca. 11.5 and 4.5 cal ka BP, which is well in agreement with the reconstruction of mean annual precipitation based on the terrestrial fossil pollen record from the same sediment core (Leipe et al., 2014). However, meltwater must be also taken into account as a factor which influenced the lake's hydrology. Geomorphologic findings suggest that the palaeo-lake level did not exceed the level recorded in September 2013 by more than 6–7 m, which is controlled by a surface outlet at Tso Moriri's southern end. These findings suggest that during this period of enhanced freshwater influx (ca. 11.5–4.5 cal ka BP) the lake regularly drained, thus added large amounts of water to the Sutlej River, the lower reaches of which were integral part of Indus Civilisation land use.

The inferred minimum freshwater input and maximum productivity between ca. 4.5–1.8 cal ka BP coincides with the reconstruction of greatest aridity and glacial advance in the Tso Moriri catchment and points to significantly reduced or probably ceased outflow activity, which, at this time, likely caused significantly higher than present salinity levels.

We further hypothesise that lowered discharge from the Sutlej as well as from other Indus tributaries caused by reduced precipitation may have led to irrigation problems and crop losses in the Indus lowlands. This, in turn, would support the theory that, firstly, Mature Harappan urbanism (ca. 4.5–3.9 cal ka BP) emerged in order to facilitate storage, protection, administration, and redistribution of crop yields and secondly, the eventual decline of the Harappan Culture (ca. 3.5–3 cal ka BP) was at least partly triggered by prolonged aridity driven by declining ISM precipitation.

There is no clear evidence for human impact in the Tso Moriri region prior to ca. 3.7/2.7 cal ka BP. For the time interval ca. 2.7–0 cal ka BP, the record provides clear indications for an occupation by humans likely subsisting on agro-pastoralism. Besides evidence for burning of grass and enhanced grazing activities, there is indication for farming activities by the presence of cultivated plants (i.e. cereals). However, as long as the pollen morphology of regional Poaceae cereal types and wild grass types remains poorly studied, certain differentiation is not possible.

In combination with the climate reconstruction based on the terrestrial pollen record from the same core, the presented record of NPPs from Tso Moriri provides a first insight in the development of the palaeolimnological conditions of the lake system. Further research is required, which should include sediment geochemical approaches to deepen our understanding of the interpretation of NPP assemblages in future studies. To test our hypotheses on the ecological and hydromorphological evolution of Tso Moriri, the reconstruction of salinity, e.g. by means of fossil ostracod shell assemblages, is considered to be a promising approach.

3.8 Acknowledgements

The present study is a contribution to the current project ‘Himalaya: Modern and Past Climates (HIMPAC)’ funded by the German Research Foundation (DFG Research Unit 1380) and to the ongoing research initiative “Bridging Eurasia”. The work of D. Demske and C. Leipe was funded by the DFG grant RI 809/24. P. Tarasov acknowledges the DFG Heisenberg Program (TA 540/5). For collection of additional surface samples in the field and laboratory preparation at FU Berlin the authors thank C. Funk. We are grateful to people living at Tso Moriri who provided information on the lake, to Mehar Chand (Mountaineering Institute Manali, India) who gave an extensive report of his hydrological observations during two decades of trekking through the Tso Moriri region and to Jaishri Sanwal (IIS Bangalore, India) who helped in accessing the study area. We would also like to thank two anonymous referees and S. Müller (FU Berlin) for providing valuable comments which greatly improved the present paper.

3.9 Supplementary material

Supplementary data associated with this article is provided in the Open Access information system PANGAEA at doi:10.1594/PANGAEA.829753.

4. Manuscript III

Vegetation and climate history of Northern Japan inferred from the 5500-year pollen record from the Oshima Peninsula, SW Hokkaido

Christian Leipe [a], Norio Kito [b], Yumi Sakaguchi [b], Pavel E. Tarasov [a]

[a] *Institute of Geological Sciences, Palaeontology, Freie Universität Berlin, Malteserstraße 74–100, Building D, 12249 Berlin, Germany*

[b] *Laboratory of Earth Science, Hokkaido University of Education, Hakodate Campus, 1–2 Hachimancho, Hakodate, Hokkaido 040-8567, Japan*

Published in *Quaternary International* 290–291 (2013) pp. 151–163

doi:10.1016/j.quaint.2012.07.014

4.1 Abstract

This study reconstructs middle and late Holocene vegetation and climate dynamics in the Oshima Peninsula, SW Hokkaido, using the published method of biome reconstruction and modern analogue technique applied to the Yakumo pollen record (42°17′03″N, 140°15′34″E) spanning the last 5500 years. Two previously published matrices assigning Japanese plant/pollen taxa to the major vegetation types (biomes) are tested using a newly compiled dataset of 78 surface pollen spectra from Hokkaido. With both matrices showing strengths and weaknesses in reconstructing cool mixed and temperate deciduous forests of Hokkaido, the results suggest the necessity to consider the whole list of identified terrestrial pollen taxa for generating robust vegetation reconstructions for northern Japan. Applied to the fossil pollen data, both biome-reconstruction approaches demonstrate consistently that oak-dominated cool mixed forest spread in the study region between 5.5 and 3.6 cal ka BP and was subsequently replaced by beech-dominated temperate deciduous forest. The pollen-based climate reconstruction suggests this change in the vegetation composition was caused by a shift from cooler and drier than present climate to warmer and wetter, similar to modern conditions about 3.6 cal ka BP. Comparing the pollen-based reconstruction results with the published marine records from the NW Pacific, the reconstructed vegetation and climate dynamics can be satisfactorily explained by the greater role played by the warm Tsushima Current in the Sea of Japan and in the Tsugaru Strait during the middle and late Holocene. An increase in sea surface temperatures west and south of the

study site would favour air temperature rise and moisture uptake and cause an increase in precipitation and snow accumulation in the western part of Hokkaido during the late Holocene.

4.2 Introduction

Palynological studies have proved to be extremely useful for reconstructing the East Asian Monsoon (EAM) dynamics (e.g. Nakagawa et al., 2008; Tarasov et al., 2011) and its influence on the regional climate, vegetation and human dynamics and adaptation strategies during the late Quaternary (e.g. Yasuda et al., 2004b; Jiang et al., 2006; Tarasov et al., 2006; Lee et al., 2010; Nakazawa et al., 2011). Likewise, pollen records and pollen-based vegetation and climate reconstructions serve as boundary conditions and/or as data for comparison with model output and are capable of improving model predictions of past and future climate changes on a global and regional level (e.g. Prentice and Jolly, 2000; Wang et al., 2005a; Kleinen et al., 2011).

The vegetation and climate of the Japanese Archipelago situated in the north-western Pacific close to the eastern edge of the Eurasian continent are greatly influenced by the EAM. The area is suitable for palaeoenvironmental studies aiming to reconstruct the past monsoon climate–vegetation–human relationships in the region, and pollen have been frequently used as a proxy to infer climate and human-induced environmental changes in prehistoric times on the Japanese Archipelago (Tsukada, 1986, 1988; Takahara et al., 2010). Whereas numerous conventional pollen studies and pollen-based qualitative environmental reconstructions have been conducted in Japan since the 1930s, the number of works performing quantitative vegetation and climate reconstructions from Japanese pollen data is rather limited.

Takahara et al. (2000) and Gotanda et al. (2002) independently adopted the biome reconstruction (also called biomization) method (Prentice et al., 1996) to derive quantitative information about the major vegetation types (biomes) during the late Quaternary. The approach was first tested with representative modern pollen datasets and then applied to fossil pollen data to calculate the dominant biome scores and to objectively discuss late Quaternary changes in vegetation. Each of the two cited studies proposed different biome-taxa matrices based on slightly different assumptions and reference datasets. For example, Takahara et al. (2000) considered all arboreal and non-arboreal pollen taxa in their regional biomization scheme. When testing the method, they achieved an agreement of 54% between pollen-derived biomes and modern natural vegetation at the surface pollen sampling sites. All samples from the areas dominated by cool conifer forest and temperate conifer forest were reconstructed incorrectly, which appeared to be the main weakness of the suggested approach. Gotanda et al. (2002) modified the approach by

allowing only 32 tree and shrub taxa commonly counted in pollen spectra from the Japanese Archipelago to be considered in the biome reconstruction. Tested with a three times greater reference modern pollen dataset, this modification increased the amount of correctly assigned pollen spectra to 78%. Despite this substantial improvement for Japan in its entirety, the utilised approach (Gotanda et al., 2002) still revealed difficulties in accurate biome reconstruction for the northern island of Hokkaido, where most samples from cool mixed forest sites were assigned to temperate deciduous forest.

Another approach frequently used to derive quantitative information about past climate (Jackson et al., 2000; Peyron et al., 2000; Nakagawa et al., 2002; Tarasov et al., 2011) and vegetation (Tarasov et al., 2007; Williams et al., 2011) from fossil pollen spectra using representative reference datasets of modern pollen and vegetation/climate data is the modern analogue technique (MAT) (Overpeck et al., 1985; Guiot, 1990). The MAT was applied to the pollen profiles from central and northern Honshu (e.g. Nakagawa et al., 2002, 2003, 2005, 2006, 2008; Yoshida and Takeuti, 2009) using the modern pollen-climate dataset representing 285 surface pollen sites from Japan compiled by Gotanda et al. (2002). Recently, Tarasov et al. (2011) significantly extended this previously published dataset to 798 sites representing the whole Northwest Pacific region, including the boreal Russian Far East and tropical Japanese islands. This dataset together with the MAT was suggested as a powerful tool suitable for reconstructing glacial–interglacial climate changes from Japanese pollen records.

The Baikal-Hokkaido Archaeology Project (BHAP) – an international and multi-disciplinary research project investigating Holocene hunter–gatherer culture dynamics in the Lake Baikal region of Siberia, Russia and in Hokkaido, Japan – was started in 2011. Together with archaeological teams from Japan, Russia, UK, Germany and Canada, BHAP also includes scientists representing palaeoenvironmental studies and climate and vegetation modelling, whose aims are robust reconstructions of the past climate and environments using high-resolution environmental archives (i.e. sedimentary cores obtained from Lake Kotokel, Siberia and Lake Kushu, Rebun Island, Japan) and regional climate models (e.g. White and Bush, 2010 and references therein). The present study discusses the applicability of the published approaches and reference dataset for reconstructing the Holocene vegetation and climate of northern Japan. For this purpose, different biomization schemes are tested with the newly compiled surface pollen data from Hokkaido and the MAT is applied to the pollen record from the Oshima Peninsula, SW Hokkaido (Kito and Takimoto, 1999), spanning the last 5500 years. The findings are discussed in the context of the regional climatic system and against the existing palaeoclimate records.

4.3 Reconstruction methods

4.3.1 Biome reconstruction method

The method of biome reconstruction is the quantitative approach adapted for reconstruction of globally recognised major vegetation types from pollen and plant macrofossil data (Prentice et al., 1996). The method allows the objective assignment of pollen taxa to plant functional types (PFTs) and to biomes on the basis of modern ecology, bioclimatic tolerance and geographical distribution of pollen producing plants. The method was tested using surface pollen data from Russia (Tarasov et al., 1998), Mongolia (Gunin et al., 1999), China (Yu et al., 2000) and Japan (Takahara et al., 2000; Gotanda et al., 2002) and further used to reconstruct the late Quaternary vegetation on a regional, extra-regional and hemispheric scale (e.g. Prentice and Jolly, 2000 and references therein). The main steps for the construction of the biome-taxa matrix and biome score calculation summarised in Prentice et al. (1996) are rather universal and include: (i) assignment of each pollen taxon to one or several plant functional types (PFT: group of plants defined by their stature, leaf form, phenology, and bioclimatic tolerance) and to biomes, using knowledge of modern plant distribution; (ii) construction of the biome-taxa matrix showing the taxa that may occur in each biome; (iii) calculation of the affinity scores for all concerned biomes as the summation of square roots of attributed pollen taxa abundance (percentage value minus 0.5% - the universal threshold suggested for minimisation of possible noise mainly due to long distance transport or re-deposition of exotic pollen grains); and (iv) the biome with the highest affinity score or the one defined by a smaller number of PFTs (when scores of several biomes are equal) is assigned for each pollen spectrum. However, the use of the method in the new area requires that the applied taxon-biome matrix reflects regional vegetation and pollen composition, which can be tested with the surface pollen data from the region (Prentice et al., 1996; Tarasov et al., 1997; Mokhova et al., 2009).

For the purpose of the present study and the BHAP focus on Hokkaido, the biome reconstruction method was tested using assignment of pollen taxa to the main Japanese biomes (Tables 4.1 and 4.2) proposed by Takahara et al. (2000) and Gotanda et al. (2002). Tests were performed on a dataset of 78 unpublished surface pollen spectra from Hokkaido. PPPBase software (Guiot and Goeury, 1996) was used for biome score calculations.

4.3.2 Climate reconstruction method

The MAT, also known as the best modern analogue or modern analogue approach, has been described in detail in many publications (e.g. Overpeck et al., 1985; Guiot, 1990; Nakagawa et al., 2002; Jackson and Williams, 2004; Tarasov et al., 2007, 2011). The method assumes that pollen assemblages with a similar composition of pollen taxa are produced by

compositionally and structurally similar vegetation communities. Proceeding from this assumption, comparison of fossil samples and modern pollen samples included in the reference dataset makes it possible to identify the closest modern analogues for each

Biome name/ Abbreviation	Pollen taxa assigned
Tundra/TUND	*Aconitum**, *Allium*, *Artemisia**, *Betula**, Caryophyllaceae*, Compositae (Asteraceae)*, Cruciferae (Brassicaceae), Cyperaceae*, *Epilobium**, Ericaceae*, Ericales*, *Gentiana**, *Geranium**, Gramineae (Poaceae)*, Leguminosae (Fabaceae)*, Liliaceae*, *Lysimachia**, *Pinus Haploxylon*-type, Polygonaceae*, *Polygonum* undiff.*, *Polygonum bistorta*-type, Ranunculaceae*, *Rhododendron*, Rosaceae*, *Salix**, *Scabiosa*, *Scheuchzeria*, *Selaginella selaginoides*, *Stellaria*, *Thalictrum**, Umbelliferae (Apiaceae)*
Cold deciduous forest/CLDE	*Aconitum**, *Allium*, *Alnaster*, *Alnus**, *Artemisia**, *Betula**, Caryophyllaceae*, Compositae*, Cruciferae, Cupressaceae-type*, *Epilobium**, Ericaceae*, Ericales*, *Gentiana**, *Geranium**, *Larix**, Leguminosae*, Liliaceae*, *Lysimachia**, *Pinus* undiff.*, Polygonaceae*, *Polygonum* undiff.*, *Polygonum bistorta*-type, Ranunculaceae*, *Rhododendron*, Rosaceae*, *Rumex**, *Salix**, *Sanguisorba**, *Scabiosa*, *Scheuchzeria*, *Stellaria*, *Thalictrum**, Umbelliferae (Apiaceae)*
Taiga/TAIG	*Abies**, *Aconitum**, *Allium*, *Alnaster*, *Alnus**, *Artemisia**, *Betula**, Caryophyllaceae*, Compositae (Asteraceae)*, Cruciferae (Brassicaceae), Cupressaceae-type*, *Epilobium**, Ericaceae*, Ericales*, *Gentiana**, *Geranium**, *Larix**, Leguminosae (Fabaceae)*, Liliaceae*, *Lysimachia**, *Picea**, *Pinus* undiff.*, *Pinus Haploxylon*-type, Polygonaceae*, *Polygonum* undiff.*, *Polygonum bistorta*-type, Ranunculaceae*, *Rhododendron*, Rosaceae*, *Rumex**, *Salix**, *Sanguisorba**, *Scabiosa*, *Scheuchzeria*, *Stellaria*, *Thalictrum**, Umbelliferae (Apiaceae)*
Cold mixed forest/CLMX	*Abies**, *Aconitum**, *Allium*, *Alnaster*, *Alnus**, *Artemisia**, *Betula**, Caryophyllaceae*, Compositae (Asteraceae)*, Cruciferae (Brassicaceae), Cupressaceae-type*, *Epilobium**, Ericaceae*, Ericales*, *Gentiana**, *Geranium**, Leguminosae (Fabaceae)*, Liliaceae*, *Lysimachia**, *Pinus* undiff.*, *Pinus Haploxylon*-type, Polygonaceae*, *Polygonum* undiff.*, *Polygonum bistorta*-type, Ranunculaceae*, *Rhododendron*, Rosaceae*, *Rumex**, *Salix**, *Sanguisorba**, *Scabiosa*, *Scheuchzeria*, *Stellaria*, *Thalictrum**, *Tsuga**, Umbelliferae (Apiaceae)*
Cool conifer forest/COCO	*Abies**, *Aconitum**, *Allium*, *Alnaster*, *Alnus**, *Artemisia**, *Betula**, Caryophyllaceae*, Compositae (Asteraceae)*, Cruciferae (Brassicaceae), Cupressaceae-type*, *Epilobium**, Ericaceae*, Ericales*, *Gentiana**, *Geranium**, Leguminosae (Fabaceae)*, Liliaceae*, *Lysimachia**, *Picea**, *Pinus* undiff.*, *Pinus Haploxylon*-type, Polygonaceae*, *Polygonum* undiff.*, *Polygonum bistorta*-type, Ranunculaceae*, *Rhododendron*, Rosaceae*, *Rumex**, *Salix**, *Sanguisorba**, *Scabiosa*, *Scheuchzeria*, *Stellaria*, *Thalictrum**, *Tsuga**, Umbelliferae (Apiaceae)*
Cool mixed forest/COMX	*Abies**, *Acanthopanax*, *Acer**, *Aconitum**, *Allium*, *Alnaster*, *Alnus**, *Artemisia**, *Betula**, *Cardamine*, *Carpinus*, *Carpinus/Ostrya**, Caryophyllaceae*, Celastraceae*, *Cercidiphyllum**, Chenopodiaceae, Chenopodiaceae/Amaranthaceae*, Cichorioideae*, *Clematis**, *Cleyera*, Compositae*, *Coptis**, *Cornus**, *Corylus**, Cruciferae, *Cryptomeria**, Cupressaceae-type*, *Epilobium**, Ericaceae*, Ericales*, *Euonymus*, *Fagus**, *Fagus crenata*, *Filipendula**, *Fraxinus**, *Gentiana**, *Geranium**, *Hamamelis*, *Humulus*, *Hygrophila*, *Impatiens**, *Juglans/Pterocarya**, Juglandaceae, Labiatae (Lamiaceae)*, Leguminosae (Fabaceae)*, Liliaceae*, *Lysimachia**, Moraceae*, *Myrica**, *Patrinaria*, *Phellodendron**, *Picea**, *Pinus* undiff.*, *Pinus Diploxylon*-type, *Pinus Haploxylon*-type, *Plantago**, Polygonaceae*, *Polygonum* undiff.*, *Polygonum bistorta*-type, *Prunus*, *Pterocarya**, *Quercus* (deciduous)*, Ranunculaceae*, *Reynoutria**, *Rhododendron*, *Rhus*, Rosaceae*, *Rumex**, *Salix**, *Sanguisorba**, *Scabiosa*, *Scheuchzeria*, *Sciadopitys**, *Sorbus**, *Stellaria*, *Symplocos*, *Thalictrum**, *Tilia**, *Tsuga**, *Ulmus**, *Ulmus/Zelkova**, Umbelliferae (Apiaceae)*, Urticaceae*, *Viburnum**, *Vitis**, *Weigela*

Temperate deciduous forest/TEDE	*Abies**, *Acanthopanax*, *Acer**, *Aconitum**, *Aesculus**, *Allium*, *Alnaster*, *Alnus**, Araliaceae*, *Artemisia**, *Betula**, *Cardamine*, *Carpinus*, *Carpinus tschonoskii*, *Carpinus/Ostrya**, Caryophyllaceae*, *Castanea*, *Castanea/Castanopsis**, Celastraceae*, *Cercidiphyllum**, Chenopodiaceae, Chenopodiaceae/Amaranthaceae*, Cichorioideae*, *Clematis**, *Cleyera*, Compositae (Asteraceae)*, *Coptis**, *Cornus**, *Corylus**, Cruciferae (Brassicaceae), *Cryptomeria**, Cupressaceae-type*, *Epilobium**, Ericaceae*, Ericales*, *Euonymus*, *Fagus**, *Fagus crenata*, *Fagus japonica*, *Filipendula**, *Fraxinus**, *Gentiana**, *Geranium**, *Hamamelis*, *Humulus*, *Hygrophila*, *Ilex**, *Impatiens**, *Juglans/Pterocarya**, Juglandaceae, Labiatae (Lamiaceae)*, Leguminosae (Fabaceae)*, Liliaceae*, *Lysimachia**, Moraceae*, *Myrica**, *Parthenocissus*, *Patrinaria*, *Phellodendron**, *Pinus* undiff.*, *Pinus Diploxylon*-type, *Pinus Haploxylon*-type, *Plantago**, Polygonaceae*, *Polygonum* undiff.*, *Polygonum bistorta*-type, *Prunus*, *Pterocarya**, *Quercus* (deciduous)*, Ranunculaceae*, *Reynoutria**, *Rhododendron*, *Rhus*, Rosaceae*, *Rumex**, *Salix**, *Sanguisorba**, *Scabiosa*, *Scheuchzeria*, *Sciadopitys**, *Sorbus**, *Stellaria*, *Symplocos*, *Thalictrum**, *Tilia**, *Tsuga**, *Ulmus**, *Ulmus/Zelkova**, Umbelliferae (Apiaceae)*, Urticaceae*, *Viburnum**, *Viscum*, *Vitis**, *Weigela*
Temperate conifer forest/TECO	*Abies**, *Acanthopanax*, *Acer**, *Aconitum**, *Aesculus**, *Allium*, *Alnaster*, *Alnus**, Araliaceae*, *Artemisia**, *Betula**, *Cardamine*, *Carpinus*, *Carpinus tschonoskii*, *Carpinus/Ostrya**, Caryophyllaceae*, *Castanea*, *Castanea/Castanopsis**, Celastraceae*, *Celtis*, *Celtis/Aphananthe**, Chenopodiaceae, Chenopodiaceae/Amaranthaceae*, Cichorioideae*, *Clematis**, *Cleyera*, Compositae (Asteraceae)*, *Coptis**, *Cornus**, *Corylus**, Cruciferae (Brassicaceae), *Cryptomeria**, Cupressaceae-type*, *Diospyros*, *Elaeagnus*, *Epilobium**, Ericaceae*, Ericales*, *Euonymus*, *Fagus**, *Fagus japonica*, *Filipendula**, *Fraxinus**, *Gentiana**, *Geranium**, *Hamamelis*, *Humulus*, *Hygrophila*, *Ilex**, *Impatiens**, *Juglans/Pterocarya**, Juglandaceae, Labiatae (Lamiaceae)*, Leguminosae (Fabaceae)*, *Ligustrum**, Liliaceae*, *Lysimachia**, *Mallotus*, Moraceae*, *Parthenocissus*, *Patrinaria*, *Pinus* undiff.*, *Pinus Diploxylon*-type, *Plantago**, *Platycarya**, *Podocarpus**, Polygonaceae*, *Polygonum* undiff.*, *Prunus*, *Quercus* (deciduous)*, Ranunculaceae*, *Reynoutria**, *Rhamnus*, *Rhododendron*, *Rhus*, Rosaceae*, *Salix**, *Scabiosa*, *Sciadopitys**, *Sorbus**, *Stellaria*, *Symplocos*, *Thalictrum**, *Tsuga**, *Ulmus**, *Ulmus/Zelkova**, Umbelliferae (Apiaceae)*, Urticaceae*, *Viburnum**, *Viscum*, *Vitis**, *Weigela*, *Zelkova*
Warm mixed forest/WAMX	*Abies**, *Acanthopanax*, *Acer**, *Aconitum**, *Aesculus**, *Allium*, *Alnaster*, *Alnus**, Araliaceae*, *Artemisia**, *Aucuba*, *Betula**, *Camellia*, *Cardamine*, *Carpinus*, *Carpinus tschonoskii*, *Carpinus/Ostrya**, Caryophyllaceae*, *Castanea*, *Castanea/Castanopsis**, *Castanopsis*, Celastraceae*, *Celtis*, *Celtis/Aphananthe**, Chenopodiaceae, Chenopodiaceae/Amaranthaceae*, Cichorioideae*, *Clematis**, *Cleyera*, Compositae (Asteraceae)*, *Coptis**, *Cornus**, *Corylus**, Cruciferae (Brassicaceae), *Cryptomeria**, Cupressaceae-type*, *Diospyros*, *Elaeagnus*, *Epilobium**, Ericaceae*, Ericales*, *Euonymus*, Euphorbiaceae, *Fagus**, *Fagus japonica*, *Filipendula**, *Fraxinus**, *Gentiana**, *Geranium**, *Hamamelis*, *Humulus*, *Hygrophila*, *Ilex**, *Illicium*, *Impatiens**, *Juglans/Pterocarya**, Juglandaceae, Labiatae (Lamiaceae)*, Leguminosae (Fabaceae)*, *Ligustrum**, Liliaceae*, *Lysimachia**, *Mallotus*, Moraceae*, *Myrica**, *Parthenocissus*, *Patrinaria*, *Pinus* undiff.*, *Pinus Diploxylon*-type, *Plantago**, *Platycarya**, *Podocarpus**, Polygonaceae*, *Polygonum* undiff.*, *Prunus*, *Quercus* (deciduous)*, *Quercus* (evergreen)*, Ranunculaceae*, *Reynoutria**, *Rhamnus*, *Rhododendron*, *Rhus*, Rosaceae*, *Salix**, *Scabiosa*, *Sciadopitys**, *Skimmia*, *Sorbus**, *Stellaria*, *Symplocos*, *Thalictrum**, *Tsuga**, *Ulmus**, *Ulmus/Zelkova**, Umbelliferae (Apiaceae)*, Urticaceae*, *Viburnum**, *Viscum*, *Vitis**, *Weigela*, *Zelkova*

Table 4.1 Biome-taxa matrix used in the calculation of biome affinity scores (after Takahara et al., 2000). All taxa which are present in the 78 modern pollen samples from Hokkaido compiled in this study are indicated by an asterisk. The affinity score for each potential biome is calculated by summation of the square roots of all attributed pollen taxa percentages (taxon percentage value minus 0.5%). The universal threshold of 0.5% is applied to all taxa as suggested by Prentice et al. (1996). The biome with the highest affinity score or the one defined by a smaller number of PFTs (when scores of several biomes are equal) is treated as the dominant biome.

Biome name/Abbreviation	Pollen taxa assigned
Taiga/TAIG	*Abies**, *Alnus**, *Betula**, Ericaceae*, *Larix**, *Myrica**, *Picea**, *Pinus**, *Rhododendron*, *Salix**, Taxodiaceae/Cupressaceae*
Cool conifer forest/COCO	*Abies**, *Aesculus**, *Alnus**, *Betula**, *Corylus**, Ericaceae*, *Larix**, *Myrica**, *Picea**, *Pinus**, *Rhododendron*, *Salix**, Taxodiaceae/Cupressaceae*, *Tilia**, *Tsuga**, *Ulmus/Zelkova**, *Viburnum**
Cool mixed forest/COMX	*Abies**, *Acer**, *Aesculus**, *Alnus**, *Betula**, *Carpinus/Ostrya**, *Corylus**, Ericaceae*, *Fraxinus**, *Juglans/Pterocarya**, *Larix**, *Myrica**, *Picea**, *Pinus**, *Quercus* (deciduous)*, *Rhododendron*, *Rhus**, *Salix**, *Symplocos*, Taxodiaceae/Cupressaceae*, *Tilia**, *Tsuga**, *Ulmus/Zelkova**, *Viburnum**
Temperate deciduous forest/TEDE	*Abies**, *Acer**, *Aesculus**, *Alnus**, *Betula**, *Carpinus/Ostrya**, *Corylus**, *Cryptomeria**, Ericaceae*, *Fagus**, *Fraxinus**, *Ilex**, *Juglans/Pterocarya**, *Myrica**, *Pinus**, *Quercus* (deciduous)*, *Rhododendron*, *Rhus**, *Salix**, *Sciadopitys**, *Symplocos*, Taxodiaceae/Cupressaceae*, *Tilia**, *Tsuga**, *Ulmus/Zelkova**, *Viburnum**
Temperate conifer forest/TECO	*Abies**, *Acer**, *Aesculus**, *Alnus**, *Carpinus/Ostrya**, *Castanea/Castanopsis**, *Corylus**, *Cryptomeria**, Ericaceae*, *Fraxinus**, *Ilex**, *Juglans/Pterocarya**, *Pinus**, *Podocarpus**, *Quercus* (deciduous)*, *Rhododendron*, *Rhus**, *Salix**, *Sciadopitys**, *Symplocos*, Taxodiaceae/Cupressaceae*, *Tilia**, *Tsuga**, *Ulmus/Zelkova**, *Viburnum**
Warm mixed forest/WAMX	*Acer**, *Aesculus**, *Alnus**, *Camellia*, *Carpinus/Ostrya**, *Castanea/Castanopsis**, *Corylus**, *Cryptomeria**, Ericaceae*, *Fraxinus**, *Ilex**, *Juglans/Pterocarya**, *Myrica**, *Pinus**, *Podocarpus**, *Quercus* (deciduous)*, *Quercus* (evergreen)*, *Rhododendron*, *Rhus**, *Salix**, *Sciadopitys**, *Symplocos*, Taxodiaceae/Cupressaceae*, *Tilia**, *Ulmus/Zelkova**, *Viburnum**

Table 4.2 Biome-taxa matrix used in the calculation of biome affinity scores (after Gotanda et al., 2002). All taxa which are present in the 78 modern pollen spectra from Hokkaido compiled in this study are indicated by an asterisk. The affinity score for each potential biome is calculated by summation of the square roots of all attributed pollen taxa percentages (taxon percentage value minus 0.5%). The universal threshold of 0.5% is applied to all taxa as suggested by Prentice et al. (1996). The biome with the highest affinity score or the one defined by a smaller number of PFTs (when scores of several biomes are equal) is treated as the dominant biome.

analysed fossil sample. The modern climate parameters affiliated with the sites of modern pollen samples serving as the closest analogues are then assigned to the analysed fossil samples and considered as reconstructed values of the past climate. The MAT used in the current study, including the performance statistics and reference pollen–climate dataset, was discussed in detail in Tarasov et al. (2011). Calculation of the modern climate at the reference pollen sampling sites used the free-access software packages Polation and Polygon (Nakagawa et al., 2002; http://dendro.naruto-u.ac.jp/~nakagawa/) and a global high-resolution (10′ × 10′ grids) dataset of surface climate averaged over a thirty-year (1961–1990) interval (New et al., 2002). All temperature estimates were corrected by taking into account a standard temperature lapse rate of −0.6 C per 100 m increase in altitude (Domrös and Peng, 1988).

As the basis for the quantitative reconstruction of past climate from the 5500-year pollen record from the Oshima Peninsula, SW Hokkaido, modern pollen and climate variables for 248 sites situated in the region between ~35–45.5°N and ~139–146°E (Fig. 4.1) were extracted from the reference dataset published by Tarasov et al. (2011). This area includes northern Honshu, Hokkaido, Kunashir and Rebun islands. It covers a 1150 × 650 km spatial window centred on the site with the fossil pollen record and represents a wide range of modern climate variables (Fig. 4.2), which exceeds possible climatic variability at the study site during the last 5500 years.

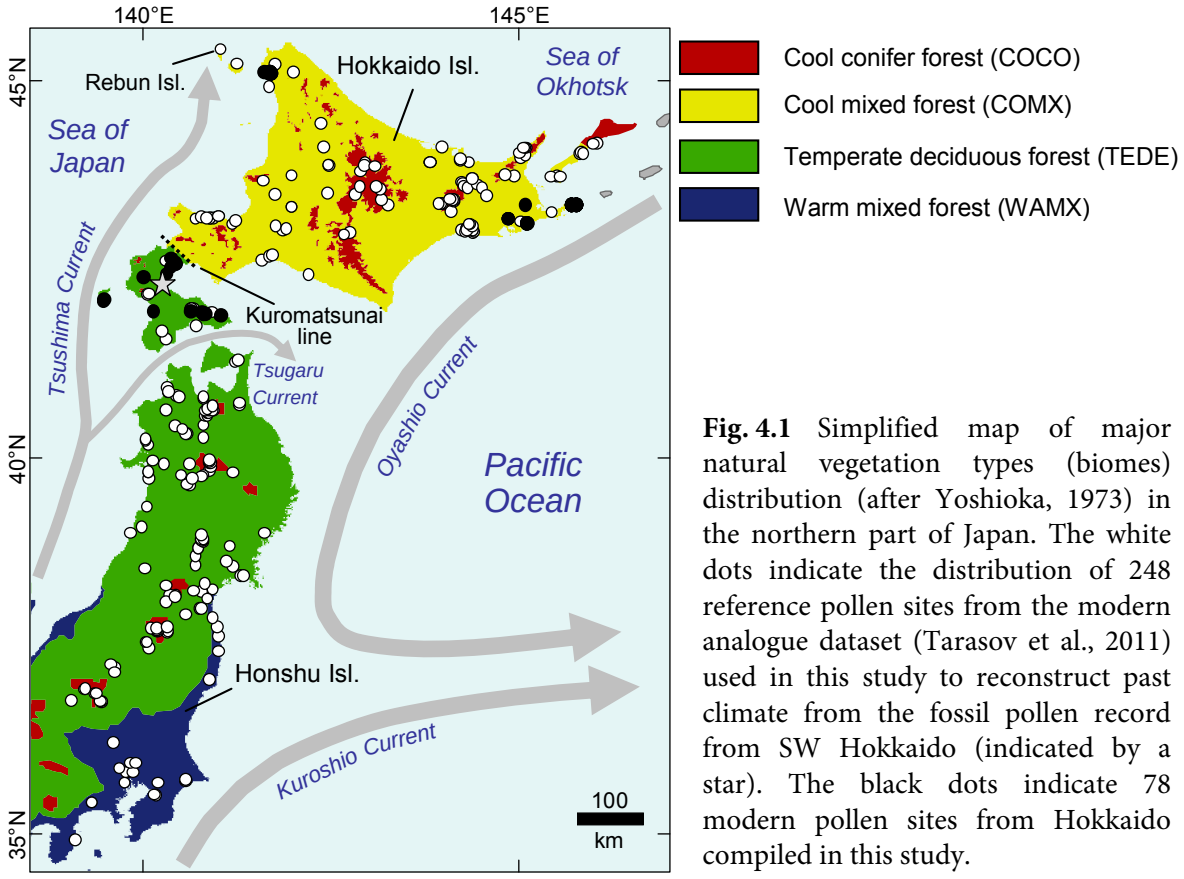

Fig. 4.1 Simplified map of major natural vegetation types (biomes) distribution (after Yoshioka, 1973) in the northern part of Japan. The white dots indicate the distribution of 248 reference pollen sites from the modern analogue dataset (Tarasov et al., 2011) used in this study to reconstruct past climate from the fossil pollen record from SW Hokkaido (indicated by a star). The black dots indicate 78 modern pollen sites from Hokkaido compiled in this study.

In addition to the climate reconstruction using the regional reference dataset from Tarasov et al. (2011), reconstruction was performed using the reference dataset updated with the 78 surface pollen spectra from Hokkaido compiled in this study. For this purpose climate variables representing the modern pollen sites were derived from the New et al. (2002) climate database using the same approach as for the rest of the sites, as described in Tarasov et al. (2011). The two sets of reconstruction results are presented in Fig. 4.7 and further compared with the other climate proxies from the larger region in Fig. 4.8.

4.4 Pollen data and modern environments

4.4.1 Surface pollen data from Hokkaido and regional environments

The number of modern pollen spectra from Hokkaido used to test the method of biome reconstruction was 6 in Takahara et al. (2000) and 64 in Gotanda et al. (2002). The reference dataset compiled by Tarasov et al. (2011) includes an even higher number of modern pollen sites from northern Japan (white dots in Fig. 4.1). However, the latter study also only considered the 32 most common arboreal pollen taxa. The current work presents 78 surface pollen spectra from Hokkaido (black dots in Fig. 4.1), which are used to test and discuss both earlier published biome reconstruction schemes.

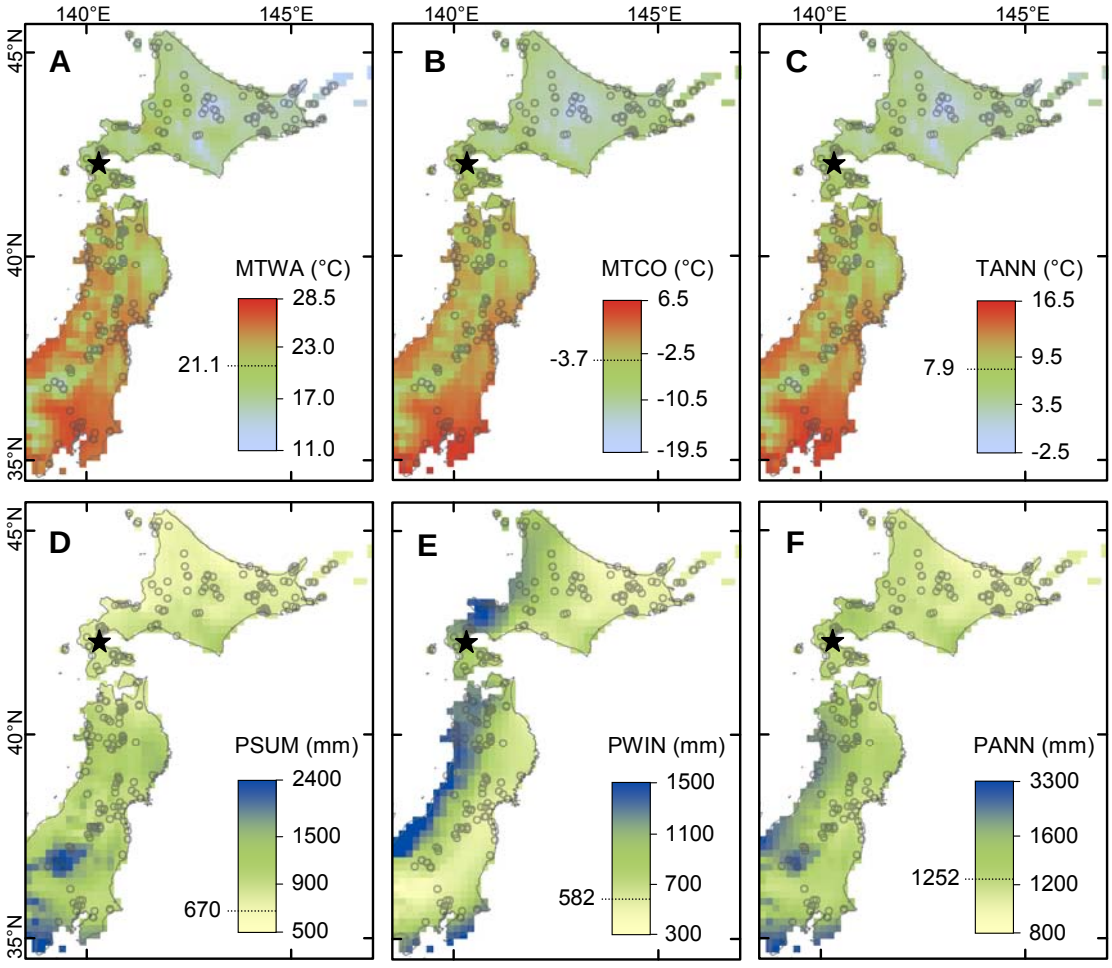

Fig. 4.2 Estimated climate variables in the study region based on the climate dataset from New et al. (2002) including (A) mean temperature of the warmest (MTWA) and (B) coldest (MTCO) month, (C) mean annual temperature (TANN), (D) precipitation of summer (PSUM) and (E) winter (PWIN), and (F) annual precipitation (PANN). The dotted line in each legend indicates modern conditions at the location of the fossil pollen record (indicated by a black star). Circles show the locations of the reference modern pollen sites.

The spatial distribution of modern pollen data is shown in Fig. 4.1. The sampling sites are clustered in three main regions, i.e. the northern, eastern and south-western parts of Hokkaido, which are covered with cool mixed forest and temperate deciduous forest, respectively (Fig. 4.1). The regional climate of Hokkaido (see Fig. 4.2 for details) is mainly controlled by marine currents and the EAM system. The Tsushima Warm Current flows northwards along the western margin of Hokkaido causing a sea surface temperature gradient between the Sea of Japan and the Pacific Ocean, which is influenced by the Oyashio Cold Current (Fig. 4.1). The west–east gradient in sea water temperature is well pronounced. According to the Japan Oceanographical Data Center (Koizumi, 2008), along 42°N latitude modern surface water temperatures west of Hokkaido change from 19–20 °C in summer to 6–7 °C in winter, whilst sea surface temperatures east of Hokkaido reach 15–16 °C in summer and about 1 °C in winter. This results in higher annual temperatures on the west coast in contrast to the east coast (Fig. 4.2).

During winter the north-west monsoon winds crossing the relatively warm Sea of Japan collect water and bring heavy snowfalls to western Hokkaido (Fig. 4.2; Igarashi, 1994; Kuroyanagi et al., 2006). In summer, the tropical air masses of the south-east monsoon affect the south-western part of Hokkaido, whereas the remaining parts are subjected to the influence of subpolar air masses throughout the year (Nakamura, 1968).

Major distribution patterns of natural vegetation of Hokkaido (Fig. 4.1) reflect features of regional climate, but can be complicated by local microenvironments due to complex topography and volcanic activities. Three major biomes are well distinguished (e.g. Tatewaki, 1958). Temperate deciduous forest (also called "beech zone") is dominated by *Fagus crenata*, accompanied by *Quercus crispula* (=*Quercus mongolica*), *Acer japonica*, *Aesculus turbinata*, *Juglans mandshurica* var. *sachalinensis*, *Pterocarya rhoifolia*, with a dense understory of *Sasa senanensis* and *Sasa kurilensis*. Cool mixed forest is a variably mixed forest of deciduous trees and conifers (*Abies sachalinensis* and *Picea jezoensis*). Most of the forest is composed only of deciduous trees dominated by *Q. crispula*, *Tilia japonica*, *Acer mono* with a dense understory of *Sasa* species. The forest is often considered as the temperate deciduous forest without *F. crenata*. Most broadleaved trees of the forest are common to those of temperate deciduous forest, but some thermophilous species, such as *P. rhoifolia*, *A. turbinata*, are absent. The forest also has *Carpinus cordata*, *Kalopanax pictus*, *Magnolia obovata*, *Magnolia kobus* var. *borealis*, *Prunus sergentii*, *Cornus controversa*, *Populus maximowiczii*, *Ulmus davidiana* var. *japonica*, *Fraxinus mandshurica* var. *japonica*, *Cercidiphyllum japonicum*, *Alnus japonica*, *Alnus hirsuta*, etc. Cool conifer forest occupies mountain areas in the most continental central part of the island and is mainly composed of *P. jezoensis*, *Picea glehnii*, *A. sachalinensis*, accompanied by *Betula platyphylla* var. *japonica*, *Betula ermanii*, *Sorbus commixta*, etc. with a dense understory of *Sasa*.

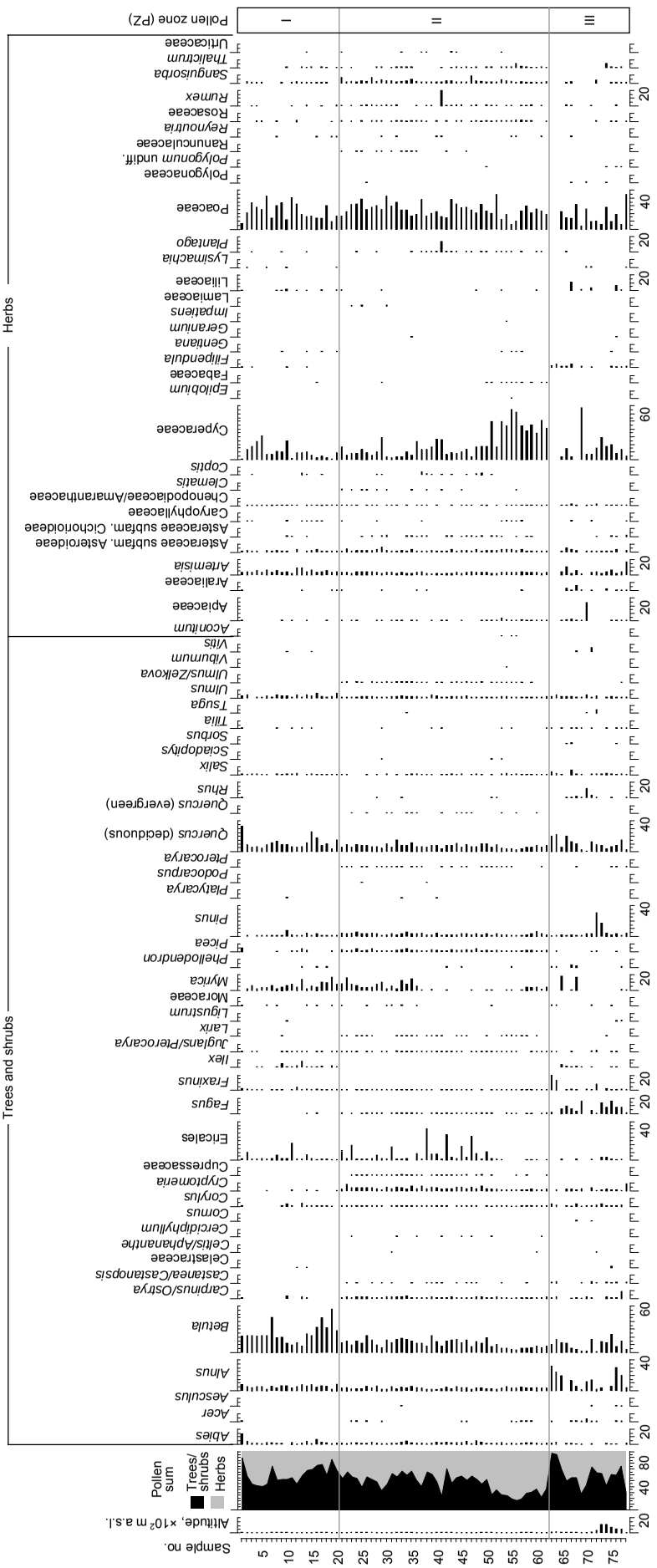

Fig 4.3 Percentage pollen diagram representing 78 modern pollen spectra from Hokkaido. Percentages of individual taxa are calculated upon the total sum of all arboreal and nonarboreal pollen taxa listed in Tables 1 and 2 and used for the biome reconstruction (Takahara et al., 2000; Gotanda et al., 2002).

Pollen taxa percentages in all 78 modern spectra were recalculated for the purpose of biome climate reconstructions based upon the sum of all arboreal and non-arboreal pollen taxa (Table 4.1) and upon the sum of 32 arboreal pollen taxa (Table 4.2). The pollen diagrams showing percentage variations of taxa considered for environmental reconstructions in this study are presented in Fig. 4.3. The pollen diagrams were created using the Tilia/Tilia-Graph/TGView software package (Grimm, 2004). Determination of the local pollen zone boundaries (Fig. 4.3) was supported by cluster analysis performed using CONISS (Grimm, 1987).

4.4.2 Fossil pollen record and environments around the coring site

This study utilised 38 fossil pollen spectra from a 280 cm long sediment core (42°17′03″N, 140°15′34″E) recovered from a peat bog located on the coastal plain, 3 km north of the town of Yakumo on the Oshima Peninsula in the south-western part of Hokkaido (Fig. 4.1). The results of pollen analysis were first published in Japanese with an English abstract (see Kito and Takimoto (1999) for original pollen diagram and details of pollen extraction and identification). The age model is based on four radiocarbon dates (Kito and Takimoto, 1999), which were converted to calendar years before present (cal BP) using Calib 3.0 (Stuiver and Reimer, 1993), as well as on the two prominent tephra layers of known age (Katsui et al., 1975; Hayakawa and Koyama, 1998) found in the upper part of the peat section.

As was done for the modern surface dataset, taxa percentages for all 38 fossil spectra were recalculated for the purpose of biome climate reconstructions based upon the sum of all arboreal and non-arboreal pollen taxa (Table 4.1) and upon the sum of 32 arboreal pollen taxa (Table 4.2). The pollen diagrams showing percentage variations of taxa considered for environmental reconstructions in this study are presented in Fig. 4.4.

The coring site is located south of the Kuromatsunai line (Fig. 4.1), which according to Itoh (1987) separates the temperate deciduous forest (to the south) from the cool mixed forest biome (to the north) and marks the northern distribution limit of *Fagus* (*F. crenata*: Japanese beech). The vegetation of the study area is described in Kito and Takimoto (1999). The plains and lowlands around the coring site are dried and cultivated, whilst slopes and mountains (reaching up to 500–1300 m) are covered by secondary forest typically characterised by temperate deciduous broadleaf trees, including *Q. crispula* (Japanese oak), *F. crenata*, *U. davidiana* var. *japonica* (Japanese elm), *Fraxinus lanuginosa* (Japanese ash), *Acer japonicum* (Downy Japanese maple) and *Castanea crenata* (Japanese chestnut). Evergreen broadleaf elements, i.e. *Ilex crenata* var. *paludosa* (Japanese holly), can also be found at lower elevations. It has been suggested that in northern Japan chestnut trees were

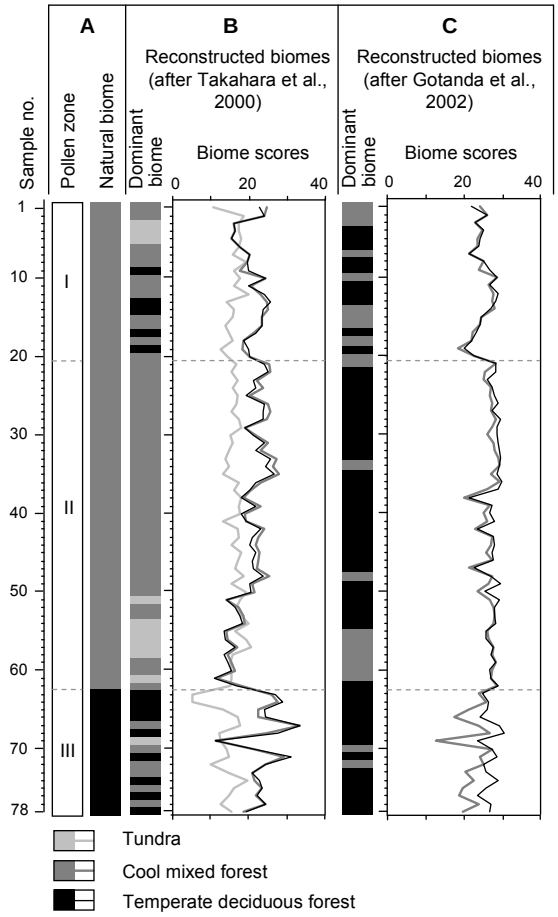

Fig. 4.4 (A) Major natural vegetation types around the modern pollen sampling sites (after Yoshioka, 1973) compared to the results of biome reconstruction (dominant biomes and numerical scores) for the set of 78 modern pollen spectra from Hokkaido using biome-taxa assignment suggested by (B) Takahara et al. (2000) and (C) by Gotanda et al. (2002).

planted for food and timber by the Jomon people from about 6000 to 5000 cal BP (Tanaka et al., 2005). *Cryptomeria* (Japanese cedar) is also counted as a human-introduced tree species which is present in the study region. *A. sachalinensis* (Sakhalin fir), native but rare in nature, is widely planted in the region (Kito and Takimoto, 1999).

Modern climate variables around the study site derived from a global climate dataset (New et al., 2002) demonstrate a seasonally warm and all-year-round wet climate, which supports natural growth of the temperate deciduous forest biome, as defined in the BIOME1 global vegetation model (Prentice et al., 1992). The estimated mean annual temperature (TANN) is 7.9 °C, the mean temperature of the warmest month (MTWA) is 21.1 °C, and the coldest month mean temperature (MTCO) drops to −3.7 °C. Mean annual precipitation (PANN) is 1252 mm in total, of which ca. 670 mm falls between April and September (PSUM) and the rest between October and March (PWIN). For comparison, the meteorological data from the nearest station averaged for 1981–2010 provide very similar values: 7.9 °C (TANN), 20.9 °C (MTWA), −3.5 °C (MTCO), 1279 mm (PANN), 709.7 mm (PSUM), and 569.3 mm (PWIN).

4.5 Results

4.5.1 Surface pollen data and pollen-derived biomes

The results of the microscopic analysis of the 78 modern pollen spectra are presented in a percentage pollen diagram (Fig. 4.3). Among the 72 terrestrial pollen taxa identified in the surface pollen dataset, 41 taxa represent trees and shrubs and the remaining 31 taxa represent herbaceous plants. In total 16 taxa show percentage values that do not exceed the universal threshold of 0.5% and, thus, could not influence the biome reconstruction. This list includes both arboreal and non-arboreal taxa, such as *Aconitum*, *Aesculus*, *Celtis/Aphananthe*, *Cercidiphyllum*, *Epilobium*, *Geranium*, *Impatiens*, Labiatae (Lamiaceae), Leguminosae (Fabaceae), *Ligustrum*, *Lysimachia*, *Platycarya*, *Podocarpus*, *Pterocarya*, Ranunculaceae and *Sciadopitys*.

The analysed pollen spectra are arranged along a latitudinal profile in north–south direction. The diagram is subdivided into three pollen zones (PZ), which represent the three main sampling areas (Fig. 4.1) and reflect the most pronounced changes in pollen composition. PZ I (samples 1–20) represents the northern part of the study area north of 45°N and west of 142°E. This zone reveals the highest percentages of cold-tolerant *Betula* and moderately abundant pollen of temperate deciduous tree taxa, including *Quercus* (deciduous) and *Ulmus*. *Ilex*, which is a cool-temperate broadleaved evergreen taxon, commonly appears in the pollen spectra, although in low abundances. PZ II (samples 21–62) represents the easternmost part of Hokkaido between 43° and 43.5°N (Fig. 4.1). This zone reveals the highest percentages of Ericaceae (heath family) pollen, moderately high percentages of *Betula* pollen, relatively low percentages of *Quercus* pollen, and an absence of *Ilex*. PZ III (samples 63–78) represents the south-western part of the study area south of 43°N (Fig. 4.1). This zone reveals the highest percentages and variety of temperate deciduous tree and shrub taxa, including *Fagus* and *Fraxinus*. In all three pollen zones, percentages of herbaceous taxa (mainly Poaceae and Cyperaceae) are relatively high, reaching 78% in PZ II, partly reflecting the natural openness of the landscape and partly human disturbances. *Artemisia* reaches its highest percentages in PZ III, which is the most densely populated part of the island.

The results of the pollen-based biome reconstruction are shown in Fig. 4.4. The assignment of all terrestrial pollen taxa to biomes (Table 4.1) following Takahara et al. (2000) reveals some differences from the results obtained with the short list of 32 arboreal taxa (Table 4.2) applied by Gotanda et al. (2002). Comparison of both tests with the natural forest biomes distinguished in the botanical maps (Fig. 4.1) demonstrates better results obtained with the biome-taxa matrix presented in Takahara et al. (2000), i.e. 56 correct reconstructions (71.8%), than with the biome-taxa matrix presented in Gotanda et al.

(2002), i.e. 34 (43.5%) correct reconstructions (Fig. 4.4A–C). In particular, the latter reconstruction (Fig. 4.4C) frequently shows the TEDE biome scores have the highest values in PZ I and PZ II, where COMX biome predominates in the natural vegetation. In general, the biome reconstruction obtained with the longer list of taxa (Fig. 4.4B) reflects the natural biome distribution in the study regions (Fig. 4.4A) better (by ca. 28%) than the results obtained with the short list of taxa (Fig. 4.4C). However, in 11 cases (ca. 14%) it demonstrates the tundra biome (Fig. 4.4B) being reconstructed in place of TEDE and COMX forest (Fig. 4.4A).

4.5.2 Fossil pollen record and pollen-based vegetation reconstruction

The percentage pollen diagram (Fig. 4.5) demonstrates the local and regional changes in the fossil pollen assemblages. Visual inspection and quantitative CONISS-based analysis allow subdivision of the pollen diagram into three major pollen zones (PZ A to C) representing extra-local and regional vegetation and six subzones (PsZ Hn-I to Hn-VI), which represent local vegetation communities (as defined in Kito and Takimoto, 1999). The main changes in the pollen assemblages can be summarised as follows.

The lowermost PZ Hn-A (~160–280 cm; ~3.6–5.5 cal ka BP) shows the highest pollen percentages of *Alnus* and *Rhus*, relatively high percentages of *Quercus* (deciduous) and almost no pollen of *Fagus*. Pollen percentages of taxa representing local vegetation communities (e.g. *Alnus*, *Rhus* and various herbs) are highest in this zone. PZ Hn-B (~59–160 cm; ~1.2–3.6 cal ka BP) reveals decreasing percentages of *Alnus* and increasing percentages of *Fagus* pollen and the virtual disappearance of *Rhus* from the pollen spectra. The highest values of locally growing *Ilex* are noticeable in PsZ Hn-IV (~134–160 cm; ~3.3–3.6 cal ka BP). Pollen assemblages of PZ Hn-C (~0–59 cm; 0–1.2 cal ka BP) are co-dominated by *Alnus*, *Betula*, *Quercus* and *Fagus*. The latter reaches its maximum throughout the whole record in this zone. Qualitative interpretation of the Yakumo record demonstrates the middle to late Holocene spread of *F. crenata* in the south-western part of Hokkaido. Beech invaded an oak-dominated forest around 3.4 cal ka BP and its population grew progressively until approximately 1.7 cal ka BP and slightly declined after that. Results of the pollen-based biome reconstruction obtained with the two different biome-taxa matrices (Fig. 4.6) are in line with the qualitative interpretation of the pollen diagram (Fig. 4.5), suggesting that the regional vegetation was predominantly cool mixed and temperate deciduous forest prior to 3.6 cal ka BP and *Fagus*-dominated communities spread in the study area after that time.

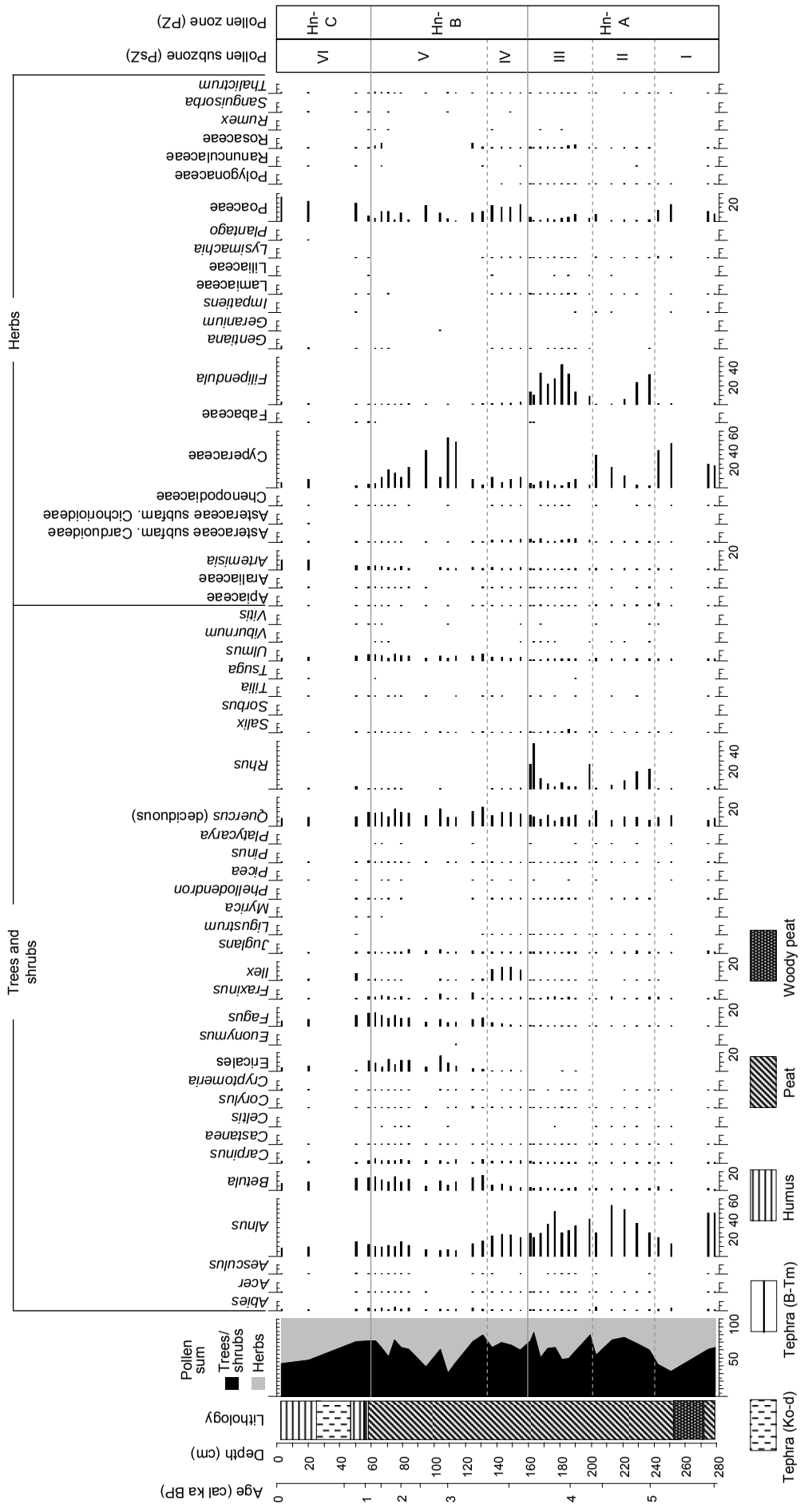

Fig. 4.5 Percentage pollen diagram representing 38 fossil pollen spectra from the Yakumo site, SW Hokkaido (modified from Kito and Takimoto, 1999). Percentages of individual taxa are calculated upon the total sum of all arboreal and non-arboreal pollen taxa listed in Tables 1 and 2 and used for the biome reconstruction (Takahara et al., 2000; Gotanda et al., 2002).

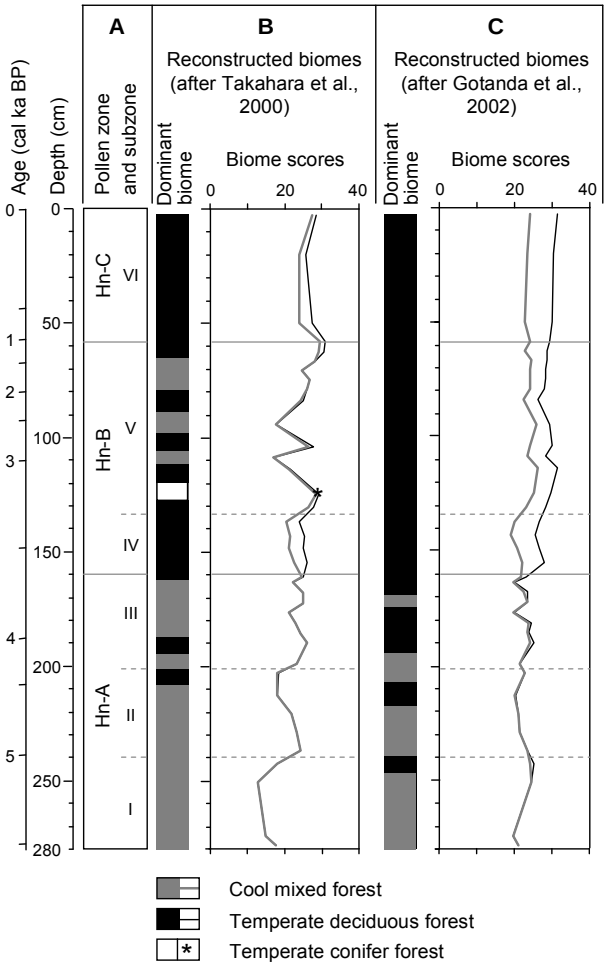

Fig. 4.6 Results of biome reconstruction (dominant biomes and numerical scores) for the set of 38 fossil pollen spectra from the Yakumo record, SW Hokkaido plotted along the depth and age scales and (A) pollen zones (adapted from Kito and Takimoto, 1999) using the biome-taxa assignment suggested by (B) Takahara et al. (2000) and (C) by Gotanda et al. (2002).

4.5.3 Pollen-based climate reconstruction

Results of the quantitative reconstruction of six climate parameters representing thermal and hydrological conditions of the Yakumo area during the last ca. 5500 years are shown in Fig. 4.7. The results obtained with a smaller (248 sites from Tarasov et al., 2011) and a larger (326 sites, including 78 additional spectra from Hokkaido) dataset show very similar features and the differences in the absolute values are within the uncertainty range of the reconstruction method (Fig. 4.7). All temperatures reconstructed from the topmost core sample using the larger reference dataset are very close to modern climate observations at the study site, while the reconstructions with the smaller dataset overestimate modern temperatures by 1.1–1.6 C (Fig. 4.7A–C). Two sets of precipitation reconstructions derived from the core top sample provide very similar values, which closely resemble modern meteorological observations (Fig. 4.7D–F). As the reconstruction obtained with the larger analogue dataset generally reproduces the modern climate better, it is considered as more robust and therefore is used in further discussion.

The temperature reconstructions (Fig. 4.7A–C) demonstrate small variations around modern values (within ~2–3 C range), indicating slightly colder than present environments in the lower part of the record (PZ Hn-A, prior to 3.6 cal ka BP), slightly warmer in the middle part (PZ Hn-B) and similar to present in the upper part of the record (PZ Hn-1, during the last millennium). MTWA (Fig. 4.7A) fluctuates between 19.6 and 22.0 °C and MTCO between −6 and −3 °C. The reconstructed changes in hydrological variables (Fig. 4.7D–F) show lower than present precipitation values prior to 3.6 cal ka BP and similar to present environments after this date, suggesting an increase in annual precipitation (Fig. 4.7F) of about 300 mm between the middle and late Holocene.

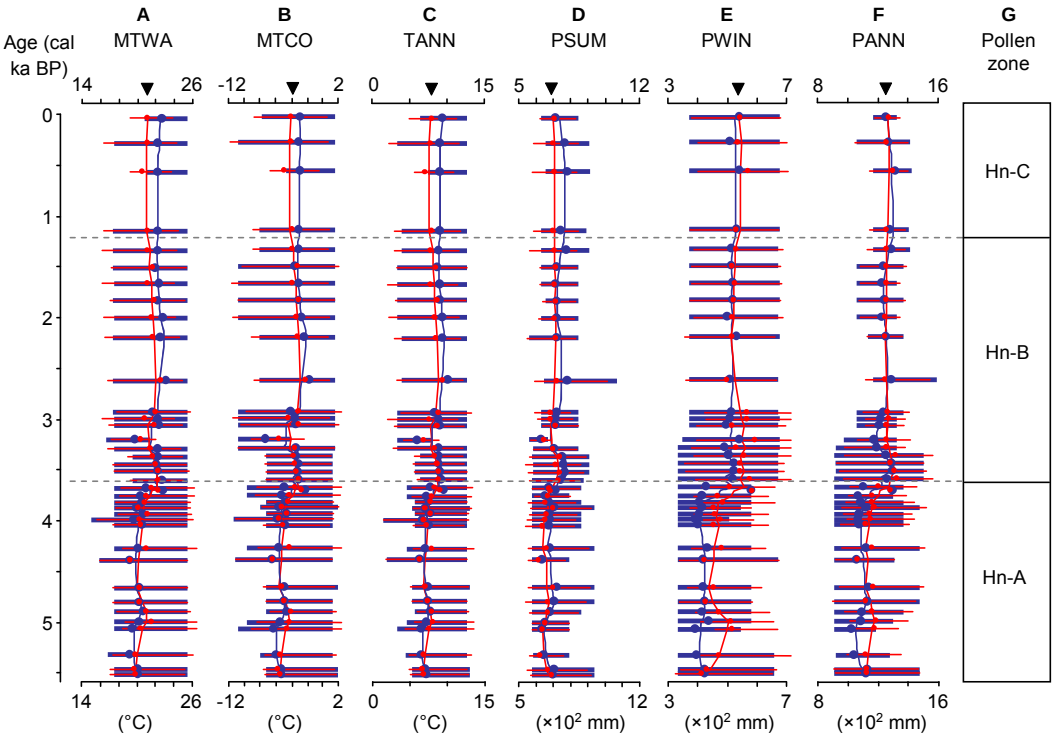

Fig. 4.7 Charts A–F show the results of the reconstruction of six climate parameters (see Fig. 4.2 caption for abbreviations) based on the modern analogue technique (adapted from Nakagawa et al., 2002; Tarasov et al., 2011) and the fossil pollen record from the Yakumo site, SW Hokkaido (Kito and Takimoto, 1999; this study). The results obtained with the set of 248 reference pollen sites from Tarasov et al. (2011) are shown in blue (large dots and thick lines) and the reconstructions obtained with the set of 326 reference pollen sites (Tarasov et al., 2011 plus 78 sites compiled in this study) are shown in red (small dots and thin lines). Dots indicate weighted averages of reconstructed variables calculated from a range of 8 closest analogues determined by the squared Euclidean distance applying a threshold of 0.4 (after Nakagawa et al., 2002; Tarasov et al., 2011). Horizontal bars indicate the analogue uncertainty range defined by the minimum and maximum value of best modern analogues assigned to each analysed fossil sample and vertical curve lines show the 3-point running averages of the reconstructed climate variables. The triangles mark modern conditions inferred from the climate dataset of New et al. (2002). Main pollen zones (G) are adopted from Kito and Takimoto (1999).

4.6 Discussion

4.6.1 Quantitative vegetation reconstructions with the pollen data from Hokkaido

Tests of the biome reconstruction method using two published matrices assigning Japanese pollen taxa to biomes were performed for the set of 78 surface pollen spectra from northern, eastern and southern Hokkaido, where natural vegetation is represented by cool mixed and temperate deciduous forests. The results of these tests suggest that both proposed schemes have their limitations in reconstructing natural vegetation. In particular, the approach (Gotanda et al., 2002) considering the short list of 32 arboreal taxa (Table 4.2) correctly assigns pollen spectra from the TEDE vegetation zone (14 of 16 cases; 88%), but fails in reconstructing the COMX biome (20 of 62 cases; 32%). Another approach (Takahara et al., 2000), which applies more arboreal and non-arboreal taxa (Table 4.1), provides seemingly better reconstruction results for COMX (47 of 62 cases; 76%) but is less reliable for TEDE (9 of 16 cases; 56%). A key difference between the two approaches causing the major discrepancies in the reconstruction results is the assignment of *Cryptomeria* to both TEDE and COMX by Takahara et al. (2000), while Gotanda et al. (2002) only assign this taxon to TEDE. Although not native to Hokkaido, *Cryptomeria* grows well in its southern and middle part, as far as Tsukigata (43°20.63′N, 141°39.70′E), i.e. in the distribution area of TEDE and (partly) of COMX. Following the concept of biomization summarised in Prentice et al. (1996) the individual taxa which occupy part of the bioclimatic space of the respective biome should be assigned to it. Indeed assignment of *Cryptomeria* to COMX in the biome-taxa matrix (Table 4.2) helps to improve the accuracy of the Gotanda et al. (2002) approach, i.e. 13 of 16 correct assignments for TEDE (81%) and 54 of 62 correct assignments for COMX (87%).

Another problem indicated by the tests with the surface pollen data and the long taxa list (Table 4.1) is the reconstruction of the tundra biome where botanical maps show a predominance of temperate deciduous (1 case) or cool mixed forest (10 cases). As tundra is not among the modern natural vegetation types of Hokkaido, the problem requires more careful investigation. The appearance of TUND in the reconstruction may reflect incorrect assignment of the taxa to biomes or/and some features of the vegetation at and around sampling sites, i.e. disturbed or azonal vegetation communities. For example, large swamps in the boreal and temperate zones very much resemble the environments and vegetation composition of the tundra. The distribution patterns of modern tree cover (expressed in % per 1×1 km pixel) can be checked using the satellite-based Advanced Very High Resolution Radiometer (AVHRR) dataset (DeFries et al., 1999, 2000a, 2000b). The AVHRR data demonstrate that tree cover percentages are very low (i.e. ~10–11%) within a 21×21 km window placed around the three pollen sampling sites from the northern

region, on which TUND has been reconstructed (Fig. 4.4B). Although the remaining 8 sites demonstrate higher tree cover percentages (i.e. ~23–46%), these are still low enough to explain high percentages of non-arboreal (mainly Poaceae and Cyperaceae) pollen (Fig. 4.3) and pollen-based reconstruction of the non-forest biome (Fig. 4.4B). In all 11 cases, however, the biome with the second highest score is COMX (Fig. 4.4B), suggesting that the reconstruction of TUND does not reflect regional climate but is caused by the local environments at and around the pollen sampling sites.

4.6.2 Middle and late Holocene climate dynamics

Among all reconstructed climate parameters (Fig. 4.8A–F), the precipitation curves show the most pronounced changes. Thus, PSUM (Fig. 4.8D) and PWIN (Fig. 4.8E) demonstrate relatively low values during the early part of the Yakumo record, followed by a gradual increase until reaching near modern values about 3.6 cal ka BP, suggesting a possible change in the EAM characteristics. The past climate reconstructions derived from various climatic and environmental archives from continental East Asia revealed a substantial weakening of the East Asian Monsoon during the middle and late Holocene (Yu et al., 1998, 2000; Xiao et al., 2004; Dykoski et al., 2005; Peng et al., 2005; Wang et al., 2005b; Tarasov et al., 2006; Hu et al., 2008; Steinke et al., 2011) related to a gradual decrease in solar insolation anomalies (Fig. 4.8M), particularly pronounced during the Northern Hemisphere summer (Berger and Loutre, 1991). Other studies (Yancheva et al., 2007; Yang and Ding, 2008) reported evidence of stronger winter monsoon winds during the Younger Dryas episode and during the middle and late Holocene, when Chinese cave stalagmites (Fig. 4.8G) suggest a weaker summer monsoon. This anti-correlation explained by migrations in the intertropical convergence zone (ITCZ) (Yancheva et al., 2007) found some support in the Chinese loess records (Fig. 4.8L) but is not accepted universally (see Steinke et al., 2011 for discussion and references).

Pollen and diatom studies on lake sediments from the western part of Japan suggest that the phases of weak summer and strong winter monsoon (for example, the Younger Dryas) revealed heavier snowfalls and the expansion of beech forests along the western coast of Honshu (Nakagawa et al., 2005, 2006; Kossler et al., 2011). Strengthening of the north-westerly winds crossing the relatively warm Sea of Japan would cause an increase in winter precipitation in SW Hokkaido, and support the spread of beech trees in the local forests during the late Holocene, as reconstructed from the Yakumo pollen record.

High resolution stalagmite $\delta^{18}O$ records from south-western China (Fig. 4.8G) show decreasing summer monsoon intensity, which is not reproduced in the PSUM reconstruction (Fig. 4.8D). Progressively drier conditions reconstructed from the middle and late Holocene pollen and isotope records from northern China (e.g. Tarasov et al., 2006; Hu

et al., 2008) are possibly connected to a more southerly position of the summer monsoon front, which also controls summer precipitation in Japan. Haug et al. (2001) and Wang et al. (2004), who reported decreasing trends in Holocene precipitation for Central America and northern South America respectively, were the first who partly linked this to a general southward movement of the ITCZ. This southward shift of the ITCZ, possibly driven by decreasing summer insolation in the Northern Hemisphere, could also cause a progressive cooling of the western Pacific warm pool (Stott et al., 2004) in line with the $\delta^{18}O$ record from Greenland (Fig. 4.8I), reflecting hemispheric change in air temperature. The cooling trend (from ~20 to ~18 °C) is also visible in the sea surface temperature (SST) reconstruction (Koizumi, 2008) derived from the diatom record of the MD01-2421 sediment core representing the NW Pacific region east of central Honshu (Fig. 4.8J). However, the reconstruction obtained for the MD01-2409 core (Koizumi, 2008) located in the Tsugaru Strait, where SST is controlled by the Tsugaru branch of the Tsushima Current (Fig. 4.1), does not reproduce this trend, but shows colder than average conditions prior to 4.5 cal ka BP, warm oscillation around 3.5 cal ka BP and generally warmer conditions during the last 2000 years (Fig. 4.8J). These differences suggest that the climate of the Yakumo area and SW Hokkaido during the last 5500 years might be influenced by another factor, which is not directly related to the hemispheric-scale changes in solar insolation and temperatures and the EAM variations.

The modern climate of the study area is strongly influenced by the Tsushima Warm Current and by the winter monsoon-associated snow precipitation, whilst the rainy season associated with the summer monsoon is not pronounced, as it is in the southern and central regions of Japan. The reconstruction of the Holocene influx of the Tsushima Current into the Sea of Japan signalled by spatial and temporal changes in the planktic foraminifer Neogloboquadrina incompta (Domitsu and Oda, 2008) suggest that the warm current started to influence the sea prior to the deposition of the K–Ah tephra (7.3 cal ka BP) and that a northern cold water mass strongly affected the south-western part of the Sea of Japan until 6.9 cal ka BP, which may have been a result of the weaker influence of the Tsushima Current during a time of lower sea level. The percentages of N. incompta in the cores from the southern part of the Sea of Japan (Domitsu and Oda, 2008) demonstrate progressive increase (Fig. 4.8K), most likely indicating the weakening impact of the cold water masses in the Sea of Japan during the last 6.9 cal ka BP, in line with the diatom record from the Tsugaru Strait (Fig. 4.8J) and with trends towards higher temperatures and precipitation derived from the Yakumo pollen record (Fig. 4.8A–F).

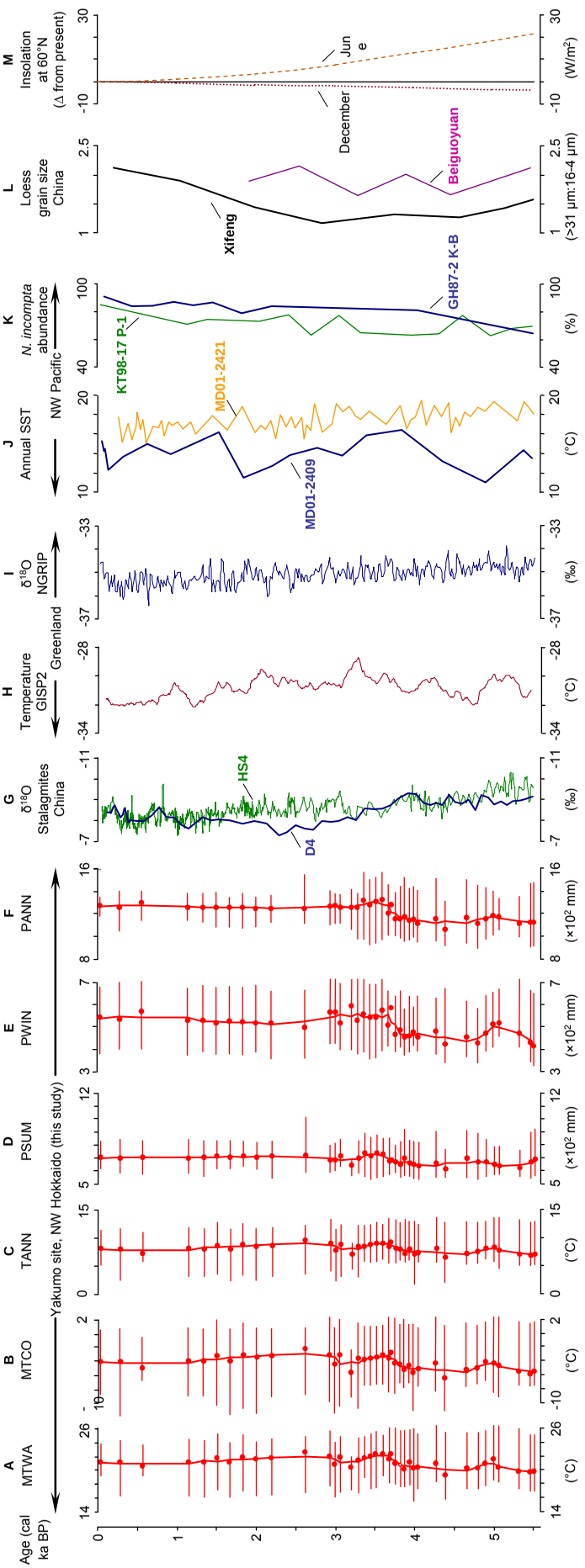
Age (cal ka BP)
Yakumo site, NW Hokkaido (this study)
A MTWA (°C)
B MTCO (°C)
C TANN (°C)
D PSUM (×10² mm)
E PWIN (×10² mm)
F PANN (×10² mm)
G δ18O Stalagmites China (‰)
HS4
D4
H Temperature GISP2 Greenland (°C)
I δ18O NGRIP (‰)
J Annual SST NW Pacific (°C)
MD01-2409
MD01-2421
K N. incompta abundance (%)
KT98-17 P-1
GH87-2 K-B
L Loess grain size China (>31 µm:16-4 µm)
Xifeng
Beiguoyuan
M Insolation at 60°N (Δ from present) (W/m²)
December
June

Fig. 4.8 Six climate variables derived from the Yakumo fossil pollen record using the set of 326 modern reference samples (A–F) along with the other climate proxies from the North Atlantic and North Pacific regions discussed in the text: (G) the $\delta^{18}O$ speleothem records from China including HS4 stalagmite (thin green line) from Heshang Cave (30°27'N, 110°25'E; after Hu et al., 2008) and D4 stalagmite (thick blue line) from Dongge cave (25°17'N, 108°5'E; after Yuan et al., 2004) showing East Asian summer monsoon intensity; (H) the GISP2 temperature reconstruction for central Greenland (after Alley, 2000); (I) the NGRIP $\delta^{18}O$ record from Greenland as an indicator of the Northern Hemisphere air temperature (after Svensson et al., 2008); (J) the diatom-inferred annual sea surface temperature (SST) for the MD01-2421 sediment core of central Japan (36.02°N, 141.78°E) from the NW Pacific east of Honshu controlled by the Kuroshio Warm Current (thin orange line) and for the MD01-2409 core (41.56°N, 141.87°E) from the Tsugaru Strait (thick blue line) controlled by the Tsugaru branch of the Tsushima Warm Current (after Koizumi, 2008); (K) relative abundance of planktic foraminifer Neogloboquadrina incompta in the core KT98-17 P-1 (35°50.6'N, 131°05.2'E) (thin green line) and in the core GH87-2 K-B (36°4.92'N, 134°59.97'E) (thick blue line) indicating the warming trend in the southern Sea of Japan (after Domitsu and Oda, 2008); (L) the grain-size variations (ratio >31 mm:16–4 mm) in the Beiguoyuan (36°37'21.3''N, 107°17'12.3''E) section (thin violet line) and Xifeng (35°32'09.4''N, 107°43'13.5''E) section (thick black line) from the Chinese Loess Plateau (after Stevens et al., 2007) indicating the strength of the East Asian winter monsoon winds; and (M) the June (dashed line) and December (dotted line) solar insolation relative to present conditions (continuous line) at 60°N (after Berger and Loutre, 1991).

4.7 Conclusions

The current study reconstructs middle and late Holocene vegetation and climate dynamics in the south-western part of Hokkaido using the method of biome reconstruction and modern analogue technique applied to the published and newly compiled surface and fossil pollen data from northern Japan.

The ability of the biomization method to predict distribution of temperate deciduous and cool mixed forest biomes on Hokkaido was tested using two previously published biome-taxa matrices applied for reconstruction of the late Quaternary vegetation in Japan and a newly compiled dataset of 78 modern surface spectra representing northern, eastern and southern Hokkaido. The results of the tests compared with the natural forest biome distribution shown in the botanical maps demonstrate better agreement obtained with the longer biome-taxa matrix presented in Takahara et al. (2000), i.e. 71.8% correct assignments, than with the shorter biome-taxa matrix presented in Gotanda et al. (2002), i.e. 43.5% correct assignments. In particular, the latter approach frequently assigns pollen spectra collected from the cool mixed forest dominated area to temperate deciduous forest. A key difference between the two approaches causing the major discrepancies is the treatment of *Cryptomeria*, which (although not native to Hokkaido) grows well in its southern and middle part and therefore should be assigned to both COMX and TEDE biomes. The assignment of *Cryptomeria* to COMX in the biome-taxa matrix (Table 4.2) helps to improve the total accuracy of the Gotanda et al. (2002) approach to 86%. This problem, however, should not influence vegetation reconstructions based on the Holocene

pollen records from Hokkaido, as *Cryptomeria* pollen contribution is minor and represents distant air transport.

The method for reconstructing cool conifer forest, which occupies relatively small areas in the mountains of central Hokkaido, could not be tested due to the lack of surface pollen samples. This gap needs to be filled, as COCO probably played a more important role on Hokkaido during the late glacial and early Holocene. The current study also demonstrates the need to use the whole list of identified terrestrial pollen taxa for constructing a biome-taxa matrix capable of providing robust vegetation reconstructions from the fossil pollen records from Hokkaido and Rebun, particularly during the colder/drier intervals of the late Quaternary when forests occupied a smaller area in comparison to the warmer/wetter Holocene climatic optimum.

The middle and late Holocene climate dynamics in the south-western part of Hokkaido were reconstructed using the modern analogue technique applied to the terrestrial pollen record from Yakumo and updated dataset of 326 reference pollen samples representing Hokkaido and northern Honshu. The reconstruction suggests a climate slightly cooler and drier than present between 5.5 and 3.6 cal ka BP and similar to present or warmer/wetter conditions after 3.6 cal ka BP when temperate deciduous forest replaced cool mixed forest in the study region. This general trend in vegetation and climate development of the Yakumo area, however, conflicts with the wide-scale features of the Northern Hemisphere climate, such as the gradual decrease in summer insolation and temperature and the weakening of the East Asian Summer Monsoon, meaning that another mechanism controlling regional environments needs to be sought. The changes in the water circulation of the Sea of Japan could provide a reasonable explanation of the reconstructed vegetation and climate changes. In particular, the expansion of the warm Tsushima Current in the Sea of Japan during the middle and late Holocene supported by the studies on diatoms and foraminifera in the marine core sediments most likely caused an increase in sea surface and air temperatures around SW Hokkaido and favoured moisture uptake leading to an increase in precipitation and snow accumulation during the late Holocene. High resolution pollen and SST records with better age control from Hokkaido and surrounding seas are necessary in order to test this hypothesis.

4.8 Acknowledgments

This work contributes to the ongoing ‘Baikal-Hokkaido Archaeology Project’ funded via the Social Sciences and Humanities Research Council of Canada and to the ‘Bridging Eurasia Research Initiative’ supported by the German Archaeological Institute, CIC FU Berlin and the German Research Foundation (DFG TA 540/4-1 and TA 540/5-1). The work of C. Leipe is funded via the DFG grant RI 809/24. We highly appreciate the

comments and suggestions of two anonymous reviewers, which helped to improve the quality of the article. We are grateful to Dr. Dustin White and Giles Shephard for polishing the English.

4.9 Supplementary data

Supplementary material associated with this article can be found in the Open Access data library PANGAEA at doi:10.1594/PANGAEA.785361.

5. Manuscript IV

Pollen-inferred late Quaternary vegetation and climate variations from the northern-most part of the East Asian Summer Monsoon domain (Sakhalin, Russian Far East)

Christian Leipe [a], Yaeko Igarashi [b], Takeshi Nakagawa [c],
Katsuya Gotanda [d], Pavel E. Tarasov [a]

[a] *Institute of Geological Sciences, Palaeontology, Freie Universität Berlin, Malteserstraße 74–100, Building D, 12249 Berlin, Germany*

[b] *Institute for Paleoenvironment of Northern Regions, Koyocho 3-7-5, Kitahiroshima 061–1134, Japan*

[c] *Department of Geography, University of Newcastle, Newcastle Upon Tyne NE1 7RU, United Kingdom*

[d] *Faculty of Policy Informatics, Chiba University of Commerce, Chiba 272–8512, Japan*

Manuscript in review at *Quaternary Science Reviews*

5.1 Abstract

A last glacial–Holocene pollen record from northern Sakhalin (51.34°N, 142.14°E, 15 m a.s.l.) spanning the last ca. 44 ka was used to infer dynamics in regional climate conditions and vegetation distribution by means of the modern analogue technique (MAT) and the biome reconstruction method. The long-term trends of the reconstructed mean annual temperature (TANN) and precipitation (PANN), total tree cover and dominant biome distribution are generally in line with key palaeoclimate records from the North Atlantic region and the Asian monsoon domain. TANN largely follows the fluctuations in solar summer output, and was mainly controlled by winter thermal conditions. During Marine Isotope Stage (MIS) 3, TANN and PANN were on average 0.2 °C and 700 mm, respectively, thus very similar to late Holocene/modern conditions. Full glacial climate deterioration with TANN of –3.3 °C and PANN of 550 mm was relatively weak as suggested by the MAT-inferred average climate parameters, which is supported by the calculated biome scores. However, error ranges of the climate reconstructions during this interval are rather large and suggest potentially much colder and drier environments in northern Sakhalin. An anti-phase relationship between mean temperature of the coldest and warmest month is documented during the last glacial, which we interpret as changes in the degree of continentality due to variations in the global sea level and glaciation cycles. Warmest and wettest climate conditions have prevailed since the end of the last

deglaciation with an optimum (TANN = 1.5 °C, PANN = 800 mm) in the middle Holocene interval (ca. 8.7–5.2 cal ka BP), which lags behind the solar insolation peak during the early Holocene. We propose that this is due to continuous Holocene sea level transgression and regional forcing factors like the Tsushima Warm Current, which reached maximum intensity during the middle Holocene. Several short-term climate oscillations are imprinted in our reconstruction results and correspond to Northern Hemisphere last glacial millennial-scale (Heinrich and Dansgaard-Oeschger events, Bølling–Allerød, Younger Dryas) and Holocene centennial-scale (Bond cycles) events. The most prominent fluctuation is registered during Heinrich event 4, which is marked by noticeably colder and drier conditions and the spread (decrease) of herbaceous (arboreal) taxa. An equivalent is not clearly traceable in the available palaeoclimate proxy records from the Asian monsoon domain and neighbouring regions. In addition, Holocene millennial-scale cold spells synchronous with Bond events are only partly registered in our biome and climate reconstruction. Although this might be due to an insufficient resolution of the presented pollen record, it appears more likely that effects of Northern Hemisphere short-term (centennial- and millennial-scale) climate oscillations on Sakhalin are partly amplified or weakened by feedbacks on regional forcing factors.

5.2 Introduction

The Asian monsoon, comprising the Indian and East Asian subsystem, is a major global atmospheric circulation system which principally controls the climate of a vast continental area stretching from the western Arabian Sea to the southern Russian Far East (RFE) including the most densely populated regions of the world (Alpat'ev et al., 1976; Wang, 2006). Numerous palaeoclimate studies from both monsoon subdomains have outlined that climate conditions have varied significantly on different time-scales during the Holocene (e.g. Leipe et al., 2014; Hu et al., 2008) and last glacial period (e.g. Wang et al., 2001b; Govil and Naidu, 2010). For predicting future climate changes model simulations have been identified to provide useful estimations (IPCC, 2001, 2007). Since the Asian monsoon system affects weather and climate in various regions of the world, precise simulation of its future development is of particular importance (Wang, 2006; Turner and Annamalai, 2012). Although numerous approaches have been proposed (IPCC, 2007), modelling the Asian monsoon and its teleconnections on short- and long-term scales (i.e. intraseasonal to orbital time scales) and to estimating future trends remains a challenging task (e.g. Turner et al., 2011; Sperber et al., 2012; Zhao and Harrison, 2012). To evaluate and further improve existing projections of both global and regional climate trends relevant for the development of human societies, it is essential to compare model outputs

with palaeoclimate data (e.g. Otto-Bliesner et al., 2009; Dallmeyer et al., 2010; Braconnot et al., 2012).

Concerning glacial–interglacial timescales, the spatiotemporal patterns and the magnitude of past variations in Asian monsoon activity and its relation with other components of the global climate system as well as extraterrestrial forcing factors remain poorly understood (e.g. Nakagawa et al., 2008; Leipe et al., 2014). To enhance our perception, additional climate reconstructions based on continuous long-term records from different regions of the Asian monsoon domain are required (e.g. Ju et al., 2007; Tarasov et al., 2011; Chabangborn et al., 2013; Jin et al., 2014). Today, numerous late Quaternary marine and terrestrial palaeoclimate proxy records are available from both the Indian Summer Monsoon (ISM) and East Asian Summer Monsoon (EASM) subdomains but are mostly derived from the core monsoon zone and seldom exceed the Holocene interval (e.g. Morrill et al., 2003; Wang et al., 2005a; Herzschuh, 2006; Fleitmann et al., 2007; Wang et al., 2010; Ran and Feng, 2013 and references therein).

Especially from the terrestrial northernmost EASM domain (ca. 45–55°N), including parts of the northeast Asian mainland (i.e. north-easternmost China and the continental southern RFE) and parts of the north-western Pacific archipelago (i.e. Hokkaido, the Kuril Islands and Sakhalin), the number of palaeoclimate studies is very scarce (e.g. Mokhova et al., 2009). In summer the area represents the transitional zone between cold air masses from high latitude polar regions and the warm and moist EASM air masses originating from the north-western Pacific. EASM influence here is strongest between June and July (Ding and Chan, 2005) when the monsoon front reaches its northernmost position at ca. 55°N (Geograficheski Atlas SSSR, 1990). In winter, the climate is generally controlled by the East Asian Winter Monsoon (EAWM) (Alpat'ev et al., 1976). During this season, the region is situated on the boundary which separates the area to the south and to the north of ca. 50°N where surface air temperature is significantly influenced by the Siberian High and the Arctic Oscillation, respectively (Wu and Wang, 2002). Thus, robust reconstructions of past thermal and hydrological conditions from this climatically sensitive region are of particular significance to enhance our understanding of past climate dynamics in the whole northeast Asian region.

Regional palaeoclimate studies available to the international community are based on a limited number of proxy records from sites in the southern RFE including the Amur river valley (e.g. Bazarova et al., 2008, 2011; Mokhova et al., 2009), Sakhalin (e.g. Igarashi et al., 2002; Takahara et al., 2010; Igarashi and Zharov, 2011) and the Kuril Islands (e.g. Razjigaeva et al., 2013 and references therein) and the Japanese island of Hokkaido (e.g. Igarashi, 2013 and references therein). The majority of these works employed fossil pollen assemblages to qualify palaeoclimate conditions and vegetation distribution. Such pollen records have also proved to be an excellent tool to quantify past variations in climate

(Jackson and Williams et al., 2004 and references therein) and vegetation cover (Williams et al., 2011 and references therein) in different parts of the world. In addition, they allow the reconstruction of changes in dominant vegetation (biome) distribution (e.g. Prentice et al., 2000), which may also be interpreted in climatic terms via vegetation models (e.g. Prentice et al., 1992; Kaplan, 2001). Therefore, they are extremely valuable for assessing climate model performances (e.g. Kaplan et al., 2003; Bartlein et al., 2011; Braconnot et al., 2012).

The so far longest terrestrial fossil pollen record from the northernmost East Asian Monsoon domain (ca. 45–55°N) was recovered from a peat bog on the north-western coast of Sakhalin (Fig. 5.1B) and spans the last ca. 44 ka. Results of the conventional pollen and spore analysis are presented and discussed in a palaeoclimatological context by Igarashi et al. (2000) and Igarashi et al. (2002). Later, the results were employed by Takahara et al. (2010) to evaluate vegetation variability in response to Dansgaard-Oeschger (DO) and Heinrich events and by Igarashi and Zharov (2011) to compare and review the climate and vegetation dynamics on Hokkaido and Sakhalin during the late last glacial. In this study we utilise the fossil pollen record from northern Sakhalin for (semi-)quantitative reconstruction of past dynamics in (i) climate conditions and tree cover based on the modern analogue technique and (ii) dominant vegetation communities based on the biome reconstruction method, which is (iii) tested with a dataset of surface pollen spectra. The results of the vegetation and environmental reconstructions are discussed in the context of other published regional and extra-regional palaeoclimate proxy records.

5.3 Environmental setting of Sakhalin

Sakhalin is an island in the western Okhotsk Sea (Fig. 5.1A). It is narrow in shape with no location further away from the coast than 67 km (Reuter et al., 2007; Jarvis et al., 2008; ESRI, 2012) and stretches ~950 km from north to south (ca. 54.5–46°N). The island is separated from the Eurasian mainland by the Tatar Strait (~8 km at the narrowest point) in the northwest and from Hokkaido by the Soya Strait (~43 km at the narrowest point) in the south. Topographically, Ivanov (2002) roughly subdivides Sakhalin into a mostly flat region, i.e. the North Sakhalin Plain, in the north (ca. 51.5–54°N) and a mountainous region in the south (ca. 46–51.5°N). The latter is dominated by the Eastern and Western Sakhalin Range, which are separated by a graben structure in the central part of the island (Fig. 5.1B). Both mountain ranges are characterised by medium elevations up to ~1600 m above sea level (a.s.l.), deep intermontane depressions and steep incised river valleys (Zhulidov et al., 1997; Kuzmin and Glascock, 2007).

5.3.1 Climate conditions

The climate of Sakhalin is mainly determined by a typical summer and winter monsoon circulation (Alpat'ev et al., 1976; Martyn, 1992). The summer monsoon is driven by low air pressure over Siberia (Asiatic Low) and high air pressure (Hawaiian High) over the northern Pacific Ocean. The development of both pressure systems results in the continuous northward migration of the East Asian polar front (Fig. 5.1A). This movement culminates in middle to late summer when the front stretches roughly from the northern tip of Sakhalin, over Mongolia, to the eastern end of Lake Balkhash. During this time, Sakhalin is affected by predominant flow of moist air masses from southern to south-eastern directions, which creates humid and thermally mild conditions (Fig. 5.1A). Due to the formation of the Aleutian Low and the Siberian High during autumn, the pressure gradient reverses and leads to the continuous southward migration of the East Asian polar front (Fig. 5.1A). In winter, when the pressure gradient is most pronounced, weather conditions on Sakhalin are predominated by south-eastward flow of continental cold and dry air masses. Simultaneously to the development of the Siberian High, the northern RFE is marked by enhanced cooling, which results in the southward shift of the Arctic front. In January it is approximately situated along the northern shore line of the Okhotsk Sea (Alpat'ev et al., 1976; Geograficheski Atlas SSSR, 1990; Ivanov, 2002; Dando, 2005).

A second factor which affects the climate on Sakhalin are the different thermal conditions of the surrounding seas driven by ocean currents (Fig. 5.1B). On the eastern coast of the island the East Sakhalin Cold Current (ESCC) flows southward. In the southwest and south of Sakhalin mean surface water temperatures are higher under the influence of the Tsushima Warm Current (TWC), which flows as a sub-branch of the Kuroshio Warm Current (KWC) northwards along the eastern margin of the Sea of Japan, and the Soya Warm Current (SWC), which flows as a TWC sub-branch between Sakhalin and Hokkaido towards the Okhotsk Sea. While the TWC gradually cools when progressing further north into the Tatar Strait, parts of the water current turn and flow southwards along the shore of the Eurasian mainland as the Liman Cold Current (LCC).

Mean temperatures and precipitation generally follow a latitudinal gradient with highest values in the southern part of the island. The mean annual temperature (TANN) is 2.1 °C at Yuzhno-Sakhalinsk (46.97°N, 142.73°E, Fig. 5.1B) in the south, drops to 0.0 °C in Poronaysk (49.22°N, 143.1°E, Fig. 5.1B) and reaches only –2.4 °C in Okha (53.52°N, 142.91°E, Fig. 5.1B) located in northern Sakhalin (Krestov, 2003). Mainly due to the maritime conditions and the influence of the TWC, winters are particularly mild in the narrow southern part of Sakhalin. The mean temperature of the coldest month (MTCO) in Yuzhno-Sakhalinsk is with –13.8 °C about six degrees higher than at Nogliki (51.81°N, 143.16°E, Fig. 5.1B) and Okha in the island's north-eastern part. A noticeable winter

temperature gradient is also recognised between southern Sakhalin and the coastal mainland areas across the Sea of Japan. In Uglegorsk (49.08°N, 142.06°E, Fig. 5.1B) the MTCO is −14.8 °C but only reaches −19.4 °C in Sovetskaya Gavan (48.97°N, 140.29°E, Fig. 5.1B), which is situated only ~130 km westwards on the same latitude (Krestov, 2003). According to the global database of average modern surface climate (1961–1990) from New et al. (2002), the main amount of the annual precipitation (PANN) on Sakhalin, ~60% on average, is received during summer (April–September). While the PANN in Okha is ~550 mm, it is almost double (~960 mm) at Cape Krilion (Krestov, 2003). Like the western coastal areas of Honshu and Hokkaido (Japan), the southern part of Sakhalin receives enhanced snow falls promoted by the predominance of winter monsoon winds which transport significant amounts of moisture absorbed over the relatively warm Sea of Japan.

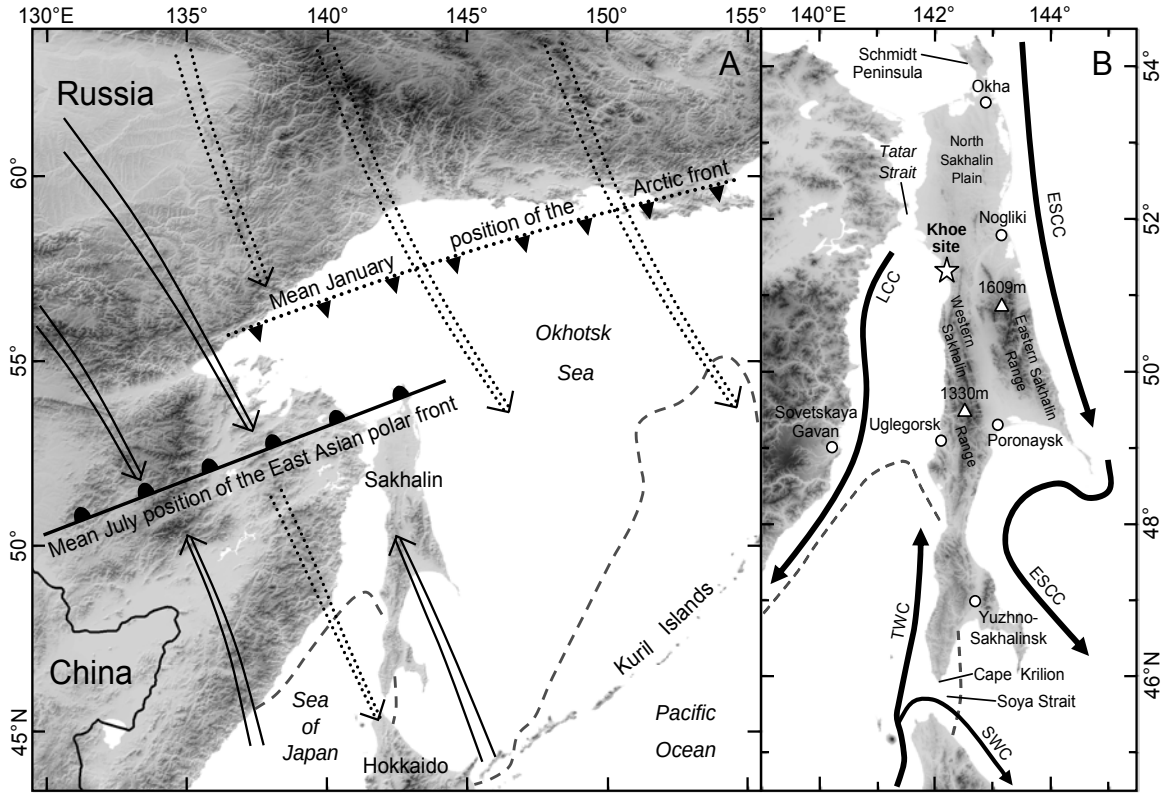

Fig. 5.1 (A) Overview map of the study region showing the mean July position of the East Asian polar front and the mean January position of the Arctic front together with the prevailing surface winds during summer (continuous arrows) and winter (dotted arrows) and (B) map of Sakhalin and adjacent regions illustrating the location of the Khoe sediment profile marked by a star; geographic features mentioned in the text; and schematic ocean currents including the East Sakhalin Cold Current (ESCC), the Liman Cold Current (LCC), the Tsushima Warm Current (TWC) and the Soya Warm Current (SWC). The boundary of the mean maximum extent of sea ice cover in the Okhotsk Sea and the Tatar Strait is indicated in both maps by a broken line (after Geograficheski Atlas SSSR, 1990).

5.3.2 Vegetation

A simplified classification of the vegetation (Bukhteeva and Reimers, 1967) and satellite-derived tree cover (DeFries et al., 2000a, 2000b) on Sakhalin is provided in Figures 5.2 and 5.3, respectively. The cool and humid climate on Sakhalin promotes the predominant growth of boreal and temperate forests, which cover most of the island (Figs. 5.2, 5.3A). The northern part (north of ca. 51.5°N) is dominated by thin larch (*Larix gmelinii*) taiga (Figs. 5.2, 5.3B) associated with Siberian dwarf pine (*Pinus pumila*). The area to the south is mainly covered by denser evergreen forests with spruce (*Picea ajanensis*) and fir (*Abies sachalinensis*) as the main components (Figs. 5.2, 5.3C). As far as ca. 48°N these dark conifer forests are dominated by *P. ajanensis* and further south by *A. sachalinensis*. An exception is the northernmost part of Sakhalin (i.e. the Schmidt Peninsula, Fig. 5.1B), where *P. ajanensis* forms pure stands. The south-westernmost end of Sakhalin is characterised by mixed forests comprising dark conifers (mostly *A. sachalinensis*) and cool temperate broadleaf trees like *Acer mono*, *Fraxinus mandshurica*, *Juglans ailantifolia*, *Juglans mandshurica, Kalopanax septemlobus*, *Phellodendron sachalinense*, *Quercus mongolica*, *Quercus crispula*, *Tilia japonica*, *Ulmus japonica* (Bukhteeva and Reimers, 1967; Alexandrova, 1982; Krestov, 2003; Nakamura and Krestov, 2005; Figs. 5.2, 3B). However, the distribution range of arboreal cool temperate broadleaf taxa is not exclusively limited to this region. Trees like *Q. mongolica* (Fig. 5.2), *Ulmus laciniata* and *U. japonica* grow sporadically in climatically favourable locations within the boreal zone of dark conifer forest as far north as ca. 51.5°N (e.g. Sokolov et al., 1977). Higher elevations south of ca. 51.5°N are characterised by mountain woodland with open *Betula ermanii* forest and shrubland with *P. pumila* and shrubby Ericaceae like *Empetrum nigrum* and *Rhododendron* spp. Wetlands are a common feature of the coastal and fluvial landscapes of Sakhalin (Fig. 5.2). The most widespread types are *Sphagnum* peat bogs of up to 7 m thickness with *Larix*, *Salix*, *Alnus* and *Myrica* growing on the ridges (Bukhteeva and Reimers, 1967; Zhulidov et al., 1997).

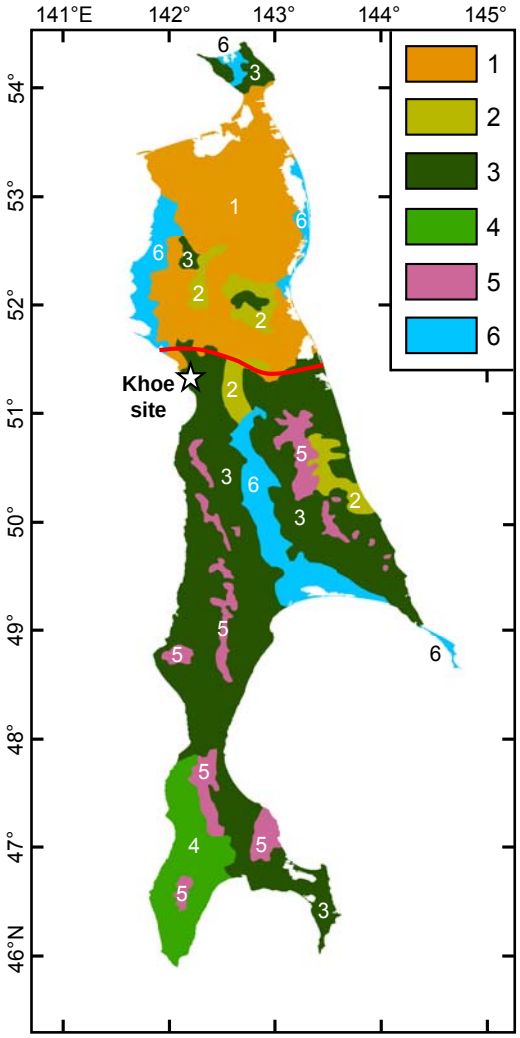

Fig. 5.2 Map of the actual vegetation distribution on Sakhalin (simplified after Bukhteeva and Reimers, 1967) showing following main vegetation types: 1 – Larix forest partly with Pinus pumila, 2 – Larix forest with Picea and Abies, 3 – Picea-Abies forest, 4 – Picea-Abies forest with cool temperate broadleaf trees, 5 – Mountain woodland with Betula forest and alpine shrubland with Pinus pumila and Ericaceae, 6 – Sphagnum peat bogs/mires partly with Larix. The location of the Khoe sediment profile is marked by a star. The red line indicates the northern distribution limit of *Quercus mongolica*.

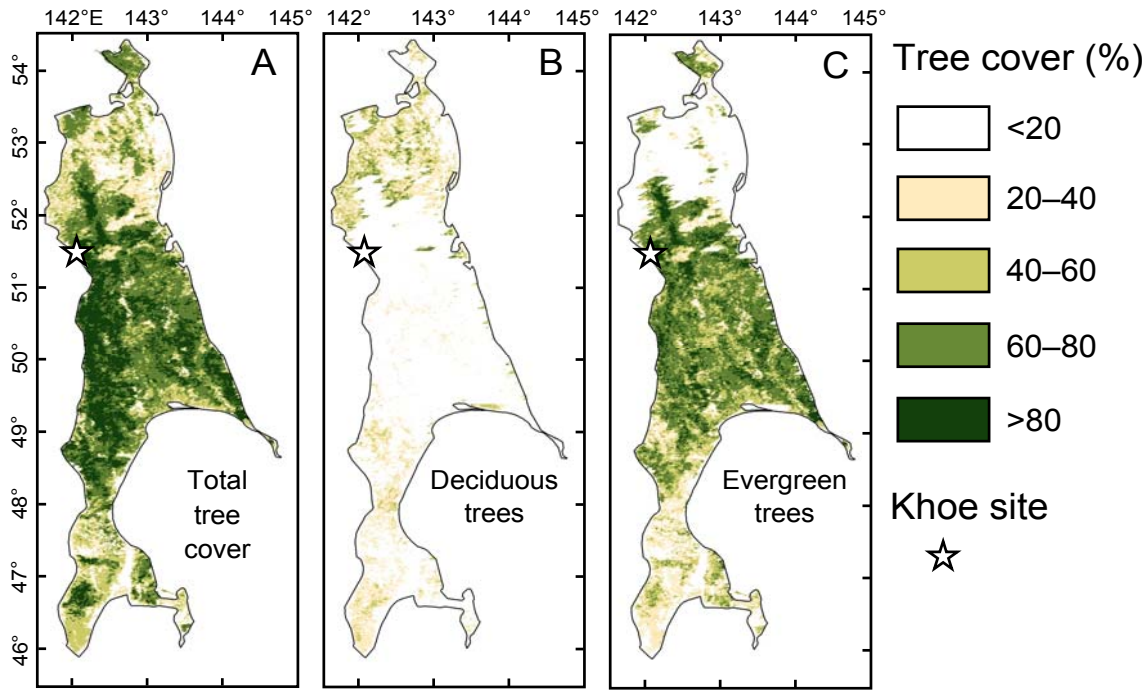

Fig. 5.3 Map compilation illustrating the AVHRR-derived concentration of the (A) total, (B) deciduous and (C) evergreen tree cover (after DeFries et al., 2000a, 2000b).

5.4 Data and methods

5.4.1 Study site and fossil pollen record

The sediment profile presented in this study was obtained from a coastal cliff, which is located ~3 km north of the settlement of Khoe on the western coast of Sakhalin facing the Tatar Strait (51.34°N, 142.14°E, 15 m a.s.l., Fig. 5.1B). The vegetation of the surrounding area is mainly characterised by boreal evergreen conifers (i.e. *Picea ajanensis* and *Abies sachalinensis*) with an admixture of *Larix gmelinii* and species of *Betula* and *Alnus*. However, cool temperate broadleaf trees like *Quercus mongolica* may also infrequently grow in the region (Fig. 5.2). There is no permanent climate station in the vicinity of Khoe. In order to get an overview of the modern climate conditions around the sampling site, we utilised the interpolated climate parameters from the New et al. (2002) dataset for the 10′ × 10′ grid surrounding the sampling site. The mean temperature of the coldest month (MTCO), which is January, falls to −18.5 °C, reaches 16.4 °C in the warmest month (MTWA), which is August, and is 0.2 °C on annual scale (TANN). Regarding the mean annual precipitation (PANN = 625 mm), 62% falls during the warm season months between April and September (PSUM = 386 mm). The abrasional coastal cliff north of Khoe exhibits a succession of Miocene–Quaternary sediments with a thickness of 15–20 m. In several places, the exposed bedrock Cape Uandi Formation (Miocene) is interrupted by tectonic depressions filled with Pliocene–Quaternary sediments. The sampled sediment profile is situated in the largest depression in the area, which has a maximum extent of 200 m in width and 13 m in depth. Samples were taken along a vertical transect spanning from the surface to a depth of 620 cm. The sediment profile is mainly composed of peat deposits (620–590 cm and 385–0 cm), which are interrupted by layers of largely silty (590–555 cm), sandy (555–455 cm) and gravelly (455–385 cm) material (Fig. 5.4). Altogether, 113 samples were collected and microscopically analysed for pollen and spore assemblages by Igarashi et al. (2000). A total of 42 arboreal (AP) and non-arboreal (NAP) terrestrial pollen types, three aquatic pollen types and six types of ferns and fern allies spore were identified. Percentages of individual pollen taxa were calculated upon the total sum of all terrestrial AP and NAP taxa. For spores, percentages were calculated using the total terrestrial pollen sum plus the sum of spores. A simplified pollen and spore diagram is illustrated in Fig. 5.4.

5.4.2 Radiocarbon dates

A total number of eight radiocarbon dates were obtained from the sediment profile from Khoe (Table 5.1). The four ^{14}C ages determined by Igarashi et al. (2002) were

supplemented by an additional four AMS dates by Igarashi and Zharov (2011). For the present study, we converted these ^{14}C ages into calendar (cal) ages (Table 5.1) using the online version of the CalPal radiocarbon calibration program (Danzeglocke et al., 2013) and the software-based CalPal-2007 program (Weninger and Jöris, 2008; Weninger et al., 2013). The obtained radiocarbon dates suggest that the Khoe sediment profile represents at least the last ca. 40 ka. For the Holocene part of the core, there are five ^{14}C dates (samples a–e, Table 5.1) available. Taking into account the overall pattern of these dates in relation to depth, the ^{14}C age of sample c (9420 ± 50 ^{14}C yr BP at 302.5 cm depth) appears to be somewhat displaced. We regard this date as too old and consequently excluded it from the age–depth model. The chronology for the Holocene part was defined by linear interpolation based on the calibrated ages of the remaining four ^{14}C dates.

In contrast, the middle and late last glacial part of the profile, which covers a time period of approximately 30 ka, are represented by only three radiocarbon dates (samples f–h, Table 5.1). Previous studies have shown that late Pleistocene–Holocene temperature records from the North Atlantic region are consistent with reconstructions from the Asian monsoon domain (e.g. Porter and An, 1995; Wang et al., 2001b; Zhao et al., 2003; Dykoski et al., 2005; Nakagawa et al., 2005). Pronounced climate fluctuations (i.e. DO and Heinrich events) reported from the North Atlantic region were also identified by variations in the relative abundances of *Larix* and *Picea* type pollen in the fossil pollen record from Khoe by Takahara et al. (2010). This encouraged us to use the well-dated mean annual surface temperature reconstruction curve (Alley, 2000) derived from the $\delta^{18}O$ record of the GISP2 ice core from central Greenland (72.58°N, 38.48°W, 3208 m a.s.l.) for correlation with the mean annual temperature reconstruction (TANN) curve based on the Khoe fossil pollen record by means of stadial and interstadial temperature oscillations to further confine the chronology for this part of the sediment profile.

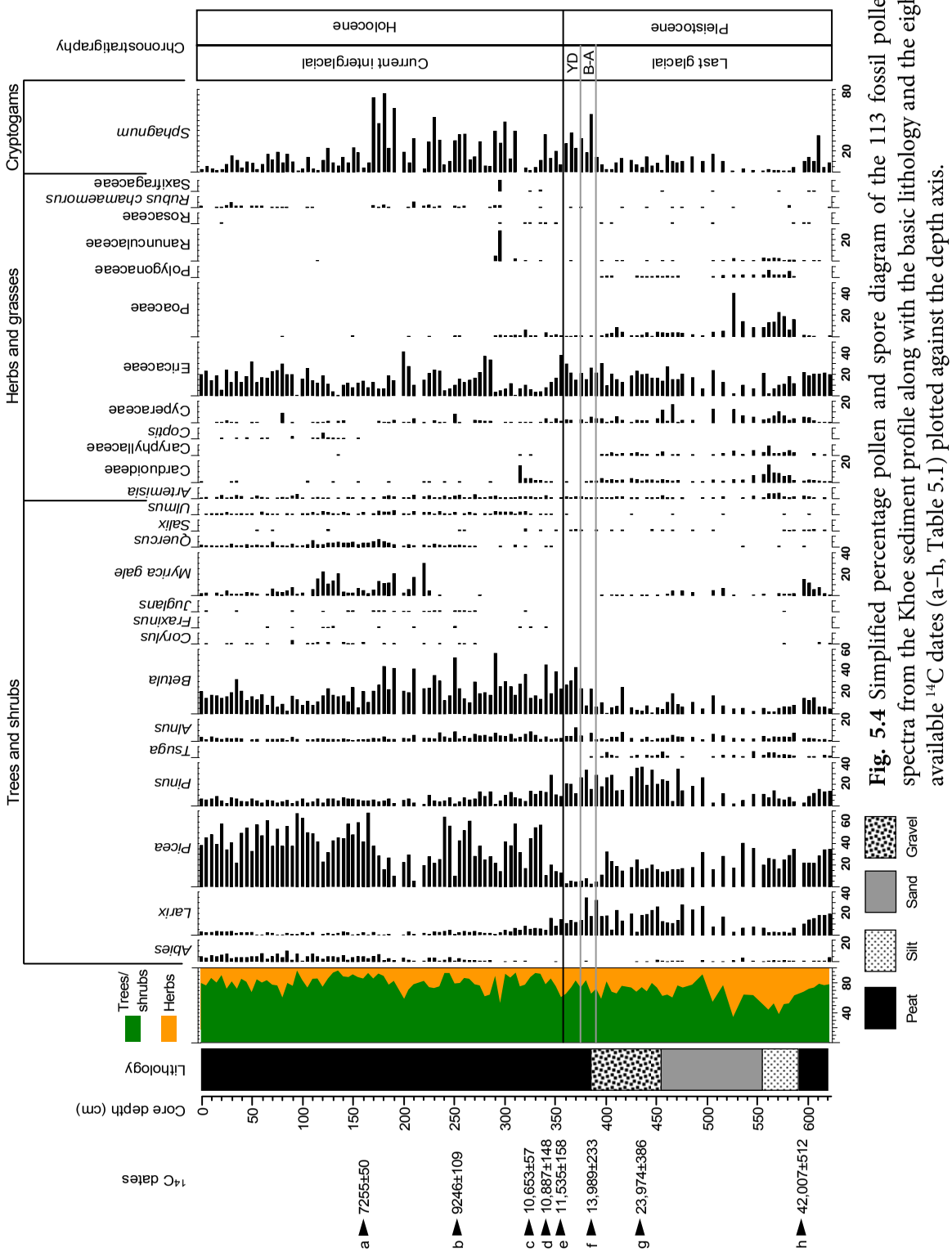

Fig. 5.4 Simplified percentage pollen and spore diagram of the 113 fossil pollen spectra from the Khoe sediment profile along with the basic lithology and the eight available ^{14}C dates (a–h, Table 5.1) plotted against the depth axis.

Sample ID	Laboratory ID	Depth (cm, mid point)	Dated material	Radiocarbon date, ^{14}C BP	Reference	Calibrated age, yr BP	Error range (95% conf. interval)	
							Upper age limit, yr BP	Lower age limit, yr BP
a	IAAA 62612	157.5	Plant fragment	6330 ± 40	Igarashi and Zharov, 2011	7255*	7160	7360
b	KIA 9557	252.5	Plant fragment	8251 ± 62	Igarashi et al., 2002	9246*	9020	9460
c	IAAA 72344	302.5	Plant fragment	9420 ± 50	Igarashi and Zharov, 2011	10653	10520	10800
d	IAAA 72345	342.5	Bulk TOC	9520 ± 50	Igarashi and Zharov, 2011	10887*	10580	11180
e	IAAA 72346	357.5	Plant fragment	10020 ± 50	Igarashi and Zharov, 2011	11535*	11250	11810
f	KIA 9558	387.5	Plant fragment	12000 ± 101	Igarashi et al., 2002	13989*	13610	14330
g	KIA 9559	432.5	Organic mud	20050 ± 230	Igarashi et al., 2002	23974*	23400	24600
h	Beta 122027	607.5	Organic debris	37270 ± 750	Igarashi et al., 2002	42007	41090	42970*

Table 5.1 Radiocarbon dates for samples from the Khoe sediment profile (Igarashi et al., 2002; Igarashi and Zharov 2011). Calibrations were performed using CALPAL-2007 (Weninger et al., 2013; Weninger and Jöris, 2008) and the online version of the CalPal radiocarbon calibration program (Danzeglocke et al., 2013). Ages marked by an asterisk were used in the age–depth model (Fig. 5.11).

5.4.3 Modern pollen data

In this study we compiled a total of 236 modern pollen spectra from existing reference datasets from Eurasia (Tarasov et al., 1998, 2005) and the southern (Mokhova et al., 2009) and northern (Edwards et al., 2000) RFE that have already been used in previous studies for quantitative vegetation and climate reconstructions (e.g. Bigelow et al., 2003; Andreev et al., 2004; Tarasov et al., 2011; Williams et al., 2011; Melles et al., 2012). The sites of the pollen samples are distributed over a large area of the RFE (Fig. 5.5) extending from ca. 46–63°N to 130–152°E including four major regions, i.e. the south-eastern Sakha Republic, the southern Magadan Oblast, the southern Khabarovsk Krai and Sakhalin, and thus cover a broad range of vegetation and climate conditions. Calculation of relative pollen abundances for each spectrum was based upon the total sum of terrestrial pollen. For plotting the pollen percentage diagrams, we employed the Tilia/Tilia-Graph/TGView software package (Grimm, 1993, 2004).

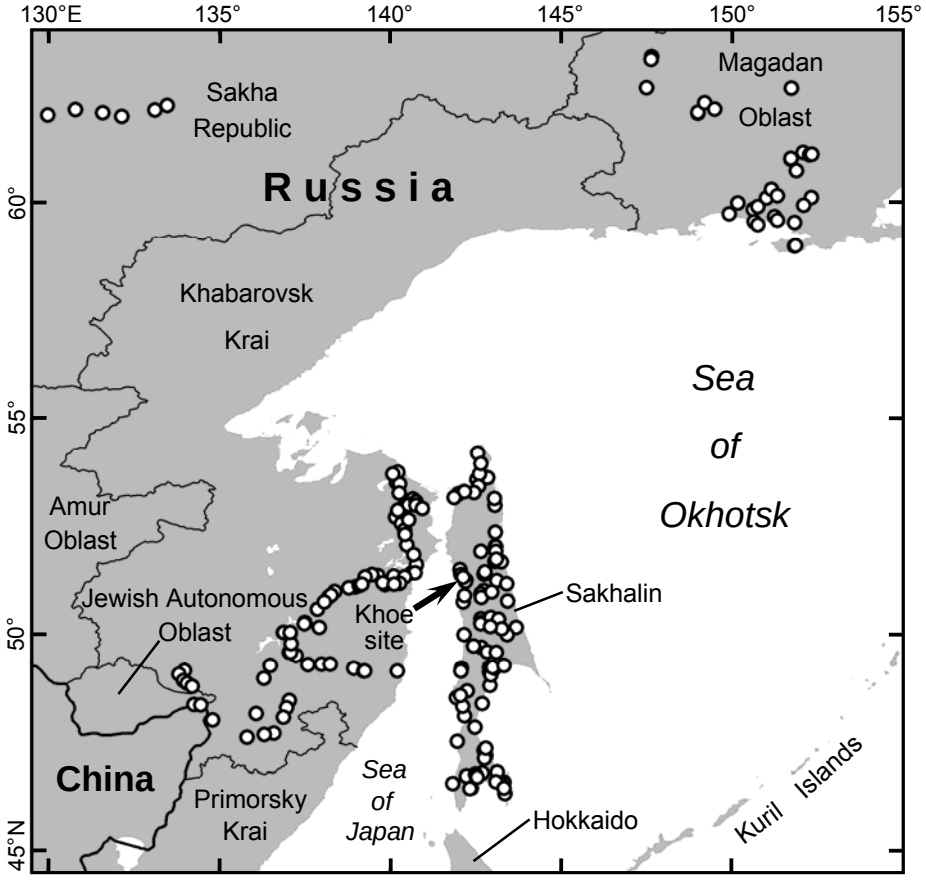

Fig. 5.5 Site distribution of 236 reference pollen spectra (indicated by white dots) from the south-eastern Sakha Republic, the southern Magadan Oblast, the southern Khabarovsk Krai and Sakhalin compiled from existing modern analogue datasets (Tarasov et al., 1998, 2005; Edwards et al., 2000; Mokhova et al., 2009) and used to reconstruct past climate and tree cover from the fossil pollen record from Khoe.

5.4.4 Biome reconstruction

The biome reconstruction method or biomisation method, which is described in detail by Prentice et al. (1996), allows the quantitative reconstruction of biomes, i.e. major vegetation types, from pollen or plant macrofossil assemblages. Basically, the approach requires (i) assignment of pollen/macrofossil taxa to plant functional types (PFTs), which are plant groups with similar characteristics in stature, leaf form, phenology and bioclimatic tolerance defined in the global BIOME1 vegetation model (Prentice et al., 1992); (ii) assignment of PFTs to one or more biome(s) in which they may occur; and (iii) determination of the affinity scores for each biome by summation of square roots of the attributed pollen/microfossil abundance. The biome with the highest affinity score, or the one defined by a smaller number of PFTs (in case several biome scores are equal), is considered as the dominant biome and assigned to the given taxa assemblage. Since the different PFTs and biomes are associated with bioclimatic ranges via vegetation models,

they allow climatic interpretation of biome reconstruction results which, in turn, may be used for comparison with climate model outputs (Kleinen et al., 2011, 2014).

The pollen-based biomisation method was verified by means of comprehensive surface pollen datasets and used to reconstruct Quaternary vegetation dynamics in the wider study region and adjacent areas including the former Soviet Union and Mongolia (Tarasov et al., 1998, 1999, 2000), the northern (Edwards et al., 2000) and southern (Mokhova et al., 2009) RFE and China (e.g. Yu et al., 1998). For the Japanese archipelago, two significantly different pollen-based biomisation approaches have been proposed. Takahara et al. (2000) considered both terrestrial AP and NAP types in the defined taxa-PFT-biome scheme. Since the entire East Asian island arc including Taiwan, the Japanese islands and Sakhalin is characterised by humid climate conditions which promote the dominance of forest biomes, Gotanda et al. (2002) suggested a different approach. Following earlier successfully applied biomisation schemes (Prentice et al., 1996; Tarasov et al., 1998; Yu et al., 1998; Williams et al., 1998), which do not attribute NAP taxa to forest biomes, Gotanda et al. (2002) proposed a taxa-PFT-biome matrix considering only 32 AP taxa. More recently, Leipe et al. (2013) tested the applicability of both approaches for reconstructing past vegetation dynamics for northern Japan using a dataset of surface pollen spectra from Hokkaido. The study revealed that assignment of both terrestrial AP and NAP pollen taxa is needed in order to provide robust vegetation reconstructions in particular for the colder/drier intervals of the late Quaternary when northern Japan was likely marked by more open landscapes in which forest generally occupied smaller areas. Therefore, the whole list of terrestrial pollen taxa is included in the taxa-PFT-biome matrix applied to the late Quaternary fossil pollen record from Sakhalin.

The defined matrix is based on previously published biomisation schemes from studies in northern Eurasia (Tarasov et al., 1998, 1999b, 2000; Müller et al., 2010) and the southern RFE (Mokhova et al., 2009). A simplified scheme showing the applied taxa-biome assignment is presented in Table 5.2. Biome scores were calculated using the percentage abundances of each attributed pollen taxon, which are based on the total sum of all terrestrial pollen grains. To minimise the noise of long-distance transported or redeposited exotic pollen grains, we excluded the pollen taxa with an abundance of less than 0.5% (Prentice et al., 1996). Biome score calculation was supported by PPPBase software (Guiot and Goeury, 1996). We tested the applicability of the proposed biomisation approaches for Sakhalin based on a set of 104 surface pollen spectra collected all across the island.

Biome name (Abbreviation)	Assigned pollen taxa
Tundra (TUND)	*Alnus*[1, 4, 9], *Betula*[1, 4], Cyperaceae[13], *Dryas*[1], Ericales[11], Poaceae[12, 14], Polemoniaceae[1], Polygonaceae[1, 14], *Rubus chamaemorus*[2], *Rumex*[1, 14], *Salix*[1, 4, 9], Saxifragaceae[1], Scrophulariaceae[1, 14]
Cold deciduous forest (CLDE)	*Alnus*[1, 4, 9], *Betula*[1, 4], Ericales[11], *Juniperus*/Cupressaceae[7], *Larix*[4], *Myrica*[4, 10], *Pinus*[7], *Populus*[4, 9], *Rubus chamaemorus*[2], *Salix*[1, 4, 9]
Taiga (TAIG)	*Abies*[3, 6], *Alnus*[1, 4, 9], *Betula*[1, 4], Ericales[11], *Juniperus*/Cupressaceae[7], *Larix*[4], *Myrica*[4, 10], *Picea*[3], *Pinus*[7], *Populus*[4, 9], *Rubus chamaemorus*[2], *Salix*[1, 4, 9]
Cold mixed forest (CLMX)	*Abies*[3, 6], *Alnus*[1, 4, 9], *Betula*[1, 4], *Corylus*[8], Ericales[11], *Juniperus*/Cupressaceae[7], *Larix*[4], *Myrica*[4, 10], *Pinus*[7], *Populus*[4, 9], *Rubus chamaemorus*[2], *Salix*[1, 4, 9], *Tilia*[8], *Ulmus*[8]
Cool conifer forest (COCO)	*Abies*[3, 6], *Alnus*[1, 4, 9], *Betula*[1, 4], *Corylus*[8], Ericales[11], *Juniperus*/Cupressaceae[7], *Larix*[4], *Myrica*[4, 10], *Picea*[3], *Pinus*[7], *Populus*[4, 9], *Rubus chamaemorus*[2], *Salix*[1, 4, 9], *Tilia*[8], *Ulmus*[8]
Temperate deciduous forest (TEDE)	*Abies*[3, 6], *Acer*[9], *Alnus*[1, 4, 9], Araliaceae[10], *Betula*[1, 4], *Castanea*[10], *Corylus*[8], Ericales[11], *Fraxinus excelsior*-type[9], *Juglans*[10], *Juniperus*/Cupressaceae[7], *Larix*[4], *Myrica*[4, 10], *Pinus*[7], *Populus*[4, 9], *Pterocarpus*/*Celtis*[10], *Quercus* (deciduous)[9], *Salix*[1, 4, 9], *Syringa*[9], *Tilia*[8], *Ulmus*[8]
Cool mixed forest (COMX)	*Abies*[3, 6], *Acer*[9], *Alnus*[1, 4, 9], *Betula*[1, 4], *Corylus*[8], Ericales[11], *Fraxinus excelsior*-type[9], *Juniperus*/Cupressaceae[7], *Larix*[4], *Myrica*[4, 10], *Picea*[3], *Pinus*[7], *Populus*[4, 9], *Quercus* (deciduous)[9], *Salix*[1, 4, 9], *Syringa*[9], *Tilia*[8], *Ulmus*[8]
Steppe (STEP)	Apiaceae[14], *Artemisia*[14], Asteraceae[14], Boraginaceae[14], Brassicaceae[14], Campanulaceae[14], Caryophylaceae[14], Chenopodiaceae[14], Fabaceae[14], Iridaceae[14], Lamiaceae[14], Liliaceae[14], Onagraceae[14], Papaveraceae[14], Plantaginaceae[14], Poaceae[12, 14], Polygonaceae[1, 14], Primulaceae[14], Ranunculaceae[14], Rosaceae[14], Rubiaceae[14], *Rumex*[1, 14], Scrophulariaceae[1, 14], *Stellera*/Thymelaeaceae[14], *Thalictrum*[14], Urticaceae[14]

Plant functional types (Abbreviation)		
[1] Arctic/alpine dwarf shrub/forbs (aa)	[6] Cool-temperate conifer (ctc)	[11] Heath (h)
[2] Arctic/boreal dwarf shrub (ab)	[7] Eurythermic conifer (ec)	[12] Grass (p)
[3] Boreal evergreen conifer (bec)	[8] Cool-temperate summergreen (ts1)	[13] Sedge (s)
[4] Boreal summergreen (bs)	[9] Temperate summergreen (ts)	[14] Steppe forb (sf)
[5] Boreal-temperate summergreen (bts)	[10] Warm-temperate summergreen (ts2)	

Table 5.2 Biome-taxa matrix used in the calculation of biome affinity scores (adopted from Tarasov et al., 1998, 1999b, 2000; Müller et al., 2010; Mokhova et al., 2009). All pollen taxa (n = 53) which are present in the compiled 236 modern pollen spectra from the study region, whose abundances exceed the universal threshold of 0.5% are assigned to one or more plant functional types (indicated by superscript numbers) and biomes. The affinity score for each potential biome is calculated by summation of the square roots of all attributed pollen taxa percentages (taxon percentage value minus 0.5%) as suggested by Prentice et al. (1996). The biome with the highest affinity score or the one defined by a smaller number of PFTs (when scores of several biomes are equal) is treated as the dominant biome.

5.4.5 Pollen-based climate and tree cover reconstruction

The modern analogue technique (MAT; Overpeck et al., 1985; Guiot, 1990) is one of the most powerful quantitative tools to reconstruct past climate and environmental conditions from fossil pollen spectra (Jackson and Williams, 2004) and has been widely

used in Quaternary palaeoenvironmental studies (e.g. Tarasov et al., 2005, 2007; Bartlein et al., 2011; Melles et al., 2012). The method is underpinned by the assumption that contemporary pollen spectra reflect the distribution of the regional vegetation from which they originate and that this vegetation distribution is in turn controlled by the character of determinant environmental factors. Moreover, two random surface pollen assemblages, which resemble each other in taxa composition and abundance, are also alike in respect to the environmental conditions under which they were deposited. Based on the concept of uniformitarianism, this may be transferred to fossil pollen assemblages. In other words, the environmental conditions which are associated with a given fossil pollen spectrum and determinant for the sample's assemblage composition may be inferred from one or more statistically "matching" modern pollen spectra (i.e. modern analogues). In palaeoenvironmental studies, the level of analogy between multivariate pollen spectra is commonly determined by means of similarity coefficients (Jackson and Williams, 2004).

In this study, we aim at reconstructing four main climate variables including MTCO, MTWA, TANN and PANN and percentage total tree cover as a property of vegetation cover, which may be easily compared with results from other proxy studies and/or model simulations. Performance tests (cross-validation) on modern reference datasets from the wider study region revealed a reasonably high correlation between pollen-inferred and observed climate variables including MTCO, MTWA, TANN, and PANN (Nakagawa et al., 2002; Li et al., 2007; Tarasov et al., 2011) and percentage total tree cover (Tarasov et al., 2007; Zheng et al., 2010), which suggests high potential for reliable reconstruction of these environmental parameters from fossil pollen assemblages. The climate variables were attributed to the reference pollen sampling sites by interpolation (Inverse Distance Weighting) from the global high-resolution (10' × 10' grid size) dataset of surface climate averaged over a thirty-year (1961–1990) period from New et al. (2002) using free-access Polation software (Nakagawa et al., 2002, http://dendro.naruto-u.ac.jp/~nakagawa/). For estimating the thermal variables, we accounted for a standard temperature lapse rate of –0.6 °C per 100 m difference in altitude (Domrös and Peng, 1988).

To reconstruct past changes in total tree cover, we utilised the satellite-based Advanced Very High Resolution Radiometer (AVHRR) dataset with a spatial resolution of 0.5' × 0.5' providing the estimated percent area covered by woody vegetation, herbs and bare ground (DeFries et al., 2000a, 2000b). Surface coverage values in the dataset range between 0–80% with the value of 80% corresponding to a coverage of ≥80%. Williams and Jackson (2003) have demonstrated that results of pollen-based reconstructions correspond best to satellite-based estimates of woody cover within a window size ranging from 20 × 20 to 150 × 150 km. Later, Tarasov et al. (2007) obtained highest correlations for northern Eurasia using a search window of 21 × 21 km (~441 km^2), which was recently confirmed for China by Zheng et al. (2010). Therefore, we first defined a "geodesic" (equal area) buffer

with a radius of 11.85 km (~441 km^2) around each reference pollen sampling site using the ArcGIS v10.0 software package (ESRI, 2012). In a second step, the AVHRR total tree cover estimates of all grid cells situated within each buffer were arithmetically averaged and assigned to the appropriate reference pollen spectrum.

Prior to method application, all pollen abundances were square root transformed in order to enhance minor taxa. The similarity between each assemblage of the Khoe fossil pollen record and each of the 236 spectra in the modern reference dataset was numerically measured by the squared cord distance (SCD) (Overpeck et al., 1985; Guiot, 1990). As frequently done (Nakagawa et al., 2002; Tarasov et al., 2007, 2011), we considered a maximum number of eight spectra with the smallest SCD and below a threshold (T = 0.15, Overpeck et al., 1985) as best modern analogues from which weighted average climate variables and percentage tree cover were determined. Calculation of the SCD was performed with the aid of the computer program C2 v1.6.8 (Juggins, 2007).

5.5 Results and interpretation

5.5.1 Modern pollen data and pollen-derived biomes

The results of the pollen analysis, the estimated values of the six climate parameters and percent tree cover, and the pollen-inferred (actual) dominant biomes of the 236 surface pollen spectra are plotted in Fig. 5.6A, B and C, respectively. Among the 64 terrestrial pollen types identified in the surface pollen dataset, eleven taxa (i.e. Caprifoliaceae, *Carpinus*, *Cornus*, *Fagus*, Gentianaceae, Geraniaceae, Moraceae, *Phellodendron*, Rutaceae, Valerianaceae, and *Viburnum*) have percentage values below the universal threshold of 0.5%. Thus, only 53 taxa were considered for the biomisation method (Table 5.2). In view of the modern climate conditions at the site of the Khoe fossil pollen record, the reference pollen dataset represents a wide range of climates covering significantly warmer/colder (Fig. 5.7A–C) and wetter/drier (Fig. 5.7D–F) environments. Regarding total tree cover, the dataset represents environments ranging from open vegetation to densely forested areas (Fig. 5.7G). The results of the analysed pollen spectra, which are subdivided into four groups according to source area (Fig. 5.5), are presented in the following paragraphs.

Region I (Sakha Republic) represents the Lena/Aldan river basin, which is mainly delineated by stands of boreal summergreen trees (i.e. *Larix* and *Betula*) and *Pinus*. The relatively high abundance of herb and grass taxa like *Artemisia*, Asteraceae and Poaceae suggests a more open landscape, which is also reflected by satellite-derived tree cover estimations. The biome reconstruction results show the dominance of cold deciduous forest (CLDE) and taiga (TAIG) in this region. The latter is derived at sites where *Picea* is a substantial element of the surrounding vegetation. The spectra from two sites contain a

significantly high amount of herbaceous taxa which are representative of the steppe (STEP) biome.

Region II (Magadan Oblast) is characterised by low percentages of *Larix* and high assemblages of *Pinus*, *Alnus* and *Betula* pollen. Like in region I, NAP taxa including heath, sedges and grasses are constantly registered. The estimated low total tree cover with values not exceeding 10% demonstrates that the pollen types of *Pinus*, *Alnus* and *Betula* belong to species with a shrubby stature. However, for most spectra from this region the biome reconstruction suggests CLDE as the dominant vegetation type. This may be explained by the assignment of *Alnus* and *Betula* to both tundra (TUND) and CLDE.

Region III (Southern Khabarovsk Krai) extends over a large latitudinal distance between ca. 54–47.5°N. The spectra are in general clearly dominated by AP. The northernmost parts (ca. 54–51°N) exhibit high abundances of cold-tolerant boreal taxa like *Abies*, *Larix*, *Picea*, *Alnus*, and *Betula*. The decrease of *Abies*, *Larix* and *Picea* towards the south (ca. 51–47.5°N), is accompanied by increasing abundances of *Pinus* pollen. South of 51°N, pollen of temperate deciduous broadleaf trees like *Corylus*, *Juglans*, *Quercus*, *Tilia*, and *Ulmus* are frequently recorded. The pollen-based biome reconstruction demonstrates that the northern part of the region is distinctively dominated by TAIG. South of 51°N, TAIG scores decrease and cool mixed forest (COMX) is reconstructed as the dominant vegetation type. Cool conifer forest (COCO) and temperate deciduous forest (TEDE) are reconstructed at four sites and one site, respectively. These biomes likely reflect local rather than regional environmental conditions, in the southern part of this source area.

Region IV (Sakhalin) has the largest latitudinal extension (ca. 54–46°N). The pollen assemblages from the northernmost part (ca. 54–52.5°N) differ considerably from the rest of the island. Here, pollen of the *Pinus*, *Alnus*, *Betula*, Ericales, Cyperaceae, and Poaceae type dominate the spectra. Cool temperate and temperate deciduous broadleaf tree pollen types are only identified in a few samples and do not exceed the biomisation threshold value of 0.5%. Towards 51.5°N, pollen abundances of *Abies* and *Picea* increase, whereas *Pinus* type pollen decrease. This section is also characterised by high percentage values of Ericales and the highest abundances of *Larix* type pollen in the surface spectra from Sakhalin. Between ca. 51.5–49°N, *Picea* type pollen predominate. Percentages of *Pinus*, *Larix*, Ericales as well as herbs and grasses are low. In this zone, pollen of cool temperate (i.e. *Acer*, *Corylus* and *Ulmus*) and temperate (i.e. *Quercus*) summergreen taxa are more frequently observed. South of 49°N, percentages of *Pinus* and *Larix* type pollen persist on low levels. While the content of *Picea* type pollen decreases, *Abies* abundances remain unchanged. This section also reveals the highest and most frequently observed abundances of *Acer*, *Corylus*, *Ulmus*, and *Quercus*. Although concentrations are mostly below the threshold value of 0.5%, *Juglans*, as a warm temperate summergreen taxon, regularly

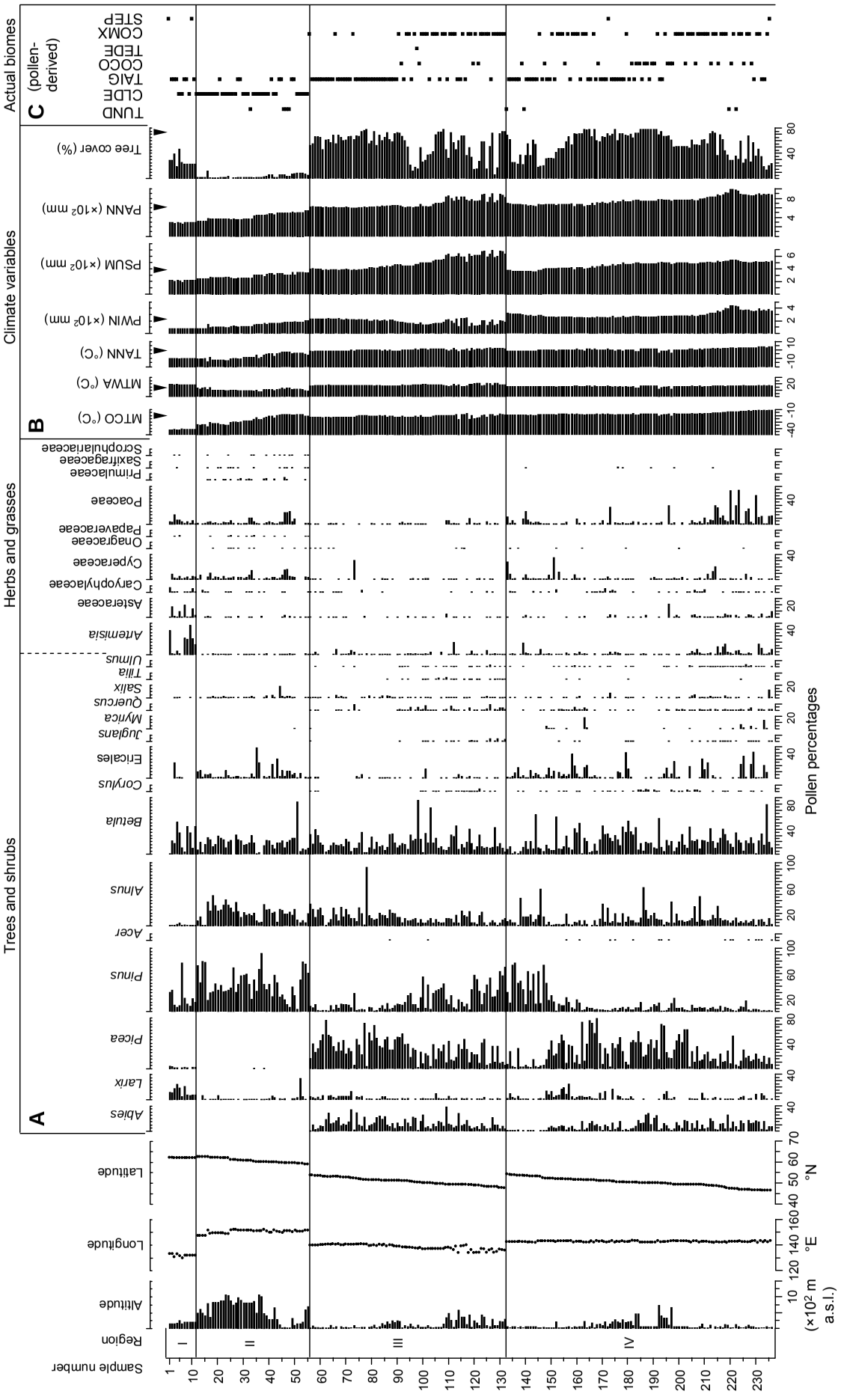
Sample number
Region
Altitude
Longitude
Latitude
Trees and shrubs
Abies
Larix
Picea
Pinus
Acer
Alnus
Betula
Corylus
Ericales
Juglans
Myrica
Quercus
Salix
Tilia
Ulmus
Artemisia
Herbs and grasses
Asteraceae
Caryophyllaceae
Cyperaceae
Onagraceae
Papaveraceae
Poaceae
Primulaceae
Saxifragaceae
Scrophulariaceae
Climate variables
MTCO (°C)
MTWA (°C)
TANN (°C)
PWIN (×10² mm)
PSUM (×10² mm)
PANN (×10² mm)
Tree cover (%)
Actual biomes (pollen-derived)
TUND
CLDE
TAIG
COCO
TEDE
COMX
STEP
Pollen percentages
(×10² m a.s.l.)
°E
°N

Fig. 5.6 Summary chart showing (A) the simplified percentage pollen diagram including 236 continuously numbered modern pollen spectra from the study area grouped by sample source area (I – Sakha Republic, II – Magadan Oblast, III – southern Khabarovsk Krai, IV – Sakhalin, see Fig. 5.5 for spatial distribution) and sorted within each group by latitudinal position (north to south) along with (B) the main climate variables (see Fig. 5.7 caption for abbreviations) inferred from the modern climate dataset from New et al. (2002) and percentage modern tree cover based on the AVHRR-derived dataset from DeFries et al. (2000a, 2000b) calculated for the location of each modern pollen spectrum using the free-access Polation software (Nakagawa et al., 2002, http://dendro.naruto-u.ac.jp/~nakagawa/) including modern conditions (triangles) at the site of the Khoe fossil pollen record (Fig. 5.1B) and (C) the results of the pollen-based (actual) biome reconstruction (Mokhova et al., 2009).

appears in the pollen assemblages from the southernmost part of Sakhalin. Another feature of this region is the significantly higher portion of Poaceae and *Artemisia* type pollen, which is a response to enhanced agricultural activities in this area. According to the results of the biomisation method, Sakhalin is dominated by TAIG and COMX. The prevalence of TAIG in the northern part (between 54.5–50.3°N) is only interrupted between 52–51.3°N, where COMX is reconstructed from a considerable number of surface spectra. The latter biome is most frequently reconstructed in the southern part (i.e. south of 49.2°N) of the island. Though less frequently, COCO sites are mainly distributed in Sakhalin's south with a minor agglomeration of sampling sites between 50.3–46.6°N. Non-forest biomes are reconstructed at six sampling sites. The spectra of these samples contain high pollen concentrations of grasses and steppe forbs (e.g. Ranunculaceae and Asteraceae) as well as grasses and sedges, which are under natural conditions representatives of the STEP and TUND biome, respectively.

5.5.2 Reconstruction of vegetation and climate conditions

The pollen-based biome score calculation (Fig. 5.8A) and dominant biome reconstructions (Fig. 5.8B) along with the results of the MAT-based temperature, precipitation and tree cover reconstructions (Fig. 5.9A–E) allow for the interpretation of past environmental conditions in the region of northern Sakhalin. Based on these results, the pollen profile from the Khoe site may be generally subdivided into seven sections.

The earliest period (620–590 cm) is marked by relatively high average values for annual precipitation and temperature ranging between 675 and 705 mm –0.3 and 0.3 °C, respectively. The error ranges are small and, regarding the upper and lower limits, similar to those of the upper half (360–0 cm) of the record. Reconstructed total tree cover ranges between 44 and 52%. The regional vegetation is dominated by forest (i.e. COCO and TAIG) composed of boreal and temperate tree taxa with low but rising scores for STEP and TUND.

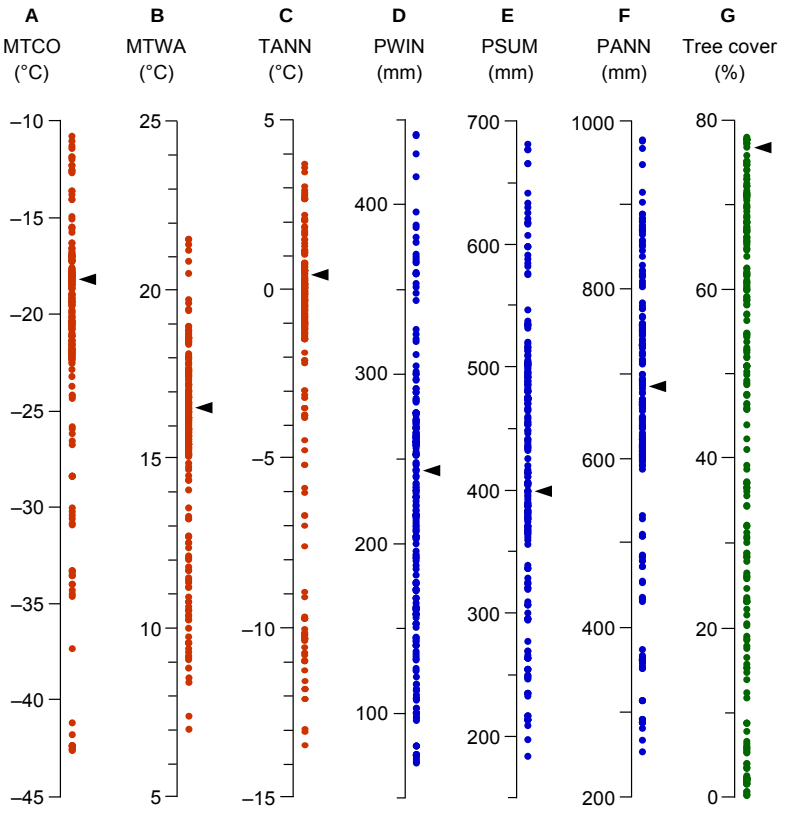

Fig. 5.7 Ranges of main climate variables including mean temperature of (A) the coldest (MTCO) and (B) warmest (MTWA) month, (C) mean annual temperature (TANN), (D) winter (PWIN, October–March) and (E) summer (PSUM, April–September) precipitation, (F) annual precipitation (PANN) and (G) percentage total tree cover represented by the set of 236 modern pollen spectra (dots) compiled in this study. Climate variables derived from the modern climate dataset from New et al. (2002) and percentage total tree cover from the AVHRR-based dataset from DeFries et al. (2000a, 2000b) were calculated for the location of each modern pollen spectrum using the free-access Polation software (Nakagawa et al., 2002, http://dendro.naruto-u.ac.jp/~nakagawa/). The triangles in each diagram indicate modern conditions at the position of the Khoe fossil pollen record (see Fig. 5.1B for spatial location).

Between 590–540 cm, reconstructions for PANN, MTCO and TANN reach minimum values of 410 mm, –36 and –8 °C, respectively. This is paralleled by maximum MTWA of 18 °C, which likely indicates more continental conditions around the Khoe site. With minimum values of approximately 30%, total tree cover reconstructions suggest a more open landscape. This is in agreement with the calculated biome scores of non-forest biomes (i.e. TUND and STEP), which reach highest values during this section. Simultaneously, scores for forest biomes broadly decrease but continue to dominate the regional vegetation. The STEP biome scores exceed the forest biome scores only at 560 cm.

The subsequent section (540–420 cm) is marked by higher average temperatures, precipitation with slight fluctuations. However, the reconstructions are partly characterised

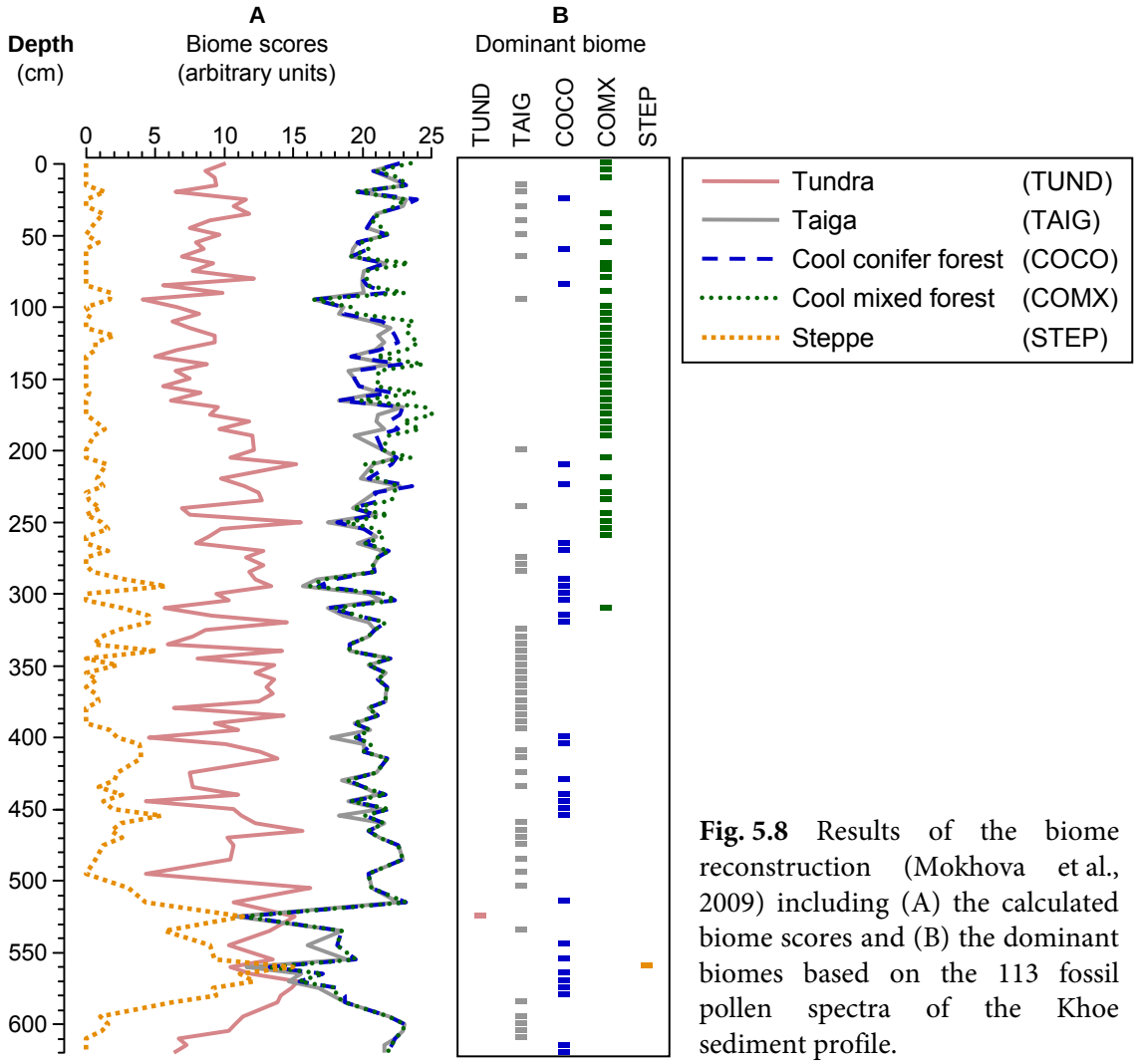

Fig. 5.8 Results of the biome reconstruction (Mokhova et al., 2009) including (A) the calculated biome scores and (B) the dominant biomes based on the 113 fossil pollen spectra of the Khoe sediment profile.

by relatively large error ranges especially in the upper part (467.5–420 cm), which suggest at least several excursions towards generally colder and drier conditions. Similarly, total tree cover shows a relatively high density, but decreases above 460 cm. While STEP scores remain on relatively high levels during the lower part of this section (540–505 cm), they are significantly lower in the upper part (505–540 cm) when the record is clearly dominated by forest biomes. The dominance of COCO and TAIG is interrupted by TUND in the lower part at 525 cm.

The MAT results indicate a phases of significant climate deterioration between 420–362.5 cm with lower TANN (between –5.5 and –0.5 °C) and reduced PANN (between 470 and 640 mm). While the MTCO is lowest in the lower part ($MTCO_{min}$ = –30 °C), it rises towards the top of this section. With average values of 14.7 °C, MTWA is lowest in the upper part of this segment. Total tree cover persists on relatively low levels of 35%. Forest (i.e. COCO and TAIG) remains the dominant vegetation type around the study site. A trend towards a more open landscape is suggested by the decline in forest and increase in

STEP biome scores in the lower part (410–390 cm), which is in line with the MAT-derived reduced precipitation and colder winter conditions.

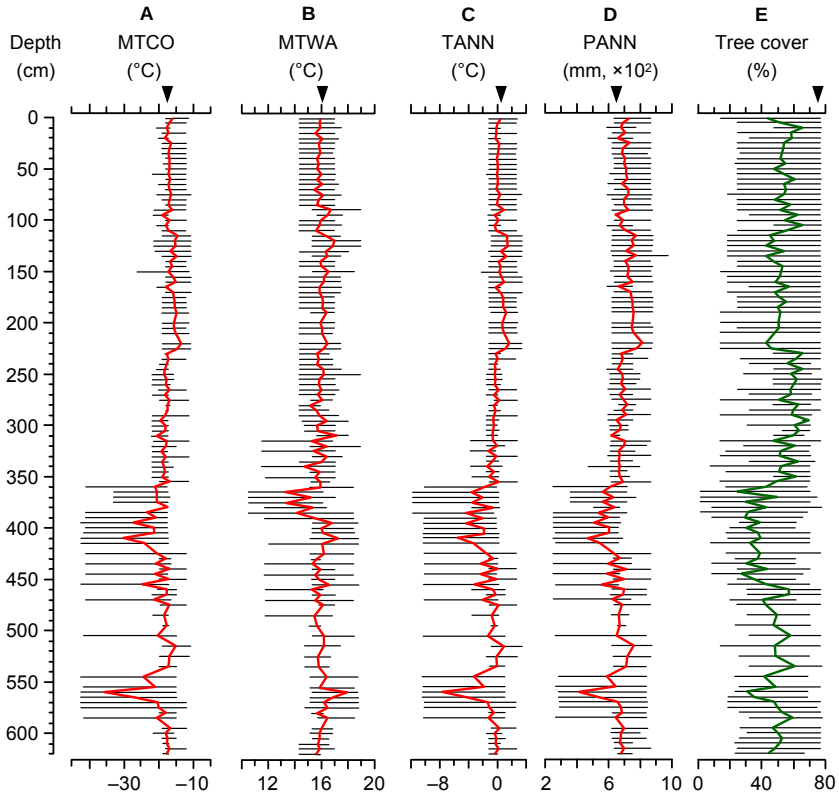

Fig. 5.9 Charts A–E show the results of the reconstruction of four climate variables (see Fig. 5.7 caption for abbreviations) and percentage total tree cover based on the MAT, the compiled set of 236 reference pollen spectra and the Khoe fossil pollen record. The curves represent the weighted averages of the five reconstructed parameters inferred from a range of eight closest analogues determined by the squared chord distance (T < 1.5). The horizontal bars indicate the analogue uncertainty range defined by the minimum and maximum value of the best modern analogues assigned to each analysed fossil sample. The traingles mark modern conditions at the site of the Khoe fossil pollen record (see Fig. 5.1B for spatial location) derived from the modern climate dataset from New et al. (2002).

The lower third (362.5–227.5 cm) of the upper half of the record shows relatively stable climate conditions, which are wetter and warmer compared to the previous core section. Reconstructions for MTCO, MTWA, TANN, and PANN range between –21 and –17 °C, 14.5 and 17 °C, –1.5 and 0.5 °C, and 620–720 mm, respectively. For this section, the highest average tree density of ca 60% (range between ca. 50 and 70%) is suggested. TAIG predominates around the sampling site until 322.5 cm. In the subsequent section (322.5–262.5 cm), COCO dominates the regional landscape, which is reflected by the increased concentration of cool temperate summergreen pollen in the spectra. Above 262.5 cm, the COMX has the highest scores, thus dominating the vegetation around Khoe, which is due to the spread of temperate summergreen taxa (e.g. *Quercus*).

Most favourable climate conditions are reconstructed between 227.5–112.5 cm. Compared to the previous part of the record, average MTCO, MTWA, TANN, and PANN

are higher by about 2.5 °C, 0.5 °C, 1.5 °C, and 70 mm, respectively. With around 50%, average total tree cover is slightly lower than in the previous period. STEP scores display very low levels. Scores for TUND decrease continuously; COMX, which reaches the highest affinity scores during this phase, generally dominates the regional vegetation. However, boreal tree and shrub taxa remain important elements of the landscape.

In the top part of the profile (112.5–0 cm), the reconstructed climate conditions are very similar to the ones registered in the lower third (362.5–227.5 cm) of the upper half of the record. The same applies to the total tree cover concentration, which is slightly higher than in the section below. The dominant vegetation type fluctuates between COMX, COCO and TAIG, thus also suggesting a trend towards climate deterioration. This is supported by the slight increase in TUND scores, which mirror enhanced growth of boreal and/or arctic herb and shrub communities in the study region.

5.5.3 Chronological framework

Figure 5.10 shows the calibrated radiocarbon dates together with the comparison between the TANN reconstruction results based on the Khoe fossil pollen record (Fig. 5.9C) and the mean annual temperature reconstruction (Alley, 2000) based on the $\delta^{18}O$ record of the GISP2 ice core. During the Holocene, the variability in both temperature reconstruction curves (Fig. 5.10A) is low and therefore difficult to correlate. The age–depth model for this period is based on linear interpolation using four available radiocarbon dates (samples a, b, d and e, Table 5.1). For the last glacial part, we correlated the two temperature records based on the 15 most prominent levels (tie points), which were identified by visual comparison (Fig. 5.10B). The calendar ages associated with theses selected levels in the GISP2 record were allocated to the corresponding tie points of the Khoe record. In addition to these tie point ages, we employed the three available ^{14}C datings including two calibrated ages (samples f and g, Table 5.1) and one lower error range limit (sample h, Table 5.1) for a 95% confidence interval to define the age–depth model based on linear interpolation for the last glacial section of the Khoe sediment profile. The resulting chronology together with the lithological properties for the Khoe profile is outlined in Fig. 5.11. The chronology illustrates a shift to significantly increased sedimentation rates at the late-glacial–Holocene transition. Synchronously, there is a change in lithological composition from mainly clastic components to organic-rich peat bog sediments at ca. 380 cm depth. If we assume that the establishment of the bog is a response to enhanced precipitation in combination with more favourable conditions for vegetation growth during the late-glacial climate amelioration, the recognised lithological change supports the defined chronology at least for this specific time interval.

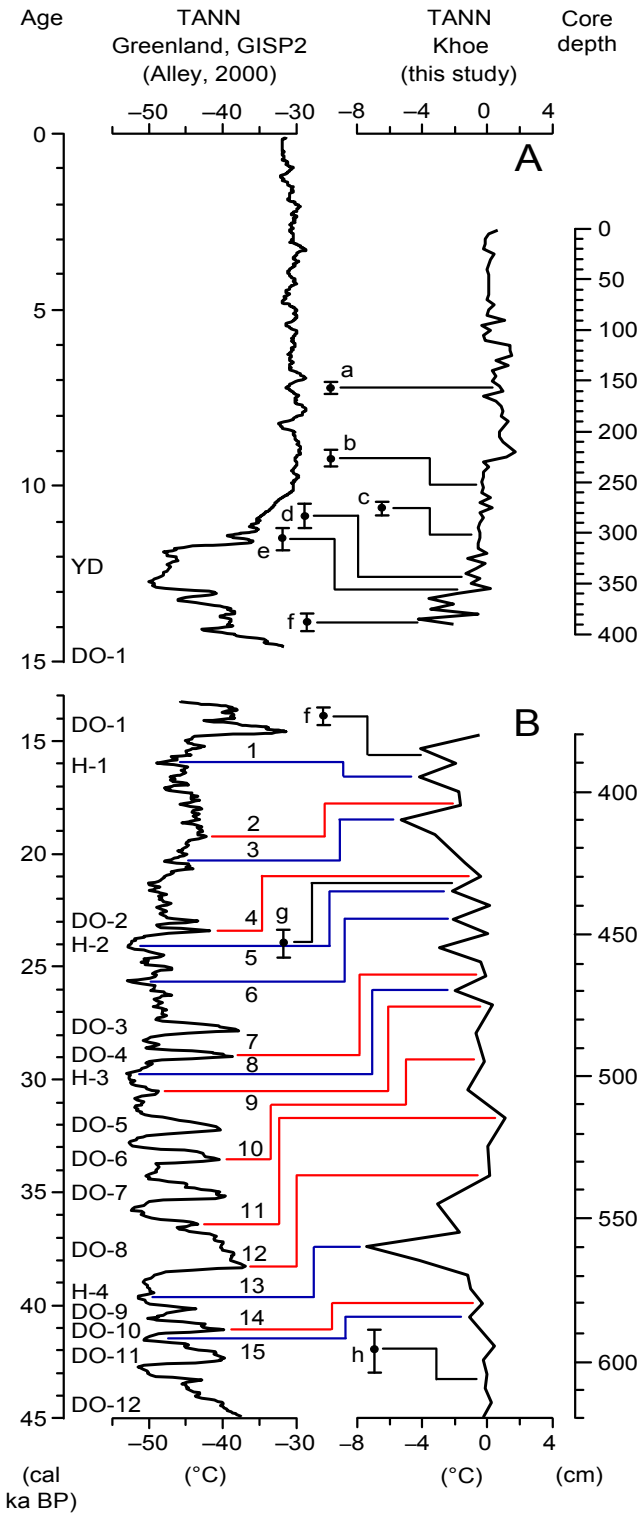

Fig. 5.10 Combined charts showing the 95% confidence intervals of the calibrated radiocarbon dates (a–h, see Table 5.1 for further details) from the Khoe sediment profile for (A) the Holocene and (B) the last glacial interval together with the correlations (tie points no. 1–15) between the MAT-based TANN reconstruction results for the Khoe fossil pollen record (this study) and the TANN reconstruction based on the $\delta^{18}O$ record from the GISP2 ice core from central Greenland (72.58°N, 38.48°W, 3208 m a.s.l.; after Alley, 2000) used to constrain the age–depth model for (B) the last glacial interval (Fig. 5.11). Heinrich (after Heinrich, 1988) and Dansgaard-Oeschger (after Dansgaard et al., 1993) events and the Younger Dryas are indicated for better orientation and denoted by "H", "DO" and "YD", respectively.

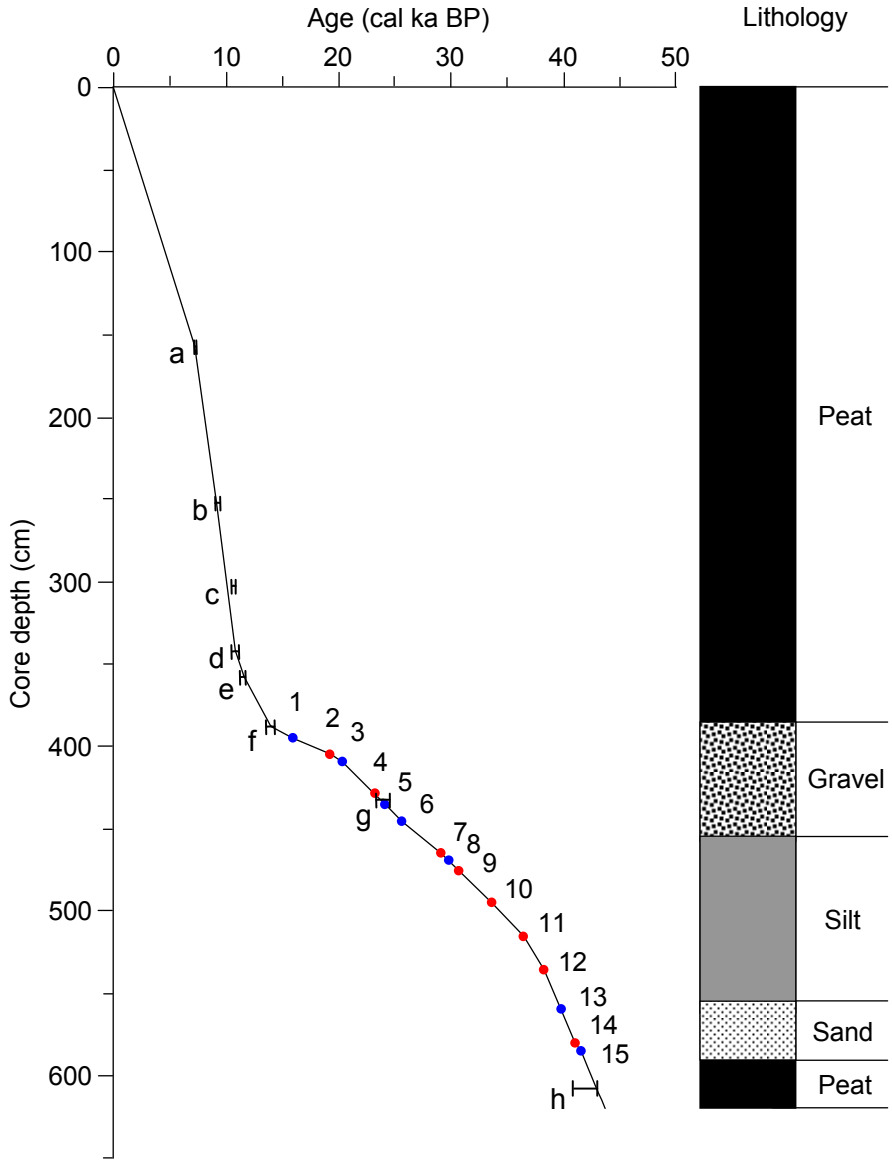

Fig. 5.11 Age–depth model and lithology for the Khoe sediment profile based on linear interpolation between seven calibrated radiocarbon dates (a, b, d–h; see Table 5.1 for further details) and 15 tie points (Fig. 5.10) identified by correlating the TANN reconstruction results based on the MAT and the Khoe fossil pollen record (this study) and the TANN reconstructions derived from the GISP2 ice core $\delta^{18}O$ record from central Greenland (after Alley, 2000).

5.6 Discussion

5.6.1 Comparison of pollen-derived biome distribution and actual vegetation on Sakhalin

The pollen-based biome reconstruction method has been successfully tested in large parts of the wider study area including the RFE and Beringia (e.g. Tarasov et al., 1998; Edwards et al. 2000; Mokhova et al., 2009). However, such a test has not been performed in detail for Sakhalin, which is characterised by a wetter and milder climate than the continental parts of the study area. The actual natural biomes allocated from the observed

regional vegetation distribution (Bukhteeva and Reimers, 1967, Fig. 5.2) and the results of the pollen-based biome reconstruction from Sakhalin are compared in Fig. 5.12A and 5.12B–F, respectively. Generally, the reconstructed dominant biomes match well with the actual vegetation distribution. The overall dominance of forest biomes is well reproduced by the biomisation method. TUND is reconstructed at four sites (Fig. 5.12B). The two samples in the north contain significant amounts of sedge and grass as well as alder and birch type pollen, which may be explained by their location in swampy riverine environments close to the shoreline. In the other two samples collected from the floodplains between two mountain ranges in the south of the island, grass type pollen account for more than half of the total pollen assemblage. This is likely due to the enhanced agricultural activities in this populated valley region.

TAIG is mainly reconstructed in the region between ca. 54–49.5°N (Fig. 5.12C). In the northern part of this area (ca. 54–53°N), the reconstructions agree with the actual dominant biome. Since the vegetation distribution of this region is mainly dominated by *Larix* and *Pinus pumila* (Fig. 5.2) intermingled with *Picea ajanensis* (Bukhteeva and Reimers, 1967), we allocated this region to TAIG (Fig. 5.12A). Towards the south, the spectra distribution extends into the zone of COCO (Fig. 5.12A), which is often referred to as southern taiga. On Sakhalin, this biome is characterised by minor presence of cool temperate broadleaf trees which are patchily distributed over this zone. TAIG is reconstructed in places where these trees are absent or so sparsely distributed that their pollen only insignificantly contribute to the overall assemblages. COCO is mainly reconstructed in the central part of Sakhalin but also for some samples collected in the northern- and southernmost parts of the island (Fig. 5.12D). At these sites, typical vegetation elements of COMX (i.e. temperate broadleaf trees including *Acer*, *Fraxinus* and *Quercus*) are lacking in the pollen spectra or have abundances which fall below the applied universal threshold of 0.5%. Where pollen concentrations of temperate broadleaf trees (mainly *Quercus*) influence the biome affinity scores, COMX is reconstructed (Fig. 5.12E). In contrast to the observed vegetation distribution, according to which COMX is restricted to the island's south-westernmost part (Bukhteeva and Reimers, 1967; Fig. 5.12A), the results of the pollen-based reconstructions indicate a distribution which stretches much further north. In fact, the spread of *Quercus mongolica* is not limited to this south-westernmost part of Sakhalin. Its habitat extents as far north as ca. 52°N (Sokolov et al., 1977, Fig. 5.2) and thus is well in agreement with the distribution of the COMX reconstructions.

STEP is reconstructed at only two locations. Like TUND, it is not a dominant biome on Sakhalin at present. Both spectra contain high pollen abundances of herbaceous taxa including Ranunculaceae, Poaceae, Asteraceae, and *Artemisia* with low concentrations of AP taxa, which probably reflects local human disturbance.

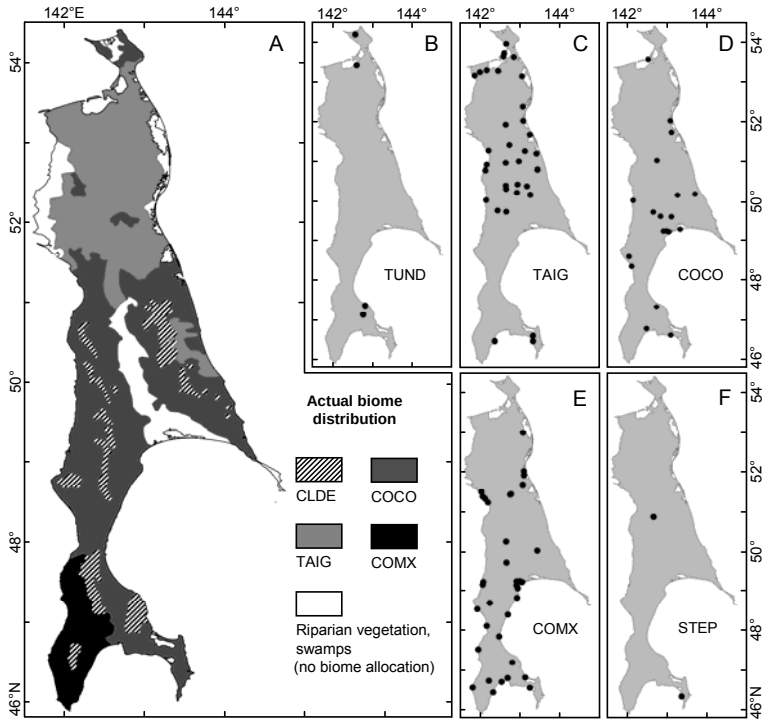

Fig. 5.12 Distribution maps of (A) the actual natural biomes on Sakhalin allocated from the observed vegetation distribution (after Bukhteeva and Reimers, 1967) and (B–F) the pollen-derived biomes at 236 surface pollen sample sites.

5.6.2 Late Quaternary vegetation and climate dynamics in northern Sakhalin

For chronological comparison, the results of the quantitative climate and tree cover reconstructions (Fig. 5.9) together with selected palaeoclimate records and insolation parameters are plotted along the age axis in Fig. 5.13. According to the defined age–depth model (Fig. 5.11), the fossil pollen record from Khoe spans the last ca. 44 cal ka BP, thus partly covering the last glacial cycle (i.e. the late Pleistocene) and the current interglacial (i.e. the Holocene). Regarding the long-term climate evolution, the derived error ranges of the climate reconstructions allow a rough subdivision of the record into two potentially milder and moister periods ca. 43.7–29.3 cal ka BP (620–467.5 cm) and ca. 11.7–0 cal ka BP (362.5–0 cm) and a cooler and drier period ca. 29.3–11.7 cal ka BP (467.5–362.5 cm), which, according to Martinson et al. 1987, largely correspond to the upper Marine Isotope Stage (MIS) 3 (ca. 59–29 cal ka BP) and MIS1 (ca. 12–0 cal ka BP) interstadials and the MIS2 stadial (ca. 29–12 cal ka BP), respectively (Fig. 5.13L).

The MAT-based climate reconstructions show that during the late Pleistocene, TANN is mainly controlled by winter temperatures, which are represented by MTCO. This corresponds with climate reconstructions from other regions of the Northern Hemisphere (NH) including North America and Northern Eurasia (e.g. Tarasov et al., 1999b; Bartlein et al., 2011; Helmens, 2014). Annual-scale trends towards cooler (warmer) conditions are

generally characterised by decreasing (increasing) MTCO and increasing (decreasing) MTWA. We assume that these cooler (warmer) intervals are linked to enhanced (reduced) continentality as a consequence of falling (rising) sea levels. This is also well reflected in the level of thermal seasonality, which is higher during cooler intervals than during warmer intervals. In our reconstructions, PANN is paralleled by MTCO, thus is negatively correlated with thermal seasonality. This matches the long-term relationship between the reconstructed TANN and PANN variation over the last ca. 450 ka in central Japan, which was determined by Nakagawa et al. (2008). Another interesting feature of the late Pleistocene climate reconstructions are the relatively high average MTWA values during cold phases. Nevertheless, they should not be overestimated since the error ranges are rather large at these levels especially during MIS2, where they suggest a potential for much colder summer temperatures. Given the biomisation results (Fig. 5.8), average values of MTCO, which are in contrast to MTWA a main controlling factor for forest biomes, appear to be more reliably reconstructed.

The climate and tree cover reconstructions of the Holocene interval are marked by comparably small error ranges, thus suggesting more robust average values. The relationship between MTCO and MTWA follows a different pattern. Unlike the late Pleistocene period, variations in both parameters appear to be in phase. This is probably a response to the complex interplay of regional interglacial climate forcings, which likely involve changes in the summer/winter solar insolation, a reduced influence of glaciation, sea ice cover and permafrost, a reduced continentality and a specific pattern of ocean currents.

The following sections provide a more detailed discussion on the pollen-inferred changes in vegetation and climate in view of the previously published regional and extra-regional palaeoclimate and palaeoenvironmental proxy records in chronostratigraphical order. Emphasis is put on long-term as well as on millennial- and centennial-scale climate oscillations. Last glacial short-term warming events, which match well with DO events identified in ice core records from Greenland (Alley, 2000, Fig. 5.13G) and Antarctica (Jouzel et al., 2007, Fig. 5.13F), are not further discussed.

5.6.2.1 The MIS3 interstadial (ca. 43.7–29.3 cal ka BP)

Given the long-term average temperature and precipitation reconstructions with relatively small error ranges, the oldest (i.e. MIS3) interval of the Khoe record represents relatively moist and thermally mild climate conditions (Fig. 5.13A–D). Average values of TANN (0 °C), MTCO (–18 °C) and PANN (690 mm) reflect favourable conditions for tree growth (Fig. 5.13E), although NAP taxa played a more important role in the regional vegetation in comparison to modern conditions (Fig. 5.8). Interestingly, the derived mean

climate conditions during the MIS3 interstadial were very close to the modern ones (Fig. 5.13A–D). Similarly, the Hulu Cave MIS3 $\delta^{18}O$ ratios (Wang et al., 2001b, MSD in Fig. 5.13H) are more or less identical with the modern and slightly higher than the early to middle Holocene optimum $\delta^{18}O$ from Dongge Cave (Yuan et al., 2004, D4 in Fig. 5.13H). In their study, Yuan et al. (2004) argue that the $\delta^{18}O$ stalagmite records from both caves, which are located ca. 1200 km apart from each other, largely replicate, thus are comparable in terms of absolute $\delta^{18}O$ variations. However, these oxygen isotope records do not provide information on absolute climate variations. Moreover, climate conditions during MIS3, which were similar to today or even warmer and wetter, are reported from several palaeoclimate proxy studies from the Asian monsoon domain including the Chinese Loess and Tibetan plateau, south-western China, and the South China Sea (see Herzschuh, 2006 and references therein). Disregarding the stadials, mild climate conditions during MIS3, which led to the extensive shrinking of the Fennoscandian Ice Sheet, are also reconstructed in Europe (Helmens, 2014). Although generally cooler than during the late MIS3 (Helmens, 2014), it is interesting to note that Bos et al. (2009) inferred similar to today's climate conditions in northern Scandinavia during the early MIS3 warming phase. As indicated by Overpeck et al. (1996) and Hodell et al. (1999), such favourable climate conditions as inferred from the Khoe pollen record and the above mentioned studies probably reflect the interplay between solar forcing and glacial climate boundary conditions during MIS3. While the summer insolation exceeded the present-day conditions (Laskar et al., 2004, Fig. 5.13K), its positive effect on the Asian summer monsoon intensity was suppressed by the NH continental ice sheets, low North Atlantic sea surface temperature (SST) and large-scale Asian snow cover. This is supported by Nakagawa et al. (2008), who postulate that during periods of minimum eccentricity – when solar forcing (mainly driven by the precession cycle; 19–23 ka) falls below a threshold level, which happened in Japan during MIS3, 2 and 1 – the control of solar forcing over the monsoon decreased relative to glacial forcing.

As indicated by both mean climate reconstructions and error bars, the broad MIS3 interstadial conditions are interrupted by a phase of distinctive climate deterioration between ca. 40.6–38.6 cal ka BP (572.5–540 cm). Regarding the pollen-inferred average thermal (TANN = 0 °C) and moisture (PANN = 690 mm) conditions prior to and after this phase, the values decrease by up to 8 °C and 300 mm, respectively. A synchronous trend towards less favourable conditions for tree growth is also evident in increasing scores for the STEP and TUND biomes and decreasing scores for forest biomes (Fig. 5.8). Although, the onset of this strong vegetation and climate shift occurs somewhat earlier, it appears to be coincident with Heinrich event 4 (H4). This time lead might depict a certain insufficiency in our age control. H4 is described as the largest of the six North Atlantic cold climate (i.e. Heinrich) events during the last glacial period (Hemming, 2004). There is

strong evidence that millennial-scale last glacial aridification trends in the NH are a response to North Atlantic temperature variations (Deplazes et al., 2014). As denoted by the MTCO and MTWA reconstructions, the massive temperature decline is attributed to the winter season. Concordant seasonal temperature patterns are reported for MIS3 cold events in the North Atlantic region and related to widespread winter sea-ice expansion across the North Atlantic Ocean (Denton et al., 2005). Such significant shifts towards drier conditions during Heinrich events are also reported from e.g. the Indian Monsoon domain by elemental and grain size records from the Indus submarine slope in the northern Arabian Sea (Deplazes et al., 2014) reflecting ISM strength and other regions within the East Asian Monsoon domain by stalagmite $\delta^{18}O$ records from Hulu (Wang et al., 2001b, Fig. 5.13H) and Sanbao (Wang et al., 2008) Cave in China used as a proxy for meteoric precipitation and cave temperature. Moreover, there is correspondence between the TANN reconstructions (T. Nakagawa, personal communication 2013) based on the SG06 high-resolution pollen record from Lake Suigetsu (Nakagawa et al., 2012) in central Japan and our results during H4. Although smaller in magnitude, the recognised phase of cooler conditions in central Japan is similarly pronounced in relation to MIS3 climate fluctuations and nearly identical in timing. Given the robust chronology of the annually laminated sediment record SG06 (Bronk Ramsey et al., 2012), these correlations would in turn enhance the confidence for the age–depth model of the Khoe sediment profile (Fig. 5.11). The more sensitive climate reaction denoted in our MAT results may be due to the location of the Khoe site at the northern limit of the EASM, which would lead to a stronger influence of cold Siberian air masses during phases of weak EASM circulation. Comparable relations between the position of palaeoclimate archives (ranging from core to outer monsoon zone) and the magnitude of precipitation variations over the Holocene interval are also identified for the ISM domain (Fleitmann et al., 2007; Leipe et al., 2014). The decrease in average TANN and PANN in combination with a rather low error limit at the end of MIS3 we associate (ca. 29.7 cal ka BP, 470 cm) with Heinrich event 3 (H3). In contrast to H4, the climate deterioration of this stadial appears less pronounced. This might be a result of the lower resolution in this part of the core section and/or shorter duration of a regional H3-related climate change. Above this, it also has to be assumed that the North Atlantic cooling had a much weaker impact on the climate of the study region than during H4.

5.6.2.2 The MIS2 stadial (ca. 29.3–11.7 cal ka BP)

The section of the Khoe record (ca. 29.3–11.7 cal ka BP, 467.5–362.5 cm), which largely represents MIS2, is generally characterised by MAT-inferred climate values showing a noticeably lower error limit (Fig. 5.13A–D), thus suggesting cooler and drier

conditions in the study region. After a phase of climate fluctuations (ca. 29.3–21.8 cal ka BP, 467.5–420 cm), including several short pulses towards climate amelioration, temperature and precipitation decrease. During the following full glacial stage (ca. 21.8–15.3 cal ka BP, 420–392.5 cm), average TANN (–3.3 °C) and PANN (550 mm) reconstructions are, compared to present-day conditions, reduced by 3.3 °C and 150 mm, respectively. Climatically more severe growing conditions are underpinned by contemporary minimum tree cover concentration levels of ca. 35%. Another indication for unfavourable growing conditions are the minimum sedimentation rates inferred from the age–depth model (Fig. 5.11), which is likely the response to lowered biomass production levels in and around the sampled tectonic depression. This trend is accompanied by reconstructed (Waelbroeck et al., 2002, Fig. 5.13I) and simulated (Peltier and Fairbanks, 2006, Fig. 5.13J) minimum global sea levels linked to the global maximum extent of ice sheets.

The coldest and driest stage during this interval, conventionally related to the last glacial maximum (LGM), is observed around 20.3 cal ka BP (410 cm). This pulse is determined by harsh winter temperatures (MTCO = –30.5 °C) and lowered precipitation (PANN = 470 mm) which coincide with the simulated absolute minimum global sea level (Peltier and Fairbanks, 2006, Fig. 5.13J) lagging the NH summer insolation minimum (Laskar et al., 2004, Fig. 5.13K) by ca. 3 ka. There is no doubt about a major global glaciation, which occurred during MIS2 (Clark et al., 2009), but still debate about the timing of this event (Hughes et al., 2013). While some authors consider that the LGM spanned the period ca. 24/23–19/18 cal ka BP with ca. 21 cal ka BP as its centre (Mix et al., 2001; MARGO Project Members, 2009), others place the event between ca. 26–21 cal ka BP (Peltier and Fairbanks, 2006) or even between 27.2–23.5 cal ka BP (Svensson et al., 2008). The most unfavourable climate conditions observed in our reconstructions are temporally in agreement with reconstructed minimum mean effective moisture (ca. 23–19 cal ka BP) based on a set of 75 palaeoclimate records from monsoonal Central Asia (Herzschuh, 2006). Although not representing maximum values, the increased $\delta^{18}O$ ratios of the MSD Hulu Cave stalagmite also suggest generally drier and cooler LGM climate conditions between ca. 23–19 cal ka BP than during MIS3 (Wang et al., 2001b, Fig. 5.13H). This might be due to LGM boundary conditions (e.g. increased distance to the moisture source and reduced humidity over southern China), which, despite colder and drier conditions, would result in more negative $\delta^{18}O$ values (Cai et al., 2010). Further confirmation for LGM climate conditions around ca. 20 cal ka BP in the wider study region comes from a fossil pollen record from the Kenbuchi Basin located in northern Hokkaido (Igarashi et al., 1993; Igarashi, 1996). After conversion of the available radiocarbon dates to calendar ages using the online version of the CalPal radiocarbon calibration program (Danzeglocke et al., 2013), the record indicates coldest and driest conditions by increasing concentration of NAP and pollen of cold-tolerant boreal trees (i.e. *Larix* and *Pinus*) around 23–20 cal ka BP.

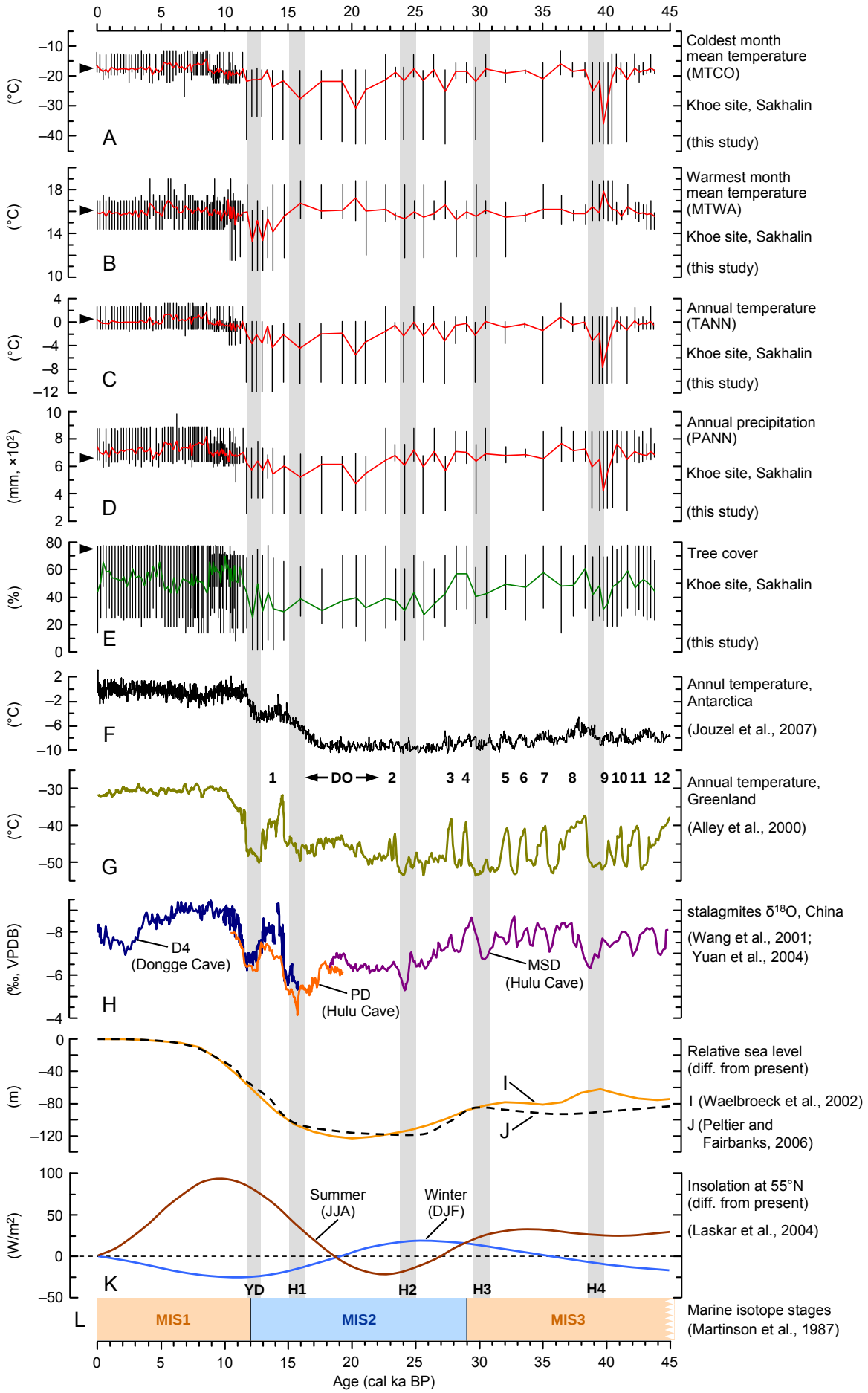
Coldest month mean temperature (MTCO)
Khoe site, Sakhalin
(this study)
Warmest month mean temperature (MTWA)
Annual temperature (TANN)
Annual precipitation (PANN)
Tree cover
Annul temperature, Antarctica
(Jouzel et al., 2007)
Annual temperature, Greenland
(Alley et al., 2000)
stalagmites δ18O, China
(Wang et al., 2001; Yuan et al., 2004)
D4 (Dongge Cave)
PD (Hulu Cave)
MSD (Hulu Cave)
Relative sea level (diff. from present)
I (Waelbroeck et al., 2002)
J (Peltier and Fairbanks, 2006)
Insolation at 55°N (diff. from present)
(Laskar et al., 2004)
Summer (JJA)
Winter (DJF)
YD
H1
H2
H3
H4
MIS1
MIS2
MIS3
Marine isotope stages (Martinson et al., 1987)
Age (cal ka BP)

Fig. 5.13 Comparison of the pollen-based (A–D) climate and (E) tree cover reconstructions from Khoe, Sakhalin (this study) and other palaeoclimate records including (F) the mean annual surface temperature reconstruction from the EPICA Dome C Ice Core (75.1°S, 123.35°E, 3270 m a.s.l.) deuterium record from Antarctica (after Jouzel et al., 2007); (G) the mean annual surface temperature derived from the Greenland GISP2 ice core (72.58°N, 38.48°W, 3208 m a.s.l.) $\delta^{18}O$ record (after Alley, 2000) with Dansgaard-Oeschger (DO) events (after Dansgaard et al., 1993); (H) the stalagmite $\delta^{18}O$ records PD and MSD from Hulu cave (23.50°N, 119.17°E, 100 m a.s.l., after Wang et al., 2001b) and D4 from Dongge cave (25.28°N, 108.08°E, 680 m a.s.l., after Yuan et al., 2004) in China; (I) the oxygen isotope ratio-based reconstructed (after Waelbroeck et al., 2002) and (J) ICE-5G(VM2) model simulated changes in relative global sea-level (after Peltier and Fairbanks, 2006); and (K) the computed mean summer (June–August) and winter (December–February) insolation at 55°N (after Laskar et al., 2004). Heinrich (H) events (after Heinrich, 1988) and the Younger Dryas (YD) are indicated by grey bars.

Like H3 (MIS3), Heinrich event 2 (H2) and 1 (H1) are much less distinct in our climate and tree cover reconstructions in comparison with H4. Accordingly, it might be considered that the climate signals of the fossil pollen assemblages in the Khoe record during both events are obscured by low sedimentation rates (ca. 30–15 cal ka BP, 472.5–392.5 cm, Fig. 5.11) and low resolution. However, H1 is suggested to be the longest stadial of the last glacial (Denton et al., 2010) with a duration of over 4 ka (ca. 19–14.6 cal ka BP; Stanford et al., 2011). It also appears to be well reflected in the stalagmite $\delta^{18}O$ records from China (Wang et al., 2001b, Fig. 5.13H; Yuan et al., 2004, Fig. 5.13H). Therefore, it is more likely that H1 is well registered in the Khoe pollen record. Compared to previous (i.e. full glacial) conditions, our reconstructions show a weak decrease in TANN of ca. 2 °C (Fig. 5.13C), which is, however, well in accord with the faint cooling trend (ca. 5 °C) in the GISP2 annual temperature record from Greenland (Alley et al., 2000, Fig. 5.13G).

The H1-related cooling trend, which was caused by warming-induced ice-sheet melting and is widely recognised in NH palaeoclimate proxy records, marks the onset of the last deglaciation (Denton et al., 2010). The subsequent climate amelioration towards the Holocene with a stepwise increase of PANN and TANN between ca. 15.3–13.2 cal ka BP (392.5–377.5 cm) is interrupted by a climate reversion between ca. 13.2–11.7 cal ka BP (377.5–362.5 cm). Both short-term trends are well in agreement with the key palaeoclimate records from the North Atlantic region (e.g. Alley, 2000, Fig. 5.13G) and Antarctica (Jouzel et al., 2007, Fig. 5.13F), thus corresponding to the late-glacial Bølling–Allerød interstadial and the Younger Dryas stadial, respectively, which are widely recognised within the Asian monsoon domain including coastal China (e.g. Wang et al., 2001b, Fig. 5.13H; Yuan et al., 2004, Fig. 5.13H; Stebich et al., 2009) and central Japan (Nakagawa et al., 2005, 2006). A North Atlantic region-like pattern of deglacial warmer/moister and cooler/drier climate conditions is also evident in different fossil pollen records from northern Japan (Hokkaido), but less distinct due to low resolution and less robust chronologies (Igarashi et al., 1993; Igarashi, 1996). According to the error bars, MTWA are suggested to be lowest during the

late-glacial period (ca. 15.3–11.7 cal ka BP, 392.5–362.5 cm). As for the previous intervals, the trend towards slightly cooler summers may represent enhanced continentality resulting in higher seasonality. We presume that this late-glacial MTWA decrease is related to the continuous rise in global sea level in response to large-scale deglaciation (Waelbroeck et al., 2002, Fig. 5.13I; Peltier and Fairbanks, 2006, Fig. 5.13J). Further explanation for lowered summer temperatures might be provided by the late-Pleistocene East Siberian Ice sheet hypothesis raised by Grosswald and Hughes, according to which large parts of the northern Okhotsk Sea were occupied by an extensive marine ice sheet that was supplied by glaciation of the north-bounding mountain ranges during the LGM (see Grosswald and Hughes, 2002 and references therein). Thawing of these ice masses would have led to the discharge of large amounts of cold water into the adjacent seas (Okhotsk Sea and Sea of Japan) of late-Pleistocene peninsular Sakhalin, which, in turn, would have induced a cooling effect there during summer. On the other hand, during winters such a cooling effect would have been outbalanced by greater maritimity. However, the existence of an East Siberian Ice sheet during the LGM–late-glacial period is strongly called into question by contrary findings of different authors (see Brigham-Grette, 2001 and references therein). Moreover, extensive glaciation in the Okhotsk Sea region is in disagreement with several studies based on marine palaeoclimate proxy records from the Okhotsk Sea floor. While some authors postulate that the sea was not influenced by larger ice sheets but non-perennial sea ice cover (e.g. Okazaki et al., 2005; Sakamoto et al., 2005; Gorbarenko et al., 2014), others argue that perennial sea ice cover was limited to the LGM (Shiga and Koizumi, 1999) or restricted to the northern sector of the Okhotsk Sea during Pleistocene full glacial stages (Yamazaki, et al., 2013).

5.6.2.3 The Holocene (ca. 11.7 cal ka BP – present)

The early Holocene (ca. 11.7–8.7 cal ka BP, 362.5–227.5 cm) is characterised by considerably warmer and wetter conditions compared to the late-glacial period, with winters slightly cooler than today but precipitation levels comparable to modern conditions. The remarkable climate amelioration is supported by tighter error bars and higher upper and lower limits in contrast to the last glacial. Although summer insolation peaked, Holocene climate optimum conditions did not occur in the study region before ca. 8.7 cal ka BP, which, at first glance, seems to be in agreement with review studies arguing for a middle Holocene climate optimum in the northern (Zhao and Yu, 2012; Ran and Feng, 2013) or entire (Herzschuh et al., 2006; Wang et al., 2010) domain of the EASM. In contrast, asynchrony with the ISM domain, where Holocene climate optimum conditions are identified during the early Holocene (see Leipe et al., 2014 and references therein), has been questioned by the works of different authors (e.g. Rudaya et al., 2009; Zhang et al.,

2011; Li et al., 2014) and thus remains controversial. Different palynological studies from Hokkaido provide further evidence for a Holocene climate optimum not having occurred before ca. 8 cal ka BP (Sakaguchi, 1992; Igarashi et al., 2002, 2011), when pollen of the cold-tolerant *Larix* disappeared from the records and pollen of the temperate broadleaved taxon *Quercus* started to strongly increase. Broadly corresponding results are also documented by the calculation of dominant biome scores (Fig. 5.8). Although climate gradually ameliorated during the early Holocene stage, taiga and cool conifer forest prevailed until ca. 10.5 and 9.4 cal ka BP, respectively, before cool mixed forest was established around the study site. In terms of climatic interpretation based on the BIOME1 vegetation model (Prentice et al., 1992), this means that MTCO did not exceed –19 °C before ca. 10.5 cal ka BP, which is in agreement with the error ranges of the MAT-derived values. In contrast, MTCO of not below –15 °C as indicated by the spread of cool mixed forest is reached ca. 0.5 ka earlier than suggested by the MAT (ca. 8.9 cal ka BP).

Holocene optimum climate with slightly increased precipitation and improved thermal conditions is reconstructed for the period ca. 8.7–5.2 cal ka BP (227.5–112.5 cm), which is well in line with maximum biome scores for cool mixed forest owing to higher concentrations of temperate deciduous tree type pollen (i.e. *Quercus*, *Fraxinus* and *Acer*). Although remaining on high levels, summer insolation had started to decrease, which indicates a mainly regional rather than orbital forcing of the early to middle Holocene climate conditions in northern Sakhalin. An important factor for the regional climate was probably the influence of the surrounding seas and ocean currents. By this time, the Sea of Japan had transgressed further north towards the modern Tatar Strait with its shoreline located fairly close to the Khoe sampling site. After its initial inflow to the Sea of Japan at the onset of the Holocene interval (e.g. Oba et al., 1991, 1995), the TWC, which today still flows along Sakhalin's south-western coast (Fig. 5.1B), is suggested to have reached a phase of highest intensity between ca. 9/8–7 cal ka BP (Oba et al., 1991, 1995; Itaki et al., 2004; Takada et al., 2006). The TWC intensity probably culminated at around 8 cal ka BP when according to Sawada and Handa (1998) the subtropical heat transport to northern latitudes of the Pacific Ocean reached a maximum. Furthermore, evidence for cool early Holocene conditions is found in the north-western and southern Okhotsk Sea. Records of ice rafted debris and marine diatom assemblages (Gorbarenko et al., 2014) and alkenones (Ternois et al., 2000) suggest that SSTs were low until ca. 9–8 cal ka BP due to persistent sea ice influence and, according to Gorbarenko et al. (2014), reached a maximum in the late middle Holocene (ca. 4–5 cal ka BP).

Interestingly, climate optimum conditions are paralleled by a slight reduction in total tree cover compared to the previous Holocene interval. A possible reason for this is that tree growth is not necessarily directly related to precipitation, but rather depends on the annual moisture availability often expressed with α (Priestley-Taylor coefficient) as the

ratio of actual evapotranspiration over potential evapotranspiration (Prentice et al., 1992), which also accounts for thermal conditions (Prentice et al., 1992). Hence, tree growth may be constrained by temperature-induced high evapotranspiration (i.e. low α) even when precipitation is on high levels. Similar findings are reported in a study of a fossil pollen record from the EASM domain in north-eastern China, where the Holocene peak period of tree pollen percentages is not in phase with warmest and wettest conditions but with the peak in MAT-based α reconstructions (Guiot et al., 2008). On the contrary, it might be also considered that higher precipitation levels were paralleled by increased moisture availability, which led to a large-scale expansion of bog conditions. This is indicated by the spread of typical bog taxa like *Sphagnum* and *Myrica gale* traced in the fossil pollen and spore assemblages (Fig. 5.4), which would in turn explain more unfavourable conditions for tree growth. However, whether bog growth was restricted to a rather small area within and/or around the sampled depression or more widespread cannot be clarified in this study. An alternative explanation for the reduced presence of trees around the study site might be anthropogenic influence. In deed, the development of sedentism is documented by several early Neolithic sites discovered in both the northern and southern part of Sakhalin, of which the ages (own calibrations of the original ^{14}C dates using CalPal online by Danzeglocke et al., 2013) of the oldest sites range between ca. 9.8–8.3 cal ka BP (Kuzmin et al., 2004; Zhushchikhovskaya and Shubina, 2006). A substantial impact on the vegetation by deforestation may yet be ruled out as the early sedentary communities of Sakhalin are reported to have subsisted on hunting, fishing and gathering (Lutaenko et al., 2007; Kuzmin and Rakov, 2011) and were likely rather dispersed.

The uppermost interval (ca. 5.2–0 cal ka BP, 112.5–0 cm) is initiated by a swing towards a drier and on average cooler environment that culminated ca. 4.4 cal ka BP with a coeval interruption in the overall dominance of the cool mixed forest by taiga. Subsequently, TANN and PANN remained on a level that was lower than during the middle Holocene but still stable. This is broadly in agreement with palaeoclimate proxy studies from the entire Asian monsoon domain (e.g. Herzschuh, 2006; Fleitmann et al., 2007; Rudaya et al., 2009; Wang et al., 2010; Ran and Feng, 2013; Li et al., 2014) and well paralleled by annual insolation decline (Laskar et al., 2004, Fig. 5.13K). Correspondingly, the tundra biome scores illustrate the continuous expansion of herbaceous and shrubby taxa to the detriment of arboreal taxa and more unstable climate conditions expressed by the fluctuation in dominant biome distribution (i.e. among cool mixed forest, cool conifer forest by taiga). Analogous late Holocene climate trends are inferred on the basis of palynological investigations from the wider study region including the lower Amur River basin (Mokhova et al., 2009; Bazarova et al., 2011) and the Kuril Islands (Razjigaeva et al., 2013). However, as reviewed by Igarashi (2013), late Holocene climate deterioration is not documented in the fossil pollen records from Hokkaido. In a recent study, Leipe et al.

(2013) applied the biomisation method and MAT to a ca. 5500-year-old pollen record from south-western Hokkaido. They concluded that between ca. 3.6 cal ka BP and today, climate was even wetter and warmer than the previous interval, which is likely caused by strengthening of the TWC. It seems well conceivable that a re-intensified TWC may have positively influenced or even outbalanced the overall solar forced development towards cooler and drier climate conditions during the late Holocene. However, the lack of additional well-dated marine records from the northern Sea of Japan and terrestrial proxy records from Sakhalin and/or northern Japan prevents us from conducting a more robust and detailed interpretation.

Several Holocene short-term pulses towards climate deterioration are imprinted in the MAT reconstructions. The four most prominent cold/dry relapses are found at around 10.3 (310 cm), 7.4 (165 cm), 4.4 (95 cm) and 0.5–0.9 (20–10 cm) cal ka BP, and thus match well with cold cycles (i.e. Bond cycles) determined in ice-rafted sediment records from the North Atlantic (Bond et al., 1997, 2001) and Greenland ice cores (Mayewski et al., 1997, 2004). Such cold events are also reconstructed for other regions within the Asian monsoon domain (Hong et al., 2003; Wang et al., 2005b; Leipe et al., 2014) and the Okhotsk Sea (Gorbarenko et al., 2014). The driving mechanisms for these NH cold climate oscillations, which show no clear cyclicity but rather a fairly complex spatiotemporal pattern, are still insufficiently understood. While some events appear to be linked to a downturn of the thermohaline circulation in the North Atlantic linked to phases of weak solar activity or enhanced meltwater influence, others seem to be additionally combined with increased volcanic activity (Wanner et al., 2008, 2011). In order to clarify whether the short-term cold spells registered in the Khoe fossil pollen record represent a direct teleconnection with one or several of the identified processes, or primarily reflect internal forcing factor variability driven by feedback effects (Bengtsson et al., 2006), further palaeoclimate proxy studies are required in the study region.

5.7 Conclusions

Covering the last ca. 44 ka, the fossil pollen assemblages from Khoe in northern Sakhalin represent the longest terrestrial record of vegetation and environmental development from the north-western corner of the Pacific region. Successful tests with a combination of previously approved biome–taxon matrices and a set of modern pollen spectra suggest that the biome reconstruction method may be reliably applied to fossil pollen records from Sakhalin. In addition to the biomisation method, we have applied the modern analogue technique to the Khoe pollen record to objectively quantify variations in temperature, precipitation and percentage tree cover in the study region. The overall

results of both methods are well in agreement and illustrate the long-term trends as well as millennial- and centennial-scale variations in vegetation and climate conditions.

The last glacial is characterised by mean average temperature (TANN = 0 °C) and precipitation (PANN = 690 mm) reconstructions, which are generally similar to late Holocene averages (TANN = 0.2 °C, PANN = 700 mm) during MIS3 (ca. 43.7–29.3 cal ka BP) and weakly reduced during the full glacial interval (ca. 21.8–15.3 cal ka BP). While the error bars of the MIS3 reconstructions are relatively small, they are larger particularly during the full glacial. Especially the low error range limits during MIS2 show the potential for lower temperature and precipitation levels. A more comprehensive pollen-climate dataset may help to provide more robust reconstructions.

Another interesting feature is the anti-phase relationship between MTCO and MTWA during the last glacial, which we relate to changes in the degree of continentality due to variations in the global sea level and glaciation cycles. However, the average MTWA reconstructions should not be overinterpreted since the error ranges are rather large and the influence of MTWA on the forest vegetation distribution is negligible. To evaluate the relatively high reconstructed last glacial MTWA averaged from the eight best modern analogues, additional fossil records of Chironomidae, Ostracoda and/or plant macro remains may be also helpful.

During the last glacial, several millennial-scale climate oscillations towards warmer/wetter and cooler/drier climate are indicated by the MAT reconstructions, which are coeval with respective warming (i.e. Dansgaard-Oeschger) and cooling (i.e. Heinrich) events registered in the North Atlantic region and Antarctica. The most prominent one is H4, which is marked by noticeably drier and cooler conditions and the spread (decrease) of herbaceous (arboreal) taxa. Although H4 was the largest cooling event during the last glacial, an equivalent is not clearly traceable in the available palaeoclimate proxy records from the Asian monsoon domain and neighbouring regions. Therefore, it might be assumed that H4 climate deterioration in northern Sakhalin was amplified by a regional driving force.

The last deglaciation is marked by a stepwise increase of TANN and PANN, which broadly coincides with the Bølling–Allerød and the Younger Dryas. Synchronously, MTWA reconstructions suggest that summer temperatures were slightly decreased, which we relate to enhanced maritimity in response to rising global sea levels.

Compared to MIS2, the climate during the Holocene interval is warmer and wetter with highest levels of tree cover in the study region and accompanied by a successive development of cool mixed forest. Reconstructed maximum tree cover indicates that annual moisture availability (α) was highest during the early Holocene (ca. 11.7–8.7 cal ka BP) when, despite peak summer insolation, a rise in annual temperatures was suppressed by the influence of low SSTs of the surrounding seas. Middle Holocene climate optimum

conditions with TANN of 1.0 °C and PANN of 750 mm (ca. 8.7–5.2 cal ka BP) are likely caused by the effect of high-level solar output, which was distinctly amplified by the rising global sea level (i.e. maritimity) and intensified flow of the Tsushima Warm Current in the Sea of Japan.

In order to disentangle the influence of global- and/or hemispherical-scale climate system processes and regional forcing factors on different time-scales in the insular north-western Pacific, additional well-dated, high-resolution palaeoclimate proxy records are needed from the region.

5.8 Acknowledgments

The work of C. Leipe was financially supported by the DFG grant RI 809/24. P. Tarasov acknowledges the DFG Heisenberg Program (TA 540/5).

6. Conclusions and future perspectives

This thesis exhibits a compilation of four palaeoenvironmental proxy studies (Chapters 2–5) based on different fossil palynomorph records originating from different regions within the ASM domain and representing different time ranges. Numerical pollen-based vegetation and climate reconstructions, which are partly combined with NPP analyses, yield implications for past variations of the ISM and EASM system as well as for past human impact in the western Trans-Himalaya and the evolution of the Harappan Civilisation. This chapter briefly highlights the most significant insights from the previous chapters grouped by subject area followed by an outline of perspectives for future research.

The Indian Summer Monsoon (ISM):

- The pollen record from the high-altitude lake Tso Moriri (western Trans-Himalaya) covering the last ca. 12 ka, reveals that the onset of the Holocene ISM indicated by a rapid increase in moisture availability, occurred at the termination of the Younger Dryas. ISM intensity was strongest between ca. 11–9.6 cal ka BP, thus suggesting an early Holocene moisture optimum.
- The Holocene moisture evolution in the western Trans-Himalaya is marked by a gradual decline, which parallels the southward migration of the mean summer position of the ITCZ in response to orbitally induced reduction of summer insolation. This confirms the existing hypothesis that the long-term ISM strength is primarily governed by the mean summer ITCZ position.
- The results of the quantitative reconstruction indicate considerable fluctuations in annual precipitation, which during the wettest interval (early Holocene) was ca. 430 mm higher and during the driest interval (late Holocene) ca. 35 mm lower compared to modern conditions (ca. 250 mm).
- Correlation with other palaeoclimate proxy records suggests that the decrease in precipitation in the regions at the northern limit of the ISM (i.e. the north-western Himalaya) was greater than in the southern parts (i.e. the western Arabian Sea region) of the ISM domain.

The East Asian Summer Monsoon (EASM):

- The climate conditions in the northern-most part of the EASM domain (Sakhalin) during late MIS3 (ca. 44–29 cal ka BP) DO cycles were similar to modern conditions. During late MIS3 Heinrich events and the entire MIS2, climate conditions were

potentially much drier and colder than today. Relatively large error ranges of the MAT results for the last glacial hamper a more precise climate interpretation for this time interval and call for an extension of the available modern reference pollen datasets.

- While cold and dry climate cycles, coeval with North Atlantic millennial-scale Heinrich events (H4–H1), are traced during the represented interval of the last glacial in the MAT reconstructions from Sakhalin, H4 exhibits by far the most extensive phase of climate deterioration. Since an equivalent event is not clearly recognisable in existing palaeoclimate proxy records from the ASM domain, it may be only presumed that H4 climate deterioration on Sakhalin was amplified by a regional driving force.
- Reconstructions of vegetation, climate and total tree cover indicate that climate ameliorated remarkably at the Younger Dryas/Holocene transition. Furthermore, annual moisture availability (α) was highest during the early Holocene (ca. 11.7–8.7 cal ka BP) accounting for the Holocene hydrological optimum. In contrast, the thermal optimum and maximum in precipitation occurred during the middle Holocene (ca. 8.7–5.2 cal ka BP). The middle Holocene climate optimum on Sakhalin is likely explained by the effect of enhanced solar insolation at high NH latitudes, which was distinctly amplified by the rising global sea level (i.e. maritimity) and intensified flow of the Tsushima Warm Current in the Sea of Japan.
- The results derived from the compiled set of modern pollen reference samples revealed that the biomisation approach which considers the whole list of terrestrial pollen taxa (including herbaceous taxa) (Takahara et al., 2000) is more suitable for reconstructing late Quaternary vegetation and climate dynamics in northern Japan than the approach which only considers AP taxa (Gotanda et al., 2002).
- MAT and biomisation method results based on the south-western Hokkaido (Yakumo) late Holocene fossil pollen record demonstrate warmer/wetter conditions initiated at ca. 3.6 cal ka BP and persisting until present compared to the previous interval (ca. 5.5–3.6 cal ka BP). As this conflicts with the broad-scale climate trends in the EASM domain and other regions of the NH, the reconstructed warming trend is probably linked to the expansion of the Tsushima Warm Current documented in previous studies on diatom and foraminifera assemblages from sediment cores from the Sea of Japan.

Influence of westerly disturbances:

- The climate reconstructions from the ISM domain (Tso Moriri) clearly illustrate several prominent centennial-scale intervals of enhanced aridification during the Holocene, which are closely synchronous with North Atlantic cold climate (i.e. Bond) events.

These dry intervals probably indicate reduced winter westerly airflow, which led to decreased winter precipitation in the north-western Himalayas.

- There is also evidence from this study and other Holocene palaeoclimate proxy records that early Holocene climate conditions are more strongly linked to North Atlantic cold events in the southern ISM domain (i.e. the western Arabian Sea region) than in the northern domain (i.e. north-western Himalayas). This may reflect a higher portion of westerly-derived moisture in the annual precipitation sum in the former region. A plausible explanation for this is the persistence of large parts of the Fennoscandian ice sheet during the early Holocene, which prevented the belt of summer westerly disturbances from migrating as far north as today. This would have led to enhanced moisture transport especially to the southern/south-western ISM domain.
- The slight increase in annual precipitation in the north-western Trans-Himalaya during the late Holocene likely reflects an intensification of the winter westerly disturbances.

The Asian Summer Monsoon (ASM):

- The results of the studies contained in this thesis suggest that the ITCZ was the common driving force of the ASM, which led to the synchronous post-glacial strengthening of both the ISM and EASM at the onset of the Holocene interval.
- Holocene climate optimum conditions show a different (i.e. asynchronous) timing in the ISM (early Holocene) and EASM (middle Holocene). However, it has to be noted that the derived climate signals from the EASM (i.e. Sakhalin) are mainly driven or overprinted by regional forcing factors such as the influence of ocean currents or changing degrees of continentality.

Human activities in the western Trans-Himalaya:

- There is no clear evidence for human impact in the Tso Moriri region prior to ca. 3.7 cal ka BP. Clear indications for an occupation by humans likely subsisting on agro-pastoralism is indicated by the pollen and NPP record no earlier than ca. 2.7 cal ka BP.

Evolution of the Harappan Civilisation:

- The results of the quantitative mean annual precipitation reconstruction, NPP analysis from Tso Moriri and geomorphologic analysis of its basin lead to the hypothesis that the evolution of the Harappan Civilisation of the greater Indus Valley was linked to climate change. First, the gradual decrease in precipitation may have caused crop yields to fall, which promoted the establishment of urban centres of the mature phase to provide an infrastructure for storage, protection, administration, and redistribution of staple crops.

Later, additional pronounced dry spells at ca. 4 and 3.2 cal ka BP in combination with enhanced ENSO-related interannual monsoon oscillations probably further hampered sufficient food supply that may have caused the protracted deurbanisation after ca. 4 cal ka BP and the eventual demise of the sophisticated Harappan Civilisation between ca. 3.5–3 cal ka BP.

Numerous studies using both palaeoclimate proxies and simulations have deepened our knowledge about spatiotemporal patterns of Asian monsoon activity during the late Quaternary and the underlying internal and external driving forces. However, to completely understand the complex mechanisms which control this major component of the global climate system remains a great challenge. Further palaeoclimate proxy records are needed from the ISM and EASM domain to better understand the mechanisms of differences and similarities in the past evolution of both subsystems.

One current issue which is frequently discussed is whether the Holocene pattern of climate development of both subsystems was synchronous or asynchronous. This study indicates that palaeoclimate proxy records from the East Asian island arc as representative for the EASM may not be sufficient to clarify this question. The EASM signal in these records may be difficult to capture since the region's climate is additionally influenced by ocean currents of the surrounding seas. Proxy records from regions which are less dominated by other atmospheric circulation systems or regional forces may provide a better understanding of past EASM variations.

A similar situation is encountered within the westernmost areas of the ISM domain. Here, the influence of westerly-derived precipitation may complicate the interpretation of proxy records of past ISM moisture evolution. A promising tool to solve this problem are e.g. ^{18}O and ^{13}C ratios of aragonitic shells of the aquatic gastropod *Radix*, which have been recently established as a proxy for climate and hydrological conditions on the Tibetan Plateau and adjacent regions on a sub-seasonal level (Taft et al., 2012, 2013, 2014).

Fossil and modern pollen assemblages are among those palaeoclimate proxies which have great potential to enhance our knowledge about the magnitude of late Quaternary climate change within the Asian monsoon domain. To improve the reliability of quantitative analogue-based climate and environmental reconstructions and to verify the biomisation method in different regions, modern reference datasets need to be further extended. This is especially crucial for the ISM domain where modern pollen spectra are especially limited and for regions of northern Japan, where cool conifer forest is the actual dominant biome at present.

This study has shown that the analysis of fossil NPP assemblages may serve as a valuable tool to supplement fossil pollen records and to strengthen the significance of their

palaeoclimatic interpretation. However, further research is required to deepen our understanding of the interpretation of NPP assemblages in future studies. Similarly, fossil Poaceae pollen assemblages from the north-western Himalayas have great potential in the study of the impact of sedentary communities. Yet a certain differentiation of regional cereal and wild grass type pollen is not feasible, due to a poor knowledge of their morphology.

Most chronologies of palaeoclimate proxy records are based on radiocarbon dating. Especially in the Himalayas and on the Tibetan Plateau, ^{14}C reservoir effects are a particular problem, which makes finding suitable palaeoclimate archives a challenging future task. This thesis also highlights the general importance of adjusting the radiocarbon-based chronologies of different palaeoclimate records when correlated with each other. Assuming that different studies from different times used different radiocarbon calibration models, chronologies have to be aligned by recalibration of ^{14}C ages to allow a reliable intercorrelation and thus interpretation.

7. Bibliography

Abram, N.J., Gagan, M.K., Liu, Z., Hantoro, W.S., McCulloch, M.T., Suwargadi, B.W., 2007. Seasonal characteristics of the Indian Ocean Dipole during the Holocene epoch. Nature 445, 299–302.

Adam, D.P., Mehringer, P.J., 1975. Modern Pollen Surface Samples – An analysis of Subsamples. Journal of Research of the U.S. Geological Survey 3 (6), 733–736.

Adams, R.M., 1981. Heartland of Cities: Surveys of Ancient Settlement and Land Use on the Central Floodplain of the Euphrates. The University of Chicago Press, Chicago. 384 pp.

Aichner, B., Herzschuh, U., Wilkes, H., Schulz, H.-M., Wang, Y., Plessen, B., Mischke, S., Diekmann, B., Zhang, C., 2012. Ecological development of Lake Donggi Cona, north-eastern Tibetan Plateau, since the late glacial on basis of organic geochemical proxies and non-pollen palynomorphs. Palaeogeography, Palaeoclimatology, Palaeoecology 313–314 (0), 140–149.

Aizen, V., Aizen, E., Melack, J., Martma, T., 1996. Isotopic measurements of precipitation on central Asian glaciers (southeastern Tibet, northern Himalayas, central Tien Shan). Journal of Geophysical Research: Atmospheres 101, 9185–9196, doi:10.1029/96JD00061.

Aldenderfer, M.S., 2003. Archaeologists seek to understand how and when people came to occupy the Andean and Tibetan plateaus. American Scientist 91, 542–549.

Aldenderfer, M.S., 2011. Peopling the Tibetan Plateau: Insights from Archaeology. High Altitude Medicine & Biology 12 (2), 141–147.

Alexandrova, A.N., 1982. Pleistotsen Sakhalina. Nauka, Moscow (in Russian).

Alley, R.B., 2000. The Younger Dryas cold interval as viewed from central Greenland. Quaternary Science Reviews 19 (1–5), 213–226.

Alpat'ev, A.M., Arkhangel'skii, A.M., Podoplelov, N.Y., Stepanov, A.Y., 1976. Fizicheskaya geografiya SSSR (Aziatskaya chast'). Vysshaya Shkola, Moscow (in Russian).

An, Z., Colman, S.M., Zhou, W., Li, X., Brown, E.T., Jull, A.J.T., Cai, Y., Huang, Y., Lu, X., Chang, H., Song, Y., Sun, Y., Xu, H., Liu, W., Jin, Z., Liu, X., Cheng, P., Liu, Y., Ai, L., Li, X., Liu, X., Yan, L., Shi, Z., Wang, X., Wu, F., Qiang, X., Dong, J., Lu, F., Xu, X., 2012. Interplay between the Westerlies and Asian monsoon recorded in Lake Qinghai sediments since 32 ka. Nature Scientific Reports 2, 619, doi:10.1038/srep00619.

An, Z., Porter, S.C., Kutzbach, J.E., Xihao, W., Suming, W., Xiaodong, L., Xiaoqiang, L., Weijian, Z., 2000. Asynchronous Holocene optimum of the East Asian monsoon. Quaternary Science Reviews 19 (8), 743–762.

Andersen, S.T., 1979. Identification of wild grass and cereal pollen. Danmarks Geologiske Undersøgelse, Årbog, 69–92.

Andreev, A.A., Grosse, G., Schirrmeister, L., Kuzmina, S.A., Novenko, E.Y., Bobrov, A.A., Tarasov, P.E., Ilyashuk, B.P., Kuznetsova, T.V., Krbetschek, M., Meyer, H., Kunitsky, V.V., 2004. Late Saalian and Eemian palaeoenvironmental history of the Bol'shoy Lyakhovsky Island (Laptev Sea region, Arctic Siberia). Boreas 33 (4), 319–348.

Andrew, T.E., Fitzsimons, A.G., 1992. Seasonality, population dynamics and production of planktonic rotifers in Lough Neagh, Northern Ireland. Hydrobiologia 246 (2), 147–164.

Ashfaq, M., Shi, Y., Tung, W.-w., Trapp, R.J., Gao, X., Pal, J.S., Diffenbaugh, N.S., 2009. Suppression of south Asian summer monsoon precipitation in the 21st century. Geophysical Research Letters 36, L01704, doi:10.1029/2008GL036500.

Bar-Matthews, M., Ayalon, A., Gilmour, M., Matthews, A., Hawkesworth, C.J., 2003. Sea–land oxygen isotopic relationships from planktonic foraminifera and speleothems in the Eastern Mediterranean region and their implication for paleorainfall during interglacial intervals. Geochimica et Cosmochimica Acta 67 (17), 3181–3199.

Bartlein, P., Harrison, S., Brewer, S., Connor, S., Davis, B., Gajewski, K., Guiot, J., Harrison-Prentice, T., Henderson, A., Peyron, O., Prentice, I., Scholze, M., Seppä, H., Shuman, B., Sugita, S., Thompson, R., Viau, A., Williams, J., Wu, H., 2011. Pollen-based continental climate reconstructions at 6 and 21 ka: a global synthesis. Climate Dynamics 37 (3), 775–802.

Basińska, A., Kuczyńska-Kippen, N., Świdnicki, K., 2010. The body size distribution of *Filinia longiseta* (Ehrenberg) in different types of small water bodies in the Wielkoposka region. Limnetica 29 (1), 171–182.

Bazarova, V.B., Klimin, M.A., Mokhova, L.M., Orlova, L.A., 2008. New pollen records of Late Pleistocene and Holocene changes of environment and climate in the Lower Amur River basin, NE Eurasia. Quaternary International 179, 9–19.

Bazarova, V.B., Mokhova, L.M., Klimin, M.A., Kopoteva, T.A., 2011. Vegetation development and correlation of Holocene events in the Amur River basin, NE Eurasia. Quaternary International 237 (1–2), 83–92.

Beall, C.M., 2001. Adaptations to altitude: a current assessment. Annual Review of Anthropology, 30, 423–56.

Behre, K.-E., 1981. The interpretation of anthropogenic indicators in pollen diagrams. Pollen et Spores 23, 225–245.

Behre, K.-E., 1988. The role of man in European vegetation history. In: Huntley, B.W., Webb, T. III (Eds.) Vegetation history. Kluwer, Dordrecht, pp. 633–672.

Behre, K.-E., 2007. Evidence for Mesolithic agriculture in and around central Europe? Vegetation History and Archaeobotany 16 (2–3), 203–219.

Bengtsson, L., Hodges, K., Roeckner, E., Brokopf, R., 2006. On the natural variability of the pre-industrial European climate. Climate Dynamics 27 (7–8), 743–760.

Bennett, K.D., Willis, K.J., 2001. Pollen. In: Smol, J.P., Birks, H.J.B., Last, W.M. (Eds.), Tracking Environmental Change using Lake Sediments, Volume 3: Terrestrial, Algal and Siliceous Indicators. Kluwer, Dordrecht, pp. 5–31.

Berger, A., Loutre, M.F., 1991. Insolation values for the climate of the last 10 million years. Quaternary Science Reviews 10 (4), 297–317.

Beug, H.J., 2004. Leitfaden der Pollenbestimmung für Mitteleuropa und angrenzende Gebiete. Dr. F. Pfeil, München (in German).

Beug, H.-J., Miehe, G., 1999. Vegetation history and human impact in the eastern central Himalaya (Langtang and Helambu, Nepal). Dissertationes Botanicae 318.

Bhattacharyya, A., 1989a. Modern pollen spectra from Rohtang range, Himachal Pradesh. Journal of Palynology 25, 121–131.

Bhattacharyya, A., 1989b. Vegetation and climate during the last 30,000 years in Ladakh. Palaeogeography, Palaeoclimatology, Palaeoecology 73 (1–2), 25–38.

Bhattacharyya, A., 1991. Ethnobotanical observations in the Ladakh Region of Northern Jammu and Kashmir state, India. Economic Botany 45 (3), 305–308.

Bigelow, N.H., Brubaker, L.B., Edwards, M.E., Harrison, S.P., Prentice, I.C., Anderson, P.M., Andreev, A.A., Bartlein, P.J., Christensen, T.R., Cramer, W., Kaplan, J.O., Lozhkin, A.V., Matveyeva, N.V., Murray, D.F., McGuire, A.D., Razzhivin, V.Y., Ritchie, J.C., Smith, B., Walker, D.A., Gajewski, K., Wolf, V., Holmqvist, B.H., Igarashi, Y., Kremenetskii, K., Paus, A., Pisaric, M.F.J., Volkova, V.S., 2003. Climate change and Arctic ecosystems: 1. Vegetation changes north of 55°N between the last glacial maximum, mid-Holocene, and present. Journal of Geophysical Research: Atmospheres 108 (D19), 8170, doi:10.1029/2002jd002558.

Birks, H.H., Birks, H.J.B., Kaland, P.E., Moe, D., 1988. The Cultural Landscape – Past, Present and Future, Part II. Cambridge University Press, Cambridge, pp. 179–468.

Birks, H.J.B., 1973. Modern pollen rain studies in some arctic and alpine environments. In: Birks, H.J.B., West, R.G. (Eds.), Quaternary Plant Ecology. Blackwell Scientific Publications, Oxford, pp. 143–168.

Birks, H.J.B., 1995. Quantitative palaeoenvironmental reconstructions. In: Maddy, D., Brew, J.S. (Eds.), Statistical Modelling of Quaternary Science Data. Technical Guide, Vol. 5. Quaternary Research Association, Cambridge, pp. 161–254.

Birks, H.J.B., 1998. Numerical tools in palaeolimnology – progress, potentialities, and progress. Journal of Palaeolimnology 20 (4), 307–332.

Bond, G., Kromer, B., Beer, J., Muscheler, R., Evans, M.N., Showers, W., Hoffmann, S., Lotti-Bond, R., Hajdas, I., Bonani, G., 2001. Persistent solar influence on North Atlantic climate during the Holocene. Science 294, 2130–2136.

Bond, G., Showers, W., Cheseby, M., Lotti, R., Almasi, P., deMenocal, P., Priore, P., Cullen, H., Hajdas, I., Bonani, G.,1997. A pervasive millennial-scale cycle in North Atlantic Holocene and glacial climates. Science 278, 1257–1266.

Bookhagen, B., Burbank, D.W., 2010. Toward a complete Himalayan hydrological budget: spatiotemporal distribution of snowmelt and rainfall and their impact on river discharge. Journal of Geophysical Research: Earth Surface 115, F03019, doi:10.1029/2009JF001426.

Bos, J.A.A., Helmens, K.F., Bohncke, S.J.P., Seppä, H., Birks, H.J.B., 2009. Flora, vegetation and climate at Sokli, northeastern Fennoscandia, during the Weichselian Middle Pleniglacial. Boreas 38 (2), 335–348.

Bos, J.A.A., Huisman, D.J., Kiden, P., Hoek, W.Z., van Geel, B., 2005. Early Holocene environmental change in the Kreekrak area (Zeeland, SW-Netherlands): A multiproxy analysis. Palaeogeography, Palaeoclimatology, Palaeoecology 227 (4), 259–289.

Braconnot, P., Harrison, S.P., Kageyama, M., Bartlein, P.J., Masson-Delmotte, V., Abe-Ouchi, A., Otto-Bliesner, B., Zhao, Y., 2012. Evaluation of climate models using palaeoclimatic data. Nature Climate Change 2 (6), 417–424.

Brantingham, P.J., Gao, X., Olsen, J.W., Ma, H., Rhode, D., Zhang, H., Madsen, D.B., 2007. A short chronology for the peopling of the Tibetan Plateau. In: Madsen, D.B., Chen, F.H., Gao, X. (Eds.) Developments in Quaternary Sciences. Elsevier, Amsterdam, pp. 129–150.

Brantingham, P.J., Rhode, D., Madsen, D.B., 2010. Archaeology augments Tibet's genetic history. Science 329, 72–75.

Brigham-Grette, J., 2001. New perspectives on Beringian Quaternary paleogeography, stratigraphy, and glacial history. Quaternary Science Reviews 20 (1–3), 15–24.

Bronk Ramsey, C., Staff, R.A., Bryant, C.L., Brock, F., Kitagawa, H., van der Plicht, J., Schlolaut, G., Marshall, M.H., Brauer, A., Lamb, H.F., Payne, R.L., Tarasov, P.E., Haraguchi, T., Gotanda, K., Yonenobu, H., Yokoyama, Y., Tada, R., Nakagawa, T., 2012. A Complete Terrestrial Radiocarbon Record for 11.2 to 52.8 kyr B.P. Science 338, 370–374.

Bukhteeva, A.V., Reimers, N.F., 1967. Vegetation map. In: Atlas Sakhalinskoi oblasti. GUGK, Moscow, pp. 106–107.

Bush, M., Gosling, W.D., 2012. Environmental change in the humid tropics and monsoonal regions. In: Matthews, J.A., (Ed.), The SAGE Handbook of Environmental Change Vol. 2. SAGE Publications Ltd, London, pp. 113–140.

Cai, Y., Tan, L., Cheng, H., An, Z., Edwards, R.L., Kelly, M.J., Kong, X., Wang, X., 2010. The variation of summer monsoon precipitation in central China since the last deglaciation. Earth and Planetary Science Letters 291 (1–4), 21–31.

Chabangborn, A., Brandefelt, J., Wohlfarth, B., 2014. Asian monsoon climate during the Last Glacial Maximum: palaeo-data–model comparisons. Boreas 43 (1), 220–242.

Chandan, P., Chatterjee, A., Gautam, P., 2008. Management planning of Himalayan high altitude wetlands. A Case Study of Tsomoriri and Tsokar Wetlands in Ladakh, India. In: Sengupta, M., Dalwani, R. (Eds.), Proceedings of Taal 2007: The 12th World Lake Conference, pp. 1446–1452.

Chang, C.-P., Wang, Z., Hendon, H., 2006. The Asian Winter monsoon. In: Wang, B. (Ed.), The Asian Monsoon. Praxis Publishing Ltd, Chichester, pp. 89–127.

Chen, F., Yu, Z., Yang, M., Ito, E., Wang, S., Madsen, D.B., Huang, X., Zhao, Y., Sato, T., John B. Birks, H., Boomer, I., Chen, J., An, C., Wünnemann, B., 2008. Holocene moisture evolution in arid central Asia and its out-of-phase relationship with Asian monsoon history. Quaternary Science Reviews 27 (3–4), 351–364.

Cheng, H., Zhang, P.Z., Spötl, C., Edwards, R.L., Cai, Y.J., Zhang, D.Z., Sang, W.C., Tan, M., An, Z.S., 2012. The climatic cyclicity in semiarid-arid central Asia over the past 500,000 years. Geophysical Research Letters 39 (1), L01705, doi:10.1029/2011GL050202.

Chinese Central Meteorological Office, 2010. Meteorological Data of China. Meteorology Press, Beijing.

CIESIN and CIAT, 2005. Gridded Population of the World, Version 3 (GPWv3): Population Density Grid for 2010. Socioeconomic Data and Applications Center (SEDAC), Columbia University, New York. Data retrieved from http://sedac.ciesin.columbia.edu/gpw (accessed 02/2014).

Clark, P.U., Dyke, A.S., Shakun, J.D., Carlson, A.E., Clark, J., Wohlfarth, B., Mitrovica, J.X., Hostetler, S.W., McCabe, A.M., 2009. The Last Glacial Maximum. Science 325, 710–714.

Clemens, S.C., Prell, W.L., 2007. The timing of orbital-scale Indian monsoon changes. Quaternary Science Reviews 26 (3–4), 275–278.

Clement, A.C., Peterson, L.C., 2008. Mechanisms of abrupt climate change of the last glacial period. Reviews of Geophysics 46 (4), RG4002, doi:10.1029/2006RG000204.

Clift, P.D., Plumb, R.A., 2008. The Asian Monsoon: causes, history and effects. Cambridge University Press, 270 pp.

Cook, E.R., Anchukaitis, K.J., Buckley, B.M., D'Arrigo, R.D., Jacoby, G.C., Wright, W.E., 2010. Asian monsoon failure and megadrought during the last millennium. Science 328, 486–489.

Cour, P., Zheng, Z., Duzer, D., Calleja, M., Yao, Z., 1999. Vegetational and climatic significance of modern pollen rain in northwestern Tibet. Review of Palaeobotany and Palynology 104 (3–4), 183–204.

Cui, X., Graf, H.-F., 2009. Recent land cover changes on the Tibetan Plateau: a review. Climatic Change 94 (1–2), 47–61.

Cullen, H.M., deMenocal, P.B., Hemming, S., Hemming, G., Brown, F.H., Guilderson, T., Sirocko, F., 2000. Climate change and the collapse of the Akkadian empire: evidence from the deep sea. Geology 28 (4), 379–382.

Dallmeyer, A., Claussen, M., Otto, J., 2010. Contribution of oceanic and vegetation feedbacks to Holocene climate change in monsoonal Asia. Climate of the Past 6 (2), 195–218.

Dando, W.A., 2005. Asia, Climates of Siberia, Central and East Asia. In: Oliver, J.E. (Ed.), Encyclopedia of World Climatology. Springer, Dordrecht, pp. 102–114.

Dansgaard, W., Johnsen, S.J., Clausen, H.B., Dahl-Jensen, D., Gundestrup, N.S., Hammer, C.U., Hvidberg, C.S., Steffensen, J.P., Sveinbjornsdottir, A.E., Jouzel, J., Bond, G., 1993. Evidence for general instability of past climate from a 250-kyr ice-core record. Nature 364, 218–220.

Danzeglocke, U., Jöris, O., Weninger, B., 2013. CalPal-2007online. http://www.calpal-online.de/.

DeFries, R.S., Hansen, M.C., Townshend, J.R.G., Janetos, A.C., Loveland, T.R., 2000a. 1 Kilometer Tree Cover Continuous Fields, 1.0. Department of Geography, University of Maryland, College Park, Maryland.

DeFries, R.S., Hansen, M.C., Townshend, J.R.G., Janetos, A.C., Loveland, T.R., 2000b. A new global 1-km dataset of percentage tree cover derived from remote sensing. Global Change Biology 6 (2), 247–254.

DeFries, R.S., Townshend, J.R.G., Hansen, M.C., 1999. Continuous fields of vegetation characteristics at the global scale at 1-km resolution. Journal of Geophysical Research: Atmospheres 104 (D14), 16911–16923, doi:10.1029/1999JD900057.

deMenocal, P., Ortiz, J., Guilderson, T., Adkins, J., Sarnthein, M., Baker, L., Yarusinsky, M., 2000. Abrupt onset and termination of the African Humid Period: rapid climate responses to gradual insolation forcing. Quaternary Science Reviews 19 (1–5), 347–361.

deMenocal, P.B., 2001. Cultural responses to climate change during the late Holocene. Science 292, 667–673.

Demske, D., Mischke, S., 2003. Palynological investigation of a Holocene profile section from the Palaeo-Gaxun-Nur-Basin. Chinese Science Bulletin 48 (14), 1418–1422.

Demske, D., Tarasov, P.E., Wünnemann, B., Riedel, F., 2009. Late glacial and Holocene vegetation, Indian monsoon and westerly circulation in the Trans-Himalaya recorded in the lacustrine pollen sequence from Tso Kar, Ladakh, NW India. Palaeogeography, Palaeoclimatology, Palaeoecology 279 (3–4), 172–185.

Denton, G.H., Alley, R.B., Comer, G.C., Broecker, W.S., 2005. The role of seasonality in abrupt climate change. Quaternary Science Reviews 24, 1159–1182.

Denton, G.H., Anderson, R.F., Toggweiler, J.R., Edwards, R.L., Schaefer, J.M., Putnam, A.E., 2010. The Last Glacial Termination. Science 328, 1652–1656.

Deplazes, G., Lückge, A., Stuut, J.-B.W., Pätzold, J., Kuhlmann, H., Husson, D., Fant, M., Haug, G.H., 2014. Weakening and strengthening of the Indian monsoon during Heinrich events and Dansgaard-Oeschger oscillations. Paleoceanography 29 (2), 2013PA002509, doi:10.1002/2013PA002509.

Dimbleby, G.W., 1985. The Palynology of Archaeological Sites. Academic Press, London, 176 pp.

Ding, Y.H., Chan, C.L., 2005. The East Asian summer monsoon: an overview. Meteorology and Atmospheric Physics 89 (1–4), 117–142.

Dollfus, P., 2012. Transformation processes in Nomadic pastoralism in Ladakh. Himalaya, the Journal of the Association for Nepal and Himalayan Studies 32 (1), 61–72.

Domitsu, H., Oda, M., 2008. Holocene influx of the Tsushima Current into the Japan Sea signalled by spatial and temporal changes in Neogloboquadrina incompta distribution. The Holocene 18 (2), 345–352.

Domrös, M., Peng, G., 1988. The Climate of China. Springer, Berlin.

Dvorský, M., Doležal, J., De Bello, F., Klimešová, J., Klimeš, L., 2011. Vegetation types of East Ladakh: species and growth form composition along main environmental gradients. Applied Vegetation Science 14 (1), 132–147.

Dykoski, C.A., Edwards, R.L., Cheng, H., Yuan, D., Cai, Y., Zhang, M., Lin, Y., Qing, J., An, Z., Revenaugh, J., 2005. A high-resolution, absolute-dated Holocene and deglacial Asian monsoon record from Dongge Cave, China. Earth and Planetary Science Letters 233 (1–2), 71–86.

Edwards, M.E., Anderson, P.M., Brubaker, L.B., Ager, T.A., Andreev, A.A., Bigelow, N.H., Cwynar, L.C., Eisner, W.R., Harrison, S.P., Hu, F.S., Jolly, D., Lozhkin, A.V., MacDonald, G.M., Mock, C.J., Ritchie, J.C., Sher, A.V., Spear, R.W., Williams, J.W., Yu, G., 2000. Pollen-based biomes for Beringia 18,000, 6000 and 0 ^{14}C yr BP. Journal of Biogeography 27 (3), 521–554.

El-Moslimany, A.P., 1990. Ecological significance of common nonarboreal pollen: examples from drylands of the Middle East. Review of Palaeobotany and Palynology 64 (1–4), 343–350.

ESRI, 2011. ArcGIS Desktop: Release 10. Environmental Systems Research Institute, Redlands, CA.

ESRI. 2012. ArcGIS Desktop: Release 10.1. Environmental Systems Research Institute, Redlands, CA.

Fægri, K., Iversen, J., 1989. Textbook of Pollen Analysis. John Wiley & Sons, Chichester.

Favre, E., Escarguel, G., Suc, J.-P., Vidal, G., Thévenod, L., 2008. A contribution to deciphering the meaning of AP/NAP with respect to vegetation cover. Review of Palaeobotany and Palynology 148 (1), 13–35.

Filippov, A., Riedel, F. 2009. The late Holocene mollusc fauna of the Aral Sea and its biogeographical and ecological interpretation. Limnologica 39, 67–85.

Firbas, F., 1937. Der pollenanalytische Nachweis des Getreidebaus. Zeitschrift für Botanik 31, 447–448.

Flad, R.K., Yuan, J., Li, S., 2007. Zooarcheological evidence for animal domestication in northwest China. In: Madsen, D.B., Chen, F.H., Gao, X. (Eds.), Developments in Quaternary Sciences. Elsevier, pp. 167–203.

Fleitmann, D., Burns, S.J., Mangini, A., Mudelsee, M., Kramers, J., Villa, I., Neff, U., Al-Subbary, A.A., Buettner, A., Hippler, D., Matter, A., 2007. Holocene ITCZ and Indian monsoon dynamics recorded in stalagmites from Oman and Yemen (Socotra). Quaternary Science Reviews 26 (1–2), 170–188.

Fleitmann, D., Burns, S.J., Mudelsee, M., Neff, U., Kramers, J., Mangini, A., Matter, A., 2003. Holocene forcing of the Indian monsoon recorded in a stalagmite from Southern Oman. Science 300, 1737–1739.

Fox, J.L., Nurbu, C., Bhatt, S., Chandola, A., 1994. Wildlife conservation and land-use changes in the Transhimalayan region of Ladakh, India. Mountain Research and Development 14 (1), 39–60.

Frenzel, B., 1994. Über Probleme der holozänen Vegetationsgeschichte Osttibets. Göttinger Geographische Abhandlungen 95, 143–166 (in German).

Fujiki, T., Zhou, Z., Yasuda, Y., 2005. The Pollen Flora of Yunnan, China, vol. I. Roli Books Pvt. Ltd., New Delhi.

Fuller, D.Q., 2006. Agricultural origins and frontiers in South Asia: a working synthesis. Journal of World Prehistory 20 (1), 1–86.

Fuller, D.Q., Madella, M., 2001. Issues in Harappan archaeobotany: retrospect and prospect. In: Settar, S., Korisettar, R. (Eds.), Indian Archaeology in Retrospect. Protohistory, Vol. II. Manohar Publishers, New Delhi, pp. 317–390.

Gadgil, S., 2003. The Indian monsoon and its variability. Annual Review of Earth and Planetary Sciences 31, 429–467.

Gagan, M.K., Hendy, E.J., Haberle, S.G., Hantoro, W.S., 2004. Post-glacial evolution of the Indo-Pacific Warm Pool and El Niño-Southern oscillation. Quaternary International 118–119, 127–143.

Gaillard, M.-J., Birks, H.J.B., Emanuelsson, U., Berglund, B.E., 1992. Modern pollen/landuse relationships as an aid in the reconstruction of past land-uses and cultural landscapes: an example from south Sweden. Vegetation History and Archaeobotany 1, 3–17.

Gaillard, M.-J., Birks, H.J.B., Emanuelson, U., Karlson, S., Lagerås, P., Olausson, D., 1994. Application of modern pollen/land-use relationships to the interpretation of pollen diagrams–reconstructions of land-use history in south Sweden, 3000–0 BP. Reviews of Palaeobotany and Palynology 82 (1–2), 47–73.

Ganjoo, R.K., and Ota, S.B., 2012. Mountain environment and early human adaptation in NW Himalaya, India: A case study from Siwalik Hill Range and Leh valley. Quaternary International 269, 31–37.

Gasse, F., 2000. Hydrological changes in the African tropics since the Last Glacial Maximum. Quaternary Science Reviews 19 (1–5), 189–211.

Gasse, F., Arnold, M., Fontes, J.C., Fort, M., Gibert, E., Huc, A., Li, B.Y., Li, Y.F., Lju, Q., Melieres, F., Van Campo, E., Wang, F.B., Zhang, Q.S., 1991. A 13,000-year climate record from Western Tibet. Nature 353, 742–745.

Gasse, F., Fontes, J.C., Van Campo, E., Wei, K.,1996. Holocene environmental changes in Bangong Co basin (Western Tibet). Part 4: discussion and conclusions. Palaeogeography, Palaeoclimatology, Palaeoecology 120 (1–2), 79–92.

Gaur, A.S., Vora, K.H., 1999. Ancient shorelines of Gujarat, India, during the Indus Civilization (Late Mid-Holocene): a study based on archaeological evidences. Current Science 77 (1), 180–185.

Gautam, P., Chandan, P., Chatterjee, A., Vidya, S., Areendran, G., Takpa, J., Saleem-ul-Haq, Bhatt, S., Chundawat, R.S., and Hussain, S.A., 2007. Management planning for Tsomoriri – Tsokar – a framework. Department of Wildlife Protection, Government of Jammu & Kashmir, Jammu, 120 pp.

Gauthier, E., Bichet, V., Massa, C., Petit, C., Vannière, B., Richard, H., 2010. Pollen and non-pollen palynomorph evidence of medieval farming activities in southwestern Greenland. Vegetation History and Archaeobotany 19 (5–6), 427–438.

Gavin, D.G., Oswald, W.W., Wahl, E.R., Williams, J.W., 2003. A statistical approach to evaluating distance metrics and analog assignments for pollen records. Quaternary Research 60 (3), 356–367.

Geograficheski Atlas SSSR. 1990. Glavnoe upravlenie geodezii i kartografii, Moskow (in Russian).

Giosan, L., Clift, P.D., Macklin, M.G., Fuller, D.Q., Constantinescu, S., Durcan, J.A., Stevens, T., Duller, G.A.T., Tabrez, A.R., Gangal, K., Adhikari, R., Alizai, A., Filip, F., Vanlaningham, S., Syvitski, J.P.M., 2012. Fluvial landscapes of the Harappan civilization. Proceedings of the National Academy of Sciences 109 (26), E1688–E1694.

Göktürk, O.M., Fleitmann, D., Badertscher, S., Cheng, H., Edwards, R.L., Leuenberger, M., Fankhauser, A., Tüysüz, O., Kramers, J., 2011. Climate on the southern Black Sea coast during the Holocene: implications from the Sofular Cave record. Quaternary Science Reviews 30 (19–20), 2433–2445.

Goldstein, M., and Beall, C. (1990). Nomads of Western Tibet: The Survival of a Way of Life. University of California Press, Berkeley, 200 pp.

Gong, D.-Y., Wang, S.-W., Zhu, J.-H., 2001. East Asian Winter Monsoon and Arctic Oscillation. Geophysical Research Letters 28 (10), 2073-2076, doi:10.1029/2000GL012311.

Gorbarenko, S.A., Artemova, A.V., Goldberg, E.L., Vasilenko, Y.P., 2014. The response of the Okhotsk Sea environment to the orbital-millennium global climate changes during the Last Glacial Maximum, deglaciation and Holocene. Global and Planetary Change 116, 76–90.

Gotanda, K., Nakagawa, T., Tarasov, P., Kitagawa, J., Inoue, Y., Yasuda, Y., 2002. Biome classification from Japanese pollen data: application to modern-day and Late Quaternary samples. Quaternary Science Reviews 21 (4–6), 647–657.

Gou, X., Chen, F., Jacoby, G., Cook, E., Yang, M., Peng, J., Zhang, Y., 2007. Rapid tree growth with respect to the last 400 years in response to climate warming, northeastern Tibetan Plateau. International Journal of Climatology 27 (11), 1497–1503.

Govil, P., Naidu, P.D., 2010. Evaporation-precipitation changes in the eastern Arabian Sea for the last 68 ka: Implications on monsoon variability. Paleoceanography 25 (1), PA1210, doi:10.1029/2008pa001687.

Grimm, E.C., 1987. CONISS: a Fortran 77 program for stratigraphically constrained cluster analysis by the method of incremental sum of squares. Computers & Geosciences 13 (1), 13–35.

Grimm, E.C.,1993. TILIA 2.0 Version b.4 (Computer Software). Illinois State Museum, Research and Collections Center, Springfield.

Grimm, E.C., 2004. TGView. Illinois State Museum, Research and Collections Center, Springfield.

Grosswald, M.G., Hughes, T.J., 2002. The Russian component of an Arctic Ice Sheet during the Last Glacial Maximum. Quaternary Science Reviews 21 (1–3), 121–146.

Guiot, J., 1990. Methodology of the last climatic cycle reconstruction in France from pollen data. Palaeogeography, Palaeoclimatology, Palaeoecology 80 (1), 49–69.

Guiot, J., Goeury, C., 1996. PPPBASE, a software for statistical analysis of paleoecological and paleoclimatological data. Dendrochronologia 14, 295–300.

Guiot, J., Hai, H.B., Jiang, W.Y., Luo, Y.L., 2008. East Asian Monsoon and paleoclimatic data analysis: a vegetation point of view. Climate of the Past 4, 137–145.

Gujja, B., Chatterjee, A., Gautam, P., and Chandan, P., 2003. Wetlands and lakes at the top of the World. Mountain Research and Development 23 (3), 219–221.

Gunin, P.D., Vostokova, E.A., Dorofeyuk, N.I., Tarasov, P.E., Black, C.C., 1999. Vegetation Dynamics of Mongolia. In: Geobotany, Vol. 26. Kluwer Academic Publishers, Dordrecht. 240 pp.

Gupta, A.K., Anderson, D.M., Overpeck, J.T., 2003. Abrupt changes in the Asian southwest monsoon during the Holocene and their links to the North Atlantic Ocean. Nature 421, 354–357.

Gupta, A.K., Das, M., Anderson, D.M., 2005. Solar influence on the Indian summer monsoon during the Holocene. Geophysical Research Letters 32 (17), L17703, doi:10.1029/2005GL022685.

Gupta, H.P., Sharma, C., 1986. Pollen Flora of North-West Himalaya. Indian Association of Palynostratigraphers, Lucknow.

Hartmann, H., 1983. Pflanzengesellschaften entlang der Kashmirroute in Ladakh. Jahrbuch des Vereins zum Schutz der Bergwelt 48, 131–173 (in German).

Hartmann, H., 1987. Pflanzengesellschaften trockener Standorte aus der subalpinen und alpinen Stufe im südlichen und östlichen Ladakh. Candollea 42, 277–326 (in English with German abstract).

Hartmann, H., 1990. Pflanzengesellschaften aus der alpinen Stufe des westlichen, südlichen und östlichen Ladakh mit besonderer Berücksichtigung der rasenbildenden Gesellschaften. Candollea 45, 525–574 (in English with German abstract).

Hartmann, H., 1995. Beitrag zur Kenntnis der subalpinen Wüsten-Vegetation im Einzugsgebiet des Indus von Ladakh (Indien). Candollea 50, 367–410 (in English with German abstract).

Hartmann, H., 1997. Zur Flora und Vegetation der Halbwüsten, Steppen und Rasengesellschaften im südöstlichen Ladakh (Indien). Jahrbuch des Vereins zum Schutz der Bergwelt 62, 129–188 (in German).

Hartmann, H., 1999. Studien zur Flora und Vegetation im östlichen Transhimalaya von Ladakh (Indien). Candollea 54, 171–230 (in German with English abstract).

Hassan, F.A., 1997. Nile floods and political disorder in early Egypt. In: Dalfes, H.N., Kukla, G., Weiss, H. (Eds.), Third Millennium B.C. Climate Change and Old World Collapse. NATO ASI Series I: Global Environmental Change, Vol. 49. Springer, Berlin, pp. 1–24.

Haug, G.H., Günther, D., Peterson, L.C., Sigman, D.M., Hughen, K.A., Aeschlimann, B., 2003. Climate and the Collapse of Maya Civilization. Science 299, 1731–1735.

Haug, G.H., Hughen, K.A., Sigman, D.M., Peterson, L.C., Röhl, U., 2001. Southward migration of the Intertropical Convergence Zone through the Holocene. Science 293, 1304–1308.

Hayakawa, Y., Koyama, M., 1998. Dates of two major eruptions from Towada and Baitoushan in the 10th century. Bulletin of the Volcanological Society of Japan 43, 403–407. (in Japanese)

He, J., Wen, M., Wang, L., Xu, H., 2006. Characteristics of the onset of the Asian summer monsoon and the importance of Asian-Australian "land bridge". Advances in Atmospheric Sciences 23 (6), 951–963.

He, Y., Theakstone, W.H., Zhonglin, Z., Dian, Z., Tandong, Y., Tuo, C., Yongping, S., Hongxi, P., 2004. Asynchronous Holocene climatic change across China. Quaternary Research 61 (1), 52–63.

Hedrick, K.A., Seong, Y.B., Owen, L.A., Caffee, M.W., Dietsch, C., 2011. Towards defining the transition in style and timing of Quaternary glaciation between the monsoon-influenced Greater Himalaya and the semi-arid Transhimalaya of Northern India. Quaternary International 236, 21–33.

Heinrich, H., 1988. Origin and consequences of cyclic ice rafting in the Northeast Atlantic Ocean during the past 130,000 years. Quaternary Research 29 (2), 142–152.

Helmens, K.F., 2014. The Last Interglacial–Glacial cycle (MIS 5–2) re-examined based on long proxy records from central and northern Europe. Quaternary Science Reviews 86, 115–143.

Hemming, S.R., 2004. Heinrich events: Massive Late Pleistocene detritus layers of the North Atlantic and their global climate imprint. Reviews of Geophysics 42 (1), RG1005, doi:10.1029/2003RG000128.

Herzschuh, U., 2006. Palaeo-moisture evolution in monsoonal Central Asia during the last 50,000 years. Quaternary Science Reviews 25 (1–2), 163–178.

Herzschuh, U., 2007. Reliability of pollen ratios for environmental reconstructions on the Tibetan Plateau. Journal of Biogeography 34 (7), 1265–1273.

Herzschuh, U., Birks, H.J.B., Liu, X., Kubatzki, C., Lohmann, G., 2009. What caused the mid-Holocene forest decline on the eastern Tibet-Qinghai Plateau? Global Ecology and Biogeography 19 (2), 278–286.

Herzschuh, U., Birks, H.J.B., Ni, J., Zhao, Y., Liu, H., Liu, X., Grosse, G., 2010. Holocene land-cover changes on the Tibetan Plateau. The Holocene 20 (1), 91–104.

Herzschuh, U., Kürschner, H., Mischke, S., 2006. Temperature variability and vertical vegetation belt shifts during the last ~50,000 yr in the Qilian Mountains (NE margin of the Tibetan Plateau, China). Quaternary Research 66 (1), 133–146.

Herzschuh, U., Tarasov, P., Wünnemann, B., Hartmann, K., 2004. Holocene vegetation and climate of the Alashan Plateau, NW China, reconstructed from pollen data. Palaeogeography, Palaeoclimatology, Palaeoecology 211 (1–2), 1–17.

Hodell, D.A., Brenner, M., Kanfoush, S.L., Curtis, J.H., Stoner, J.S., Xueliang, S., Yuan, W., Whitmore, T.J., 1999. Paleoclimate of southwestern China for the past 50,000 yr inferred from lake sediment records. Quaternary Research 52 (3), 369–380.

Holmes, J.A., Cook, E.R., Yang, B., 2009. Climate change over the past 2000 years in Western China. Quaternary International 194 (1–2), 91–107.

Hong, Y.T., Hong, B., Lin, Q.H., Shibata, Y., Hirota, M., Zhu, Y.X., Leng, X.T., Wang, Y., Wang, H., Yi, L., 2005. Inverse phase oscillations between the East Asian and Indian Ocean summer monsoons during the last 12 000 years and paleo-El Niño. Earth and Planetary Science Letters 231 (3–4), 337–346.

Hong, Y.T., Hong, B., Lin, Q.H., Zhu, Y.X., Shibata, Y., Hirota, M., Uchida, M., Leng, X.T., Jiang, H.B., Xu, H., Wang, H., Yi, L., 2003. Correlation between Indian Ocean summer monsoon and North Atlantic climate during the Holocene. Earth and Planetary Science Letters 211 (3–4), 371–380.

Hooghiemstra, H., 2012. Non-pollen palynomorphs: From unknown curiosities to informative fossils. Celebrating the scientific career of Bas van Geel. Review of Palaeobotany and Palynology 186 (0), 2–4.

Hou, J., D'Andrea, W.J., Liu, Z., 2012. The influence of ^{14}C reservoir age on interpretation of paleolimnological records from the Tibetan Plateau. Quaternary Science Reviews 48, 67–79.

Hu, C., Henderson, G.M., Huang, J., Xie, S., Sun, Y., Johnson, K.R., 2008. Quantification of Holocene Asian monsoon rainfall from spatially separated cave records. Earth and Planetary Science Letters 266 (3–4), 221–232.

Huang, E., Tian, J., Steinke, S., 2011. Millennial-scale dynamics of the winter cold tongue in the southern South China Sea over the past 26 ka and the East Asian winter monsoon. Quaternary Research 75 (1), 196–204.

Hughes, P.D., Gibbard, P.L., Ehlers, J., 2013. Timing of glaciation during the last glacial cycle: evaluating the concept of a global 'Last Glacial Maximum' (LGM). Earth-Science Reviews 125, 171–198.

Hutchinson, G.E., 1937. Limnological studies in Indian Tibet. Internationale Revue der gesamten Hydrobiologie und Hydrographie 35, 134–177.

Igarashi, Y., 1994. Quaternary forest and climate history of Hokkaido, Japan, from marine sediments. Quaternary Science Reviews 13 (4), 335–344.

Igarashi, Y., 1996. A lateglacial climatic reversion in Hokkaido, northeast Asia, inferred from the *Larix* pollen record. Quaternary Science Reviews 15 (10), 989–995.

Igarashi, Y., 2013. Holocene vegetation and climate on Hokkaido Island, northern Japan. Quaternary International 290–291, 139–150.

Igarashi, Y., Igarashi, T., Daimaru, H., Yamada, O., Miyagi, T., Matsushita, K., Hiramatsu, K., 1993. Vegetation history of Kenbuchi Basin and Furano Basin in Hokkaido, North Japan, since 32,000 yrs BP. The Quaternary Research 32, 89–105 (in Japanese with English abstract).

Igarashi, Y., Murayama, M., Igarashi, T., Higake, T., Fukuda, M., 2002. History of *Larix* forest in Hokkaido and Sakhalin, northeast Asia since the last glacial. Acta Palaeontologica Sinica 41 (4), 524–533.

Igarashi, Y., Sagayama, T., Higake, T., Fukuda, M., 2000. Late Quaternary environmental change in central and north Sakhalin, Russia. Journal of Geography 109 (2), 165–173 (in Japanese with English abstract).

Igarashi, Y., Zharov, A.E., 2011. Climate and vegetation change during the late Pleistocene and early Holocene in Sakhalin and Hokkaido, northeast Asia. Quaternary International 237, 24–31.

IPCC, 2001. Climate change 2001: The scientific basis. Cambridge University Press, Cambridge, pp. 881.

IPCC, 2007. Climate change 2007: The physical science basis. Cambridge University Press, Cambridge, pp. 996.

IPCC, 2013. Climate change 2013: The physical science basis. Cambridge University Press, Cambridge, pp. 1535.

Itaki, T., Ikehara, K., Motoyama, I., Hasegawa, S., 2004. Abrupt ventilation changes in the Japan Sea over the last 30 ky: evidence from deep-dwelling radiolarians. Palaeogeography, Palaeoclimatology, Palaeoecology 208 (3–4), 263–278.

Itoh, S.,1987. Hokkaido No Shokusei (Vegetation of Hokkaido). Hokkaido University Press, Sapporo (in Japanese).

Ivanochko, T.S., Ganeshram, R.S., Brummer, G.-J.A., Ganssen, G., Jung, S.J.A., Moreton, S.G., Kroon, D., 2005. Variations in tropical convection as an amplifier of global climate change at the millennial scale. Earth and Planetary Science Letters 235 (1–2), 302–314. Jarvis, A., Reuter, H.I., Nelson, A., Guevara, E., 2008. Hole-filled Seamless SRTM Data V4. International Centre for Tropical Agriculture (CIAT).

Ivanov, A., 2002. The Far East. In: Shahgedanova, M. (Ed.), The physical geography of Northern Eurasia. Oxford University Press, Oxford, pp. 422–447.

Iversen, J., 1949. The influence of prehistoric man on vegetation. Danmarks geologiske Undersgelse, Series IV 3 (6), 1–25.

Kala, C.P., Mathur, V.B., 2002. Patterns of plant species distribution in the Trans-Himalayan region of Ladakh, India. Journal of Vegetation Science 13 (6), 751–754.

Jackson, S.T., Webb, R.S., Anderson, K.H., Overpeck, J.T., Webb III, T., Williams, J.W., Hansen, B.C.S., 2000. Vegetation and environment in eastern North America during the Last Glacial Maximum. Quaternary Science Reviews 19 (6), 489–508.

Jackson, S.T., Williams, J.W., 2004. Modern analogs in Quaternary paleoecology: here today, gone yesterday, gone tomorrow? Annual Review of Earth and Planetary Sciences 32, 495–537.

Jankovská, V., Komárek, J., 1995. Pediastrum orientale from subfossil layers. Folia Geobotanica et Phytotaxonomica 30, 319–329.

Jankovská, V., Komárek, J., 2000. Indicative value of *Pediastrum* and other coccal green algae in palaeoecology. Folia Geobotanica 35, 59–82.

Jarvis, A., Reuter, H.I., Nelson, A., Guevara, E., 2008. Hole-filled Seamless SRTM Data V4. International Centre for Tropical Agriculture (CIAT).

Jiang, W., Guo, Z., Sun, X., Wu, H., Chu, G., Yuan, B., Hatté, C., Guiot, J., 2006. Reconstruction of climate and vegetation changes of Lake Bayanchagan (Inner Mongolia): Holocene variability of the East Asian monsoon. Quaternary Research 65 (3), 411–420.

Jin, L., Chen, F., Ganopolski, A., Claussen, M., 2007. Response of East Asian climate to Dansgaard/Oeschger and Heinrich events in a coupled model of intermediate complexity. Journal of Geophysical Research 112 (D6), D06117, doi:10.1029/2006JD007316.

Jin, L., Schneider, B., Park, W., Latif, M., Khon, V., Zhang, X., 2014. The spatial–temporal patterns of Asian summer monsoon precipitation in response to Holocene insolation change: a model-data synthesis. Quaternary Science Reviews 85, 47–62.

Jouzel, J., Masson-Delmotte, V., Cattani, O., Dreyfus, G., Falourd, S., Hoffmann, G., Minster, B., Nouet, J., Barnola, J.M., Chappellaz, J., Fischer, H., Gallet, J.C., Johnsen, S., Leuenberger, M., Loulergue, L., Luethi, D., Oerter, H., Parrenin, F., Raisbeck, G., Raynaud, D., Schilt, A., Schwander, J., Selmo, E., Souchez, R., Spahni, R., Stauffer, B., Steffensen, J.P., Stenni, B., Stocker, T.F., Tison, J.L., Werner, M., Wolff, E.W., 2007. Orbital and millennial Antarctic climate variability over the past 800000 years. Science 317, 793–796.

Ju, L., Wang, H., Jiang, D., 2007. Simulation of the Last Glacial Maximum climate over East Asia with a regional climate model nested in a general circulation model. Palaeogeography, Palaeoclimatology, Palaeoecology 248 (3–4), 376–390.

Juggins, S., 2007. C2 Version 1.5 User guide. Software for ecological and palaeoecological data analysis and visualisation. Newcastle University, Newcastle upon Tyne, UK.

Kaiser, K., Miehe, G., Barthelmes, A., Ehrmann, O., Scharf, A., Schult, M., Schlütz, F., Adamczyk, S., Frenzel, B., 2008. Turf-bearing topsoils on the central Tibetan Plateau, China: Pedology, botany, geochronology. CATENA 73 (3), 300–311.

Kalnay, E., Kanamitsu, M., Kistler, R., Collins, W., Deaven, D., Gandin, L., Iredell, M., Saha, S., White, G., Woollen, J., Zhu, Y., Leetmaa, A., Reynolds, R., Chelliah, M., Ebisuzaki, W., Higgins, W., Janowiak, J., Mo, K.C., Ropelewski, C., Wang, J., Jenne, R., Joseph, D., 1996. The NCEP/NCAR 40-Year Reanalysis Project. Bulletin of the American Meteorological Society 77 (3), 437–471.

Kaplan, J.O., 2001. Geophysical applications of vegetation modeling, Ph.D. thesis, Department of Ecology. Lund University, Lund, 132 pp.

Kaplan, J.O., Bigelow, N.H., Prentice, I.C., Harrison, S.P., Bartlein, P.J., Christensen, T.R., Cramer, W., Matveyeva, N.V., McGuire, A.D., Murray, D.F., Razzhivin, V.Y., Smith, B., Walker, D.A., Anderson, P.M., Andreev, A.A., Brubaker, L.B., Edwards, M.E., Lozhkin, A.V., 2003. Climate change and Arctic ecosystems: 2. Modeling, paleodata-model comparisons, and future projections. Journal of Geophysical Research: Atmospheres 108 (D19), 8171, doi:10.1029/2002jd002559.

Katsui, Y., Yokoyama, I., Fujita, T., Ehara, Y., 1975. Komagatake, Its volcanic geology, history of eruption, present state of activity and prevention of disaster. Committee for Prevention of Disasters of Hokkaido, Sapporo (in Japanese).

Kenoyer, J.M., 2010. Measuring the Harappan world: insights into the Indus order and cosmology. In: Morley, I., Renfrew, C. (Eds.), The Archaeology of Measurement: Comprehending Heaven, Earth and Time in Ancient Societies. Cambridge University Press, New York, pp. 106–121.

Khuroo, A.A., Weber, E., Malik, A.H., Reshi, Z.A., Dar, G.H., 2011. Altitudinal distribution patterns of the native and alien woody flora in Kashmir Himalaya, India. Environmental Research 111, 967–977.

Kito, N., Takimoto, F., 1999. Population growth and migration rate of *Fagus crenata* during the Holocene in southwestern Hokkaido, Japan. The Quaternary Research 38 (4), 297–311 (in Japanese with English abstract).

Klein, J.A., Harte, J., Zhao, X.-Q., 2007. Experimental warming, not grazing, decreased rangeland quality on the Tibetan Plateau. Ecological Applications 17 (2), 541–557.

Kleinen, T., Hildebrandt, S., Prange, M., Rachmayani, R., Müller, S., Bezrukova, E., Brovkin, V., Tarasov, P.E., 2014. The climate and vegetation of Marine Isotope Stage 11 – Model results and proxy-based reconstructions at global and regional scale. Quaternary International, doi:10.1016/j.quaint.2013.12.028.

Kleinen, T., Tarasov, P.E., Brovkin, V., Andreev, A.A., Stebich, M., 2011. Comparison of modeled and reconstructed changes in forest cover through the past 8000 years: Eurasian perspective. The Holocene 21 (5), 723–734.

Klimeš, L., 2003. Life-forms and clonality of vascular plants along an altitudinal gradient in E Ladakh (NW Himalayas). Basic and Applied Ecology 4 (4), 317–328.

Klimeš, L., Dickoré, B., 2005. A contribution to the vascular plant flora of Lower Ladakh (Jammu & Kashmir, India). Willdenowia 35, 125–153.

Koizumi, I., 2008. Diatom-derived SSTs (*Td'* ratio) indicate warm seas off Japan during the middle Holocene (8.2–3.3 kyr BP). Marine Micropaleontology 69, 263–281.

Kołaczek, P., Karpińska-Kołaczek, M., Worobiec, E., Heise, W., 2012. *Debarya glypto-sperma* (De Bary) Wittrock 1872 (Zygnemataceae, Chlorophyta) as a possible air-borne alga – a contribution to its palaeoecological interpretation. Acta Palaeobotanica 52 (1), 139–146.

Kossler, A., Tarasov, P., Schlolaut, G., Nakagawa, T., Marshall, M., Brauer, A., Staff, R., Ramsey, C.B., Bryant, C., Lamb, H., Demske, D., Gotanda, K., Haraguchi, T., Yoko-yama, Y., Yonenobu, H., Tada, R., 2011. Onset and termination of the late-glacial climate reversal in the high-resolution diatom and sedimentary records from the annually laminated SG06 core from Lake Suigetsu, Japan. Palaeogeography, Palaeo-climatology, Palaeoecology 306 (3–4), 103–115.

Kramer, A., Herzschuh, U., Mischke, S., Zhang, C., 2010. Late Quaternary environmental history of the south-eastern Tibetan Plateau inferred from the Lake Naleng non-pollen palynomorph record. Vegetation History and Archaeobotany 19 (5–6), 453–468.

Krestov, P., 2003. Forest vegetation of easternmost Russia (Russian Far East). In: Kolbek, J., Šrůtek, M., Box, E.O. (Eds.), Forest Vegetation of Northeast Asia. Springer, pp. 93–180.

Kuhry, P., 1997. The palaeoecology of a treed bog in western boreal Canada: a study based on microfossils, macrofossils and physico-chemical properties. Reviews of Pa-laeobotany and Palynology 96, 183–224.

Kummerow, C., Barnes, W., Kozu, T., Shiue, J., Simpson, J., 1998. The Tropical Rainfall Measuring Mission (TRMM) Sensor Package. Journal of Atmospheric and Oceanic Technology 15 (3), 809–817.

Kuroyanagi, A., Kawahata, H., Narita, H., Ohkushi, K.i., Aramaki, T., 2006. Reconstruction of paleoenvironmental changes based on the planktonic foraminiferal assemblages off Shimokita (Japan) in the northwestern North Pacific. Global and Planetary Change 53 (1–2), 92–107.

Kuzmin, Y.V., Glascock, M.D., 2007. Two Islands in the Ocean: Prehistoric Obsidian Exchange between Sakhalin and Hokkaido, Northeast Asia. The Journal of Island and Coastal Archaeology 2 (1), 99–120.

Kuzmin, Y.V., Rakov, V.A., 2011. Environment and prehistoric humans in the Russian Far East and neighbouring East Asia: Main patterns of interaction. Quaternary International 237 (1–2), 103–108.

Kuzmin, Y.V., Vasilevski, A.A., Gorbunov, S.V., Burr, G.S., Jull, A.J.T., Orlova, L.A., Shubina, O.A., 2004. Chronology of prehistoric cultural complexes of Sakhalin Island (Russian Far East). Radiocarbon 46 (1), 353–362.

Lami, A., Turner, S., Musazzi, S., Gerli, S., Guilizzoni, P., Rose, N.L., Yang, H., Wu, G., Yang, R., 2010. Sedimentary evidence for recent increases in production in Tibetan plateau lakes. Hydrobiologia 648 (1), 175–187.

Lang, T.J., Barros, A.P., 2004. Winter storms in the central Himalayas. Journal of the Meteorological Society of Japan 82 (3), 829–844.

Laskar, J., Robutel, P., Joutel, F., Gastineau, M., Correia, A.C.M., Levrard, B., 2004. A long-term numerical solution for the insolation quantities of the Earth. Astronomy and Astrophysics 428 (1), 261–285.

Le Masson, V., Nair, K., 2012. Does climate modelling help when studying adaptation to environmental changes? The case of Ladakh, India. In: Lamadrid, A., Kelman, I. (Eds.), Climate Change Modeling For Local Adaptation In The Hindu Kush-Himalayan Region. Emerald Group Publishing Limited, Bingley, pp. 1–16.

Lee, C.Y., Liew, P.M., Lee, T.Q., 2010. Pollen records from southern Taiwan: implications for East Asian summer monsoon variation during the Holocene. The Holocene 20 (1), 81–89.

Leipe, C., Demske, D., Tarasov, P.E., 2014. A Holocene pollen record from the northwestern Himalayan lake Tso Moriri: Implications for palaeoclimatic and archaeological research. Quaternary International 348, 93–112.

Leipe, C., Kito, N., Sakaguchi, Y., Tarasov, P.E., 2013. Vegetation and climate history of northern Japan inferred from the 5500-year pollen record from the Oshima Peninsula, SW Hokkaido. Quaternary International 290–291, 151–163.

Lesher, R.S., 2011. Climate change impacts to a high altitude lake in the Indian Himalaya. MSc thesis, Department of Geography, San Diego State University, xii + 73 pp. at http://hdl.handle.net/10211.10/1283 (accessed 10/2013).

Li, X., Zhao, K., Dodson, J., Zhou, X., 2011. Moisture dynamics in central Asia for the last 15 kyr: new evidence from Yili Valley, Xinjiang, NW China. Quaternary Science Reviews 30 (23–24), 3457–3466.

Li, Y., Wang, N.a., Zhou, X., Zhang, C., Wang, Y., 2014. Synchronous or asynchronous Holocene Indian and East Asian summer monsoon evolution: A synthesis on Holocene Asian summer monsoon simulations, records and modern monsoon indices. Global and Planetary Change 116, 30–40.

Li, Y., Xu, Q., Liu, J., Yang, X., Nakagawa, T., 2007. A transfer-function model developed from an extensive surface-pollen data set in northern China and its potential for palaeoclimate reconstructions. The Holocene 17 (7), 897–905.

Lister, G.S., Kelts, K., Zao, C.K., Yu, J.-Q., Niessen, F., 1991. Lake Qinghai, China: closed-basin like levels and the oxygen isotope record for ostracoda since the latest Pleistocene. Palaeogeography, Palaeoclimatology, Palaeoecology 84 (1–4), 141–162.

Litt, T., Schölzel, C., Kühl, N., Brauer, A., 2009. Vegetation and climate history in the Westeifel Volcanic Field (Germany) during the past 11 000 years based on annually laminated lacustrine maar sediments. Boreas 38 (4), 679–690.

Liu, X., Herzschuh, U., Shen, J., Jiang, Q., Xiao, X., 2008. Holocene environmental and climatic changes inferred from Wulungu Lake in northern Xinjiang, China. Quaternary Research 70 (3), 412–425.

Lutaenko, K.A., Zhushchikhovskaya, I.S., Mikishin, Y.A., Popov, A.N., 2007. Mid-holocene climatic changes and cultural dynamics in the basin of the sea of japan and adjacent areas. In: Anderson, D.G., Maasch, K.A., Sandweis, D.H., (Eds.), Climate Change and Cultural Dynamics: A Global Perspective on Mid-Holocene Transitions. Elsevier, Amsterdam, pp. 331–406.

MacDonald, G., 2011. Potential influence of the Pacific Ocean on the Indian summer monsoon and Harappan decline. Quaternary International 229, 140–148.

Madella, M., Fuller, D.Q., 2006. Palaeoecology and the Harappan Civilisation of South Asia: a reconsideration. Quaternary Science Reviews 25, 1283–1301.

Maher, B.A., Hu, M., 2006. A high-resolution record of Holocene rainfall variations from the western Chinese Loess Plateau: antiphase behaviour of the African/Indian and East Asian summer monsoons. The Holocene 16 (3), 309–319.

Maher Jr, L.J., 1981. Statistics for microfossil concentration measurements employing samples spiked with marker grains. Review of Palaeobotany and Palynology 32 (2–3), 153–191.

MARGO Project Members, 2009. Constraints on the magnitude and patterns of ocean cooling at the Last Glacial Maximum. Nature Geosciences 2, 127–132.

Martinson, D.G., Pisias, N.G., Hays, J.D., Imbrie, J., Moore Jr, T.C., Shackleton, N.J., 1987. Age dating and the orbital theory of the ice ages: Development of a high-resolution 0 to 300,000-year chronostratigraphy. Quaternary Research 27 (1), 1–29.

Martyn, D., 1992. Developments in Atmospheric Science 18 – Climates of the World. Elsevier, Amsterdam.

Marzin, C., Braconnot, P., 2009. Variations of Indian and African monsoons induced by insolation changes at 6 and 9.5 kyr BP. Climate Dynamics 33 (2–3), 215–231.

Marzin, C., Kallel, N., Kageyama, M., Duplessy, J.C., Braconnot, P., 2013. Glacial fluctuations of the Indian monsoon and their relationship with North Atlantic climate: new data and modelling experiments. Climate of the Past 9 (5), 2135–2151.

Mayewski, P.A., Meeker, L.D., Twickler, M.S., Whitlow, S., Yang, Q., Lyons, W.B., Prentice, M., 1997. Major features and forcing of high-latitude northern hemisphere atmospheric circulation using a 110,000-year-long glaciochemical series. Journal of Geophysical Research: Oceans 102 (C12), 26345–26366, doi:10.1029/96JC03365.

Mayewski, P.A., Rohling, E.E., Curt Stager, J., Karlén, W., Maasch, K.A., David Meeker, L., Meyerson, E.A., Gasse, F., van Kreveld, S., Holmgren, K., Lee-Thorp, J., Rosqvist, G., Rack, F., Staubwasser, M., Schneider, R.R., Steig, E.J., 2004. Holocene climate variability. Quaternary Research 62 (3), 243–255.

Melles, M., Brigham-Grette, J., Minyuk, P.S., Nowaczyk, N.R., Wennrich, V., DeConto, R.M., Anderson, P.M., Andreev, A.A., Coletti, A., Cook, T.L., Haltia-Hovi, E., Kukkonen, M., Lozhkin, A.V., Rosén, P., Tarasov, P., Vogel, H., Wagner, B., 2012. 2.8 Million Years of Arctic Climate Change from Lake El'gygytgyn, NE Russia. Science 337, 315–320.

Miehe, G., Miehe, S., Kaiser, K., Jianquan, L., Zhao, X., 2008. Status and Dynamics of the Kobresia pygmaea Ecosystem on the Tibetan Plateau. AMBIO: A Journal of the Human Environment 37 (4), 272–279.

Miehe, G., Miehe, S., Kaiser, K., Reudenbach, C., Behrendes, L., Duo, L., and Schlütz, F., 2009a. How old is pastoralism in Tibet? An ecological approach to the making of a Tibetan landscape. Palaeogeography, Palaeoclimatology, Palaeoecology 276, 130–147.

Miehe, G., Miehe, S., Schlütz, F., 2002. Vegetation and Pollen Records from the Muktinath Valley (Tibetan Himalaya, Nepal): A Contribution to the Environmental History of the Old World's Mountain Semi-Deserts. Erdkunde 56 (3), 268–285 (in German with English abstract).

Miehe, G., Miehe, S., Schlütz, F., 2009b. Early human impact in the forest ecotone of southern High Asia (Hindukush, Himalaya). Quaternary Research 71, 255–265.

Miehe, G., Miehe, S., Schlütz, F., Kaiser, K., Duo, L., 2006. Palaeoecological and experimental evidence of former forests and woodlands in the treeless desert pastures of Southern Tibet (Lhasa, A.R. Xizang, China). Palaeogeography, Palaeoclimatology, Palaeoecology 242 (1–2), 54–67.

Miehe, G., Winiger, M., Böhner, J., Yili, Z., 2001. The climatic diagram map of High Asia: purpose and concepts. Erdkunde 55 (1), 94–97.

Mishra, P.K., Anoop, A., Menzel, P., Gaye, B., Basavaiah, N., Jehangir, A., Prasad, S., 2013. Holocene climatic variability in the Indian Monsoon domain. Geophysical Research Abstracts 15, EGU2013-2071.

Mix, A.C., Bard, E., Schneider, R., 2001. Environmental processes of the ice age: land, oceans, glaciers (EPILOG). Quaternary Science Reviews 20 (4), 627–657.

Mokhova, L., Tarasov, P., Bazarova, V., Klimin, M., 2009. Quantitative biome reconstruction using modern and late Quaternary pollen data from the southern part of the Russian Far East. Quaternary Science Reviews 28 (25–26), 2913–2926.

Montoya, E., Rull, V., van Geel, B., 2010. Non-pollen palynomorphs from surface sediments along an altitudinal transect of the Venezuelan Andes. Palaeogeography, Palaeoclimatology, Palaeoecology 297 (1), 169–183.

Moore, P.D., Webb, J.A., Collinson, M.E., 1991. Pollen Analysis. Blackwell Science, Oxford.

Morrill, C., Overpeck, J.T., Cole, J.E., 2003. A synthesis of abrupt changes in the Asian summer monsoon since the last deglaciation. The Holocene 13 (4), 465–476.

Morrill, C., Overpeck, J.T., Cole, J.E., Liu, K.-b., Shen, C., Tang, L., 2006. Holocene variations in the Asian monsoon inferred from the geochemistry of lake sediments in central Tibet. Quaternary Research 65 (2), 232–243.

Moy, C.M., Seltzer, G.O., Rodbell, D.T., Anderson, D.M., 2002. Variability of El Niño/Southern Oscillation activity at millennial timescales during the Holocene epoch. Nature 420, 162–165.

Müller, M.J., Baltes, K., Werle, D., 1996. Handbuch ausgewählter Klimastationen der Erde. Gerold Richter, Trier (in German).

Müller, S., Tarasov, P.E., Andreev, A.A., Tütken, T., Gartz, S., Diekmann, B., 2010. Late Quaternary vegetation and environments in the Verkhoyansk Mountains region (NE Asia) reconstructed from a 50-kyr fossil pollen record from Lake Billyakh. Quaternary Science Reviews 29 (17–18), 2071–2086.

Murti, S.K., 2001. Flora of Cold Deserts of Western Himalaya: Volume I (Monocotyledons). Botanical Survey of India, Calcutta.

Nakagawa, T., 2007. Double-L channel: an amazingly non-destructive method of continuous sub-sampling from sediment cores. Quaternary International 167–168 (Supplement), 298.

Nakagawa, T., Gotanda, K., Haraguchi, T., Danhara, T., Yonenobu, H., Brauer, A., Yokoyama, Y., Tada, R., Takemura, K., Staff, R.A., Payne, R., Bronk Ramsey, C., Bryant, C., Brock, F., Schlolaut, G., Marshall, M., Tarasov, P., Lamb, H., Suigetsu 2006 Project Members, 2012. SG06, a fully continuous and varved sediment core from Lake Suigetsu, Japan: stratigraphy and potential for improving the radiocarbon calibration model and understanding of late Quaternary climate changes. Quaternary Science Reviews 36, 164–176.

Nakagawa, T., Kitagawa, H., Yasuda, Y., Tarasov, P.E., Gotanda, K., Sawai, Y., 2005. Pollen/event stratigraphy of the varved sediment of Lake Suigetsu, central Japan from 15,701 to 10,217 SG yr BP (Suigetsu varve years before present): description,

interpretation, and correlation with other regions. Quaternary Science Reviews 24 (14–15), 1691–1701.

Nakagawa, T., Kitagawa, H., Yasuda, Y., Tarasov, P.E., Nishida, K., Gotanda, K., Sawai, Y., Yangtze River Civilization Program Members, 2003. Asynchronous climate changes in the North Atlantic and Japan during the last termination. Science 299, 688–691.

Nakagawa, T., Okuda, M., Yonenobu, H., Miyoshi, N., Fujiki, T., Gotanda, K., Tarasov, P.E., Morita, Y., Takemura, K., Horie, S., 2008. Regulation of the monsoon climate by two different orbital rhythms and forcing mechanisms. Geology 36 (6), 491–494.

Nakagawa, T., Tarasov, P.E., Kitagawa, H., Yasuda, Y., Gotanda, K., 2006. Seasonally specific responses of the East Asian monsoon to deglacial climate changes. Geology 34 (7), 521–524.

Nakagawa, T., Tarasov, P.E., Nishida, K., Gotanda, K., Yasuda, Y., 2002. Quantitative pollen-based climate reconstruction in central Japan: application to surface and Late Quaternary spectra. Quaternary Science Reviews 21 (18–19), 2099–2113.

Nakamura, J., 1968. Palynological Aspects of the Quaternary in Hokkaido, Vol. 17. Research Reports of the Kochi University, pp. 39–51 (in Japanese with English abstract).

Nakamura, Y., Krestov, P.V., 2005. Coniferous forests of the temperate zone of Asia. In: Andersson, F.A. (Ed.), Ecosystems of the World Vol. 6: Coniferous forests. Elsevier, Amsterdam, pp. 163–220.

Nakazawa, Y., Iwase, A., Akai, F., Izuho, M., 2011. Human responses to the Younger Dryas in Japan. Quaternary International 242 (2), 416–433.

Namgail, T., 2009. Mountain ungulates of the Trans-Himalayan region of Ladakh, India. International Journal of Wilderness 15, 35–40.

Namgail, T., Bhatnagar, Y., Mishra, C., Bagchi, S., 2007. Pastoral Nomads of the Indian Changthang: Production System, Landuse and Socioeconomic Changes. Human Ecology 35 (4), 497–504.

Namgail, T., Rawat, G.S., Mishra, C., van Wieren, S.E., Prins, H.H.T., 2012. Biomass and diversity of dry alpine plant communities along altitudinal gradients in the Himalayas. Journal of Plant Research 125, 93–101.

NASA Land Processes Distributed Active Archive Center, 2011. ASTER GDEM Version 2 - 1 arc-second (30 m). U.S. Geological Survey, Sioux Falls, USA.

NASA Landsat Program, 2009. Landsat 7 ETM+ scene L71146037_03720060923_B20, USGS, Sioux Falls, USA (image capture date: 09/23/2006).

Negi, S.S., 2002. Cold Deserts of India, 2nd edition. Indus Publishing Company, New Delhi.

New, M., Lister, D., Hulme, M., Makin, I., 2002. A high-resolution data set of surface climate over global land areas. Climate Research 21 (1), 1–25.

Nissen, H.-J., 1988. The Early History of the Ancient Near East: 9000–2000 B.C. University of Chicago Press, Chicago.

Oba, T., Kato, M., Kitazato, H., Koizumi, I., Omura, A., Sakai, T., Takayama, T., 1991. Paleoenvironmental changes in the Japan Sea during the last 85,000 years. Paleoceanography 6, 499–518, doi:10.1029/91PA00560.

Oba, T., Murayama, M., Matsumoto, E., Nakamura, T., 1995. AMS-^{14}C ages of Japan Sea cores from the Oki Ridge. The Quaternary Research 34, 289–296 (in Japanese with English abstract).

Ohnishi, O., 1998. Search for the wild ancestor of buckwheat – I. Description of new *Fagopyrum* (Polygonaceae) species and their distribution in China and the Himalayan hills. Fagopyrum 15, 18–28.

Okazaki, Y., Takahashi, K., Katsuki, K., Ono, A., Hori, J., Sakamoto, T., Uchida, M., Shibata, Y., Ikehara, M., Aoki, K., 2005. Late Quaternary paleoceanographic changes in the southwestern Okhotsk Sea: Evidence from geochemical, radiolarian, and diatom records. Deep Sea Research Part II: Topical Studies in Oceanography 52 (16–18), 2332–2350.

Ota, S.B., 1993. Evidences of transhumance from Ladakh Himalayas, Jammu & Kashmir, India. In: Ganjoo, R.K., Ota, S.B. (Eds.), Current Advances in Indian Archaeology, Vol. 1. Dattsons, Nagpur, pp. 79–95.

Otto-Bliesner, B., Schneider, R., Brady, E.C., Kucera, M., Abe-Ouchi, A., Bard, E., Braconnot, P., Crucifix, M., Hewitt, C.D., Kageyama, M., Marti, O., Paul, A., Rosell-Melé, A., Waelbroeck, C., Weber, S.L., Weinelt, M., Yu, Y., 2009. A comparison of PMIP2 model simulations and the MARGO proxy reconstruction for tropical sea surface temperatures at last glacial maximum. Climate Dynamics 32 (6), 799–815.

Overpeck, J., Anderson, D., Trumbore, S., Prell, W., 1996. The southwest Indian Monsoon over the last 18 000 years. Climate Dynamics 12 (3), 213–225.

Overpeck, J.T., Cole, J.E., 2007. Climate change: Lessons from a distant monsoon. Nature 445, 270–271.

Overpeck, J.T., Webb, T., Prentice, I.C., 1985. Quantitative interpretation of fossil pollen spectra: dissimilarity coefficients and the method of modern analogs. Quaternary Research 23 (1), 87–108.

Pals, J.P., Van Geel, B., Delfos, A., 1980. Paleoecological studies in the Klokkeweel bog near hoogkarspel (prov. of Noord-Holland). Review of Palaeobotany and Palynology 30, 371–418.

Panigrahy, S., Patel, JG, Parihar, J.S., 2012. National Wetland Atlas: High Altitude Lakes of India. Space Applications Centre, ISRO, Ahmedabad, India.

Peel, M.C., Finlayson, B.L., McMahon, T.A., 2007. Updated world map of the Köppen-Geiger climate classification. Hydrology and Earth System Sciences 11, 1633–1644.

Peltier, W.R., Fairbanks, R.G., 2006. Global glacial ice volume and Last Glacial Maximum duration from an extended Barbados sea level record. Quaternary Science Reviews 25 (23–24), 3322–3337.

Peng, Y., Xiao, J., Nakamura, T., Liu, B., Inouchi, Y., 2005. Holocene East Asian monsoonal precipitation pattern revealed by grain-size distribution of core sediments of Daihai Lake in Inner Mongolia of north-central China. Earth and Planetary Science Letters 233 (3–4), 467–479.

Petrov, Ye.S., Novorotskiy, P.V., Lenshin, V.T., 2000. Klimat Khabarovskogo kraya i Yevreiskoy Avtonomnoy Oblasti. Dak'nauka, Vladivostok-Khabarovsk. (in Russian).

Peyron, O., Jolly, D., Bonnefille, R., Vincens, A., Guiot, J., 2000. Climate of east Africa 6000 ^{14}C yr BP as inferred from pollen data. Quaternary Research 54 (1), 90–101.

Pfister, O., 2004. Birds and mammals of Ladakh. Oxford University Press, New Delhi, 361 pp.

Philip, G., Mathew, J., 2005. Climato-tectonic impression on Trans Himalayan lakes: a case study of Kyun Tso basin of the Indus Suture Zone in NW Himalaya using remote sensing techniques. Current Science 89 (11), 1941–1947.

Philip, G., Mazari, R.K., 2000. Shrinking lake basins in the proximity of the Indus Suture Zone of northwestern Himalaya: a case study of Tso Kar and StartsapukTso, using 1RS-1C data. International Journal of Remote Sensing 21 (16), 2973–2984.

Pointet, A., 2008. Ladakh & Zanskar Trekking Map e South. Olizane, Geneva. Ponton, C., Giosan, L., Eglinton, T.I., Fuller, D.Q., Johnson, J.E., Kumar, P., Collett, T.S., 2012. Holocene aridification of India. Geophysical Research Letters 39, L03704, doi:10.1029/2011GL050722.

Polunin, O., Stainton, A., 1984. Flowers of the Himalaya. Oxford University Press, Oxford, 580 pp.

Porter, S.C., An, Z., 1995. Correlation between climate events in the North Atlantic and China during the last glaciation. Nature 375, 305–308.

Possehl, G.L., 1997. The transformation of the Indus Civilization. Journal of World Prehistory 11 (4), 425–472.

Possehl, G.L., 2002. The Indus Civilization: a Contemporary Perspective. AltaMira Press, Lanham.

Possehl, G.L., 2004. Mehrgarh. In: Fagan, B. (Ed.), Oxford Companion to Archaeology. Oxford University Press, Oxford (online version accessed 10/2013).

Prasad, S., Enzel, Y., 2006. Holocene paleoclimates of India. Quaternary Research 66 (3), 442–453.

Prentice, I.C., 1980. Multidimensional scaling as a research tool in Quaternary palynology: A review of theory and methods. Review of Palaeobotany and Palynology 31, 71–104.

Prentice, I.C., Cramer, W., Harrison, S.P., Leemans, R., Monserud, R.A., Solomon, A.M., 1992. A global biome model based on plant physiology and dominance, soil properties and climate. Journal of Biogeography 19 (2), 117–134.

Prentice, I.C., Guiot, J., Huntley, B., Jolly, D., Cheddadi, R., 1996. Reconstructing biomes from palaeoecological data: a general method and its application to European pollen data at 0 and 6 ka. Climate Dynamics 12 (3), 185–194.

Prentice, I.C., Jolly, D., BIOME 6000 Participants, 2000. Mid-Holocene and glacial-maximum vegetation geography of the northern continents and Africa. Journal of Biogeography 27 (3), 507–519.

Punt et al., 1976–2009, In: Punt, W., Blackmore, S., Hoen, P., Stafford, P. (Eds.), The Northwest European Pollen Flora Vols. I–IX, Elsevier, Amsterdam (1976–2009) http://stage.bio.uu.nl/palaeo/research/NEPF/nepf.htm, Parts 1–70 updated: April 2010.

Punt, W., Malotaux, M., 1984. Cannabaceae, Moraceae and Urticaceae. Review of Palaeobotany and Palynology 42 (1–4), 23–44.

Ralska-Jasiewiczowa, M., van Geel, B., 1992. Early human disturbance of the natural environment recorded in annually laminated sediments of Lake Gosciaz, central Poland. Vegetation History and Archaeobotany 1, 33–42.

Ramachandra, T.V., Mahapatra, D.M., Boominathan, M., Rao, K.S., Bhat, H.R., 2011. Environmental impact assessment of the National Large Solar Telescope Project and its ecological impact in Merak area. CES Technical Report XXM, Energy & Wetland Research Group, Centre for Ecological Sciences, Indian Institute of Science, Bangalore, India, 88 pp.

Ran, M., Feng, Z., 2013. Holocene moisture variations across China and driving mechanisms: A synthesis of climatic records. Quaternary International 313–314, 179–193.

Rawat, G.S., Adhikari, B.S., 2005. Millenia of grazing history in eastern Ladakh, India, reflected in rangeland vegetation. In: Proceedings of 2nd global mountain biodiversity assessment, La Paz Bolivia. CRC Press, Boca Raton, pp. 201–212.

Razjigaeva, N.G., Ganzey, L.A., Grebennikova, T.A., Belyanina, N.I., Mokhova, L.M., Arslanov, K.A., Chernov, S.B., 2013. Holocene climatic changes and vegetation development in the Kuril Islands. Quaternary International 290–291, 126–138.

Redman, C.L., Hassan, F.A., Hole, F., Morais, J., Riedel, F., Scarborough, V.L., Tainter, J.A., Turchin, P., Yasuda, Y., 2007. Group report: millennial perspectives on the dynamic interaction of climate, people, and resources. In: Costanza, R., Graumlich, L.J., Steffen, W. (Eds.), Sustainability or Collapse? An Integrated History and Future of People on Earth. MIT Press, Cambridge, pp. 115–148.

Reinmüller, J., 2010. Klimaverhältnisse in extremen Hochgebirgen der Erde. Diplom thesis. University of Graz (in German).

Ren, G., 2000. Decline of the mid- to late Holocene forests in China: climatic change or human impact? Journal of Quaternary Science 15, 273–281.

Ren, J., Qin, D., Kang, S., Hou, S., Pu, J., Jing, Z., 2004. Glacier variations and climate warming and drying in the central Himalayas. Chinese Science Bulletin 49 (1), 65–69.

Reuter, H.I., Nelson, A., Jarvis, A., 2007. An evaluation of void filling interpolation methods for SRTM data. International Journal of Geographic Information Science 21 (9), 983–1008.

Rhode, D., Haiying, Z., Madsen, D.B., Xing, G., Jeffrey Brantingham, P., Haizhou, M., Olsen, J.W., 2007. Epipaleolithic/early Neolithic settlements at Qinghai Lake, western China. Journal of Archaeological Science 34 (4), 600–612.

Ricketts, R.D., Johnson, T.C., Brown, E.T., Rasmussen, K.A., Romanovsky, V.V., 2001. The Holocene paleolimnology of Lake Issyk-Kul, Kyrgyzstan: trace element and stable isotope composition of ostracodes. Palaeogeography, Palaeoclimatology, Palaeoecology 176 (1–4), 207–227.

Rösch, M., 1992. Human impact as registered in the pollen record: some results from the western Lake Constance region, Southern Germany. Vegetation History and Archaeobotany 1 (2), 101–109.

Rohling, E.J., 1994. Review and new aspects concerning the formation of eastern Mediterranean sapropels. Marine Geology 122 (1–2), 1–28.

Rossignol-Strick, M., 1999. The Holocene climatic optimum and pollen records of sapropel 1 in the eastern Mediterranean, 9000–6000 BP. Quaternary Science Reviews 18, 515–530.

Rudaya, N., Tarasov, P., Dorofeyuk, N., Solovieva, N., Kalugin, I., Andreev, A., Daryin, A., Diekmann, B., Riedel, F., Tserendash, N., Wagner, M., 2009. Holocene environments and climate in the Mongolian Altai reconstructed from the Hoton-Nur pollen and diatom records: a step towards better understanding climate dynamics in Central Asia. Quaternary Science Reviews 28 (5–6), 540–554.

Rull, V., López-Sáez, J., Vegas-Vilarrúbia, T., 2008. Contribution of non-pollen palynomorphs to the paleolimnological study of a high-altitude Andean lake (Laguna Verde Alta, Venezuela). Journal of Paleolimnology 40 (1), 399–411.

Sakaguchi, Y., 1992. Cooling of Hokkaido around 9000 BP caused by permafrost meltwater burst. Bullettin of the Deptartement of Geography of the University of Tokyo 24, 1–6.

Sakamoto, T., Ikehara, M., Aoki, K., Iijima, K., Kimura, N., Nakatsuka, T., Wakatsuchi, M., 2005. Ice-rafted debris (IRD)-based sea-ice expansion events during the past 100

kyrs in the Okhotsk Sea. Deep Sea Research Part II: Topical Studies in Oceanography 52 (16–18), 2275–2301.

Sawada, K., Handa, N., 1998. Variability of the path of the Kuroshio ocean current over the past 25,000 years. Nature 392, 592–595.

Sawada, M., Viau, A.E., Vettoretti, G., Peltier, W.R., Gajewski, K., 2004. Comparison of North-American pollen-based temperature and global lake-status with CCCma AGCM2 output at 6 ka. Quaternary Science Reviews 23 (3–4), 225–244.

Schlütz, F., Lehmkuhl, F., 2009. Holocene climatic change and the nomadic Anthropocene in Eastern Tibet: palynological and geomorphological results from the Nianbaoyeze Mountains. Quaternary Science Reviews 28, 1449–1471.

Schlütz, F., Zech, W., 2004. Palynological investigations on vegetation and climate change in the Late Quaternary of Lake Rukche area, Gorkha Himal, Central Nepal. Vegetation History and Archaeobotany 13 (2), 81–90.

Schmidt, G.A., 2010. Enhancing the relevance of palaeoclimate model/data comparisons for assessments of future climate change. Journal of Quaternary Science 25, 79–87.

Schulz, H., von Rad, U., Erlenkeuser, H., 1998. Correlation between Arabian Sea and Greenland climate oscillations of the past 110,000 years. Nature 393, 54–57.

Schweinfurth, U.,1957. Die horizontale und vertikale Verbreitung der Vegetation im Himalaya. Bonner Geographische Abhandlungen 20, 1–370 (in German).

Sharma, K.K., Rajagopalan, G., and Choubey, V.M., 1989. Radiocarbon dating of charcoal from pre-Indus civilization fireplace, upper Indus valley, Ladakh. Current Science 58 (6), 306–308.

Shiga, K., Koizumi, I., 1999. Latest Quaternary oceanographic changes in the Okhotsk Sea based on diatom records. Marine Micropaleontology 38 (2), 91–117.

Singh, G., 1971. The Indus Valley culture seen in the context of postglacial climatic and ecological studies in north-west India. Archaeology and Physical Anthropology of Oceania 6 (2), 177–189.

Singh, J.S., Singh, S.P.,1987. Forest vegetation of the Himalaya. The Botanical Review 53 (1), 80–192.

Singh, O., Rai, S.P., Kumar, V., Sharma, M.K., Choubey, V.K., 2008. Water quality and eutrophication status of some lakes of the western Himalayan region. In: Sengupta, M., Dalwani, R. (Eds.), Proceedings of Taal 2007: The 12th World Lake Conference, 286–291.

Sinha, A., Berkelhammer, M., Stott, L., Mudelsee, M., Cheng, H., Biswas, J., 2011. The leading mode of Indian Summer Monsoon precipitation variability during the last millennium. Geophysical Research Letters 38 (15), L15703, doi:10.1029/2011GL047713.

Sirocko, F., Sarnthein, M., Erlenkeuser, H., Lange, H., Arnold, M., Duplessy, J.C., 1993. Century-scale events in monsoonal climate over the past 24,000 years. Nature 364, 322–324.

Sokolov, S.J., Svjazeva, O.A., Ogureeva, G.N., 1977. Arealy derev'ev i kustarnikov SSSR 1. Nauka, Leningrad (in Russian).

Sorsa, P., 1964. Studies on the spore morphology of Fennoscandian fern species. Annales Botanici Fennici 1, 179–201.

Sperber, K.R., Annamalai, H., Kang, I.S., Kitoh, A., Moise, A., Turner, A., Wang, B., Zhou, T., 2013. The Asian summer monsoon: an intercomparison of CMIP5 vs. CMIP3 simulations of the late 20th century. Climate Dynamics 41 (9–10), 2711–2744.

Srivastava, S.K., 2010. Floristic diversity and conservation strategies in cold desert of western Himalaya, India. Botanica Orientalis – Journal of Plant Science 7, 18–25.

Stanford, J.D., Rohling, E.J., Bacon, S., Roberts, A.P., Grousset, F.E., Bolshaw, M., 2011. A new concept for the paleoceanographic evolution of Heinrich event 1 in the North Atlantic. Quaternary Science Reviews 30 (9–10), 1047–1066.

Staubwasser, M., Sirocko, F., Grootes, P.M., Erlenkeuser, H., 2002. South Asian monsoon climate change and radiocarbon in the Arabian Sea during early and middle Holocene. Paleoceanography 17 (4), 1063, doi:10.1029/2000PA000608.

Staubwasser, M., Sirocko, F., Grootes, P.M., Segl, M., 2003. Climate change at the 4.2 ka BP termination of the Indus valley civilization and Holocene south Asian monsoon variability. Geophysical Research Letters 30 (8), 1425, doi:10.1029/2002GL016822.

Stebich, M., Mingram, J., Han, J., Liu, J., 2009. Late Pleistocene spread of (cool-)temperate forests in Northeast China and climate changes synchronous with the North Atlantic region. Global and Planetary Change 65, 56–70.

Steinke, S., Glatz, C., Mohtadi, M., Groeneveld, J., Li, Q., Jian, Z., 2011. Past dynamics of the East Asian monsoon: no inverse behaviour between the summer and winter monsoon during the Holocene. Global and Planetary Change 78,170–177.

Stevens, T., Thomas, D.S.G., Armitage, S.J., Lunn, H.R., Lu, H., 2007. Reinterpreting climate proxy records from late Quaternary Chinese loess: a detailed OSL investigation. Earth-Science Reviews 80 (1–2), 111–136.

Stockmarr, J., 1971. Tablets with spores used in absolute pollen analysis. Pollen et Spores 13, 614–621.

Stott, L., Cannariato, K., Thunell, R., Haug, G.H., Koutavas, A., Lund, S., 2004. Decline of surface temperature and salinity in the western tropical Pacific Ocean in the Holocene epoch. Nature 431 (7004), 56–59.

Stuiver, M., Reimer, P.J., 1993. Extended ^{14}C data base and revised CALIB 3.0 ^{14}C age calibration program. Radiocarbon 35 (1), 215–230.

Sun, Y., Clemens, S.C., Morrill, C., Lin, X., Wang, X., An, Z., 2012. Influence of Atlantic meridional overturning circulation on the East Asian winter monsoon. Nature Geoscience 5 (1), 46–49.

Svensson, A., Andersen, K.K., Bigler, M., Clausen, H.B., Dahl-Jensen, D., Davies, S.M., Johnsen, S.J., Muscheler, R., Parrenin, F., Rasmussen, S.O., Roethlisberger, R., Seierstad, I., Steffensen, J.P., Vinther, B.M., 2008. A 60 000 year Greenland stratigraphic ice core chronology. Climate of the Past 4 (1), 47–57.

Taft, L., Mischke, S., Wiechert, U., Leipe, C., Rajabov, I., Riedel, F., 2014. Oxygen and carbon isotope ratios in *Radix* (Gastropoda) shells indicate changes of glacial meltwater flux and temperature since 4,200 cal yr BP at Lake Karakul, eastern Pamirs (Tajikistan). Journal of Paleolimnology, doi:10.1007/s10933-014-9776-4.

Taft, L., Wiechert, U., Riedel, F., Weynell, M., Zhang, H.C., 2012. Sub-seasonal oxygen and carbon isotope variations in shells of modern *Radix* sp. (Gastropoda) from the Tibetan Plateau: potential of a new archive for palaeoclimatic studies. Quaternary Science Reviews 34, 44–56.

Taft, L., Wiechert, U., Zhang, H., Lei, G., Mischke, S., Plessen, B., Weynell, M., Winkler, A., Riedel, F., 2013. Oxygen and carbon isotope patterns archived in shells of the aquatic gastropod Radix: Hydrologic and climatic signals across the Tibetan Plateau in submonthly resolution. Quaternary International 290–291, 282-298.

Takada, H., Itaki, T., Ikehara, K., Yamada, K., Takayasu, K., 2006. Significant Tsushima Warm Current during the Early–Middle Holocene along the San-in District coast inferred from foraminiferal profiles. The Quaternary Research 45, 249–256 (in Japanese with English abstract).

Takahara, H., Igarashi, Y., Hayashi, R., Kumon, F., Liew, P.-M., Yamamoto, M., Kawai, S., Oba, T., Irino, T., 2010. Millennial-scale variability in vegetation records from the East Asian Islands: Taiwan, Japan and Sakhalin. Quaternary Science Reviews 29, 2900–2917.

Takahara, H., Sugita, S., Harrison, S.P., Miyoshi, N., Morita, Y., Uchiyama, T., 2000. Pollen-based reconstructions of Japanese biomes at 0, 6000 and 18,000 ^{14}C yr BP. Journal of Biogeography 27 (3), 665–683.

Tanaka, T., Yamamoto, T., Suzuki, M., 2005. Genetic diversity of *Castanea crenata* in northern Japan assessed by SSR markers. Breeding Science 55 (3), 271–277.

Tarasov, P., Granoszewski, W., Bezrukova, E., Brewer, S., Nita, M., Abzaeva, A., Oberhansli, H., 2005. Quantitative reconstruction of the last interglacial vegetation and climate based on the pollen record from Lake Baikal, Russia. Climate Dynamics 25 (6), 625–637.

Tarasov, P., Jin, G., Wagner, M., 2006. Mid-Holocene environmental and human dynamics in northeastern China reconstructed from pollen and archaeological data. Palaeogeography, Palaeoclimatology, Palaeoecology 241 (2), 284–300.

Tarasov, P., Williams, J.W., Andreev, A., Nakagawa, T., Bezrukova, E., Herzschuh, U., Igarashi, Y., Müller, S., Werner, K., Zheng, Z., 2007. Satellite- and pollen-based quantitative woody cover reconstructions for northern Asia: verification and application to late-Quaternary pollen data. Earth and Planetary Science Letters 264, 284–298.

Tarasov, P.E., Guiot, J., Cheddadi, R., Andreev, A.A., Bezusko, L.G., Blyakharchuk, T.A., Dorofeyuk, N.I., Filimonova, L.V., Volkova, V.S., Zernitskaya, V.P., 1999a. Climate in northern Eurasia 6000 years ago reconstructed from pollen data. Earth and Planetary Science Letters 171 (4), 635–645.

Tarasov, P.E., Jolly, D., Kaplan, J.O., 1997. A continuous Late Glacial and Holocene record of vegetation changes in Kazakhstan. Palaeogeography, Palaeoclimatology, Palaeoecology 136 (1–4), 281–292.

Tarasov, P.E., Nakagawa, T., Demske, D., Österle, H., Igarashi, Y., Kitagawa, J., Mokhova, L., Bazarova, V., Okuda, M., Gotanda, K., Miyoshi, N., Fujiki, T., Takemura, K., Yonenobu, H., Fleck, A., 2011. Progress in the reconstruction of Quaternary climate dynamics in the Northwest Pacific: a new modern analogue reference dataset and its application to the 430-kyr pollen record from Lake Biwa. Earth-Science Reviews 108 (1–2), 64–79.

Tarasov, P.E., Peyron, O., Guiot, J., Brewer, S., Volkova, V.S., Bezusko, L.G., Dorofeyuk, N.I., Kvavadze, E.V., Osipova, I.M., Panova, N.K., 1999b. Last Glacial Maximum climate of the former Soviet Union and Mongolia reconstructed from pollen and plant macrofossil data. Climate Dynamics 15 (3), 227–240.

Tarasov, P.E., Thompson III, W., Andreev, A.A., Afanas'eva, N.B., Berezina, N.A., Bezusko, L.G., Blyakharchuk, T.A., Bolikhovskaya, N.S., Cheddadi, R., Chernavskaya, M.M., Chernova, G.M., Dorofeyuk, N.I., Dirksen, V.G., Elina, G.A., Filimonova, L.V., Glebov, F.Z., Guiot, J., Gunova, V.S., Harrison, S.P., Jolly, D., Khomutova, V.I., Kvavadze, E.V., Osipova, I.M., Panova, N.K., Prentice, I.C., Saarse, L., Sevastyanov, D.V., Volkova, V.S., Zernitskaya, V.P., 1998. Present-day and mid-Holocene biomes reconstructed from pollen and plant macrofossil data from the former Soviet Union and Mongolia. Journal of Biogeography 25 (6), 1029–1053.

Tarasov, P.E., Volkova, V.S., Webb III, T., Guiot, J., Andreev, A.A., Bezusko, L.G., Bezusko, T.V., Bykova, G.V., Dorofeyuk, N.I., Kvavadze, E.V., Osipova, I.M., Panova, N.K., Sevastyanov, D.V., 2000. Last Glacial Maximum Biomes Reconstructed from Pollen and Plant Macrofossil Data from Northern Eurasia. Journal of Biogeography 27 (3), 609–620.

Tatewaki, M., 1958. Forest ecology of the islands of the North Pacific Ocean. Journal of the Faculty of Agriculture, Hokkaido University 50 (4), 371–486.

ter Braak, C.J.F., 1987. Ordination. In: Jongman, R., Ter Braak, C.J.F., Van Tongeren, O. (Eds.), Data Analysis in Community and Landscape Ecology. Pudoc, Wageningen, pp. 91–173.

Ternois, Y., Kawamura, K., Ohkouchi, N., Keigwin, L., 2000. Alkenone sea surface temperature in the Okhotsk Sea for the last 15 kyr. Geochemical Journal 34, 283–293.

Thelaus, M., 1992. Some characteristics of the mire development in Hongyuan County, eastern Tibetan Plateau. In: Proceedings of the Ninth International Peat Congress, Uppsala, Sweden, pp. 334–351.

Thompson, L.G., Yao, T., Davis, M.E., Henderson, K.A., Mosley-Thompson, E., Lin, P.-N., Beer, J., Synal, H.-A., Cole-Dai, J., Bolzan, J.F.,1997. Tropical climate instability: the last glacial cycle from a Qinghai–Tibetan ice core. Science 276, 1821–1825.

Trenberth, K.E., Stepaniak, D.P., Caron, J.M., 2000. The Global Monsoon as Seen through the Divergent Atmospheric Circulation. Journal of Climate 13 (22), 3969–3993.

Tripathi, C. Verma, B.C., Arora, R.K., 1988. Lower and Middle Palaeolithic artifacts from the Quaternary sediments of upper Indus valley, Ladakh Himalaya, J & K State, India. Bulletin of the Indian Geologist's Association 21 (1), 81–88.

Tsukada, M., 1986. Vegetation in prehistoric Japan: the last 20,000 years. In: Pearson, R.J., Barnes, G.L., Hutterer, K.L. (Eds.), Windows on the Japanese Past: Studies in Archaeology and Prehistory. Center for Japanese Studies, The University of Michigan, Ann Arbor, pp. 11–56.

Tsukada, M., 1988. Japan. In: Huntley, B., Webb III, T. (Eds.), Vegetation History. Kluwer Academic Publishers, Dordrecht, pp. 459–518.

Turner, A., Sperber, K.R., Slingo, J., Meehl, G., Mechoso, C.R., Kimoto, M., Giannini, A., 2011. Modelling monsoons: Understanding and predicting current and future behaviour. In: Chang, C.-P., Ding, Y., Lau, N.-C., Johnson, R.H., Wang, B., Yasunari, T. (Eds.), The Global Monsoon System – research and forcast, 2nd Edition. World Sientific, New Jersey, pp. 421–454.

Turner, A.G., Annamalai, H., 2012. Climate change and the South Asian summer monsoon. Nature Climate Change 2, 587–595.

Tweddle, J., Edwards, K., Fieller, N.J., 2005. Multivariate statistical and other approaches for the separation of cereal from wild Poaceae pollen using a large Holocene dataset. Vegetation History and Archaeobotany 14 (1), 15–30.

United States Geological Survey EROS Center, 1995. CORONA Satellite Photograph DS1107-1104DA026 Mission 1107-1. USGS, Sioux Falls, USA (image capture date: 30/07/1969).

Van Campo, E., Cour, P., Sixuan, H., 1996. Holocene environmental changes in Bangong Co basin (Western Tibet). Part 2: the pollen record. Palaeogeography, Palaeoclimatology, Palaeoecology 120 (1–2), 49–63.

Van Campo, E., Gasse, F., 1993. Pollen- and diatom-inferred climatic and hydrological changes in Sumxi Co Basin (western Tibet) since 13,000 yr B.P. Quaternary Research 39 (3), 300–313.

van Geel, B., 1978. A palaeoecological study of Holocene peat bog sections in Germany and The Netherlands, based on the analysis of pollen, spores and macro- and microscopic remains of fungi, algae, cormophytes and animals. Review of Palaeobotany and Palynology 25 (1), 1–120.

van Geel, B., 1986. Application of fungal and algal remains and other microfossils in palynological analyses. In: Berglund, B.E. (Ed.), Handbook of Holocene Palaeoecology and Palaeohydrology. John Wiley & Sons, Chichester, pp. 497–505.

van Geel, B., 2001. Non-pollen palynomorphs. In: Smol, J.P., Birks, H.J.B., Last, W.M. (Eds.), Tracking Environmental Change using Lake Sediments, Volume 3: Terrestrial, Algal and Siliceous Indicators. Kluwer, Dordrecht, pp. 99–119.

van Geel, B., Buurman, J., Brinkkemper, O., Schelvis, J., Aptroot, A., van Reenen, G., and Hakbijl, T., 2003. Environmental reconstruction of a Roman Period settlement site in Uitgeest (The Netherlands), with special reference to coprophilous fungi. Journal of Archaeological Science 30, 873–883.

van Geel, B., Coope, G.R., van der Hammen, T., 1989. Palaeoecology and stratigraphy of the Lateglacial type section at Usselo (The Netherlands). Reviews of Palaeobotany and Palynology 60, 25–129.

van Geel, B., Hallewas, D.P., Pals, J.P., 1983. A late holocene deposit under the Westfriese Zeedijk near Enkhuizen (Prov. of Noord-Holland, The Netherlands): Palaeoecological and archaeological aspects. Review of Palaeobotany and Palynology 38 (3–4), 269–335.

van Geel, B., Van der Hammen, T., 1978. Zygnemataceae in Quaternary Columbian sediments. Review of Palaeobotany and Palynology 25 (5), 377–391.

Vera, F.W.M., 2000. Grazing ecology and forest history. CAB International, Wallingford.

von Oheimb, P.V., Albrecht, C., Riedel, F., Bössneck, U., Zhang, H.C., Wilke, T., 2013. Testing the role of the Himalaya Mountains as a dispersal barrier in freshwater gastropods (*Gyraulus* spp.). Biological Journal of the Linnean Society 109, 526–534.

von Oheimb, P.V., Albrecht, C., Riedel, F., Du, L.N., Yang, J.X., Aldridge, D.C., Bößneck, U., Zhang, H.C., Wilke, T., 2011. Freshwater biogeography and limnological evolution of the Tibetan Plateau - Insights from a plateau-wide distributed gastropod taxon (*Radix* spp.). PLoS ONE 6, e26307

Waelbroeck, C., Labeyrie, L., Michel, E., Duplessy, J.C., McManus, J.F., Lambeck, K., Balbon, E., Labracherie, M., 2002. Sea-level and deep water temperature changes derived from benthic foraminifera isotopic records. Quaternary Science Reviews 21 (1–3), 295–305.

Wahl, E.R., Morrill, C., 2010. Toward understanding and predicting monsoon patterns. Science 328, 437–438.

Walker, I.R., 2001. Midges: Chironomidae and Related Diptera. In: Smol, J., Birks, H.J., Last, W. (Eds.), Tracking Environmental Change using Lake Sediments. Kluwer, Dordrecht, pp. 43–66.

Wallace, J.M., Rasmusson, E.M., Mitchell, T.P., Kousky, V.E., Sarachik, E.S., von Storch, H., 1998. On the structure of ENSO-related climate variability in the tropical Pacific: Lessons from TOGA. Journal of Geophysical Research 103 (C7), 14241–14259, doi:10.1029/97JC02905.

Wang, B., 2006. The Asian Monsoon. Praxis Publishing Ltd, Chichester, 787 pp.

Wang, B., Clemens, S.C., Liu, P., 2003. Contrasting the Indian and East Asian monsoons: implications on geologic timescales. Marine Geology 201 (1–3), 5–21.

Wang, B., Wu, R., Lau, K.M., 2001a. Interannual Variability of the Asian Summer Monsoon: Contrasts between the Indian and the Western North Pacific–East Asian Monsoons. Journal of Climate, 14 (20), 4073–4090.

Wang, F., Chien, N., Zhang, Y., Yang, H., 1997. Pollen Flora of China, second ed. Science Press, Beijing. Wang, J.X., Feng, Z.J., 1994. A study on the pollen morphology of the genus Polygonum in China. Acta Phytotaxonomica Sinica 32 (3), 219–231.

Wang, L., Li, J., Lu, H., Gu, Z., Rioual, P., Hao, Q., Mackay, A.W., Jiang, W., Cai, B., Xu, B., Han, J., Chu, G., 2012. The East Asian winter monsoon over the last 15,000 years: its links to high-latitudes and tropical climate systems and complex correlation to the summer monsoon. Quaternary Science Reviews 32, 131–142.

Wang, P.X., Clemens, S., Beaufort, L., Braconnot, P., Ganssen, G., Jian, Z.M., Kershaw, P., Sarnthein, M., 2005a. Evolution and variability of the Asian monsoon system: state of the art and outstanding issues. Quaternary Science Reviews 24 (5–6), 595–629.

Wang, X., Auler, A.S., Edwards, R.L., Cheng, H., Cristalli, P.S., Smart, P.L., Richards, D.A., Shen, C.-C., 2004. Wet periods in northeastern Brazil over the past 210 kyr linked to distant climate anomalies. Nature 432 (7018), 740–743.

Wang, Y., Cheng, H., Edwards, R.L., Kong, X., Shao, X., Chen, S., Wu, J., Jiang, X., Wang, X., An, Z., 2008. Millennial- and orbital-scale changes in the East Asian monsoon over the past 224,000 years. Nature 451, 1090–1093.

Wang, Y., Liu, X., Herzschuh, U., 2010. Asynchronous evolution of the Indian and East Asian Summer Monsoon indicated by Holocene moisture patterns in monsoonal central Asia. Earth-Science Reviews 103 (3–4), 135–153.

Wang, Y.J., Cheng, H., Edwards, R.L., An, Z.S., Wu, J.Y., Shen, C.C., Dorale, J.A., 2001b. A high-resolution absolute-dated Late Pleistocene monsoon record from Hulu Cave, China. Science 294, 2345–2348.

Wang, Y.J., Cheng, H., Edwards, R.L., He, Y., Kong, X., An, Z., Wu, J., Kelly, M.J., Dykoski, C.A., Li, X., 2005b. The Holocene Asian monsoon: links to solar changes and North Atlantic climate. Science 308, 854–857.

Wanner, H., Beer, J., Bütikofer, J., Crowley, T.J., Cubasch, U., Flückiger, J., Goosse, H., Grosjean, M., Joos, F., Kaplan, J.O., Küttel, M., Müller, S.A., Prentice, I.C., Solomina, O., Stocker, T.F., Tarasov, P., Wagner, M., Widmann, M., 2008. Mid- to Late Holocene climate change: an overview. Quaternary Science Reviews 27 (19–20), 1791–1828.

Wanner, H., Solomina, O., Grosjean, M., Ritz, S.P., Jetel, M., 2011. Structure and origin of Holocene cold events. Quaternary Science Reviews 30 (21–22), 3109–3123.

Weber, S.A., 2003. Archaeobotany at Harappa: indications for change. In: Weber, S.A., Belcher, W.R. (Eds.), Indus Ethnobiology. New Perspectives from the Field. Lexington Books, Lanham, pp. 175–198.

Webster, P.J., 2006. The coupled monsoon system. In: Wang, B. (Ed.), The Asian Monsoon. Praxis Publishing Ltd, Chichester, pp. 3–66.

Webster, P.J., Magana, V.O., Palmer, T.N., Shukla, J., Tomas, R.A., Yanai, M., Yasunari, T., 1998. Monsoons: processes, predictability, and the prospects for prediction. Journal of Geophysical Research: Oceans 103 (C7), 14451–14510, doi:10.1029/97JC02719.

Weiss, H., 1997. Late third millennium abrupt climate change and social collapse in West Asia and Egypt. In: Dalfes, H.N., Kukla, G., Weiss, H. (Eds.), Third Millennium B.C. Climate Change and Old World Collapse. NATO ASI Series I: Global Environmental Change, vol. 49. Springer, Berlin, pp. 711–723.

Weiss, H., Bradley, R.S., 2001. What drives societal collapse? Science 291, 609–610.

Weninger, B., Clare, L., Rohling, E., Bar-Yosef, O., Boehner, U., Budja, M., Bundschuh, M., Feurdean, A., Gebe, H.G., Joeris, O., Lindstaedter, J., Mayewski, P., Muehlenbruch, T., Reingruber, A., Rollefson, G., Schyle, D., Thissen, L., Todorova, H., Zielhofer, C., 2009. The impact of rapid climate change on prehistoric societies during the Holocene in the Eastern Mediterranean. Documenta Praehistorica 36, 7–59.

Weninger, B., Jöris, O., 2008. A ^{14}C age calibration curve for the last 60 ka: the Greenland-Hulu U/Th timescale and its impact on understanding the Middle to Upper Paleolithic transition in Western Eurasia. Journal of Human Evolution 55 (5), 772–781.

Weninger, B., Jöris, O., Danzeglocke, U., 2013. CalPal-2007. Cologne Radiocarbon Calibration & Palaeoclimate Research Package. http://www.calpal.de/.

White, D., Bush, A.B.G., 2010. Holocene climate, environmental change, and Neolithic biocultural discontinuity in the Baikal region. In: Weber, A.W., Katzenberg, M.A., Schurr, T.G. (Eds.), Prehistoric Hunter–Gatherers of the Baikal Region, Siberia: Bioarchaeological Studies of Past Life Ways. University of Pennsylvania, Museum Press, PA, USA, pp. 1–26.

Williams, J.W., Jackson, S.T., 2003. Palynological and AVHRR observations of modern vegetational gradients in eastern North America. The Holocene 13 (4), 485–497.

Williams, J.W., Summers, R.L., Webb III, T., 1998. Applying plant functional types to construct biome maps from eastern North American pollen data: comparison with model results. Quaternary Science Reviews 17 (6–7), 607–627.

Williams, J.W., Tarasov, P., Brewer, S., Notaro, M., 2011. Late Quaternary variations in tree cover at the northern forest-tundra ecotone. Journal of Geophysical Research 116, G01017, doi:10.1029/2010JG001458.

World Bank, 2014. Population data 2012. Data retrieved from the World Bank database at http://data.worldbank.org (accessed 03/2014).

Wright, R.P., Bryson, R.A., Schuldenrein, J., 2008. Water supply and history: Harappa and the Beas regional survey. Antiquity 82 (315), 37–48.

Wu, B., Wang, J., 2002. Winter Arctic Oscillation, Siberian High and East Asian Winter Monsoon. Geophysical Research Letters 29 (19), 1897, doi:10.1029/2002gl015373.

Wu, W., Liu, T., 2004. Possible role of the "Holocene Event 3" on the collapse of Neolithic Cultures around the Central Plain of China. Quaternary International 117 (1), 153–166.

Wünnemann, B., Demske, D., Tarasov, P., Kotlia, B.S., Reinhardt, C., Bloemendal, J., Diekmann, B., Hartmann, K., Krois, J., Riedel, F., Arya, N., 2010. Hydrological evolution during the last 15 kyr in the Tso Kar lake basin (Ladakh, India), derived from geomorphological, sedimentological and palynological records. Quaternary Science Reviews 29 (9–10), 1138–1155.

Wünnemann, B., Reinhardt, C., Kotlia, B.S., and Riedel, F., 2008. Observations on the Relationship between Lake Formation, Permafrost Activity and Lithalsa Development during the last 20 000 years in the Tso Kar Basin, Ladakh, India. Permafrost and Periglacial Processes 19, 341–358.

Wulf, H., Bookhagen, B., Scherler, D., 2010. Seasonal precipitation gradients and their impact on fluvial sediment flux in the Northwest Himalaya. Geomorphology 118, 13–21.

Xiao, J., Xu, Q., Nakamura, T., Yang, X., Liang, W., Inouchi, Y., 2004. Holocene vegetation variation in the Daihai Lake region of north-central China: a directindication of the Asian monsoon climatic history. Quaternary Science Reviews 23 (14–15), 1669–1679.

Yamazaki, T., Inoue, S., Shimono, T., Sakamoto, T., Saburo Sakai, S., 2013. Sea-ice conditions in the Okhotsk Sea during the last 550 kyr deduced from environmental magnetism. Geochemistry Geophysics Geosystems 14 (12), 5026–5040, doi:10.1002/2013GC004959.

Yancheva, G., Nowaczyk, N.R., Mingram, J., Dulski, P., Schettler, G., Negendank, J.F.W., Liu, J.Q., Sigman, D.M., Peterson, L.C., Haug, G.H., 2007. Influence of the intertropical convergence zone on the East Asian monsoon. Nature 445 (7123), 74–77.

Yang, S., Ding, Z., 2008. Advance-retreat history of the East-Asian summer monsoon rainfall belt over northern China during the last two glacialeinterglacial cycles. Earth and Planetary Science Letters 274 (3–4), 499–510.

Yasuda, Y., Fujiki, T., Nasu, H., Kato, M., Morita, Y., Mori, Y., Kanehara, M., Toyama, S., Yano, A., Okuno, M., Jiejun, H., Ishihara, S., Kitagawa, H., Fukusawa, H., Naruse, T., 2004a. Environmental archaeology at the Chengtoushan site, Hunan Province, China, and implications for environmental change and the rise and fall of the Yangtze River civilization. Quaternary International 123–125, 149–158.

Yasuda, Y., Kitagawa, H., Nakagawa, T., 2000. The earliest record of major anthropogenic deforestation in the Ghab Valley, northwest Syria: a palynological study. Quaternary International 73–74, 127–136.

Yasuda, Y., Yamaguchi, K., Nakagawa, T., Fukusawa, H., Kitagawa, J., Okamura, M., 2004b. Environmental variability and human adaptation during the Lateglacial/Holocene transition in Japan with reference to pollen analysis of the SG4 core from Lake Suigetsu. Quaternary International 123–125, 11–19.

Yoshida, A., Takeuti, S., 2009. Quantitative reconstruction of palaeoclimate from pollen profiles in northeastern Japan and the timing of a cold reversal event during the Last Termination. Journal of Quaternary Science 24 (8), 1006–1015.

Yoshioka, K., 1973. Plant Geography. Kyoritsu-Shuppan Publishing House, Tokyo (in Japanese).

Yu, G., Chen, X., Ni, J., Cheddadi, R., Guiot, J., Han, H., Harrison, S.P., Huang, C., Ke, M., Kong, Z., Li, S., Li, W., Liew, P., Liu, G., Liu, J., Liu, Q., Liu, K.B., Prentice, I.C., Qui, W., Ren, G., Song, C., Sugita, S., Sun, X., Tang, L., Campo, E.V., Xia, Y., Xu, Q., Yan, S., Yang, X., Zhao, J., Zheng, Z., 2000. Palaeovegetation of China: a pollen data-based synthesis for the mid-Holocene and last glacial maximum. Journal of Biogeography 27 (3), 635–664.

Yu, G., Prentice, I.C., Harrison, S.P., Sun, X., 1998. Pollen-based biome reconstructions for China at 0 and 6000 years. Journal of Biogeography 25 (6), 1055–1069.

Yuan, D., Cheng, H., Edwards, R.L., Dykoski, C.A., Kelly, M.J., Zhang, M., Qing, J., Lin, Y., Wang, Y., Wu, J., Dorale, J.A., An, Z., Cai, Y., 2004. Timing, duration, and transitions of the Last Interglacial Asian Monsoon. Science 304, 575–578.

Zhang, J., Chen, F., Holmes, J.A., Li, H., Guo, X., Wang, J., Li, S., Lü, Y., Zhao, Y., Qiang, M., 2011. Holocene monsoon climate documented by oxygen and carbon isotopes from lake sediments and peat bogs in China: a review and synthesis. Quaternary Science Reviews 30 (15–16), 1973–1987.

Zhao, J.-X., Wang, Y.-J., Collerson, K.D., Gagan, M.K., 2003. Speleothem U-series dating of semi-synchronous climate oscillations during the last deglaciation. Earth and Planetary Science Letters 216 (1–2), 155–161.

Zhao, M., Kong, Q.-P., Wang, H.-W., Peng, M.-S., Xie, X.-D., Wang, W.-Z., Jiayang, Duan, J.-G., Cai, M.-C., Zhao, S.-N., Cidanpingcuo, Tu, Y.-Q., Wu, S.-F., Yao, Y.-G., Bandelt, H.-J., Zhang, Y.-P., 2009a. Mitochondrial genome evidence reveals successful Late Paleolithic settlement on the Tibetan Plateau. Proceedings of the National Academy of Sciences 106 (50), 21230–21235.

Zhao, Y., Harrison, S.P., 2012. Mid-Holocene monsoons: a multi-model analysis of the inter-hemispheric differences in the responses to orbital forcing and ocean feedbacks. Climate Dynamics 39 (6), 1457–1487.

Zhao, Y., Herzschuh, U., 2009. Modern pollen representation of source vegetation in the Qaidam Basin and surrounding mountains, north-eastern Tibetan Plateau. Vegetation History and Archaeobotany 18 (3), 245–260.

Zhao, Y., Liu, H., Li, F., Huang, X., Sun, J., Zhao, W., Herzschuh, U., Tang, Y., 2012. Application and limitations of the Artemisia/Chenopodiaceae pollen ratio in arid and semi-arid China. The Holocene 22 (12), 1385–1392.

Zhao, Y., Yu, Z., 2012. Vegetation response to Holocene climate change in East Asian monsoon-margin region. Earth-Science Reviews 113 (1–2), 1–10.

Zhao, Y., Yu, Z., Chen, F., 2009b. Spatial and temporal patterns of Holocene vegetation and climate changes in arid and semi-arid China. Quaternary International 194 (1–2), 6-18.

Zhao, Y., Yu, Z., Chen, F., Ito, E., Zhao, C., 2007. Holocene vegetation and climate history at Hurleg Lake in the Qaidam Basin, northwest China. Review of Palaeobotany and Palynology 145 (3–4), 275–288.

Zhao, Y., Yu, Z., Chen, F., Liu, X., Ito, E., 2008. Sensitive response of desert vegetation to moisture change based on a near-annual resolution pollen record from Gahai Lake in the Qaidam Basin, northwest China. Global and Planetary Change 62 (1–2), 107–114.

Zhao, Y., Yu, Z., Chen, F., Zhang, J., Yang, B., 2009c. Vegetation response to Holocene climate change in monsoon-influenced region of China. Earth-Science Reviews 97 (1–4), 242–256.

Zheng, Y., Zheng, Z., Tarasov, P., Qian, L., Huang, K., Wei, J., Luo, C., Xu, Q., Lu, H., Luo, Y., 2010. Palynological and satellite-based MODIS observations of modern vegetational gradients in China. Quaternary International 218, 190–201.

Zhou, W., Yu, X., Jull, A.J.T., Burr, G., Xiao, J.Y., Lu, X., Xian, F., 2004. High-resolution evidence from southern China of an early Holocene optimum and a mid-Holocene dry event during the past 18,000 years. Quaternary Research 62 (1), 39–48.

Zhulidov, A.V., Headley, J.V., Robarts, R.D., Nikanorov, A.M., Ischenko, A.A., 1997. Atlas of Russian Wetlands: Biogeography and metal concentrations. National Hydrology Research Institute, Saskatchewan, 309 pp.

Zhushchikhovskaya, I.S., Shubina, O.A., 2006. Pottery making and the culture history of Neolithic Sakhalan. In: Dumond, D.E., Bland, R.L. (Eds.), Archaeology in Northeast Asia: on the pathway to Bering Strait. Anthropological Papers No. 76, University of Oregon, Eugene, pp. 91–128.

Zippi, P.A., Yung, Y.-T., Welbourn, P.M., Norris, G., McAndrews, J.H., 1991. Extraction of zygnematacean zygospores from lake sediments and their potential as paleo-indicators of lake acidification. RAC Project No. 464G. Ontario Ministry of the Environment.

8. Appendix

8.1 Supplementary material

Supplementary data associated with the four individual articles presented in this thesis are available in the Open Access information system PANGAEA. Detailed information on provided data and on data access via internet is provided in Table 8.1.

Manuscript no./chapter	PANGAEA issue title/ • contained datasets	Digital Object Identifier (doi)
I/2.	**Fossil pollen record of composite sediment core TMD from Tso Moriri, analysis of modern surface pollen samples, mean annual precipitation reconstruction, and digitisation and recalibration of different discussed palaeoclimate proxy records.**	doi:10.1594/PANGAEA.808958
	• Pollen and spore counts of the Holocene part of the TMD composite core from Tso Moriri.	doi:10.1594/PANGAEA.808952
	• Pollen and spore counts of eight modern surface pollen samples.	doi:10.1594/PANGAEA.808953
	• Mean annual precipitation reconstruction derived from the A/C ratio of the TMD composite core from Tso Moriri.	doi:10.1594/PANGAEA.809246
	• Revised chronology of the $\delta^{18}O$ record from Qinghai Lake.	doi:10.1594/PANGAEA.808954
	• Revised chronology of the A/C ratio record from Sumxi Co.	doi:10.1594/PANGAEA.808955
	• Age-depth model for the G. bulloides concentration record of ODP Hole 117-723A, western Arabian Sea.	doi:10.1594/PANGAEA.808956
	• Globigerina bulloides concentration record of ODP Hole 117-723A, western Arabian Sea.	doi:10.1594/PANGAEA.808957
II/3.	**Pollen and non-pollen palynomorph records of the Holocene part of the composite sediment core TMD from lake Tso Moriri (NW India) and of modern surface samples from the Tso Moriri region.**	doi:10.1594/PANGAEA.829753
	• Results of the Poaceae (terrestrial) and aquatic pollen analysis of the Holocene part of the TMD composite core from lake Tso Moriri.	doi:10.1594/PANGAEA.829748
	• Results of the non-pollen palynomorph (NPP) analysis of the Holocene part of the TMD composite core from lake Tso Moriri.	doi:10.1594/PANGAEA.829749
	• Results of the pollen and non-pollen palynomorph (NPP) analysis beyond the regular count of the Holocene part of the TMD composite core from lake Tso Moriri.	doi:10.1594/PANGAEA.829750
	• Results of the terrestrial and aquatic pollen analysis of 16 surface samples from the Tso Moriri area.	doi:10.1594/PANGAEA.829751

	• Results of the non-pollen palynomorph (NPP) analysis of 16 surface samples from the Tso Moriri area.	doi:10.1594/PANGAEA.829752
III/4.	**Reference datasets and pollen record from sediment core YAK, Yakumo, SW Hokkaido**	doi:10.1594/PANGAEA.785361
	• Modern climate variables of 326 modern surface pollen sampling sites from northern Japan.	doi:10.1594/PANGAEA.785252
	• Reference pollen dataset of 326 modern surface spectra from northern Japan.	doi:10.1594/PANGAEA.785247
	• Percentage pollen diagram representing 38 fossil pollen spectra of sediment core YAK, Yakumo, SW Hokkaido.	doi:10.1594/PANGAEA.785340
	• Reconstructed climate variables derived from the pollen record of sediment core YAK, Yakumo, SW Hokkaido, based on a reference dataset including 248 sites.	doi:10.1594/PANGAEA.785354
	• Reconstructed climate variables derived from the pollen record of sediment core YAK, Yakumo, SW Hokkaido, based on a reference dataset including 326 sites.	doi:10.1594/PANGAEA.785358
IV/5.	**Supplementary data will be provided as soon as the manuscript is submitted for publication.**	

Table 8.1 Overview of the supplementary material associated with the four article manuscripts incorporated in the present doctoral thesis.

8.2 List of publications

Main authorship articles:

Leipe, **C.**, Igarashi, Y., Nakagawa, T., Gotanda, K., Tarasov, P.E., *Manuscript in review at Quaternary Science Reviews*. Pollen-inferred late Quaternary vegetation and climate variations from the northernmost part of the East Asian Summer Monsoon domain (Sakhalin, Russian Far East).

Leipe, **C.**, Demske, D., Tarasov, P.E., Wünnemann, B., Riedel, F., HIMPAC Project Members, 2014. Potential of pollen and non-pollen palynomorph records from Tso Moriri (Trans-Himalaya, NW India) for reconstructing Holocene limnology and human–environmental interactions. *Quaternary International* 348, 113–129, doi:10.1016/j.quaint.2014.02.026.

Leipe, **C.**, Demske, D., Tarasov, P.E., HIMPAC Project Members, 2014. A Holocene pollen record from the northwestern Himalayan lake Tso Moriri: Implications for palaeoclimatic and archaeological research. *Quaternary International* 348, 93–112, doi:10.1016/j.quaint.2013.05.005.

Leipe, **C.**, Kito, N., Sakaguchi, Y., Tarasov, P.E., 2013. Vegetation and climate history of northern Japan inferred from the 5500-year pollen record from the Oshima Peninsula, SW Hokkaido. *Quaternary International* 290–291, 151–163, doi:10.1016/j.quaint.2012.07.014.

Co-authorship articles:

Taft, L., Mischke, S., Wiechert, U., **Leipe**, **C.**, Rajabov, I., Riedel, F., 2014. Oxygen and carbon isotope ratios in *Radix* (Gastropoda) shells indicate changes of glacial meltwater flux and temperature since 4,200 cal yr BP at Lake Karakul, eastern Pamirs (Tajikistan). *Journal of Paleolimnology* 52 (1–2), 27–41, doi:10.1007/s10933-014-9776-4.

Tarasov, P.E., Andreev, A.A., Anderson, P.M., Lozhkin, A.V., **Leipe**, **C.**, Haltia, E., Nowaczyk, N.R., Wennrich, V., Brigham-Grette, J., Melles, M., 2013. A pollen-based biome reconstruction over the last 3.562 million years in the Far East Russian Arctic – new insights into climate-vegetation relationships at the regional scale. *Climate of the Past* 9 (6), 2759–2775, doi:10.5194/cp-9-2759-2013.

Riedel, F., Henderson, A.G., Heußner, K.-U., Kaufmann, G., Kossler, A., **Leipe**, **C.**, Shemang, E., Taft, L., 2013. Dynamics of a Kalahari long-lived mega-lake system: hydromorphological and limnological changes in the Makgadikgadi Basin (Botswana) during the terminal 50 ka. *Hydrobiologia* 739 (1), 25–53, doi:10.1007/s10750-013-1647-x.

Tarasov, P.E., Müller, S., Zech, M., Andreeva, D., Diekmann, B., **Leipe**, **C.**, 2013. Last glacial vegetation reconstructions in the extreme-continental eastern Asia: Potentials of pollen and *n*-alkane biomarker analyses. *Quaternary International* 290–291, 253–263, doi:10.1016/j.quaint.2012.04.007.

Wagner, M., Tarasov, P., Hosner, D., Fleck, A., Ehrich, R., Chen, X., **Leipe**, **C.**, 2013. Mapping of the spatial and temporal distribution of archaeological sites of northern China during the Neolithic and Bronze Age. *Quaternary International* 290–291, 344–357, doi:10.1016/j.quaint.2012.06.039.

8.3 Curriculum vitae

Due to data protection regulations, the curriculum vitae is not included in the online version of this doctoral thesis.

Due to data protection regulations, the curriculum vitae is not included in the online version of this doctoral thesis.

8.4 Declaration

I certify that this thesis is my own work and effort and that it has not been previously submitted and approved for the award of a degree by this or any other university. Where other sources of information have been used, they are properly acknowledged.

Berlin, 19 May 2014

Christian Leipe